Macroscopic Discontinuity Modeling for Multiclass Multilane Traffic Flow Operations

Dong NGODUY

Delft University of Technology, 2006

Macroscopic Discontinuity Modeling for Multiclass Multilane Traffic Flow Operations

Proefschrift

ter verkrijging van de graad van doctor

aan de Technische Universiteit Delft,

op gezag van de Rector Magnificus prof. dr. ir J.T. Fokkema,

voorzitter van het College voor Promoties,

in het openbaar te verdedigen op donderdag 13 april 2006 om 15.30 uur

door

Dong NGODUY

Master of Science in Engineering

geboren te Vietnam

Dit proefschrift is goedgekeurd door de promotor:
Prof. dr. H.J. van Zuylen

Toegevoegd promotor: Dr. ir. S.P. Hoogendoorn

Samenstelling promotiecommissie :

Rector Magnificus	voorzitter
Prof. dr. H.J. van Zuylen	Technische Universiteit Delft, promotor
Dr. ir. S.P. Hoogendoorn	Technische Universiteit Delft, toegevoegd promotor
Prof. dr. ir. P.H.L Bovy	Technische Universiteit Delft
Prof. dr. G.S. Stelling	Technische Universiteit Delft
Prof. dr.-ing. M. Papageorgiou	Technical University of Crete, Greece
Prof. dr. J.P. Lebacque	Gretia-Inrets, Entpe, Eivp, France
Prof. dr. D. Helbing	Dresden University of Technology, Germany

This thesis is the result of a Ph.D. study carried out from 2002 to 2006 at Delft University of Technology, Faculty of Civil Engineering and Geosciences, Transport and Planning Section.

TRAIL Thesis Series no. T2006/3, The Netherlands TRAIL Research School

TRAIL
P.O. Box 5017
2600 GA Delft
The Netherlands
Phone: +31 (0) 15 278 6046
Fax: +31 (0) 15 278 4333
E-mail: info@rsTRAIL.nl

ISBN 90-5584-075-0

Printed in The Netherlands

”Imagination is more important than knowledge”
- Albert Einstein

Preface

Since Lighthill and Whitham first applied a simple continuum model to describe the evolution of traffic flow on freeways much effort has been devoted to the further development and application of continuum traffic flow models. These efforts have however mainly concentrated on describing uninterrupted traffic flow. Relatively little progress has been made in the investigation of interrupted traffic flow. In this thesis we develop a continuum traffic flow model pertaining to the modeling of discontinuities of traffic flow at bottlenecks on multilane freeway and in urban networks. The proposed model refines and extends the work of Hoogendoorn by introducing the so-called *mandatory lane-changing* process based on microscopic driving principles. Based on the details of this *mandatory lane-changing* process, a relevant control measure at on–and off–ramps (ramp metering), or design of infrastructure (acceleration lane length, exclusive lane at intersection) can be applied in order to obtain a better traffic operation. The results presented in this thesis are a part of AMICI program (Advanced Multi–agent Information and Control for Integrated multi–class traffic networks). Within the framework of AMICI program, several research projects have been carried out. As a core of AMICI program, this thesis provides traffic conditions for the control part.

During the research, several people in my department have helped me a lot. I would like to thank to each who has contributed to this thesis. Most thanks go to Serge Hoogendoorn, my daily supervisor. His ideas and modeling skills have set the light for the work developed in this thesis. I would also like to thank my promotor, Professor Henk van Zuylen, who gives me invaluable discussions and much freedom in carrying out the research. I am also owing to Professor Piet H.L. Bovy for spending time on providing valuable comments. Several people reviewed the first versions of this thesis. I am indebted to Chris Tampere for giving me your very useful comments especially in numerical solutions, to Thomas Dijker for checking my English. Finally, I would like to thank my parents, for their love and tolerance throughout the time I am absent.

Dong NGODUY, October 2005

Contents

List of Figures

List of Tables

Notation

The main shorthand and symbols that are used in the development of our model (Chapter 3 to Chapter 6) are presented as follows:

Shorthand

$p.d.f$	:	probability density function
$c.d.f$	:	cumulative distribution function
PSD	:	phase-space density
ILC	:	immediate lane-change
SLC	:	spontaneous lane-change
MLC	:	mandatory lane-change
$MLMC$	:	multilane and multiclass

Independent variables

x	:	location (m)
x_0	:	location of the beginning of acceleration (auxiliary) lane (m)
x_{end}	:	location of the end of acceleration (auxiliary) lane (m)
t	:	time (s)
u	:	vehicle class
i	:	roadway lane
a	:	link index
L	:	length of the acceleration (auxiliary) lane (m)

Microscopic variables and parameters

v	:	speed of an individual vehicle (m/s)
T	:	reaction time (s)
l	:	length of a vehicle (m)
d	:	distance headway (m)
d_{min}	:	safety margin (m)

Mesoscopic variables and parameters

$\rho_i^u(x,v,t)$	:	lane and class specific *PSD* (veh/m)
$f_i^u(x,h,t)$	:	lane and class specific *p.d.f* of distance gap
$f_{lead,i}^u(x,h,t)$	:	lane and class specific *p.d.f* of lead gap
$f_{lag,i}^u(x,h,t)$	:	lane and class specific *p.d.f* of lag gap
$F_i^u(x,h,t)$	:	lane and class specific *c.d.f* of distance gap
$F_{lead,i}^u(x,h,t)$	:	lane and class specific *c.d.f* of lead gap
$F_{lag,i}^u(x,h,t)$	:	lane and class specific *c.d.f* of lag gap
$\tilde{f}(x,h,t)$	:	Laplace transform of the *p.d.f* of distance gap
$\bar{h}$	:	average distance gap (m)
$p_{i,j}^u$	:	immediate lane-changing probability
Ω_i^u	:	fraction of vehicles giving-way at bottlenecks
$\tilde{\nu}^{\pm}$	:	Mandatory lane-changing rate (veh/(m.s))
$\alpha_{i,j}^u$	:	fraction of (mandatory) lane-changing vehicles
$\pi_{i,j}^u$	:	mandatory lane-changing probability at on–and off–ramps
$\tilde{\pi}_{i,j}^u$	:	mandatory lane-changing probability at weaving sections
μ	:	ramp factor

Macroscopic variables and parameters

$r_i^u(x,t)$	:	lane and class specific traffic density (veh/m)
$V_i^u(x,t)$	:	lane and class specific mean speed (m/s)
$V_{max,i}^u$	:	lane and class specific free mean speed (m/s)
$V_u^{\pm}(x,t)$	:	mean speed of traffic entering or exiting the freeway (m/s)
$q_i^u(x,t)$	:	lane and class specific mean flow rate (veh/s)
$V_{e,i}^u$	:	lane and class specific equilibrium speed (m/s)
$\Theta_i^u(x,t)$	:	lane and class specific mean speed variance (m^2/s^2)
Ψ_i^u	:	Interaction rates in conservation equation (veh/(m.s))
Φ_i^u	:	Interaction rates in momentum equation (veh/(m.s))
$\Delta_{i,j}^u$	:	Spontaneous lane-changing rate (1/s)
$\nu^{\pm}$	:	Mandatory lane-changing rate (veh/(m.s))
Ξ	:	traffic demand at intersection (veh/s)
Σ	:	traffic supply at intersection (veh/s)
ξ	:	traffic demand of upstream link at intersection (veh/s)
σ	:	traffic supply of downstream link at intersection (veh/s)
$A(r_i^u)$	:	lane and class specific pre-factor speed variance function
$\gamma(r)$	:	vehicle space requirement factor
$r_{max,i}^u$	:	lane and class specific jam density (veh/m)
$r_{cr,i}^u$	:	lane and class specific critical density (veh/m)
τ_i^u	:	lane and class specific relaxation time (s)

Chapter 1

Introduction

Traffic congestion on freeways and in urban areas is a major social problem worldwide. It causes direct economic losses, such as delays and accidents, and indirect losses, such as air pollution. While congested conditions are of such importance, at the same time it is very complicated to grasp the mechanisms that determine the traffic characteristics in congestion, because of the complex interactions in these conditions between the drivers that travel through the network, all with own behavioral characteristics. Consequently, to enable the description of the situations that typically are the origin of the congestion, that are, 'bottlenecks', it is essential to explicitly model the traffic operations near on– and off–ramps, lane–drops, incidents, accidents, and at intersections.

This thesis presents research carried out to construct a more generalized macroscopic model that describes the dynamics of multiclass traffic flow on multilane freeways including ramp entries and in urban networks at a microscopic level, with particular focus on the lane-changing processes at bottlenecks and intersections. The key to the approach is the introduction of a *gap-acceptance* model to describe the lane-changing processes, especially at entries. In this thesis, 'gap' indicates the space gap, that is, the distance between the front ends of two successive vehicles driving in the same lane. In case of lane-changing, a vehicle is able to change to its target lane when both the *lead-gap* and *lag-gap* are accepted. The *lead-gap* is accepted if the space between the lane-changing vehicle after the lane-change and the leader in the target lane is larger than a certain threshold distance (critical gap). The *lag-gap* is also accepted if the space between the lane-changing vehicle after the lane-change and the follower in the target lane is larger than a certain critical gap. Here, these critical gaps are defined as the minimal gaps required to avoid rear-end collisions with the leaders and the follower, respectively. Based on the relation between microscopic and macroscopic traffic characteristics, in this thesis the (microscopic) *gap-acceptance* model is implemented in a macroscopic traffic flow model for (road) discontinuities.

This introductory chapter is organized as follows. Section 1.1 presents the main problem formulation for this thesis. In Section 1.2 the objectives and scope of the research are described. Contributions of this thesis to modern state-of-the-art of traffic flow theory are discussed in Section 1.3. Finally, the set-up of this thesis is outlined in Section 1.5.

1.1 Problem formulation

Since societal and environmental constraints prohibit large-scale extension of available road networks, solutions need to be sought in using the existing traffic networks more efficiently. Dynamic Traffic Management (DTM) provides efficient tools to reduce the congestions within the boundaries of a sustainable transportation system. To this end, a number of traffic control measures such as ramp-metering, speed limits, specific lane for trucks and buses, etcetera, have been proposed and implemented in practice. A good understanding of the mechanisms in congested traffic near bottlenecks is very useful for the development of suitable control measures (Hegyi et al. (2003)). This motivates the requirement of an operational model that is able to conditionally predict the state of the traffic flow given specific control configurations.

Different modeling approaches have been applied to understand the various characteristic properties of traffic flow on freeways (Hoogendoorn (1999a)). These approaches can be classified as microscopic, mesoscopic and macroscopic traffic flow modeling. While microscopic models deal with the dynamics of individual vehicles, the macroscopic models describe the dynamics of aggregate flow quantities such as density, speed and flow rate. Mesoscopic models deal with traffic flow in more aggregate terms than microscopic models (medium level of detail) by using probabilistic descriptions. In principle, microscopic models are very suited for dealing with the dynamics of multiclass traffic on multilane freeways and urban networks. However, for purposes of control applications they have several drawbacks such as the incapability to allow the analytical derivation of theoretical results and high requirements for computational effort. For these reasons, a macroscopic traffic flow approach is preferred, which has the following strengths:

- the ability to give insight into observed traffic phenomena such as shock wave dynamics, and stop–and–go traffic (phantom traffic jams).
- the applicability of analytical macroscopic flow models in model-based estimation and control approaches.
- the relatively small number of parameters to be calibrated, hence, less demand for computational capacity.
- the applicability to very large traffic networks, independent of the number of simulated vehicles.

Research on macroscopic models has been performed since the 1950s, for example by Lighthill and Whitham (1955) and Richards (1956), who independently developed a continuum model for traffic flow operations on freeways. Nowadays these models are still developed and extended frequently. In general, these efforts have mainly concentrated on describing uninterrupted traffic flow. Relatively little progress has been made in the investigation of interrupted traffic flow, such as situations with on- and off-ramps. In most macroscopic models, traffic operations at on-ramps and off-ramps are often oversimplified and inadequately treated by

neglecting the length of acceleration lanes (for instance, the 'point–like model' (Liu et al. (1996))). In recent research (Helbing et al. (1999b)), the impact of acceleration lane length on traffic performance has been investigated. However, the probabilistic nature of traffic flow has not yet been considered explicitly. Pioneering research on the effects of lane-drops and on-ramps on freeway traffic flow has been performed by Munjal and Pipes (1971a) and Munjal et al. (1971b) using simulation approaches. Recently, the research on traffic flow at on-ramps of a freeway has revealed some physics-like phenomena that received interest from scientists like Helbing et al. (1999b), Kerner (2002), Kerner and Klenov (2003), etcetera. The impact of on-ramp flows is important in the formation of stop-and-go traffic flow near the ramp. This congested traffic state indicates the complex phenomena associated with ramps which result in a hysteretic phase transition, reproduced by Papageorgiou et al. (1990), Helbing et al. (1999b), Kerner (1998) and Lee et al. (1999). To this end, this thesis puts forward an elaborate macroscopic continuum model that is able to take into account explicitly the interactions between traffic on the acceleration lane and traffic on the main lanes. Based on the derivation approach, a model that describes drivers' lane-changing behavior at multilane intersections in urban networks will be developed in this thesis.

1.2 Research objectives

The research presented in this thesis is project 2 of the multi-university program AMICI (Advanced Multi–agent Information and Control for Integrated multi–class traffic networks). The AMICI research program focuses on traffic congestion management in and around large cities, such as Beijing, Rotterdam, Amsterdam and Shanghai. In particular, it aims at coming up with solutions to efficiently reduce traffic congestion by means of Dynamic Traffic Management.

It is argued that to improve congestion management, approaches should consider the freeway networks and the underlying urban and rural networks in an integrated way. Furthermore, traffic management measures should be coordinated rather than isolated: important gains are possible by jointly considering ramp metering and providing queue length information. Finally, efficient approaches will need to anticipate on future traffic conditions, rather than merely react to the current state. To attain the envisaged research objectives, five research themes have been set-up:

- Impact of travel information and traffic control on travel behavior
- Multiclass traffic flow theory for modeling of motorway and urban traffic networks
- Development of advanced multi-agent control strategies for multi-class traffic networks
- Optimal presentation of travel information based on personal preferences and needs
- Market for traveler information

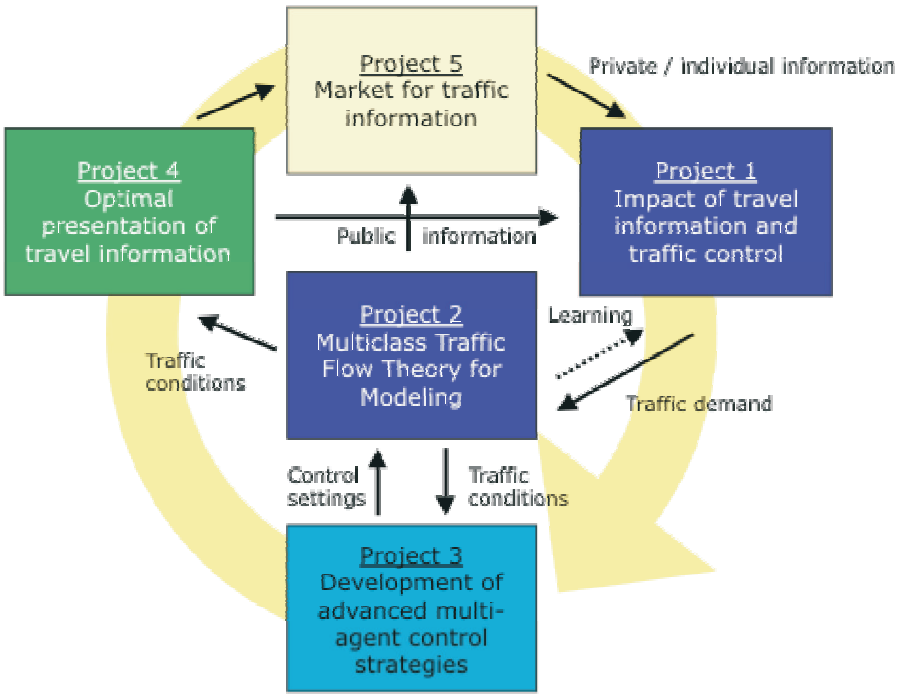

Figure 1.1: Relation between research projects within AMICI.

The link between these research projects are illustrated in Figure 1.1

As a core part of the AMICI program, the objectives of this thesis are to extend and refine the generalized multilane and multiclass model of Hoogendoorn (1999a), especially by:

- modeling the lane-changing processes of different user-classes (immediate, spontaneous and mandatory lane-changes are to be implemented and refined) at bottlenecks.
- developing a theory–based model for the analysis of multilane mixed traffic flow operations in urban networks
- developing a relevant numerical scheme for simulating the proposed model. We will show that an inappropriate numerical scheme may result in deviate or erratic model behavior, such as large numerical dissipations, numerical instabilities, etcetera.
- developing an automated procedure for the calibration of the proposed model for case-studies.

Modeling the lane–changing process, especially at bottlenecks and intersections, is very complex due to a number of factors that a driver considers before making a decision. Consequently, an essential part of the modeling effort in this thesis is to find a balance between simplifying the model and representing the real-life process. The envisaged theory provides a genuine extension and generalization of current macroscopic traffic flow theory.

We expect that the proposed model provides additional new insights into both the interactions between vehicles when making a lane-change and the nature of the control problem at hand,

given complex multi–type traffic network configurations and dynamic traffic management, yielding a better understanding of the response of heterogeneous traffic flows to multiple control measures.

1.3 Thesis contributions

This thesis contributes to the state-of-the-art in modeling discontinuities in macroscopic traffic models. It improves the contemporary models of Shvetsov and Helbing (1999), Hoogendoorn (1999a), Hoogendoorn and Bovy (1999b), Helbing et al. (1999a) by modeling in detail the lane–changing processes at bottlenecks and at intersections in traffic networks based on microscopic driving principles but without requiring as many parameters as microscopic models. Another major contribution of this thesis is introducing a novel numerical solution to macroscopic traffic flow models, which will be proven robust, fast and reliable. Furthermore, to assess the performance of the model with real-life data, an automated calibration procedure is proposed.

1. Contribution to the modeling approach: taking into account more details of the lane-changing process. More specifically:
    - The exchanges of vehicles within freeway lanes due to interactions between fast vehicles and slow vehicles (immediate lane–changes) are modeled based on microscopic driving principles. That is, drivers who desire to change lanes when catching up with slower vehicles are able to do so when they find sufficient gaps in the chosen target lanes.
    - In existing macroscopic models merging and diverging behavior of a driver at on–and off–ramps are treated as all-or-nothing type deterministic behavior. That is, the traffic flow merges (or diverges) immediately at a single location at the on–ramp (or off–ramp) if there is an opportunity (or waits otherwise). The proposed model captures the fact that drivers merge (or diverge) along a considerable stretch of freeway (for example, in an acceleration lane) until they find a sufficient gap in the chosen target lane. When drivers approach the end of the acceleration lane, they accept smaller gaps as sufficient. That is, merging (or diverging) drivers are willing to apply more risky choices than they do in the case of immediate lane–changes. Consequently, they disturb the traffic flow in the target lane more significantly than in immediate lane–changes.
    - The proposed model is able to analytically show the impact of the acceleration lane length on the traffic operations on the main carriageway, which has only been captured explicitly in microscopic models but not yet in a continuum model. That is, for example, choosing an appropriate acceleration lane length can help reduce the potential traffic congestion in a merging section.
    - The modeling approach presented in this thesis allows to model traffic dynamics at multilane intersections. The proposed model takes into account explicitly

the interactions of different traffic streams such as left-turning, right-turning and crossing stream. This allows to accurately model the dynamics of traffic flowing in and out of a multilane intersection, which have often been overestimated by current modeling approaches.

2. Contribution to mathematical and numerical solutions: as with other macroscopic traffic flow models, numerical treatment of the developed model is very complex. To numerically solve macroscopic traffic flow models including the model developed in this thesis, a new solution is introduced. The proposed numerical solution represents physical properties described by the model and always satisfies the positivity constraints of conservative traffic variables under different traffic conditions.

3. Contribution to model calibration/validation:

   - A methodology to estimate the model parameters using real-life data is proposed. Accordingly, we establish an automated calibration procedure for macroscopic traffic models in which a direct search optimization algorithm is employed. The optimal model parameters are obtained by minimizing the total mean square errors between measured data and model prediction.
   - The optimal model parameters are used to simulate the model with other data sets (validation). The results are cross-compared with other simulation models. Based on this comparison, conclusions on model performance can be made.

1.4 Research relevance

The research relevance of this thesis may be described in terms of theoretical achievements and practical results.

Theoretical relevance

The developed model will provide an extension and refinement of the current macroscopic traffic flow theory of Hoogendoorn (1999a). That is, the developed model takes into account the interactions between the main carriageway lanes and the acceleration lanes in detail. We envisage that the developed model gives insights into the impact of road geometry (for instance, acceleration lane length) on traffic dynamics. Furthermore, the urban network version of the developed model can account for the interactions between traffic streams going through the multilane intersections. Consequently, the dynamics of multiclass traffic flow at multilane intersections can be predicted accurately.

Practical relevance

The research results can be applied for operational traffic control. The distinction between lanes and user classes, the detailed consideration of road geometry and intersection design

are very useful for the development of suitable control measures. This yields a more efficient utilization of the existing road system given available traffic control tools by incorporating the developed model in model-based control approaches. This is the objective of project 3 in AMICI program (see Figure 1.1).

1.5 Thesis outline

This section provides an outline of this thesis and briefly gives information about each chapter.

Chapter 2 presents an overview of the state-of-the-art of traffic flow theory. In this chapter, we discuss the advantages and disadvantages of different traffic modeling approaches. Based on this discussion, the choice of the modeling approach applied for the objectives of the AMICI project described in Section 1.2 is treated.

Chapter 3 is based on Ngoduy et al. (2004b), Ngoduy et al. (2004c), Ngoduy et al. (2004d) and Ngoduy (2005b). In this chapter, we introduce the concept of *renewal theory* and its application in traffic flow dynamics. Based on this concept, a model to calculate lane–changing processes at on–ramps, off–ramps, and weaving sections is developed. With this model, we develop a generalized gas-kinetic traffic flow model that describes the dynamics of the so-called *phase-space density* of multiclass vehicles at bottlenecks.

Chapter 4, based on Ngoduy et al. (2006), derives a generalized macroscopic model for multiclass traffic flow dynamics at bottlenecks. We show that, on the one hand, the model is able to replicate traffic congested states on freeways in a similar fashion as existing models. On the other hand, the impact of acceleration lane length on the traffic operations in the main carriageway is shown analytically.

Chapter 5 is based on Ngoduy and Hoogendoorn (2003b) and Ngoduy et al. (2004a). In this chapter, we analyze the mathematical properties of the general second order macroscopic traffic models, based on which the numerical solutions are employed. We argue that choosing an inappropriate numerical scheme may result in very poor performance of the model. Accordingly, we propose a numerical scheme which is proven to satisfy all positivity constraints of the conservative traffic variables. The performance of the proposed solution is cross-compared with the current solutions using real-life data. We show that the proposed scheme is more robust, fast and reliable than the others.

Chapter 6, based on Ngoduy et al. (2005a), develops a macroscopic model that describes the dynamics of multiclass traffic flow in multilane urban networks. In this chapter, the interactions between all traffic streams (left-turning, right-turning and through streams) at multilane intersections are modeled in detail. This results in a proposed model that is able to accurately represent traffic flowing in and out of a multilane intersection, which has not yet been captured in currently existing macroscopic models.

Chapter 7 is based on Hegyi et al. (2003) and Ngoduy and Hoogendoorn (2003a). In this chapter we discuss the performance of the proposed model using real-life data. To this end,

an automated calibration procedure, in which a direct search optimization algorithm is employed, is proposed. The developed model is calibrated using data collected on a Dutch freeway. The optimal parameters obtained are used to validate the model. Finally, the results are cross-compared with a macroscopic model.

Chapter 8 concludes the thesis and gives some research directions for the future.

Figure 1.2 shows the structure of the main contributions in this thesis.

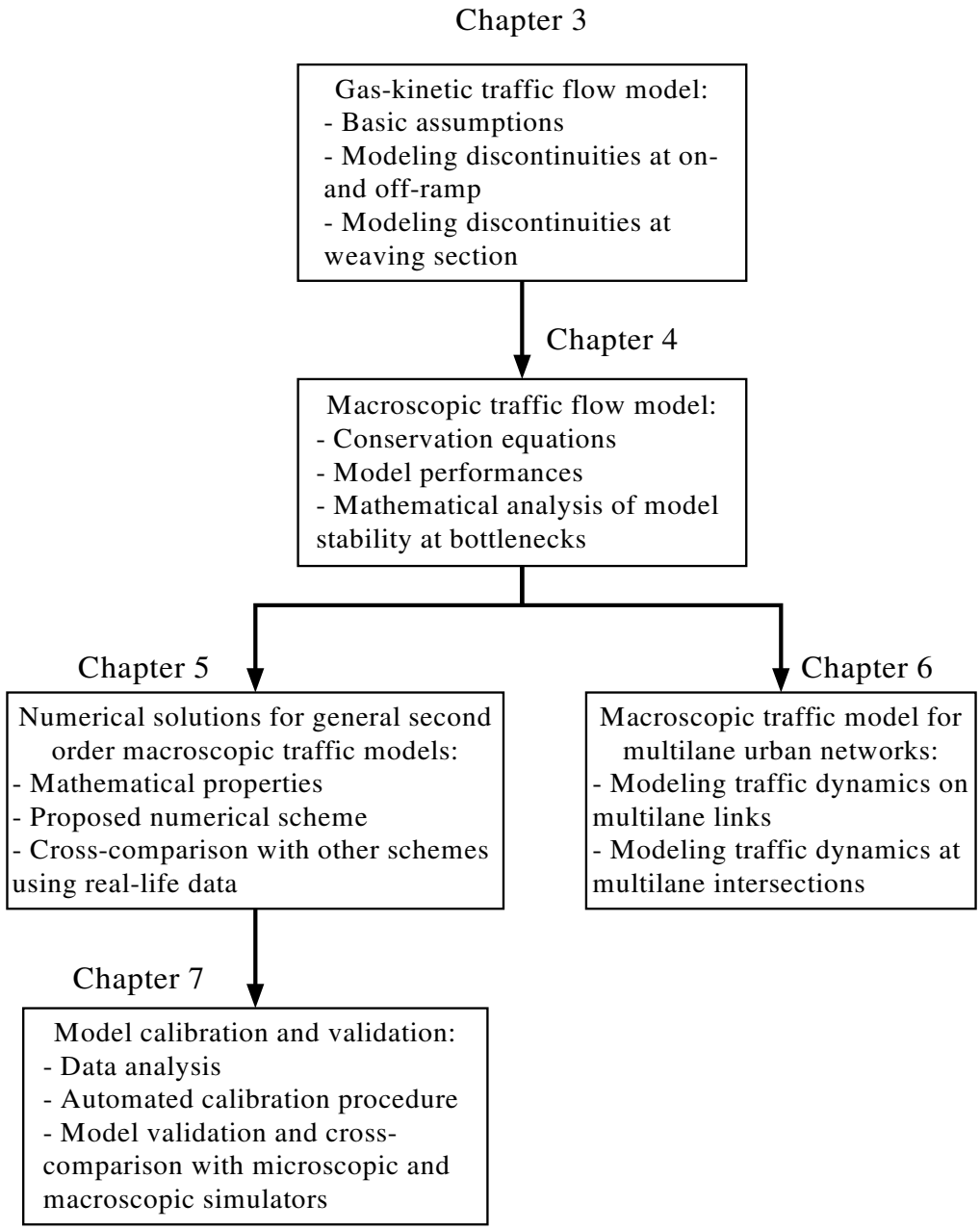

Figure 1.2: Structure of model derivation and application.

Chapter 2

State-of-the-art of traffic flow modelling

With the rise of the automobile as one of the most important means of transport in the modern world, traffic problems have become one of the main societal and economical issues in almost all industrialized countries. Consequently, traffic issues often play an important role in both policy and research. In the 1950s scientists from many disciplines started to model the movement of traffic with the aim to improve the traffic operations. One of the pioneering contributions to traffic flow theory was the model of Lighthill and Whitham (1955). They proposed a macroscopic traffic model, modeling traffic flow as a continuum akin to the dynamics of particles in a fluid. To date, many efforts have been undertaken to improve the original model of Lighthill and Whitham. The course of these developments of modern traffic flow theories is closely related to improvements in computer technology, and concepts of modern physics, mathematics, operations research and engineering.

The phenomena involved in traffic flow processes, such as traffic congestion, meta stability, nonlinear waves, etcetera, are commonly investigated by three types of modeling approaches categorized by the level of behavioral detail: microscopic, mesoscopic or macroscopic. At a microscopic level, the time-space behavior of the traffic system (vehicles and drivers) as well as their interactions is modeled at a high level of detail. At the mesoscopic level, the traffic model does not distinguish or trace vehicles and driver behavior individually but in more aggregate terms (medium level of detail) by using probabilistic descriptions. A typical example of this modeling approach is the gas-kinetic model type, in which traffic is treated as a flow of interacting particles. At the macroscopic level, the traffic model deals with traffic flow in terms of aggregate variables (low level of detail) by assuming that the aggregate behavior of drivers depends on the traffic conditions in the drivers' direct environment. That is, traffic is treated as a one-dimensional compressible fluid. In macroscopic models, individual vehicle maneuvers, such as lane-changing processes (Helbing (1997b), Hoogendoorn (1999a)), are not explicitly represented. There have been debates on which approach is the most useful in modeling traffic. However, the answer depends on the type of traffic phenomena being modeled and the type of application. According to Helbing (2001), there are some well-defined criteria for good traffic models. In terms of robustness and calibration/validation, such models should contain only a few parameters and variables, and these should have an intuitive meaning. They should be easy to observe and the measured values should be realistic. In

terms of qualitative properties, a good model should reproduce all known features of traffic flow, such as, localized jams, hysteretic phenomena, and the existence of all transition states of congestion. Furthermore, its dynamics should not lead to vehicle collisions or exceed the maximum density. In terms of computational efficiency, the model should allow for a fast simulation.

The main aim of this thesis is to develop a model describing the discontinuities of traffic flow at bottlenecks in freeways (for instance, at on– and off–ramps, weaving sections) and at intersections of urban networks. In the newly developed model, the lane–changing processes are determined explicitly based on microscopic driving principles. The model should be able to describe the dynamics of traffic flow at bottlenecks and intersections microscopically without requiring as many parameters as microscopic models. To this end, this chapter gives an overview of some important traffic flow models with emphasis on the macroscopic models on which the work presented in the remainder of this thesis is built. By synthesis of the current traffic models, we are able to develop the modeling approach that will be chosen in this thesis.

This chapter is organized as follows. Section 2.1 describes briefly the history of microscopic traffic flow models. The overview of gas-kinetic theory is given in Section 2.2. Section 2.3 focuses on the historical development of macroscopic (continuum) traffic models. Finally, Section 2.4 summarizes this chapter.

2.1 Microscopic traffic models

Microscopic traffic flow models describe the dynamics of traffic flow at the level of each individual vehicle. They have existed since the 1960s with the typical car-following models. This section reviews mainly some different car-following models since they serve as a basis for the model development in this thesis.

Car-following models describe the processes in which drivers follow each other in the traffic stream. The car-following process is one of the main processes in all microscopic models as well as in modern traffic flow theory. In car-following models, each vehicle is considered separately and its behavior is modeled as it reacts and anticipates to vehicles in front by its own dynamic equation having the following form:

$$\dot{v}_n(t+T) = f(v_n(t), d_n(t), \dot{v}_{n-1}(t), v_{n-1}(t)) \tag{2.1}$$

In equation 2.1 , T is the reaction time, d_n is the distance headway with respect to the vehicle in front, and v_n is the speed of the considered vehicle.

Different functions of f result in various types of car-following models: safe-distance models, stimulus-response models and psycho-spacing models. An extensive review of car-following models can be found in Brackstone and McDonald (2000), Rothery (1999).

Safe-distance models

Some of the early contributions to the concept of car-following were those of Reuschel (1950) and Pipes (1953). Pipes assumed that the follower wishes to maintain at least the length of the car between him and the vehicle ahead for every 10mph (that is, the equivalent of 16.1km/h) of speed. By using this assumption, the required gross distance headway d_n of vehicle n driving with speed v with respect to vehicle n-1 in front is determined as the linear function of speed of the considered vehicle as shown below:

$$d_n(v) = l_n(1 + v/16.1) \tag{2.2}$$

In equation 2.2, l_n denotes the length of vehicle n.

Another, slightly different, model of Forbes et al. (1958) assumed that the minimal gross time headway $h_n(v)$ is equal to the class specific reaction time T and the time required for the vehicle to travel a distance equal to its length. This formulation is described in an equation as follows:

$$h_n(v) = T + l_n/v \tag{2.3}$$

From expression 2.3, the minimal gross distance headway is calculated as follows:

$$d_n(v) = l_n + Tv \tag{2.4}$$

Some refinements of these models have been conducted to date. Lately, Jepsen (1998) assumed that the gross-distance headway effectively occupied by vehicle n driving with speed v is a function of the vehicle's length l_n, a constant minimal distance with respect to the vehicle in front d_{min}, the reaction time T and a speed risk factor F, as depicted by the following equation:

$$d_n(v) = l_n + d_{min} + Tv + Fv^2 \tag{2.5}$$

where v is the speed of the following vehicle. The speed-risk factor F stems from the observation that experienced drivers do not only aim to prevent rear-end collision but also desire to minimize the potential damage or injuries of a collision, hence are aware of the important role of speed in this aspect.

The safe-distance model of Jepsen (1998) will be used in the *gap-acceptance* model to account for the finite-space requirement of a vehicle, which is presented in Chapter 3.

Stimulus-response models

Other types of car-following models were developed by scientists at General Motors (GM), such as, Chadler et al. (1958), Herman et al. (1959), Herman and Rothery (1963). They conducted research on the sensitivity-stimulus framework, which is the basis for most car-following models. According to this framework, the follower tries to conform to the behavior of the preceding vehicle. The response the follower applies is calculated as given below:

$$response(t + T) = sensitivity(t + T) \times stimulus(t) \tag{2.6}$$

In equation 2.6, the $response$ is acceleration or deceleration chosen by the follower, delayed by a reaction time T. The model assumed that the $stimulus$ is the leader's relative speed. Depending on the the specifications chosen for the $sensitivity$ term, several models result. Details of these models (also called GM models) can be found in Chadler et al. (1958) or Herman et al. (1959).

Psycho-spacing model

Wiedemann (1974) and Leutzbach (1988) identified two unrealistic behavioral aspects in the GM models. Firstly, when the distance headway is very large, drivers still react to speed differences and, secondly, slow drivers are drawn by faster vehicles ahead. To remedy these problems, they introduced the perceptual threshold, which defines a minimal value for the stimulus. The perceptual threshold value increases with the space headway. The basic rules of this psycho-spacing model type are described as: a) at large distance headways, the follower is not influenced by the speed difference; and b) at small distance headways the alertness of drivers is increased. This means that some combinations of relative speeds and distance headway do not create a response of the follower. A faster vehicle will get closer to its leader until the deceleration perceptual threshold is reached. The driver than decelerates in order to adapt to the leader's speed. Because drivers cannot perform this action perfectly the distance headway will then increase again until the acceleration threshold is crossed. The driver then accelerates again. In this modeling approach, both the lane-changing and overtaking processes are incorporated. The psycho-spacing models are used in a few contemporary microscopic simulation models such as FOSIM (Vermijs et al. (1995)) and AIMSUN2 (Barcelo et al. (1998)), etcetera.

In additions there are some other car-following models worth being mentioned such as the models of Gipps (1981), Bando et al. (1995), Del Castillo (1996), Mason and Woods (1998), Minderhoud (1999), Kerner (2002), Kerner and Klenov (2003), Ossen and Hoogendoorn (2005), Ossen et al. (2006).

Optimal speed models

In car-following models, the follower's acceleration tends to zero in the absence of the leader. To remedy this, another type of models was introduced based on the assumption that each driver has a safe speed which depends on the distance headway to the leader. This modeling approach is called *optimal speed*. According to this approach, the follower adapts its speed to a certain optimal value, rather than to the leader's speed. Some contributions to this type of models are Newell (1961), Bando et al. (1998), Gipps (1981), Krauss (1998), Wolf (1999), Tomer et al. (2000) and Treiber et al. (2000). It has been shown by these models that under certain conditions, small perturbations are amplified and lead to jams. Therefore, these models are able to replicate stop-and-go waves in traffic flow.

2.2 Mesoscopic traffic models

There are three types of mesoscopic models: headway distribution models, cluster models and gas-kinetic models. In this section, we focus on the latter modeling approach because it is the foundation of the development of macroscopic models in the remainder of this thesis.

The development of gas-kinetic traffic models started in the 1960s with a simple model of Prigogine and Andrews (1960) and Prigogine (1961). In gas-kinetic models, vehicles and drivers' behavior are described in more aggregate terms than in microscopic models, by means of probability distribution functions. However, the behavioral rules are still described at an individual level. The dynamics of these distributions are generally governed by various processes, such as, acceleration, interactions between vehicles, and lane-changing, describing the individual drivers' behavior.

The gas-kinetic traffic flow models are based on descriptions of the dynamics of the phase-space (or time-location) density, that is, the dynamics of the speed distribution functions of vehicles in the traffic flow. Given the knowledge of the phase profile of density, one can determine the continuum (macroscopic) traffic variables such as density, mean speed, or flow rate, by means of the method of moments, described in Section 2.3. Let $\rho(x, v, t)$ denote the phase-space density function (*PSD*), which is interpreted as follows: at instant time t the expected number of vehicles present at a small cell $[x, x + dx]$ driving with a speed in the region $[v, v + dv]$ is equal to $\rho(x, v, t)dxdv$. Based on the conservation law, the equation for the dynamics of $\rho(x, v, t)$ can be found. Let us begin with the model of Prigogine and Andrews (1960), Prigogine (1961), and Prigogine and Herman (1971). The latter, in fact, is the summarized version of the former two. Therefore, from now on, we refer to the model of Prigogine and Herman (1971).

2.2.1 Prigogine and Herman's model

The model of Prigogine and Herman (1971) assumes that the dynamic changes of the *PSD* are caused by a number of processes which are described in the following equation:

$$\frac{\partial \rho}{\partial t} + \underbrace{v\frac{\partial \rho}{\partial x}}_{\text{convection}} = \underbrace{\left(\frac{\partial \rho}{\partial t}\right)_{int}}_{\text{interaction}} + \underbrace{\left(\frac{\partial \rho}{\partial t}\right)_{rel}}_{\text{relaxation}} \tag{2.7}$$

The left hand side (*LHS*) of equation 2.7 describes the changes of the *PSD* due to the motion of vehicles along the road, while the right hand side (*RHS*) describes the changes of the *PSD* due to events such as deceleration or relaxation. The model consists of *convection*, *interaction* and *relaxation*, which are described in detail below:

- the *convection* term describes the continuous change of the *PSD* due to the inflow into and outflow from a small cell $[x, x + dx]$ within time period $[t, t + dt]$.
- the *relaxation* term reflects the continuous change of the *PSD* due to the tendency of drivers to relax to the desired speed distribution.

- the *interaction* term describes the discontinuous change of the *PSD* due to the interaction between fast and slow vehicles. When a faster vehicle catches up with a slower one, it has to slow down (break) to avoid a collision.

Interaction process In the model of Prigogine and Herman (1971), it was assumed that when a faster vehicle driving with speed v catches up with a slower one driving with speed w ($w < v$), the former either slows down to the speed of the latter or overtakes in order to avoid a collision. To determine the interaction term in equation 2.7, the following assumptions are used:

- If the faster vehicle overtakes, it does not change its speed.
- The slower vehicle is not influenced by the vehicle behind.
- The vehicles are considered 'points' (the length of vehicles is neglected).
- The fast vehicle slows down instantaneously
- The vehicles are uncorrelated (vehicular chaos)
- Interactions affecting more than two vehicles are neglected.

Based on these assumptions, the interaction term in equation 2.7 is determined as follows:

$$\left(\frac{\partial \rho}{\partial t}\right)_{int} = (1-p)\int_{v}^{\infty}(w-v)f(x,t,v,w)dw - (1-p)\int_{0}^{v}(v-w)f(x,t,v,w)dw \quad (2.8)$$

In equation 2.8 , p denotes the probability for overtaking, $f(x,t,v,w)$ is the pair-distribution function of density. The assumption of vehicular chaos means that the correlation between vehicles is neglected. That is, the pair-distribution function can be decomposed as follows:

$$f(x,t,v,w) = \rho(x,v,t)\rho(x,w,t) \quad (2.9)$$

By substituting equation 2.9 into equation 2.8 the interaction term is reduced to:

$$\begin{aligned}\left(\frac{\partial \rho}{\partial t}\right)_{int} &= (1-p)\rho(x,v,t)\int_{v}^{\infty}|w-v|\rho(x,w,t)dw \\ &\quad -(1-p)\rho(x,v,t)\int_{0}^{v}|w-v|\rho(x,v,t)dw \end{aligned} \quad (2.10)$$

Equation 2.10 reflects the fact that faster vehicles with speed w interact with slower vehicles with speed v at a rate $|w-v|\rho(x,v,t)\rho(x,w,t)$, describing how often vehicles with speed w and v encounter at location x and time instant t. If the faster vehicle can not overtake, it decelerates to the speed of the slower vehicle. This deceleration process increases the *PSD* $\rho(x,v,t)$ accordingly (the plus term of the *RHS*). When a vehicle with speed v catches up with a slower vehicle with speed w, if the faster vehicle is unable to overtake, it decelerates to the speed w. This process decreases the *PSD* $\rho(x,v,t)$ (the minus term of the *RHS*).

Relaxation process Prigogine and Herman (1971) proposed the relaxation term in equation 2.7 as follows:

$$\left(\frac{\partial \rho}{\partial t}\right)_{rel} = -\frac{\partial}{\partial v}\left(\rho \frac{V_{max}(v|x,t) - v}{\tau}\right) \tag{2.11}$$

In equation 2.11, $V_{max}(v|x,t)$ denotes the desired speed distribution, τ is the density-dependent relaxation time.

With this model, Prigogine and Herman (1971) found that the transition from the free to the congested traffic state occurs when the density is higher than a certain critical value. This congested state is characterized by the appearance of a second maximum of the speed distribution at $v = 0$. That means, there are some vehicles still moving, while the others are at standstill.

2.2.2 Paveri-Fontana's model

The assumption of vehicular chaos in the model of Prigogine and Herman (1971) has been criticized. According to Munjal and Pahl (1969), this assumption is only valid in the situations when no vehicles form a platoon (for instance, dilute traffic). When overtaking is not possible, the overtaking vehicle is forced to follow the slower one ahead. During the following time interval its speed cannot be considered statistically independent. The improvement of Prigogine and Herman's model has been carried out by many researchers, such as Paveri-Fontana (1975), Philips (1977), Philips (1979), Nelson (1995), Helbing (1996), Helbing (1997b), Wegener and Klar (1996), Klar and Wegener (1997), Hoogendoorn (1999a), Hoogendoorn and Bovy (1999b), Tampere (2004) etcetera. They modified the acceleration term, introduced speed correlation, a lane-changing term, and considered the space requirements. The basic improvement by Paveri-Fontana (1975) is described in this section. In this model, two extreme cases were considered in the case of a free-flowing vehicle catching up with a slow moving jam as shown below :

- The approaching free-flowing vehicle passes the whole queue as if it were only one vehicle.
- It passes each car in the queue independently.

Paveri-Fontana (1975) showed that the vehicular chaos assumption of Prigogine and Herman (1971) belongs to the second case, while the real traffic situation falls between these two cases. Paveri-Fontana (1975) also showed that the acceleration term in equation 2.7 could describe the jumps in speed and that the relaxation term yields a desired speed distribution that depends on a property of the road environment but not on the drivers. This contradicts the so-called personality condition in which the driver's personality is unchanged to the changing traffic environments: driving fast, aggressively, or timidly. Paveri-Fontana (1975) resolved these problems by introducing the extended *PSD* which depends also on the desired speed,

denoted as $\tilde{\rho}(x,t,v,v_0)$. From this definition, he proposed the new formula for the relaxation process term as given below:

$$\left(\frac{\partial\tilde{\rho}}{\partial t}\right)_{rel} = -\frac{\partial}{\partial v}\left(\tilde{\rho}\frac{v_0 - v}{\tau}\right) \tag{2.12}$$

The interaction term, which accounts for the interaction between a faster vehicle driving with speed v while having desired speed v_0 and a slower vehicle driving with speed w while having desired speed w_0, is determined analogously to Prigogine and Herman's model as follows:

$$\begin{aligned}\left(\frac{\partial\tilde{\rho}}{\partial t}\right)_{int} &= (1-p)\rho(v)\int_v^{\infty}|w-v|\tilde{\rho}(w,w_0)dw \\ &- (1-p)\tilde{\rho}(v,v_0)\int_0^{v}|w-v|\rho(w)dw \end{aligned}\tag{2.13}$$

In equation 2.13 , the shorthand notations $\tilde{\rho}(v,v_0) = \tilde{\rho}(x,t,v,v_0)$ and $\rho(v) = \rho(x,v,t)$ are used. By definition, the following equations hold:

$$\rho(x,v,t) = \int_{v_0}\tilde{\rho}(x,t,v,v_0)dv_0 \tag{2.14}$$

$$r(x,t) = \int_v \rho(x,v,t)dv = \int_v\int_{v_0}\tilde{\rho}(x,t,v,v_0)dvdv_0 \tag{2.15}$$

Despite these differences, the macroscopic equations derived from Paveri-Fontana's model for density and mean speed are the same as the equations derived by Prigogine and Herman (1971). However, the equations for speed variance, and covariance (higher order equations) are different.

2.2.3 Generalized *MLMC* gas-kinetic models

In reality, traffic is heterogeneous, that is, it consists of multiple user classes moving on multiple lanes roadway. The distinction of user classes gives rise to an asymmetric braking process of faster vehicles. That is, vehicles of faster user classes (for instance, cars) catch up with the vehicles of slower user classes (for example, trucks) more frequently than vice-versa. The distinction of lanes results in lane-changing processes, which will be described in detail in the ensuing of this thesis.

To account for the heterogeneous quality of traffic, a generalization of the gas-kinetic models as well as macroscopic models has been proposed by many researchers such as Rorbech (1976), Michalopoulos et al. (1984), Daganzo (1997), Helbing (1997a), Helbing (1997b), Shvetsov and Helbing (1999), Helbing et al. (1999a), Helbing et al. (2002), Hoogendoorn (1999a), Hoogendoorn and Bovy (1999b), Tampere (2004), and so on.

This section describes a generalized multilane and multiclass (*MLMC*) gas-kinetic traffic flow model (Shvetsov and Helbing (1999), Hoogendoorn (1999a), Hoogendoorn and Bovy

(1999b), Helbing et al. (2002)):

$$\frac{\partial \rho_i^u}{\partial t} + \underbrace{v\frac{\partial \rho_i^u}{\partial x}}_{\text{convection}} + \underbrace{\frac{\partial}{\partial v}\left(\rho_i^u \frac{V_i^{u,max} - v}{\tau_i^u}\right)}_{\text{acceleration}} = \underbrace{\left(\frac{\partial \rho_i^u}{\partial t}\right)_{int}}_{\text{interaction}} + \underbrace{\left(\frac{\partial \rho_i^u}{\partial t}\right)_{lc}}_{\text{lane-changing}} \tag{2.16}$$

In equation 2.16, ρ_i^u denotes the *PSD* of vehicle class u $(u = 1, 2, \ldots, U)$ driving in lane i $(i = 1, 2, \ldots, I)$. $V_i^{u,max}$ is the desired speed of vehicle class u in lane i. In this equation, the convection term, acceleration term, and interaction term are defined the same as in Prigogine and Herman's model. The lane-changing term accounts for the changes of the *PSD* due to lane-changing processes consisting of three components described as follows:

$$\left(\frac{\partial \rho_i^u}{\partial t}\right)_{lc} = \underbrace{\left(\frac{\partial \rho_i^u}{\partial t}\right)_{lc}^{int}}_{\text{immediate}} + \underbrace{\left(\frac{\partial \rho_i^u}{\partial t}\right)_{lc}^{spon}}_{\text{spontaneous}} + \underbrace{\left(\frac{\partial \rho_i^u}{\partial t}\right)_{lc}^{man}}_{\text{mandatory}} \tag{2.17}$$

In equation 2.17, the *immediate lane changing* term (*ILC*) describes the fact that a faster vehicle catches up with a slower one and changes lanes in order to maintain the desired speed. The *spontaneous lane changing* term (*SLC*) describes the preference of drivers to use a particular lane. The last term is defined as *mandatory lane changing* (*MLC*), which accounts for the fact that a vehicle is forced to change lanes due to a blockage at the end of its current lane.

Both the *ILC* and *SLC* terms have been determined by Helbing (1997a), Shvetsov and Helbing (1999), Hoogendoorn (1999a), Hoogendoorn and Bovy (1999b), Helbing et al. (2002). This section reviews briefly the expressions for these terms. For detailed derivations, we refer to Helbing (1997a).

Interaction lane-changing process

To take into account the space requirements of vehicles (that is, vehicles are not considered point objects), it is assumed that a driver responds to an obstacle ahead at a certain safe distance D. Let $\Psi_i^{u,s}$ be the interaction rate of vehicle class u driving at speed v at location x in lane i with all vehicles classes s downstream driving with speed $w < v$ at location $(x + D)$. Similarly, let $\Phi_i^{u,s}$ be the interaction rate of vehicle class u driving at speed w at location x on lane i with all vehicles class s ahead driving with speed $v < w$ at location $x + D$.The following formulae for the interaction rate were proposed:

$$\Psi_i^{u,s} = \gamma_i \int_0^v (v - w) f_i^{u,s}(x, v, x + D_i^u, w, t) dw \tag{2.18}$$

$$\Phi_i^{u,s} = \gamma_i \int_v^\infty (w - v) f_i^{u,s}(x, v, x + D_i^u, w, t) dw \tag{2.19}$$

In equations 2.18 and 2.19, $f_i^{u,s}$ denotes the pair-distribution function of vehicle class u driving with speed v interacting with vehicle class s driving with speed w in lane i downstream at a safe distance D_i^u. γ_i is the factor that reflects the increase in the real interactions

with increasing density, determined by equation 2.20. The safe distance D_i^u between vehicle class u and any vehicle downstream in lane i is calculated by equation 2.21 as given below:

$$\gamma_i^u = \frac{1}{1 - r_i(x + T_u V_i^u, t) D_i^u} \tag{2.20}$$

$$D_i^u = l_u + d_{min} + T_u V_i^u \tag{2.21}$$

In equations 2.20 and 2.21 l_u and T_u denote the length and reaction time of vehicle class u, d_{min} is the minimal distance between vehicles (safety margin), V_i^u denotes the mean speed of vehicle class u in lane i, and r_i is the total density (regardless of vehicle class) in lane i.

The *interaction* term and *ILC* term take the form:

$$\left(\frac{\partial \rho_i^u}{\partial t}\right)^{int} = \left(1 - p_{i,i+1}^u - p_{i,i-1}^u\right) \sum_{s \in U} \left(\Phi_i^{u,s} - \Psi_i^{u,s}\right) \tag{2.22}$$

$$\left(\frac{\partial \rho_i^u}{\partial t}\right)_{lc}^{int} = \sum_{s \in U} \left(p_{i-1,i}^u \Phi_{i-1}^{u,s} - p_{i,i-1}^u \Psi_i^{u,s} + p_{i+1,i}^u \Phi_{i+1}^{u,s} - p_{i,i+1}^u \Psi_i^{u,s}\right) \tag{2.23}$$

In equations 2.22 and 2.23, $p_{i,j}^u$ denotes the probability for vehicle class u changing from current lane i to either adjacent lanes $j = i \pm 1$. This term will be determined in the remainder of this thesis.

Spontaneous lane-changing process

The spontaneous lane-changing term is assumed proportional to the density (see Helbing et al. (2002), etcetera) as follows:

$$\left(\frac{\partial \rho_i^u}{\partial t}\right)_{lc}^{spon} = \triangle_{i-1,i}^u \rho_{i-1}^u - \triangle_{i,i-1}^u \rho_i^u + \triangle_{i+1,i}^u \rho_{i+1}^u - \triangle_{i,i+1}^u \rho_{i+1}^u \tag{2.24}$$

In equation 2.24, $\triangle_{i,j}^u$ denotes the spontaneous lane-changing rate of vehicle class u from current lane i to adjacent lane $j = i \pm 1$, which is considered a function of density:

$$\triangle_{i,j}^u = g_{i,j}^u \left(\frac{r_j}{r_{max}}\right)^{\beta_1} \left(1 - \frac{r_j}{r_{max}}\right)^{\beta_2} \tag{2.25}$$

In equation 2.25, $g_{i,j}^u$, β_1, β_2 are the lane-changing factors, r_{max} is the jam density.

Mandatory lane-changing process

The *mandatory lane-changing* process concerns forced lane changes, which occur when the road is narrowed (lane-drop), when traffic diverges at an off–ramp, or merges from an on–ramp. A more generalized and elaborate formulation of the *MLC* process will be captured in the remainder of this thesis.

2.3 Macroscopic traffic models

Macroscopic (continuum) traffic models deal with traffic flow in terms of aggregate variables as a function of location and time. They describe the dynamics of traffic density $r(x,t)$, mean speed $V(x,t)$ and/or flow rate $q(x,t)$. Macroscopic models often require less information input than microscopic models. This simplifies the calibration and validation process, which make this type of model very suitable for online applications and control purposes. According to Helbing et al. (2002) macroscopic models have a number of advantages over the others, such as better agreement with real data, suitability for analytical investigations, simple treatment of inflow from ramps, etcetera. For these reasons we have chosen the gas-kinetic and macroscopic flow modeling approach for the development of a model for interrupted traffic flow, like on-and off-ramps, and intersections.

The first equation of a macroscopic model is the so-called conservation equation, which describes that the number of vehicles flowing into a cell $[x, x+dx]$ during time interval $[t, t+dt]$ is equal to the number of vehicles remaining in that cell and the number of vehicles flowing out from that cell. The conservation equation is formulated as follows:

$$\frac{\partial r}{\partial t} + \frac{\partial q}{\partial x} = 0 \tag{2.26}$$

The second equation depicts the relation between density, speed and flow rate as follows:

$$q = rV \tag{2.27}$$

Equations 2.26 and 2.27 form a system of two independent equations with three unknown variables. In order to solve this system, another independent equation is needed. The different formulations of the third equation result in a series of macroscopic models. In this section, we discuss the four major types of macroscopic traffic models, namely the first order type model, the second order type models, the third order type models, and the generalized *(MLMC)* models.

2.3.1 First order type model

The first and most popular macroscopic model was developed by Lighthill and Whitham (1955), and Richards (1956) independently (therefore, is called *LWR* model). In the *LWR* model, the speed and/or flow rate are simply considered a function of density:

$$V(x,t) = V_e(r(x,t)) \tag{2.28}$$

$$q(x,t) = q_e(r(x,t)) = r(x,t)V_e(r(x,t)) \tag{2.29}$$

In expression 2.28, V_e denotes the equilibrium speed. The relation between density $r(x,t)$ and speed or flow rate is called fundamental diagram. The speed function is monotonically decreasing, while the flow function is convex.

By substituting expression 2.29 into equation 2.26, we obtain:

$$\frac{\partial r}{\partial t} + C(r)\frac{\partial r}{\partial x} = 0 \tag{2.30}$$

In equation 2.30, $C(r)$ denotes the so-called density-dependent kinematic wave speed, determined as:

$$C(r) = \frac{dq_e}{dr} = V_e + r\frac{dV_e}{dr} \tag{2.31}$$

In equation 2.31, dV_e/dr is always negative; hence $C(r) < V_e$. This means that the kinematic waves always propagate backwards with respect to the traffic itself. The curves $dx(t)$=$C(r)dt$ are called characteristic curves. When $\partial C(r(x,0))/\partial x < 0$ the characteristic curves intersect, and the shock wave forms, otherwise rarefaction wave forms. The shock wave speed is determined by the so-called Rankine-Hugoniot conditions as:

$$C_s = \frac{q_2 - q_1}{r_2 - r_1} \tag{2.32}$$

Equation 2.32 states that the speed C_s of the shock is equal to the ratio between the jump in local flow rate and the jump in the density shock. Obviously the sign of C_s depends on the sign of the jump in flow rate (outflow from the shock minus inflow into the shock).

Since equation 2.30 does not produce a continuous solution while in real traffic there is no discontinuity, the so-called entropy or vanishing viscosity solutions are used to smooth the shock. Accordingly, an additional term of second order is included into the *RHS* of equation 2.30 as given below:

$$\frac{\partial r}{\partial t} + C(r)\frac{\partial r}{\partial x} = \epsilon\frac{\partial^2 r}{\partial x^2} \tag{2.33}$$

In equation 2.33, ϵ denotes the diffusion factor. Owing to the diffusion factor, the wave fronts are smoothed. Although this implementation solves the shock wave problems, the model is still unable to replicate non-equilibrium situations arising nearby, for instance, on-ramps, lane-drops, as well as stop-and-go traffic or phantom jams. This serious drawback requires a higher order model for describing the dynamics of speed. The different approaches result in various types of high order macroscopic traffic models, which are discussed in the next sections.

2.3.2 Second order type models

The second order type models consider the dynamics of speed in another independent equation. Payne (1971) proposed the following equation for the dynamics of speed based on a car-following model from Newell (1961):

$$\frac{\partial V}{\partial t} + \underbrace{V\frac{\partial V}{\partial x}}_{\text{convection}} = \underbrace{-\frac{C(r)}{r}\frac{\partial r}{\partial x}}_{\text{anticipation}} + \underbrace{\frac{V_e(r) - V}{\tau}}_{\text{relaxation}} \tag{2.34}$$

In equation 2.34, the convection term describes the changes of the mean speed $V(x,t)$ due to vehicles flowing into and from a cell $[x, x+dx]$. The anticipation term reflects the response of drivers with respect to the traffic conditions downstream. The relaxation term describes the tendency of drivers to relax to the equilibrium situation. The parameter τ denotes the relaxation time. $V_e(r)$ is the equilibrium speed, which is considered a monotonically decreasing

function of density. $C(r)$ denotes the anticipation factor, determined by the following equation:

$$C(r) = C_0 = -\frac{1}{2\tau}\frac{dV_e}{dr} \tag{2.35}$$

One of the serious drawbacks of the original Payne type model is its stability in linear approximation of the stationary solution to smaller perturbations for all values of density. However, in reality, at high density traffic becomes unstable, that is, a small perturbation can result in a phantom jam or stop-and-go wave. To remedy this drawback, the so-called traffic pressure was introduced by Philips (1979) as follows:

$$C(r) = dP_e/dr \quad \text{with} \quad P_e = r\Theta_e \tag{2.36}$$

In expression 2.36, P_e is the traffic pressure that reflects the anticipation of drivers to traffic conditions downstream and Θ_e denotes the density dependent speed variance, determined by:

$$\Theta_e = \Theta_0\,(1 - r/r_{max}) \tag{2.37}$$

In expression 2.37, Θ_0 is a positive constant that needs to be estimated.

By substituting expression 2.36 into equation 2.34 we obtain the model of Philips (1979):

$$\frac{\partial V}{\partial t} + V\frac{\partial V}{\partial x} = -\frac{1}{r}\frac{\partial P_e}{\partial x} + \frac{V_e(r) - V}{\tau} \tag{2.38}$$

Stability analysis of Philips' model for stationary solution shows that when density increases beyond a certain critical value r_{cr} the model becomes unstable to small perturbations. This property allows the description of the phantom jam or stop-and-go waves due to random perturbations, but it is not numerically robust. When traffic density is high, the traffic pressure decreases with density, which means that vehicles can accelerate in the congested region. This is not realistic.

Kerner and Konhauser (1993) considered the speed variance a positive constant only, and introduced the viscosity term of second order into the *RHS* of Philips' model in order to smooth the discontinuities as below:

$$\frac{\partial V}{\partial t} + V\frac{\partial V}{\partial x} = -\frac{\Theta_0}{r}\frac{\partial r}{\partial x} + \frac{\eta_0}{r}\frac{\partial^2 V}{\partial x^2} + \frac{V_e(r) - V}{\tau} \tag{2.39}$$

In equation 2.39 η_0 denotes the viscosity coefficient.

The model of Kerner and Konhauser (K-K model) is analogous to Navier-Stokes' equation for compressible fluid. This model is stable to both small and large values of density and unstable for medium values of density. The K-K model allows the replication of the formation and development of traffic clusters. However, this model also shows negative speed, that is, vehicles moving backwards (Helbing (1995)). Some other contributions to Payne type models are the models of Zhang (2000), Aw and Rascle (2000), or in the discrete type as Hilliges and Weidlich (1995).

Payne-type models use the empirical relation of speed and density, while recent publications by Kerner and Rehborn (1996a), Kerner and Rehborn (1997), Kerner (1998) showed that it is more desirable to have macroscopic traffic models that are able to replicate the non-linear phenomena and their characteristic properties. These types of models are reviewed and discussed in the next sections.

2.3.3 Third order type models

In the previous second order models, the dynamics of mean speed were formulated akin to the classical thermodynamic equations. However, there is another approach for the development of the macroscopic models from gas-kinetic models using the so-called *method of moments* (see Leutzbach (1988), Helbing (1997a), Hoogendoorn (1999a)). The relations between the macroscopic variables and the mesoscopic variables are defined as follows:

$$V(x,t) = \frac{1}{r(x,t)} \int_0^\infty v\rho(x,v,t)dv \tag{2.40}$$

$$\Theta(x,t) = \frac{1}{r(x,t)} \int_0^\infty (v-V)^2\rho(x,v,t)dv \tag{2.41}$$

First, let us briefly describe the working of the *method of moments*. According to the *method of moments,* the macroscopic traffic variables can be expressed in terms of the moments of the phase-space density. The k^{th} order of moments of the *PSD* is:

$$m_k(x,t) = \int_0^\infty v^k\rho(x,v,t)dv = r\langle v^k\rangle \tag{2.42}$$

By multiplying both sides of equation 2.7 with v^k and integrating them with respect to speed v between $[0,\infty)$, we obtain a differential equation for the k^{th} moment:

$$\frac{\partial m_k}{\partial t} + \frac{\partial m_{k+1}}{\partial x} = -k\frac{m_k - m_{0,k}}{\tau} + (1-p)\left(m_1 m_k - r m_{k+1}\right) \tag{2.43}$$

Where $m_{0,k} = rV_{max}\langle v^{k-1}\rangle$

Based on equation 2.43, for $k=0$ we obtain the conservation equation, for $k=1$ we get the equation for the dynamics of the mean speed, and for $k=2$ we obtain the equation for the dynamics of the speed variance. The model of Helbing (1995) is described by the following equations:

$$\frac{\partial V}{\partial t} + V\frac{\partial V}{\partial x} = -\frac{1}{r}\frac{\partial P}{\partial x} + \frac{V_e(r) - V}{\tau} \tag{2.44}$$

$$\frac{\partial \Theta}{\partial t} + V\frac{\partial \Theta}{\partial x} = -\frac{2P}{r}\frac{\partial V}{\partial x} + \frac{2(\Theta_e(r) - \Theta)}{\tau} \tag{2.45}$$

In equations 2.44 and 2.45, P denotes the traffic pressure, reflecting the anticipation of drivers to the downstream traffic situation (for instance, accelerate or decelerate when traffic is free or congested), which is determined as:

$$P(x,t) = r(x,t)\Theta(x,t) \tag{2.46}$$

The dynamic equilibrium speed is a function of not only density but also speed variance as:

$$V_e = V_{max} - \tau(1-p)P \tag{2.47}$$

Where p denotes the overtaking probability.

To close the system of equations 2.26, 2.44 and 2.45, the equilibrium speed variance needs to be determined. Helbing (1995) proposed the following formula for the equilibrium speed variance:

$$\Theta_e = \Theta_{max} - 2\tau(1-p)P\sqrt{\Theta/\pi} \tag{2.48}$$

In expression 2.47 and 2.48, V_{max} and Θ_{max} denote the free speed and free speed variance.

By using a similar approach, Treiber et al. (1999) derived a model in which the space requirements and non-local interactions (vehicle reacts to another vehicle at a certain distance downstream) are taken into account in the relaxation term. Since the model was developed in relation to the K-K model (Kerner and Konhauser (1993)), it is able to reproduce non-linear phenomena such as sequences of stable, linear unstable and meta stable regimes raised by Kerner and Rehborn (1996a), the local breakdown effect raised by Kerner et al. (1995), the local cluster effect as in Kerner and Konhauser (1993) and the formation of the so-called dipole-like layers at high densities (Kerner et al. (1996b)). The non-local interaction implies also the smoothing property like the viscosity term in the K-K model, but it does not smooth the shock in downstream direction. That means that the non-local model maintains driver's anisotropic property.

2.3.4 Generalized *MLMC* macroscopic models

Recently, research on macroscopic models of multilane traffic and multiclass traffic on freeways has become suitable for application in areas such as traffic state prediction and in optimization of traffic control (model based). These strategies can allow network operators to use the existing infrastructure more efficiently. Specific examples of control measures that can only be modeled in a class-specific framework are dynamic truck overtaking prohibitions, accommodation of uninterrupted passages for buses at metered on-ramps, and dynamic lane allocation control. The significant contributions to these research topics are the works by Helbing (1997b), Helbing et al. (1999a), Shvetsov and Helbing (1999), Treiber et al. (1999), Hoogendoorn (1999a), Hoogendoorn and Bovy (1999b), etcetera. Most of these models are developed from the generalized *MLMC* gas-kinetic model presented in Section 2.2 using the *method of moments*. The governing equations for the dynamics of density and flow rate of vehicle class u ($u = 1, 2, \ldots, U$) in lane i ($i = 1, 2, \ldots, I$) are:

Conservation law ($k = 0$)

$$\frac{\partial r_i^u}{\partial t} + \underbrace{\frac{\partial q_i^u}{\partial x}}_{\text{convection}} = \underbrace{\sum_{s\in U}\sum_{j=i\pm1}\left(p_{j,i}^u \Psi_j^{u,s} - p_{i,j}^u \Psi_i^{u,s}\right)}_{\text{immediate lane-changing}} + \underbrace{\sum_{j=i\pm1}\left(\triangle_{j,i}^u r_j^u - \triangle_{i,j}^u r_i^u\right)}_{\text{spontaneous lane-changing}} \tag{2.49}$$

Momentum dynamics ($k = 1$)

$$\frac{\partial q_i^u}{\partial t} + \underbrace{\frac{\partial E_i^u}{\partial x}}_{\text{convection}} = \underbrace{\frac{r_i^u V_i^{u,e} - q_i^u}{\tau_i^u}}_{\text{relaxation}} + \underbrace{\sum_{s\in U}\sum_{j=i\pm1}\left(p_{j,i}^u \Phi_j^{u,s} - p_{i,j}^u \Phi_i^{u,s}\right)}_{\text{immediate lane-changing}} + \underbrace{\sum_{j=i\pm1}\left(\triangle_{j,i}^u q_j^u - \triangle_{i,j}^u q_i^u\right)}_{\text{spontaneous lane-changing}} \tag{2.50}$$

$$E_i^u = r_i^u \left[(V_i^u)^2 + \Theta_i^u\right] \tag{2.51}$$

In equations 2.49 and 2.50, V_i^u and Θ_i^u denote the mean speed and speed variance of vehicle class u in lane i, respectively. $p_{i,j}^u$ denotes the probability of vehicle class u to change immediately from its current lane i to either adjacent lane $j = i \pm 1$. The spontaneous lane-changing rate $\triangle_{i,j}^u$ of vehicle class u from lane i to either adjacent lane $j = i \pm 1$ is determined by equation 2.25. The dynamic equilibrium speed $V_i^{u,e}$ is calculated as:

$$V_i^{u,e} = V_i^{u,max} - \left(1 - p_{i,j}^u\right) \sum_{s\in U} \Pi_i^{u,s} \tag{2.52}$$

Where $V_i^{u,max}$ is the class and lane specific free speed.

The lane-changing factor functions $\Psi_i^{u,s}$, $\Phi_i^{u,s}$ and braking factor function $\Pi_i^{u,s}$ are determined by Shvetsov and Helbing (1999), Helbing et al. (1999a), Hoogendoorn (1999a), Hoogendoorn and Bovy (1999b), Helbing et al. (2002) as follows:

$$\Psi_i^{u,s} = \gamma(\acute{r}_i) r_i^u \acute{r}_i^s \sqrt{S_i^{u,s}} \left[\phi\left(\delta V_i^{u,s}\right) + \delta V_i^{u,s} \varphi\left(\delta V_i^{u,s}\right)\right] \tag{2.53}$$

$$\Phi_i^{u,s} = \gamma(\acute{r}_i) r_i^u \acute{r}_i^s S_i^{u,s} \left[\frac{V_i^u}{\sqrt{S_i^{u,s}}} \phi\left(\delta V_i^{u,s}\right) + \left(\frac{\Theta_i^u}{S_i^{u,s}} + \frac{V_i^u}{\sqrt{S_i^{u,s}}} \delta V_i^{u,s}\right) \varphi\left(\delta V_i^{u,s}\right)\right] \tag{2.54}$$

$$\Pi_i^{u,s} = \gamma(\acute{r}_i) r_i^u \acute{r}_i^s S_i^{u,s} \left[\delta V_i^{u,s} \phi\left(\delta V_i^{u,s}\right) + \left(1 + \left(\delta V_i^{u,s}\right)^2\right) \varphi\left(\delta V_i^{u,s}\right)\right] \tag{2.55}$$

In expressions 2.53 , 2.54 and 2.55, $\delta V_i^{u,s}$ denotes the so-called *normalized speed difference* factor between vehicle class u (V_i^u) and vehicle class s ($\acute{V}_i^s$) at a safe distance ahead in lane i, calculated as:

$$\delta V_i^{u,s} = \frac{V_i^u - \acute{V}_i^s}{S_i^{u,s}} \quad \text{with} \quad S_i^{u,s} = \Theta_i^u + \acute{\Theta}_i^s \tag{2.56}$$

The standard Gaussian distribution function $\phi\left(\delta V_i^{u,s}\right)$ and error function $\varphi\left(\delta V_i^{u,s}\right)$ in expressions 2.53 , 2.54 and 2.55 are calculated as shown below:

$$\phi\left(\delta V_i^{u,s}\right) = \frac{e^{-\left(\delta V_i^{u,s}\right)^2/2}}{\sqrt{(2\pi)}} \quad \text{and} \quad \varphi\left(\delta V_i^{u,s}\right) = \frac{1}{\sqrt{(2\pi)}} \int_{-\infty}^{\delta V_i^{u,s}} e^{-z^2/2} dz \tag{2.57}$$

To close the system of equations 2.49 and 2.50, an empirical relation between the speed variance and the other variables, such as density and mean speed is proposed (Helbing et al. (2002)):

$$\Theta_i^u = A\left(r_i^u\right)\left(V_i^u\right)^2 \tag{2.58}$$

where $A(r)$ is the so-called pre-factor density dependent function, calculated as:

$$A\left(r_i^u\right) = A_i^{u,0} + \delta A_i^u \left[1 + exp\left(\frac{r_i^{u,cr} - r_i^u}{\delta r_i^u}\right)\right]^{-1} \tag{2.59}$$

In expression 2.59, $A_i^{u,0}$, δA_i^u, δr_i^u are the lane and class specific model parameters, and $r_i^{u,cr}$ denotes the lane and class specific critical density that needs to be estimated.

The effective cross section factor γ reflects the increase of the effective number of interactions in dense traffic and is calculated by the following equation:

$$\gamma(r_i) = 1 + \frac{V_i^{max}\left(T_i\right)^2}{\tau_i A\left(r_{i,max}\right)} \frac{r_i}{\left(1 - r_i/r_{i,max}\right)^2} \tag{2.60}$$

Note that the variables without class index u represent the weighted averages of the variables belonging to the different user classes, which are calculated, for example, as:

$$T_i = \sum_u T_i^{u \in U} \frac{r_i^u}{r_i} \tag{2.61}$$

The generalized model considers the effect of non-local interactions which itself satisfies the anisotropic property of traffic flow, which remedies the drawback of the Payne-type models. Furthermore, according to Shvetsov and Helbing (1999), the *MLMC* model is able to describe the development of different congested traffic states raised in Kerner and Rehborn (1996a), Kerner et al. (1996b), or Helbing et al. (1999b) such as stop-and-go waves, traffic clusters, and the synchronized traffic state. The influence of trucks on traffic operations has also been shown by Hoogendoorn and Bovy (1999b).

2.3.5 On- and off-ramp models

Research on the effects of lane-drops and on-ramps on freeway traffic flow has been initiated by Munjal and Pipes (1971a), Munjal et al. (1971b) by simulation. Recently, various research efforts on phenomena induced by traffic from ramps have been conducted such as in Kerner and Konhauser (1994), Kerner et al. (1995), Lee et al. (1999), Helbing et al. (1999b), Tampere (2004), and so on. Usually, ramps have been modeled by adding a source term in to the continuum (macroscopic) equations. Based on Payne's model (Payne (1971)), some authors such as Cremer and Ludwig (1986), Papageorgiou et al. (1989), Michalopoulos et al. (1993) and Liu et al. (1996) introduced the so-called traffic friction term into the momentum equation. Traffic friction is defined as the impact of the merging or diverging flow on the speed of the main flow. The general governing equations for interrupted traffic flow are described as given below:

$$\frac{\partial r}{\partial t} + \frac{\partial q}{\partial x} = g(x,t) \tag{2.62}$$

$$\frac{\partial V}{\partial t} + V\frac{\partial V}{\partial x} = \frac{V_e - V}{\tau} - C(r)\frac{\partial r}{\partial x} + G(x,t) \tag{2.63}$$

In equations 2.62 and 2.63, $g(x,t)$ denotes the so-called generation term which represents the impact of traffic flow from on–ramps and/or to off–ramps on the main carriageway, and $G(x,t)$ is the *traffic friction*. Different formulations of the *traffic friction* result in various models as follows:

- When $G(x,t) = -\frac{\nu_0}{\tau} g(x,t)/r$ Cremer and Ludwig (1986)'s model is obtained, where ν_0 is an anticipation parameter.
- Choosing $G(x,t) = -\delta|g(x,t)|V/r$ yields the model of Papageorgiou et al. (1989), where δ is a constant parameter depending on the layout of the ramp (for example, acceleration lane length).
- For $G(x,t) = -\nu r^{\epsilon} g(x,t)$ the model of Michalopoulos et al. (1993) is obtained, where ν is a geometry parameter depending on the acceleration lane length, and ϵ is a dimensionless constant.
- When $G(x,t) = -\nu|g(x,t)|q$ the model of Liu et al. (1996) is obtained, where all the parameters are the same as in the model of Michalopoulos et al.

The generation term $g(x,t)$ in the models above is determined as a function of the density in the target lane and the traffic flow that needs to merge or diverge. The example below shows the equation to calculate the generation term in a merging case:

$$g(x,t) = \frac{q_{in}(t)}{L}\left[1 - \left(\frac{r}{r_{max}}\right)^{\beta}\right] \tag{2.64}$$

In equation 2.64 , L is the acceleration lane length, r_{max} denotes the jam density of the main carriageway, $q_{in}(t)$ denotes the traffic demand from the on-ramp.

Other models are obtained from distinct approaches such as the ramp model of Kerner et al. (1995). In this model, the acceleration lane length is neglected and the impact of ramp flow is only considered in the conservation equation, as a result of which the equation for speed dynamics 2.39 holds. The conservation law equation reads:

$$\frac{\partial r}{\partial t} + \frac{\partial q}{\partial x} = q_{in}(t)\varphi(x - x_i) \tag{2.65}$$

In equation 2.65, $\varphi(x - x_i)$ denotes the denotes the spatial distribution function, localized at ramp location x_i.

The ramp model of Helbing et al. (1999b) takes into account the impact of acceleration lane length on the dynamics of traffic flow in a deterministic way:

$$\frac{\partial r}{\partial t} + \frac{\partial q}{\partial x} = \frac{q_{in}(t)}{(nL)} \tag{2.66}$$

In equation 2.66, L and n are the acceleration lane length and the number of main carriageway lanes downstream of the ramp. Simulations for the model of Helbing et al. (1999b) showed that longer ramps lead to higher roadway capacities.

In Tampere (2004), the acceleration lane length is also taken into account and the impact of on–ramp flow on the speed equation is considered in two ways. For one, on-ramp traffic carries momentum in the flow so that ramp traffic that has not adjusted its speed to the speed of main traffic gives rise to a speed drop. For another, merging events cause a change in driver behavior through a sudden increase of the activation level of drivers. This approach allows modeling delayed jam formation.

In general, in current continuum traffic models, the merging or diverging behavior of a driver is treated as an all-or-nothing type deterministic behavior. That is, traffic often merges or diverges immediately at on–and off–ramps if there is an opportunity while in practice it merges or diverges along a considerable stretch of freeway (such as, an acceleration lane) until it finds sufficient gaps in the target lane. In the remainder of this thesis we develop an on–and off–ramp continuum model that is able to describe merging and diverging behavior based on microscopic modeling principles. The developed model will show analytically that the acceleration lane length plays an important role in the stability of the main traffic, that is, it distributes and spreads out the disturbance due to traffic from an on–ramp.

2.3.6 Application of macroscopic models for urban networks

This section gives an overview of current continuum (macroscopic) models applied to urban networks. In general, it is assumed that a traffic network consists of a set of nodes n ($n \in N$) and a set of links a ($a \in L$). Traffic originates at origin nodes o ($o \in O$ and $O \in N$) and is directed to destination nodes d ($d \in D$ and $D \in N$) via chosen paths that are determined from a traffic assignment model (route-choice model). The route-choice model is used to determine the fraction of traffic going from link a to link b ($b \in L$), which is then used as input to predict traffic dynamics on links.

To build up a model for urban networks, the most important part is to handle discontinuities at intersections. This is very a difficult task because there exist various traffic movements in the same physical location. As far as the continuum models are concerned, there are a few (first-order) macroscopic traffic models for intersections (both controlled and uncontrolled) in urban networks reported in literature. The basic concept of intersection models is illustrated in SSMT model of Lebacque (1984). In the METACOR model, developed by Elloumi et al. (1994), the urban part is modeled based on an overlapping cell approach. Another approach, namely non-overlapping exchange zones that accommodate several movements, has been implemented in STRADA by Buisson et al. (1996). This intersection model is reported not to satisfy the so-called invariance principle explained in Section 2.3.6. Daganzo (1994) considered a node a merging or diverging node consisting of only three links (incoming or outgoing) and then proposed a priority rule for merging and a maximum flow rule for diverging with a FIFO upstream flow. This approach is of a pointwise intersection type, however, according to Lebacque (2005) this approach lacks realism. Lebacque and Khoshyaran (1998) and Lebacque (2005) proposed a maximum entropy-like model (or optimization model), which is constrained by upstream demand and downstream supply. This model has been shown to remedy the shortcomings of the previous models. However, it treats the net-

works as aggregate lanes and, therefore, can overestimate the traffic flow through multilane intersections. In terms of higher order models, Hilliges and Weidlich (1995) introduced a semi-discretized model in which the intersection is considered a point. The main drawback of this model is that the model characteristics depend on the discretization factors such as time and space steps. When these factors tend to zero the convergence of the model is not guaranteed.

In the ensuing of this section, three types of approaches dealing with modeling discontinuities at intersections, namely a pointwise, an exchange zone, and an optimization approach, are presented in detail.

Pointwise modeling approach

This approach has been proposed, amongst the others, by Daganzo (1994), Lebacque (1996), Lebacque and Khoshyaran (1998). The intersection is represented by a point, which means that the dimension of the intersection is ignored. In order to calculate the intersection demands (denoted as $\Xi(t)$) and intersection supplies (denoted as $\Sigma(t)$), the stationary solution of the intersection is used. That means, the upstream demands and downstream supplies are considered constant. Let us consider a merging node in Figure 2.1

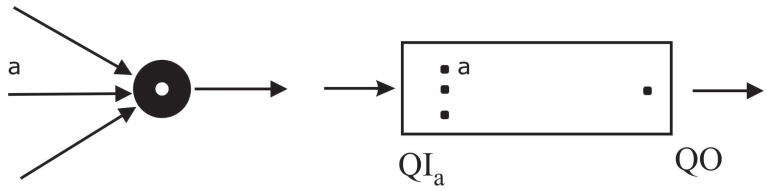

Figure 2.1: Stationary solution of a merging node.

The total intersection supply is split linearly into separate supplies that correspond to each upstream link as :$\Sigma_a(t) = \beta_a \Sigma(t)$, where β_a is a so-called supply-split coefficient. Let $NI(t)$ denote the total number of vehicles flowing into the intersection, $NI_a(t)$ denote the number of vehicles flowing into the intersection via link a and let $NO_b(t)$ denote the number of vehicles flowing out from the intersection via link b. The total traffic demand and traffic supply are calculated by $\Xi(t) = \Xi^e(NI)$ and $\Sigma(t) = \Sigma^e(NI)$, where Ξ^e and Σ^e are the empirical equilibrium functions, determined from fundamental diagrams. The total inflow $QI(t)$ and the partial inflow $QI_a(t)$ from link a to intersection becomes:

$$\begin{aligned} QI(t) &= \min\left[\Sigma(t), \sum_{a\in L} \min\left(\beta_a \Sigma(t), \xi_a(t)\right)\right] \\ QI_a(t) &= \frac{\min\left(\beta_a \Sigma(t), \xi_a(t)\right) \Sigma(t)}{\max\left[\Sigma(t), \sum_{a\in L} \min\left(\beta_a \Sigma(t), \xi_a(t)\right)\right]} \end{aligned} \tag{2.67}$$

where ξ_a denotes the upstream demand of an incoming link a, and the total outflow from intersection $QO(t)$ is determined as follows:

$$QO(t) = \min\left(\Xi(t), \sigma(t)\right) \tag{2.68}$$

where σ denotes the downstream supply of an outgoing link.

When the node is a of diverging type (Figure 2.2), the partial intersection demands are determined by the FIFO-principle as: $\Xi_b(t) = \tilde{\beta}_b \Xi(t)$, where $\tilde{\beta}_b$ denotes the composition coefficient via link b. By definition, the composition coefficient is calculated as $\tilde{\beta}_b = NO_b(t)/NT(t)$, hence, $\sum_{b \in L} \tilde{\beta}_b = 1$.

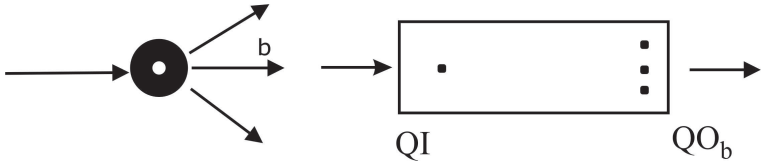

Figure 2.2: Stationary solution of a diverging node.

The inflow $QI(t)$ is calculated as $QI(t) = \min(\xi(t), \Sigma(t))$, while the outflows $QO_a(t)$ are determined by: $QO_b(t) = \min\left(\sigma_b(t), \tilde{\beta}_b \Xi(t)\right)$.

The constraints that apply for the inflow and outflow are positivity constraints and conservation constraints:

$$QI_a \geq 0 \quad \text{and} \quad QO_b \geq 0 \quad \forall a, b \tag{2.69}$$
$$\sum_{a \in L} QI_a = \sum_{b \in L} QO_b$$

Exchange zone approach

This approach has been proposed in the STRADA model (Buisson et al. (1996)), in which movements overlap. This approach is similar to the pointwise approach in principle, but the intersection is modeled as an exchange zone, which is similar to a cell with multiple entry points a and multiple exit points b (Figure 2.3).

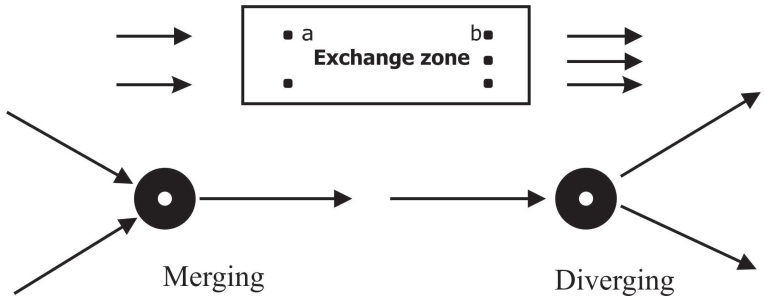

Figure 2.3: Layout of an exchange zone.

In this model, the inflows are obtained by comparing the zone partial supplies $\Sigma_a(t)$ and demands $\Xi_b(t)$ to the upstream link demands $\Xi_{i,a}(t)$ and downstream supplies $\Sigma_{j,b}(t)$. By definition, the partial upstream link demand $\Xi_{i,a}(t)$ is the traffic demand from upstream link

i to entry point a of exchange zone, and the downstream supply $\Sigma_{j,b}(t)$ is traffic supply of link j for exit point b. The partial inflow from link a to the exchange zone is:

$$QI_a(t) = \frac{\min\left(\Sigma_{j,b}(t), \Xi_b(t)\right)\Sigma(t)}{\max\left[\Sigma(t), \sum_{b\in L}\min\left(\Sigma_{j,b}(t), \Xi_b(t)\right)\right]} \tag{2.70}$$

and the outflow from the exchange zone to link b is:

$$QO_b(t) = \min\left(\Sigma_{j,b}(t), \Xi_a(t)\right) \tag{2.71}$$

Where the partial demands and partial supplies are calculated linearly by the FIFO-principle as: $\Xi_b(t) = \beta_b \Xi(t)$ and $\Sigma_a(t) = \beta_a \Sigma(t)$. However, there are other models for these relations based on driver behavior (Buisson et al. (1996)). Obviously, at an intersection, the inflow and outflow QI_a and QO_b, respectively, as a function of the boundary data, must be invariant by the following transformation:

$$\begin{aligned} \sigma_b &\longrightarrow QO_{b,max} \ \text{ if } \ QO_b < \sigma_b \\ \xi_a &\longrightarrow QI_{a,max} \ \text{ if } \ QI_a < \xi_a \end{aligned} \tag{2.72}$$

This is a so-called invariance principle (Lebacque and Khoshyaran (1998) and Lebacque (2005)). It has been shown that the intersection model in STRADA does not satisfy the invariance principle and it can only be used as a discretized and phenomenological model (Lebacque and Khoshyaran (1998) and Lebacque (2005)). A sufficient condition for the invariance principle is captured in the model described in the next section.

Flow maximizing approach

This model is built on the concept of an entropy solution at intersections by Lebacque and Khoshyaran (1998). That is, the partial inflows and outflows at an intersection are calculated by maximizing some concave increasing flow functions, subject to supply and demand constraints.

- In a merging node, the inflows $QI_a(t)$ are calculated by the following optimization problem:

$$\begin{aligned} &\max \quad \sum_{a\in L}\phi_a\left(QI_a(t)\right) \\ &\text{subject to} \\ &QO(t) = \sum_{a\in L} QI_a(t) \leq \quad \min\left(\sigma, q_{max}\right) \\ &QI_a(t) \leq \xi_a \end{aligned} \tag{2.73}$$

  Where q_{max} is the maximum flow through the intersection, ϕ_a is concave increasing functions describing the behavior of users at the intersection. A specific form of the function ϕ_a is:

$$\phi_a(q) = q - \frac{q^2}{2\min\left(\beta_a\sigma, \xi_a\right)} \tag{2.74}$$

Solving this optimization problem gives:

$$QI_a = \frac{\min\left(\beta_a \sigma, \xi_a\right) \sigma}{\max\left[\sigma, \sum_{a \in L} \min\left(\beta_a \sigma, \xi_a\right)\right]} \tag{2.75}$$

- In a diverging node, the outflows $QO_b(t)$ are calculated by the following optimization problem:

$$\begin{aligned} &\max \quad \sum_{a \in L} \phi_a \left(QO_b(t)\right) \\ &\text{subject to} \\ &QI(t) = \sum_{b \in L} QO_b(t) \leq \quad \min\left(\xi, q_{max}\right) \\ &QO_b(t) \leq \sigma_b \end{aligned} \tag{2.76}$$

The solutions of this optimization problem are either:

$$\begin{aligned} QI &= \min\left(\xi, \sigma_b / \alpha_b\right) \\ QO_b &= \alpha_b QI \end{aligned} \tag{2.77}$$

if we assume the FIFO rule of upstream drivers, or:

$$\begin{aligned} QO_b &= \min\left(\alpha_b \xi, \sigma_b\right) \\ QI &= \sum_{b \in L} QO_b \end{aligned} \tag{2.78}$$

if a non–FIFO rule is used.

Where α_b denotes the assignment coefficients.

In all models described above, the traffic interactions between lanes (left-turning, right-turning with other traffic streams) are not taken into account explicitly, therefore, they may overestimate the probability of traffic flow to exit or to enter the intersection. In the remainder of this thesis we introduce a macroscopic model for links and intersections based on *MLMC* traffic flow theory, in which the inflows and outflows at intersections are determined based on a *gap-acceptance* model and a *renewal process*.

2.4 Summary

This chapter gave a historical review of the vehicular traffic flow modeling relevant for our project. Such models were classified into three levels of detail, namely microscopic, mesoscopic and macroscopic. Since the main purpose of this thesis is to develop a continuum model for interrupted traffic networks, we put emphasis on the mesoscopic (gas-kinetic) and macroscopic models. For simplicity, we have chosen a safe–distance model as a basis for

modeling the lane–changing processes in our model. In this chapter, we showed that the gas-kinetic model is the most appropriate foundation for the development of the macroscopic model in this thesis. It enables modeling processes of discontinuous events in the flow such as deceleration (due to interaction) and lane-changing without the need to describe the time-space behavior of these events.

Issues with respect to the properties of macroscopic models and question of order (*LWR* or Payne-type models) were discussed. Other types of macroscopic models developed by Helbing or the generalized model of Hoogendoorn that includes the dynamics of speed variance for multilane and multiclass traffic flow have shown theoretical improvements over the other approaches.

The overview of the application of macroscopic models to the modeling of traffic flow dynamics at bottlenecks and intersections was also discussed in this chapter. We have argued that the current modeling approaches often simplify the traffic flow operations at bottlenecks on freeways and overestimate the traffic flow through multilane intersections in urban networks. In order to overcome these shortcomings, in the remainder of this thesis we will refine and extend the generalized *MLMC* model of Hoogendoorn with the aim to describe the dynamics of traffic at bottlenecks and intersections.

Chapter 3

Generalized *MLMC* gas-kinetic model for interrupted traffic flow

In this chapter, we will formulate equations to describe the dynamics of traffic operations that are interrupted by on– and off–ramps, weaving sections, and so on. These equations take into account the processes that yield changes in the phase-space density (*PSD*) due to the inflow and outflow of vehicles at the (infrastructure) discontinuities.

As described in Chapter 2, since Lighthill and Whitham (1955) first applied a simple continuum (macroscopic) model to describe the evolution of traffic flow on freeways, significant efforts have been undertaken to further develop and employ continuum traffic flow models. These efforts have, however, mainly concentrated on describing uninterrupted traffic flow. In contrast, relatively little progress has been made in the investigation of interrupted traffic flow. Especially with respect to macroscopic models, traffic operations at on–and off–ramp are often inadequately treated, which is generally related to oversimplification, for instance, by neglecting the length of the acceleration lane and, instead, treating a ramp as a singular point ('point-like model'). For example, in order to take into account the influence of the merging flow on the main flow, the so-called *traffic friction* is added to the right hand side of the continuum (macroscopic) model (see Section 2.3.5).

The main contribution of this chapter to the state-of-the-art in continuum traffic flow models concerns the modeling of discontinuities of heterogeneous traffic flow on multilane freeways. The proposed model refines and extends the work of Hoogendoorn (1999a) by introducing the so-called *mandatory lane-changing* (*MLC*) process into the right hand side of the current multilane and multiclass (*MLMC*) gas–kinetic models based on microscopic driving principles within freeway sections with on–and off–ramp. This model serves as an intermediate step towards the development of the macroscopic model for interrupted traffic stream in Chapter 4. The developed model describes in detail how an individual driver merges and/or diverges within on–and off–ramp section. It is assumed that a vehicle chooses a gap in its target lane in order to merge and/or diverge based on the interaction with all vehicles around it and the layout of the acceleration lane (such as, the length of the acceleration lane). Based on the details of this *MLC* process, a relevant control measure at on–and off–ramps (ramp

metering), or a certain design of the infrastructure (acceleration lane length) can be applied in order to obtain better operations of freeways. The developed model is expected to represent the following situations:

- Drivers merge and/or diverge along a considerable stretch of freeway (acceleration lane).
- Drivers are willing to accept smaller gaps as approaching the end of an on–and/or off–ramp.
- Drivers in the shoulder lane are cooperative in the sense that they change to the left lane in order to give way to merging vehicles.

This chapter is organized as follows. Several behavioral assumptions are made in Section 3.1. Section 3.2 presents some empirical foundations for the development of our model. Section 3.3 presents the modeling approach which is used throughout this thesis. Section 3.4 describes the generic gas-kinetic equation for the dynamics of the phase-space density at on– and off–ramps. Section 3.5 shows the calculation of immediate lane-changing rate. In Section 3.6 we formulate the mandatory lane-changing rate of traffic flow at on– and off–ramps. In Section 3.7 we show the extension of the on– and off–ramp model to calculate the lane-changing probabilities at weaving sections. Section 3.8 summarizes this chapter.

Before going into detail on our modeling approach, let us start with the most important behavioral assumptions for developing the gas-kinetic equations for interrupted traffic stream.

3.1 Behavioral assumptions

The assumptions covered in this section are concerned with the driver behavior when making lane-changes (Minderhoud (1999), Hoogendoorn (1999a), Ahmed (1999), Toledo (2003)).

General lane–changing assumptions

1. The speed of lane–changing vehicles is not influenced by the lane-changing maneuver. That is, the lane–changing vehicles do not reach the target lanes instantaneously with a higher/lower speed.
2. The speeds of the following and the leading vehicles in the target lanes are unaffected instantaneously by the lane-changing maneuver.
3. Only one vehicle can change lanes during each time interval. That is, lane changes are not executed instantaneously.

Immediate lane–changing assumptions

4. When a faster vehicle catches up with a slower vehicle, the faster vehicle always intends to change to the left adjacent lane in order to maintain its desired speed.

5. Lane selection model: when a driver intends to change lanes, first the target lane needs to be selected. The probability that a lane is selected as the target lane depends on a number of factors, such as the speed of the concerned vehicle, the user-class, traffic conditions in the current lane and the target lane. A lane selection model can be of either a discrete type (Ben-Akiva and Lerman (1995)) or a probabilistic type (Ahmed (1999)). The result of the lane selection model is the probability to select either the right lane, the left lane or to remain in the current lane. If either the right lane or the left lane is selected, the vehicle will seek for an acceptable gap in the selected lane. The traffic regulations can also be in-cooperated in this model. For example, under European traffic regulations, the first option is always to move to the left when a slower vehicle needs to be passed.

6. Gap acceptance: in this thesis, 'gap' stands for the space gap, that is, the distance between the front ends of two successive vehicles in the same lane. A vehicle is able to change to the target lane when both the *lead-gap* and the *lag-gap* are accepted (Section 3.3.2). The *lead-gap* is accepted if, after the lane change has been carried out, the space between the lane-changing vehicle and the leader in the target lane is larger than a certain threshold distance (*critical lead gap*). The *lag-gap* is accepted if, after the lane-change has been carried out, the space between the lane-changing vehicle and the follower in the target lane is larger than *critical lag gap*.

7. The *critical gaps* are considered single values, which are a linear function of speed and the reaction time of the follower. The presence of various vehicle classes result in different *critical gaps* due to the differences in reaction time. For example, a truck in general requires a larger gap compared to a passenger car due to longer reaction times ($T_{truck} > T_{car}$).

Mandatory lane–changing assumptions

8. Drivers are willing to accept smaller gaps when approaching the end of the current lane. That is, the remaining distance to the end of the current lane influences the gap-acceptance behavior.

9. The follower in the target lane may create gaps for the lane–changing vehicles by changing lanes to the left if there is an opportunity to do so.

10. The adaptation of the speeds of (mandatory) lane-changing vehicles to the speeds of vehicles on the destination lane by acceleration an/or deceleration is ignored.

3.2 Empirical foundations

This section illustrates some empirical foundations which are concerned with the distributions of individual vehicle speeds and distance gaps.

1. The individual vehicle speeds can be sufficiently approximated by a Gaussian distribution (see Figure 3.1).

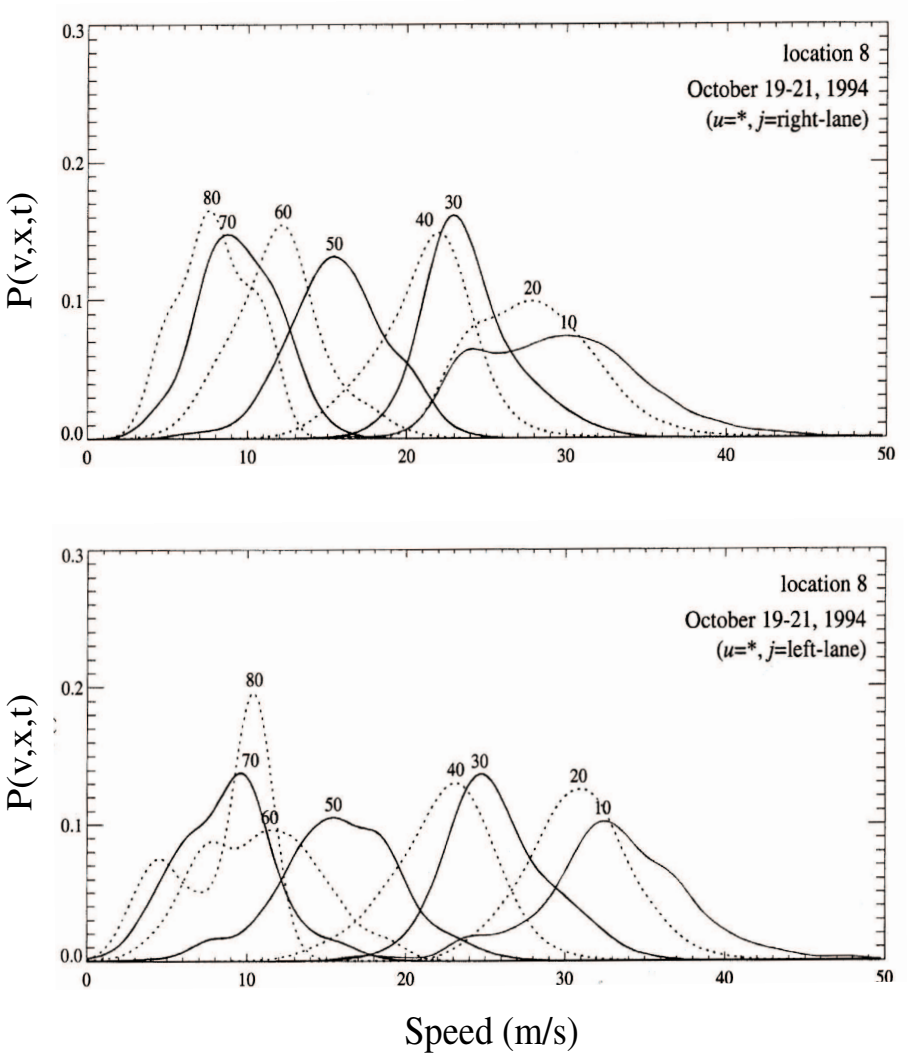

Figure 3.1: Aggregate-class speed distributions of traffic in the left and the right-lane respectively of a two lane freeway A9 in The Netherlands. Source: Hoogendoorn (1999a).

2. The gap distribution is known. For analytical purposes, we use the exponential distribution of gaps. However, the derived model can be solved numerically with other types of distributions, such as, the M3 distribution type (Cowan (1975)).

3.3 Modeling approach

This section describes the approach applied to model the lane-changing processes in a gas-kinetic traffic flow model. This modeling approach takes into account explicitly the behavior of (class specific) drivers when making a lane-change, especially at merging and/or diverging areas on freeways, and at intersections in urban networks. For these purposes, we start with a microscopic model which describes the behavior of each vehicle within lane (*safe–distance model*). Following is the behavior of drivers to assess traffic conditions in the adjacent lanes for a lane-change (*gap-acceptance model*). In the *gap–acceptance model*, gap distributions will be determined by a *renewal theory*.

3.3.1 Safe–distance model

As mentioned in Section 2.1 (Chapter 2), the microscopic safe–distance model of Jepsen (1998) is used as basis for the development of our model. The second order term is neglected in the development of our model due to its small contribution, which is approximately $0.022v^2$ (Hoogendoorn (1999a)). Therefore, the model of Jepsen (1998) reads:

$$d(v(t)) = d_{min} + l + Tv(t) \tag{3.1}$$

Here, d denotes the distance gap between two successive vehicles, l, T, and v are, respectively, the length, reaction time, and speed of the considered vehicle. d_{min} is the safe margin.

This equation is used in the *gap–acceptance model* to determine the distance *lead-gap* and *lag-gap* as shown in the next section.

3.3.2 Gap acceptance model

In this section, we describe how a *gap–acceptance* model functions in lane-changing processes. The *gap–acceptance* model expresses the drivers' assessment whether or not gaps on the target lanes are acceptable for a lane-change (Tanner (1962)). Let *lead-gap* and *lag-gap* denote the gap between the subject vehicle and its leader and between the subject vehicle and its follower in the target lane, respectively (Figure 3.2). For simplicity, Figure 3.2 only illustrates merging and diverging behavior on a two lane freeway, however, the model for multilane freeways still holds.

In the case of merging (Figure 3.2(a)), the decision to make a lane change from the acceleration lane to the shoulder lane is based on both the *lag-gap* between the merging vehicle and the follower (vehicle $n-1$) and the *lead-gap* between the merging vehicle and the leader (vehicle n). When these gaps suffice, the subject vehicle can merge to the main carriageway. To model a merging event, we consider the situation when the follower in the shoulder lane change lanes to the left in order to give way to the merging vehicle.

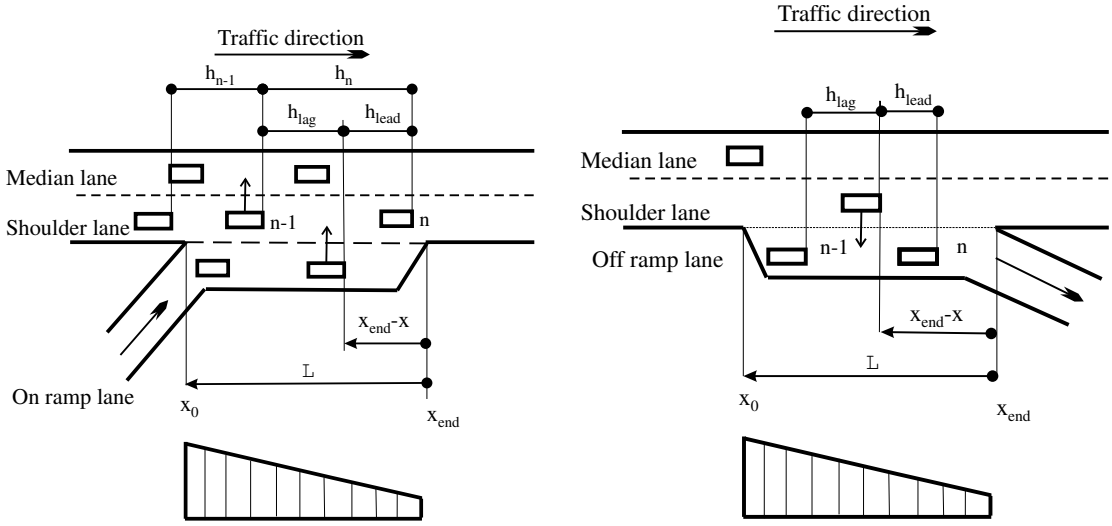

(a) Merging (b) Diverging

Figure 3.2: Layout of a merging and diverging zone.

In the case of diverging, the subject vehicle can exit from the main carriageway if the *lead-gap* between the subject vehicle and its leader (vehicle n) and the *lag-gap* between the subject vehicle and its follower (vehicle $n-1$) in the off-ramp lane are sufficient.

Let d_{lag} and d_{lead} denote the *critical lag-gap* and the *critical lead-gap* of vehicle, respectively, for lane-changing maneuvers. By using the safe–distance model we obtain the following results: $d_{lead} = d^{min} + l + \mu(x)Tv$ and $d_{lag} = d^{min} + l + Tw$; where v and w are the speed of the subject vehicle and of the following vehicle in the target lane, respectively. d^{min} is the minimal distance reflecting the safety-margin acceptance of the vehicles on the target lane, l and T are the length and reaction time of vehicle, respectively. The factor $\mu(x)$ ($\mu(x_0) = \mu_{max}$, $\mu(x_{end}) = \mu_{min}$ and $\mu(x) = 1$ when $x \leq x_0$ and $x \geq x_{end}$, $\mu_{min}^{max} \in [0, 1]$) considers the willingness to accept a smaller gap of subject drivers when approaching the end of the ramp. x_0 and x_{end} are, respectively, the start and the end locations of acceleration lane.

Let $\mathcal{A}^{u,s}(v|x,t)$ be the event that a vehicle of class u driving with speed v finds a sufficient gap between vehicles regardless of class (so denoted by s) in the target lane at location x and time instant t. According to the *gap–acceptance* model, the probability that event $\mathcal{A}^{u,s}$ occurs is:

$$P\left(\mathcal{A}^{u,s}\right) = P\left(h_{lag} \geq d_{lag}^{s}(w) \& h_{lead} \geq d_{lead}^{u}(v)\right) \tag{3.2}$$

where $d_{lag}^{s}(w) = d_{u}^{min} + l_u + T_s w$ and $d_{lead}^{u}(v) = d_{s}^{min} + l_s + T_u v$ because the distance gaps are determined by the total length of the leading vehicle, the safe margin and the product of the speed and the reaction time of the follower (see Figure 3.2).

As argued by Ahmed (1999) and Toledo (2003), the events that a vehicle accepts simultaneously a *lead-gap* and a *lag-gap* in the target lanes are assumed independent. That is:

$$P\left(\mathcal{A}^{u,s}\right) = \underbrace{P\left(h_{lag} \geq d^{s}_{lag}(w)\right)}_{(1)} \underbrace{P\left(h_{lead} \geq d^{u}_{lead}(v)\right)}_{(2)} \tag{3.3}$$

where (1) is the probability to find a sufficient *lag-gap* and (2) is the probability to find a sufficient *lead-gap* in the target lane. To determine $P\left(\mathcal{A}^{u,s}\right)$, we need to calculate the probability distribution function (*p.d.f*) of the *lead-gap* and the *lag-gap* using a so-called *renewal process*. This is described in Section 3.3.3.

3.3.3 Renewal process in traffic stream

The concept of *renewal processes* can be found in statistical literature, for example in Cox (1962). In this section, we briefly describe the definition of a *renewal process* and discuss its application in traffic flow modeling.

> *Definition (Cox (1962)): suppose that we have a population of events and that failure time, x, is a continuous variable with* p.d.f $f(x)$. *Let us start with a new event at time $x_0 = 0$. This event fails at time x_1, then it will be replaced immediately by a new event with failure time x_2. Hence, the second failure will occur after $x_1 + x_2$. Let this process be continued, an event being replaced immediately on failure by a new event. The failure time of the nth event used is x_n, and the nth failure time occurs at time $X_n = x_1 + x_2 + \ldots + x_n$. If $\{x_1, x_2, \ldots, x_n\}$ are independently, identically distributed non-negative random variables, all with* p.d.f $f(x)$*, the system is called a renewal process.*

In traffic flow events are replaced by time or distance gaps, and failure time is replaced by rejected time or distance when a vehicle wants to change lanes.

Let us consider a stream of vehicles which constitutes a *renewal process* $\mathcal{N}$. Let h_n denote the total gap between two successive vehicles located at x_n and x_{n-1}. Let us assume that $\{h_1, h_2, \ldots, h_n\}$ are independently identically distributed random variables with *p.d.f* $f(h)$. Suppose that we interrupt the *renewal process* $\mathcal{N}$ by inserting a vehicle at some specified location x between x_n and x_{n-1} (see Figure 3.3). Let h_{lag} and h_{lead} denote the distance between x and the next vehicle upstream of x and between x and the next vehicle downstream of x. That is, $h_{lag} = x - x_{n-1}$ and $h_{lead} = x_n - x$. In the terminology of the *renewal process*, the *lead-gap* h_{lead} acts as *excess life*, the *lag-gap* h_{lag} acts as *current life* and the total gap $h = h_{lead} + h_{lag}$ acts as *total life*.

- The distribution of the *lead-gap* or the *excess life* is calculated as:

$$f_{lead} = \frac{1 - F(h)}{\bar{h}} \tag{3.4}$$

  where $F\left(h\right)$ denotes the *cumulative gap distribution* and $\bar{h}$ is the expected unoccupied space between two successive vehicles, defined as the road length that is not occupied

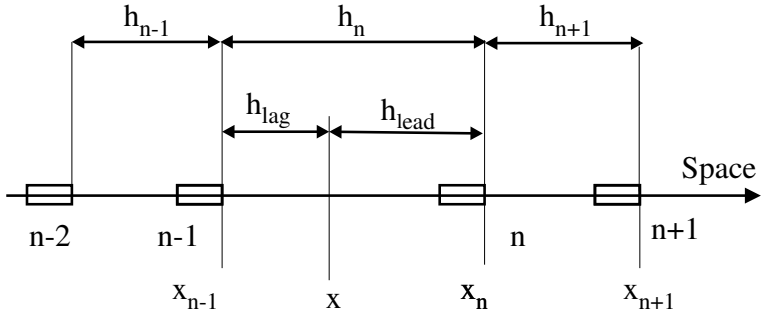

h_{lag} = current life = $x - x_{n-1}$

h_{lead} = excess life = $x_n - x$

h_n = total life = $h_{lag} + h_{lead}$

Figure 3.3: Excess, current, and total life at location x.

by a vehicle taking into account its space requirement. The expected unoccupied space is calculated by the following formula by Hoogendoorn et al. (2002):

$$\bar{h} = \frac{1 - \sum_{s \in U} r_s \left(d_s^{min} + l_s + T_s V_s\right)}{\sum_{s \in U} r_s} = \frac{1}{\gamma \sum\limits_{s \in U} r_s}$$

$$\text{with } \gamma = \frac{1}{1 - \sum_{s \in U} r_s \left(d_s^{min} + l_s + T_s V_s\right)} \tag{3.5}$$

Where γ denotes the space requirement factor, accounting for the size of the vehicles.

- The distribution of the *lag-gap* or the *current life* is calculated based on the total clear gap between the next vehicle upstream of x and the next vehicle downstream of x. For example, when vehicle $n-1$ changes lanes, the total clear gap becomes $h_n + h_{n-1}$. If both vehicle $n-1$ and vehicle $n+1$ change lanes, the total clear gap becomes $h_{n+1} + h_n + h_{n-1}$.

  In general, let $H_n = h_1 + h_2 + \ldots + h_n$ $(n = 1, 2, \ldots)$ denote the total clear gap. The *p.d.f* of the *lag-gap* is calculated as:

$$f_{lag}(h) = \frac{1 - F(H_n)}{\bar{H}_n} \tag{3.6}$$

Where $\bar{H}_n = n\bar{h}$. To calculate the *c.d.f* of the total clear gap $F(H_n)$ in equation 3.6, the so-called *Laplace transform theorem* is used below:

- *Definition of Laplace transform: let* $f(x)$ *be the* p.d.f *of a non-negative random variable* ***X****. The Laplace transform,* $\tilde{f}(s)$*, is defined as:*

$$\mathcal{L}\{f(x); s\} = \tilde{f}(s) = E\left(e^{-s\boldsymbol{X}}\right) = \int_0^{+\infty} e^{-sx} f(x) dx \tag{3.7}$$

- *Sums of independent random variables: let x_i ($i = 1 \ldots n$) be nonnegative random variables independently distributed with the p.d.f: $f_i(x)$. The Laplace transform of the p.d.f of the sum $\boldsymbol{X} = \sum_{i=1}^{n} x_i$ is determined as follows:*

$$\begin{aligned} \mathcal{L}\{f(\boldsymbol{X}); s\} &= E\left(e^{-s\sum_{i=1}^{n} x_i}\right) = E\left(\prod_{i=1}^{n} e^{-sx_i}\right) \\ &= \prod_{i=1}^{n} E\left(e^{-sx_i}\right) = \prod_{i=1}^{n} \tilde{f}_i(s) \end{aligned} \tag{3.8}$$

Assumption of the exponential distribution of gaps leads to:

$$f(h) = \gamma r e^{-\gamma r h} \quad \text{and} \quad F(h) = 1 - e^{-\gamma r h} \tag{3.9}$$

the corresponding *Laplace* transform of $f(h)$ will be:

$$\mathcal{L}\{f(h); s\} = \gamma r/(\gamma r + s) \tag{3.10}$$

Hence, the *Laplace* transform of $f(H_n = \sum_n h_n)$ becomes:

$$\mathcal{L}\{f(H_n); s\} = (\gamma r)^n/(\gamma r + s)^n \tag{3.11}$$

It turns out that this is the *Laplace* transform of the *Gamma* distribution function:

$$f(H_n) = \frac{\gamma r(\gamma r h)^{n-1} e^{-\gamma r h}}{\Gamma(n)} \tag{3.12}$$

The corresponding *c.d.f* $F(H_n)$ is:

$$F(H_n) = -\frac{(\gamma r h)^{n-1} e^{-\gamma r h}}{\Gamma(n)} + F(H_{n-1} = (n-1)h) \tag{3.13}$$

Where Γ denotes the gamma function, defined by $\Gamma(n) = \int_0^\infty x^{n-1} e^{-x} dx$. Since n is a positive integer, $\Gamma(n) = (n-1)!$.

By using equation 3.4, equation 3.6 and equation 3.13, distributions of the *lead-gap* and the *lag-gap* are determined.

The next section will present a gas-kinetic model for multilane and multiclass traffic flow including entries (that is, with on– and off–ramps).

3.4 Gas-kinetic model for interrupted traffic flow

This section establishes the gas-kinetic equations for interrupted traffic streams (for instance, with on–and off–ramps) as follows.

Let i denote the lane index, which is decreasing from the median lane to the shoulder lane ($i = 1$), and let $i = 0$ denote the index of the acceleration lane. Since the traffic from an on–ramp does not directly influence the traffic flow in the lanes further to the left of the shoulder lane ($i \geq 2$), the generalized *MLMC* gas-kinetic model of Hoogendoorn (1999a), Shvetsov and Helbing (1999) is applied for those lanes. This model holds also for those lanes in the diverging case when traffic that intends to exit at an off–ramp must move to the shoulder lane before the off–ramp is reached. The only difference in our model is that the *immediate lane–changing* probability $p^u_{i,j}$ of vehicle class u from lane i to either adjacent lane j is determined in detail by the *gap acceptance* model as described in Section 3.3.2.

For traffic operations in the shoulder lane and the acceleration lane (that is, either at an on–ramp or an off–ramp) or auxiliary lane (in ramp weaving sections) we need to determine the *mandatory lane–changing (MLC)* rate of equation 2.17 in Chapter 2. According to Helbing et al. (2002), the *MLC* rate is proportional to the traffic that intends to (mandatorily) change lanes and inversely proportional to the acceleration lane length.

Let $\tilde{\nu}^+_{i,u}(x, v, t)$ and $\tilde{\nu}^-_{i,u}(x, v, t)$ denote the incoming and outgoing flow rate to and from the main carriageway, respectively, at location x and time instant t. Let $(\partial\rho^u_i/\partial t)^{man}_{lc}$ denote the changes of the phase–space density (*PSD*) due to the inflow and/or outflow of vehicles at on–and off–ramps, respectively. The flow rates are determined as follows:

- In the case of merging, since $\rho^u_0(x, v, t)v$ denotes the expected volume of vehicle class u driving with speed v and having to merge at location x and time instant t, and $\pi^u_{0,1}(x, t)$ denotes the expected probability to do so, the expected *MLC* rate equals:

$$\tilde{\nu}^+_{i,u}(x, v, t) = \left(\frac{\partial\rho^u_i}{\partial t}\right)^{man}_{lc} = (-1)^{i+1}\delta(x)\frac{\rho^u_0(x, v, t)v\pi^u_{0,1}}{L} \tag{3.14}$$

- In the case of diverging, let $\alpha^u_{1,0}$ denote the fraction of vehicle class u that intends to exit the main carriageway, which is calculated from traffic counts or from a traffic assignment solution, and let $\pi^u_{1,0}(x, t)$ denote the expected probability to do so. The expected *MLC* rate equals:

$$\tilde{\nu}^-_{i,u}(x, v, t) = \left(\frac{\partial\rho^u_i}{\partial t}\right)^{man}_{lc} = (-1)^{i}\delta(x)\frac{\alpha^u_{1,0}\rho^u_1(x, v, t)v\pi^u_{1,0}}{L} \tag{3.15}$$

- In weaving sections, let $\alpha^u_{i,j}$ denote the fraction of weaving flow ($j = i \pm 1$) or non-weaving flow ($j = i$). The expected *MLC* rate equals:

$$\begin{aligned}
\tilde{\nu}^+_{i,u}(x, v, t) &= \left(\frac{\partial\rho^u_i}{\partial t}\right)^{man}_{lc} = (-1)^{i+1}\delta(x)\frac{\alpha^u_{0,1}\rho^u_0(x, v, t)v\tilde{\pi}^u_{0,1}}{L} \\
\tilde{\nu}^-_{i,u}(x, v, t) &= \left(\frac{\partial\rho^u_i}{\partial t}\right)^{man}_{lc} = (-1)^{i}\delta(x)\frac{\alpha^u_{1,0}\rho^u_1(x, v, t)v\tilde{\pi}^u_{1,0}}{L}
\end{aligned} \tag{3.16}$$

Where $\delta(x) = 0$ if $x < x_0$ or $x > x_{end}$, and $\delta(x) = 1$ otherwise. L denotes the length of the acceleration lane (or, of the auxiliary lane). $\tilde{\pi}^u_{1,0}$ denotes the expected probability of vehicle class u changing from the shoulder lane to the auxiliary lane within weaving sections and $\tilde{\pi}^u_{0,1}$ is the expected probability of vehicle class u changing from the auxiliary lane to the shoulder lane within weaving sections.

The generalized *MLMC* gas-kinetic models of Shvetsov and Helbing (1999), Hoogendoorn (1999a), and so on, are extended for the description of interrupted traffic stream as:

$$\begin{aligned}&\frac{\partial \rho_i^u}{\partial t} + \underbrace{v\frac{\partial \rho_i^u}{\partial x}}_{\text{convection}} + \underbrace{\frac{\partial}{\partial v}\left(\rho_i^u \frac{V_i^{u,max} - v}{\tau_i^u}\right)}_{\text{acceleration}} \\ &= \underbrace{\left(\frac{\partial \rho_i^u}{\partial t}\right)_{int}}_{\text{interaction}} + \underbrace{\left(\frac{\partial \rho_i^u}{\partial t}\right)^{int}_{lc}}_{\text{interaction LC}} + \underbrace{\left(\frac{\partial \rho_i^u}{\partial t}\right)^{spon}_{lc}}_{\text{spontaneous LC}} + \underbrace{\left(\frac{\partial \rho_i^u}{\partial t}\right)^{mand}_{lc}}_{\text{mandatory LC}}\end{aligned} \tag{3.17}$$

Equation 3.17 describes the dynamics of the *MLMC* phase-space density $\rho_i^u(x,t)$ due to longitudinal processes and lateral processes on a freeway with on– and off–ramps, which are presented in the following sections.

3.4.1 Longitudinal processes

Longitudinal traffic flow processes describe within-lane operations. These processes consist of:

- Convection. This process reflects the changes of the *PSD* due to vehicles flowing from cell x to cell $[x + dx]$.
- Acceleration. Free–flowing vehicles in cell x driving with speed v accelerate to their desired speed $w > v$. This causes a reduction in the *PSD* $\rho(x, v, t)$. However, vehicles driving with speed $w < v$ may accelerate to speed v, which causes an increase in the *PSD* $\rho(x, v, t)$.
- Deceleration. When a faster vehicle driving with speed v catches up with a slower vehicle driving with speed $w < v$ and is unable to change lanes immediately, the faster vehicle has to slow down to the speed of the slower vehicle. This causes a reduction of the *PSD* $\rho(x, v, t)$ and, equally, an increase of the *PSD* $\rho(x, w, t)$.

These process have been calculated in the literature (Shvetsov and Helbing (1999), Hoogendoorn (1999a)) as reviewed in Chapter 2.

The refinement and extension of our model concerns the implementation of the lateral processes for interrupted traffic flow, which are described in the ensuing of this chapter.

3.4.2 Lateral processes

Lateral traffic flow processes entail the lane-changes of vehicles. In this thesis, lane–changing processes are categorized into a *discretionary* and a *mandatory* type (Ahmed (1999), Hoogendoorn (1999a), Minderhoud (1999), Toledo (2003)).

1. Discretionary lane-changes. This process occurs when a vehicle is not satisfied with his driving conditions in the current lane due to:
   - catching up with a slower vehicle and have to change to an adjacent lane to maintain their current speed (*Interaction lane-changes* or *Immediate lane-changes (ILC)*).
   - preference for the adjacent lanes (*Spontaneous lane-changes (SLC)*).
2. Mandatory lane-changes. The concept of a mandatory lane-changing process is used to model lane-changes of vehicles at discontinuities on freeways. This process occurs if staying in the current lane is not possible any more due to:
   - Traffic regulations (for instance, truck or bus-reserved lanes)
   - Lane drops in work zones
   - Merging from an on-ramp
   - Diverging to an off-ramp.

Both of these lane-changing processes are formally established and implemented in the ensuing of this chapter. Because the mandatory lane-changing process has a more compulsory nature than the discretionary lane-changing process, the two types of lane changing use different parameters. For example, a driver is more likely to accept smaller gaps when making a mandatory lane-change than when making a discretionary lane-change. Consequently, mandatory lane-changes can disturb the traffic flow on the target lane more significantly than discretionary lane-changes. This behavior is also captured in the model developed in this chapter.

In equation 3.17, the *SLC* rate between the shoulder lane and the median lane is specified the same as in Chapter 2. The *MLC* rate only contributes to the changes of the *PSD* in the acceleration lane and in the shoulder lane of the main carriageway at on– and off–ramps, which is determined as follows:

$$\left(\frac{\partial \rho_i^u}{\partial t}\right)_{lc}^{mand} = \tilde{\nu}_{i,u}^{+} + \tilde{\nu}_{i,u}^{-} \tag{3.18}$$

Let $\mathcal{B}_j^u$ be the event that the following vehicle in the target lane j is of class u.

Let $P\left(\mathcal{C}_j^u\right)$ denote the probability that a vehicle of class u chooses lane j as the target lane. The target lane choice set contains up to three alternatives: the driver may stay in the current

lane or may change lanes to either the adjacent lanes. The target lane choice has been modeled in literature (see Ben-Akiva and Lerman (1995) or Ahmed (1999)). For example, the target lane model of Ahmed (1999) reads:

$$P\left(\mathcal{C}_j^u\right) = \frac{exp\left(\mathbf{X}_j^u \boldsymbol{\beta}_j^u\right)}{\sum_{k=j-1,j,j+1} exp\left(\mathbf{X}_k^u \boldsymbol{\beta}_k^u\right)} \tag{3.19}$$

Where $\mathbf{X}_j^u$ and $\boldsymbol{\beta}_j^u$ denote the set of explanatory variables, such as desired speed, speed differences between the lanes, fractions of heavy trucks, and the set of corresponding parameters, respectively.

The lane-changing probability of vehicle class u from the current lane i to the target lane j regardless of the vehicle class in the target lane, denoted by $p_{i,j}^u$, is:

$$p_{i,j}^u = \sum_{s \in U} P\left(\mathcal{A}_{i,j}^{u,s}\right) P\left(\mathcal{B}_j^s\right) P\left(\mathcal{C}_j^u\right) \tag{3.20}$$

Where $\mathcal{A}_{i,j}^{u,s}$ denotes the event that a vehicle class u driving in lane i find a sufficient gap between two successive vehicle regardless of class type in lane j (equation 3.3).

In equation 3.20, the probability that a vehicle in the target lane that interacts with vehicle class u is of class s is calculated as:

$$P\left(\mathcal{B}_j^s\right) = \frac{r_j^s}{r_j} \quad \text{with} \quad r_j = \sum_{s \in U} r_j^s \tag{3.21}$$

In the next sections, we show how to model the lane-changing probabilities (both immediate and mandatory) based on the *gap-acceptance* model and *renewal process* described previously.

3.5 Immediate lane changing probability

In this section, we refine the *immediate lane-changing* models of Hoogendoorn (1999a), Helbing et al. (1999a) and Shvetsov and Helbing (1999) by including driver behavior. The application of the *gap-acceptance* model to the *ILC* process is shown in Figure 3.4.

In this situation a vehicle approaches a slower vehicle and intends to change lanes to either adjacent lane if available. The subject vehicle then seeks for an sufficient gap in its selected target lane and changes lanes immediately when an appropriate gap is found. If the preferred target lane (that is, the right lane in compliance with European driving rules) is failed, the subject vehicle will consider the other lane for a lane-change (that is, the left lane). If all of these choices are failed, the subject vehicle will stay in the current lane.

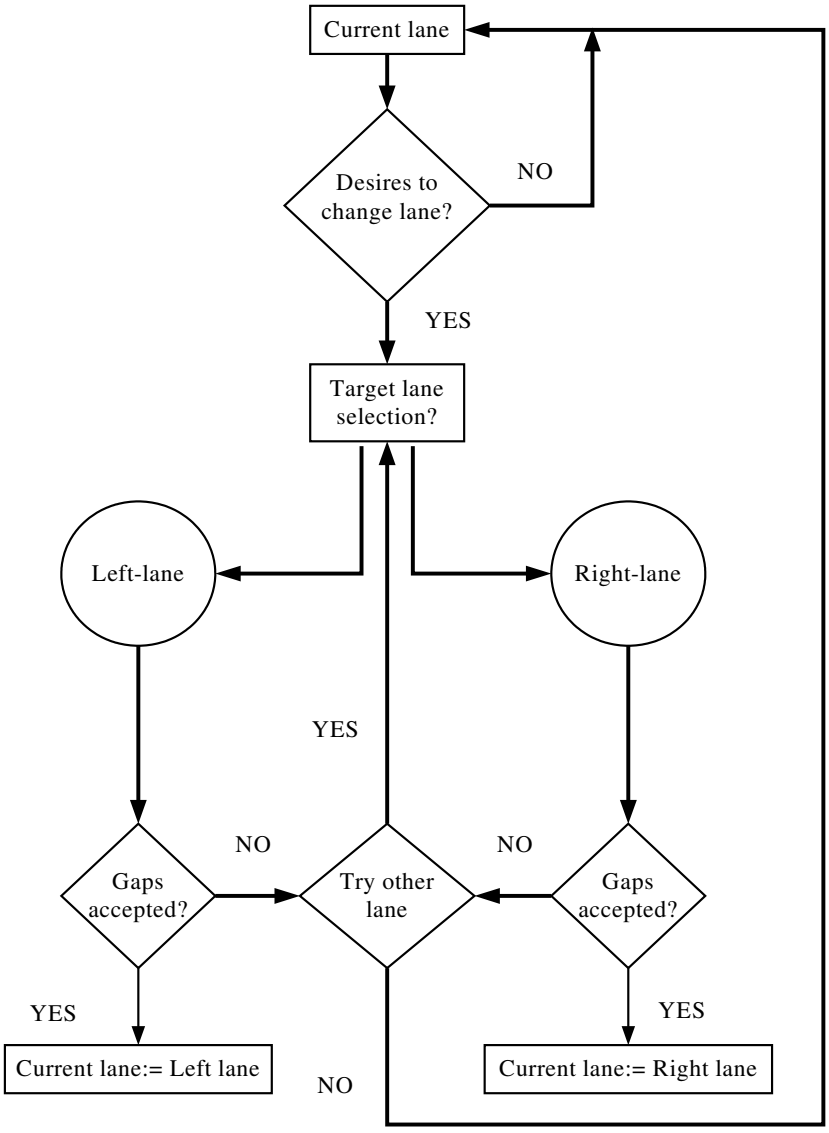

Figure 3.4: Structure of immediate lane-changing decision of a driver.

We rewrite equation 3.3 as follows:

$$P\left(\mathcal{A}^{u,s}\right) = \left[1 - \left\langle F_{lag}\left(d^{s}_{lag}(w)\right)\right\rangle_{w}\right]\left[1 - \left\langle F_{lead}\left(d^{u}_{lead}(v)\right)\right\rangle_{v}\right] \tag{3.22}$$

In equation 3.22 , $\langle \ldots \rangle_v$ denotes the mean operator with respect to speed v. By definition, the mean value of any function $\psi(x)$ ($x \in \mathbb{R}$) is determined by the following equation:

$$\langle \psi(x) \rangle_x = \int_{-\infty}^{+\infty} \psi(y) f(y) dy \tag{3.23}$$

Where $f(x)$ denotes the *p.d.f* of variable x.

In the context of the *immediate lane-changing* process (Figure 3.5), the follower in the selected target lane does not change lanes due to the lane-changing event. That is, the *lag-gap*

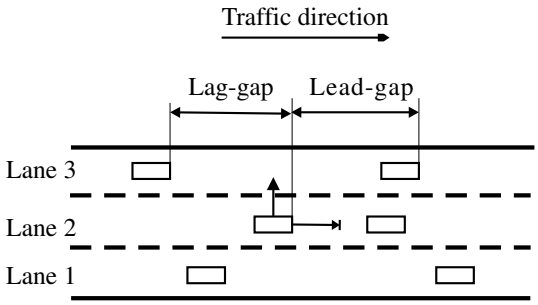

Figure 3.5: Immediate lane-changing on a multilane roadway

p.d.f in lane j for an *ILC* event is deduced from equation 3.6 as:

$$f_{lag,j}(h) = \gamma_j r_j \left(1 - F_j(h)\right) \tag{3.24}$$

From equations 3.4 and 3.24 we obtain the *c.d.f* of the *lead-gap* and the *lag-gap* for a lane-change as:

$$\begin{aligned} F_{lead}\left(d_{lead}^{u,i}(v)\right) &= \gamma_j r_j \int_0^{d_{lead}^{u,i}(v)} \left[1 - F_j(h)\right] dh \\ F_{lag}\left(d_{lag}^{s,j}(w)\right) &= \gamma_j r_j \int_0^{d_{lag}^{s,j}(w)} \left[1 - F_j(h)\right] dh \end{aligned} \tag{3.25}$$

Substituting expression 3.25 into equation 3.22 results in the probability that event $\mathcal{A}_{i,j}^{u,s}$ occurs:

$$\begin{aligned} P\left(\mathcal{A}_{i,j}^{u,s}\right) &= \left[1 - \langle \int_0^{d_{lead}^{u,i}(v)} f_{lead}^{u,j}(h)dh\rangle_v\right]\left[1 - \langle \int_0^{d_{lag}^{s,j}(w)} f_{lag}^{s,j}(h)dh\rangle_w\right] \\ &= \langle 1 - \int_0^{d_{lead}^{u,i}(v)} f_{lead}^{u,i}(h)dh\rangle_v \langle 1 - \int_0^{d_{lag}^{s,j}(w)} f_{lag}^{s,j}(h)dh\rangle_w \\ &= \langle \int_{d_{lead}^{u,i}(v)}^{\infty} f_{lead}^{u,i}(h)dh\rangle_v \langle \int_{d_{lag}^{s,j}(w)}^{\infty} f_{lag}^{s,j}(h)dh\rangle_w \\ &= \left(\gamma_j r_j\right)^2 \langle \int_{d_{lead}^{u,i}(v)}^{\infty} \left[1 - F_j(h)\right] dh\rangle_v \langle \int_{d_{lag}^{s,j}(w)}^{\infty} \left[1 - F_j(h)\right] dh\rangle_w \end{aligned} \tag{3.26}$$

Assumption of the exponential distribution of gaps results in:

$$\begin{aligned} P\left(\mathcal{A}_{i,j}^{u,s}\right) &= \langle exp\left(-\gamma_j r_j d_{lag}^{s,j}(w)\right)\rangle_w \langle exp\left(-\gamma_j r_j d_{lead}^{u,i}(v)\right)\rangle_v \\ &= \langle exp\left[-\gamma_j r_j \left(d_u^{min} + l_u + T_j^s w\right)\right]\rangle_w \\ &\quad \langle exp\left[-\gamma_j r_j \left(d_s^{min} + l_s + T_i^u v\right)\right]\rangle_v \\ &= exp\left[-\gamma_j r_j \left(d_u^{min} + l_u\right)\right] \langle exp\left(-\gamma_j r_j T_j^s w\right)\rangle_w \\ &\quad exp\left[-\gamma_j r_j \left(d_s^{min} + l_s\right)\right] \langle exp\left(-\gamma_j r_j T_i^u v\right)\rangle_v \end{aligned} \tag{3.27}$$

By substituting the Taylor expansion $e^x = \sum_0^\infty \frac{x^n}{n!}$ to equation 3.27 we get:

$$\begin{aligned} P\left(\mathcal{A}_{i,j}^{u,s}\right) &= exp\left[-\gamma_j r_j \left(d_u^{min} + l_u\right)\right] \sum_0^\infty \frac{(-1)^n (\gamma_j r_j T_j^s)^n}{n!} \langle w^n\rangle_w \\ &\quad exp\left[-\gamma_j r_j \left(d_s^{min} + l_s\right)\right] \sum_0^\infty \frac{(-1)^n (\gamma_j r_j T_i^u)^n}{n!} \langle v^n\rangle_v \end{aligned} \tag{3.28}$$

Let $M_k = \langle (v - V)^k \rangle$ denote the k^{th} moment of the speed distribution ($k \geq 2$) , the assumption of Gaussian speed distribution leads to $M_{2i+1} = 0$ ($i = 1, 2, \ldots$). Using the definition of mean values for speed V and speed variance Θ as $\langle v \rangle = V$ and $\langle (v - V)^2 \rangle = \Theta$, expansion of the k^{th} moment leads to:

$$\begin{aligned} &M_2 = \langle (v - V)^2 \rangle = \Theta \\ &M_3 = \langle (v - V)^3 \rangle = \langle v^3 \rangle - V^3 = 0 \\ &\ldots \\ &M_k = (v - V)^k \rangle = \langle v^k \rangle - V^k - 0.5k(k-1)V^{k-2}\Theta = 0 \end{aligned} \tag{3.29}$$

Hence:

$$\langle v^k \rangle = V^k + 0.5k(k-1)V^{k-2}\Theta \tag{3.30}$$

By substituting expression 3.30 into equation 3.28, after a straightforward algebraic calculation (see Appendix A), we end up with:

$$\begin{aligned} P(\mathcal{A}_{i,j}^{u,s}) &= e^{-\gamma_j r_j \left(d_s^{min} + l_s + T_i^u V_i^u\right)} \left[1 + 0.5\Theta_i^u \left(\gamma_j r_j T_i^u\right)^2\right] \\ &\quad e^{-\gamma_j r_j \left(d_u^{min} + l_u + T_j^s V_j^s\right)} \left[1 + 0.5\Theta_j^s \left(\gamma_j r_j T_j^s\right)^2\right] \end{aligned} \tag{3.31}$$

The probability that a vehicle of class u is able to change from lane i to adjacent lane j is:

$$p_{i,j}^{u} = \sum_{s \in U} \frac{r_j^s}{r_j} P(\mathcal{A}_{i,j}^{u,s}) P\left(\mathcal{C}_j^u\right) \tag{3.32}$$

From equations 3.31 and 3.32, we can see that the immediate lane-changing probability depends on the density in the adjacent lanes, the speeds and speed variances in the current lane and the adjacent lanes.

The lane changing probabilities determined by equation 3.32 is always decreasing with increasing density and belong strictly to [0, 1] as proven below:

- When traffic in the target lane is in an equilibrium state, that is, for example the density of lane j can well be equal to $r_j^e = 1/(d_0 + l + TV_j)$, the lane changing probability limits to:

$$\lim_{r_j \to r_j^e} (p_{i,j}) = \lim_{\gamma_j \to +\infty} (p_{i,j}) = 0 \tag{3.33}$$

  since $\lim_{x \to +\infty} \frac{x^m}{e^x} = 0$

- When traffic in the target lane is very dilute, that is the density of lane j can go to zero, the lane changing probability limits to:

$$\lim_{r_j \to 0} (p_{i,j}) = 1 \tag{3.34}$$

Because the lane-changing probability is monotonically decreasing with increasing density (Figure 3.6), $\lim_{r_j \to r_j^e} (p_{i,j}) \leq p_{i,j} \leq \lim_{r_j \to 0} (p_{i,j})$. Consequently, $p_{i,j}$ belongs strictly to [0,1]

3.6 Mandatory lane changing probability

According to Ahmed (1999), the so-called mandatory lane-changes exhibit different behavior compared to the immediate lane-changes presented in the previous section. Mandatory lane-changes often occur at bottlenecks and cause a major impact on road capacity due to the increase of traffic demand, which leads to traffic breakdown. In the remainder of this chapter, traffic dynamics at a merging zone, a diverging zone, and a weaving zone are discussed. Other bottlenecks such as lane-drops or road works, which are not discussed in this chapter, are comparable to bottlenecks at merging, diverging, and weaving zones.

The structure of a mandatory lane-changing process is shown in Figure 3.7, in which there is no target lane selection model. That is, vehicles are forced to change to a fixed target lane.

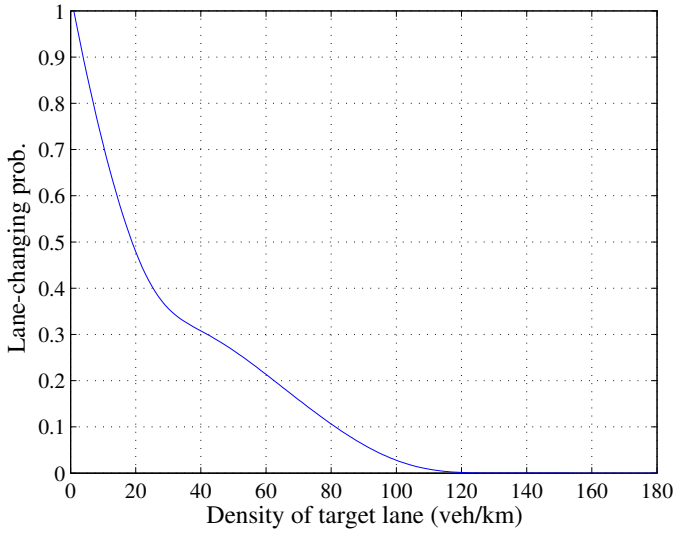

Figure 3.6: Immediate lane-changing probability as a decreasing function of density. The figure is plotted from equation 3.32 for aggregate vehicle class.

3.6.1 Merging probability

For causes of clarity, we assume that there is only one acceleration lane (but the derivation for a multilane ramp is straightforward by treating possible lane-changes between acceleration lanes as *immediate lane-changes*). Let us denote the lane index in decreasing order from the median lane I to the shoulder lane 1 and index 0 for the acceleration lane. To determine the *mandatory lane-changing* probability at location x and time instant t, we need to take into account the lane-changing rate from the shoulder lane to the median lane in order to give way to merging vehicles (see Figure 3.2(a)). Let Ω_1^u be the fraction of the vehicle class u in the shoulder lane which is willing to change to the adjacent lane (cooperative drivers) and let $p_{1,2}^u$ be the probability to do so. While the *lead-gap p.d.f* is determined by equation 3.4, the *lag-gap p.d.f* is determined by equation 3.6 in 3 situations as follows:

- If the following vehicle of class u in the shoulder lane is not willing to change to the adjacent lane (non-cooperative driver) with probability $(1 - \Omega_1^u)$, the total gap available for the merging event is h_n, and the *lag-gap p.d.f* is calculated by the following equation:

$$f_{lag,1}^u(h) = \frac{1 - F_1^u(h)}{\bar{h}} \tag{3.35}$$

- If the following vehicle of class u in the shoulder lane is willing to change to the adjacent lane (cooperative driver) with probability Ω_1^u and is able to do so, the total gap available for the merging event becomes $(h_n + h_{n-1})$, and the *lag-gap p.d.f* is calculated by the following equation:

$$f_{lag,2}^u(h) = \frac{1 - F_1^u(2h)}{2\bar{h}} \tag{3.36}$$

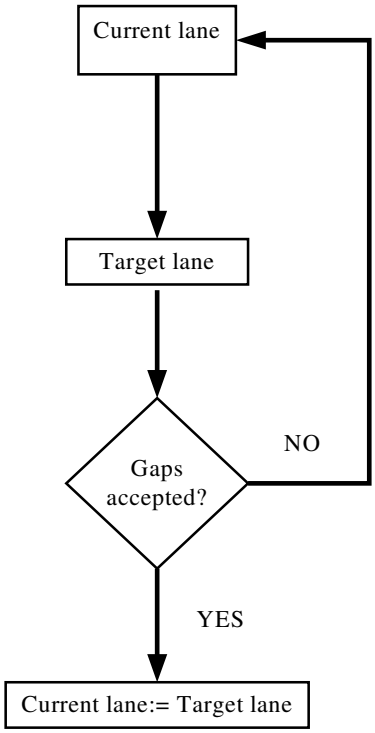

Figure 3.7: Structure of mandatory lane-changing decision of a driver.

- If the following vehicle of class u in the shoulder lane is willing to change to the adjacent lane (cooperative driver) with probability Ω_1^u but is unable to do so, the total gap available for the merging event remains h_n, and the *lag-gap p.d.f* is calculated by the following equation:

$$f_{lag,3}^u(h) = \frac{1 - F_1^u(h)}{\bar{h}} \tag{3.37}$$

From equations 3.35, 3.36 and 3.37 we obtain:

$$\begin{aligned} f_{lag}^u(h) &= \left(1 - \Omega_1^u\right) f_{lag,1}^u(h) + \Omega_1^u p_{1,2}^u f_{lag,2}^u(h) + \Omega_1^u \left(1 - p_{1,2}^u\right) f_{lag,3}^u(h) \\ &= \left(1 - \Omega_1^u p_{1,2}^u\right) \frac{1 - F_1^u(h)}{\bar{h}} + \Omega_1^u p_{1,2}^u \frac{1 - F_1^u(2h)}{2\bar{h}} \end{aligned} \tag{3.38}$$

and the *c.d.f* of the *lag-gap* on the shoulder lane for merging becomes:

$$\begin{aligned} F_{lag}^u\left(d_{lag}^{u,1}\right) &= \left(1 - \Omega_1^u p_{1,2}^u\right) \gamma_1 r_1 \int_0^{d_{lag}^{u,1}(w)} \left[1 - F_1^u(h)\right] dh \\ &+ 0.5 \Omega_1^u p_{1,2}^u \gamma_1 r_1 \int_0^{d_{lag}^{u,1}(w)} \left[1 - F_1^u(2h)\right] dh \end{aligned} \tag{3.39}$$

Hence, the probability that event $\mathcal{A}_{0,1}^{u,s}$ occurs becomes

$$\begin{aligned} & P\left(\mathcal{A}_{0,1}^{u,s}\right) = \left[1 - F_{lead}^{u}\left(d_{lead}^{u,1}\right)\right]\left[1 - F_{lag}^{s}\left(d_{lag}^{s,1}\right)\right] \\ & = \left(\gamma_1 r_1\right)^2 \langle \int_{d_{lead}^{u,0}(v)}^{\infty} \left[1 - F_1^u(h)\right] dh \rangle_v \\ & \langle \int_{d_{lag}^{s,1}(w)}^{\infty} \{\left(1 - \Omega_1^s p_{1,2}^s\right)\left[1 - F_1^s(h)\right] + 0.5\Omega_1^s p_{1,2}^s \left[1 - F_1^s(2h)\right]\} dh \rangle_w \end{aligned} \tag{3.40}$$

Given the gap distribution in the shoulder lane $F_1^u(h)$, the *c.d.f* $F_1^u(2h)$ is determined using the *Laplace* transform, and the merging probability (denoted by $\pi_{0,1}^u$ in order to distinguish from the immediate lane-changing probability $p_{i,j}^u$) is obtained as follows:

$$\begin{aligned} & \pi_{0,1}^u = \sum_{s \in U} \frac{r_1^s}{r_1} P\left(\mathcal{A}_{0,1}^{u,s}\right) \\ & = \left(\gamma_1\right)^2 r_1 \sum_{s \in U} r_1^s \langle \int_{d_{lead}^{u,0}(v)}^{\infty} \left[1 - F_1^s(h)\right] dh \rangle_v \\ & \langle \int_{d_{lag}^{s,1}(w)}^{\infty} \{\left(1 - \Omega_1^s p_{1,2}^s\right)\left[1 - F_1^s(h)\right] + 0.5\Omega_1^s p_{1,2}^s \left[1 - F_1^s(2h)\right]\} dh \rangle_w \end{aligned} \tag{3.41}$$

By applying equation 3.13 in formulae 3.39 for $n = 1$ and $n = 2$ the *lag-gap c.d.f* in the shoulder lane is determined as:

$$F_{lag}(d_{lag}^{u,1}) = 1 - e^{-\gamma_1 r_1 d_{lag}^{u,1}} - 0.5\Omega_1^u p_{1,2}^u \gamma_1 r_1 d_{lag}^{u,1} e^{-\gamma_1 r_1 d_{lag}^{u,1}} \tag{3.42}$$

Let $\Lambda_i^u = 0.5\Omega_i^u p_{i,i+1}^u \gamma_i r_i$, the probability that a vehicle of class u from the on–ramp finds an appropriate gap between vehicles regardless of class (denoted by s) in the shoulder lane is:

$$\begin{aligned} P(\mathcal{A}_{0,1}^{u,s}) &= \langle exp\left(-\gamma_1 r_1 d_{lead}^{u,0}(v)\right)\rangle_v \\ &\quad \langle exp\left(-\gamma r_1 d_{lag}^{s,1}(w)\right) + \Lambda_1^s d_{lag}^{s,1}(w) exp\left(-\gamma_1 r_1 d_{lag}^{s,1}(w)\right)\rangle_w \\ &= \langle exp\left[-\gamma_1 r_1\left(d_s^{min} + l_s + \mu(x) T_0^u v\right)\right]\rangle_v \\ &\quad \langle exp\left[-\gamma r_1\left(d_u^{min} + l_u + T_1^s w\right)\right]\left[1 + \Lambda_1^s\left(d_u^{min} + l_u + T_1^s w\right)\right]\rangle_w \\ &= exp\left[-\gamma_1 r_1\left(d_s^{min} + l_s\right)\right] \sum_0^{\infty} \frac{(-1)^n (\mu(x)\gamma_1 r_1 T_0^u)^n}{n!} \langle v^n \rangle_v \\ &\quad \{\left[1 + \Lambda_1^s\left(d_u^{min} + l_u\right)\right] exp\left[-\gamma_1 r_1\left(d_u^{min} + l_u\right)\right] \sum_0^{\infty} \frac{(-1)^n (\gamma_1 r_1 T_1^s)^n}{n!} \langle w^n \rangle_w \\ &+ \Lambda_1^s T_1^s \sum_0^{\infty} \frac{(-1)^n (\gamma_1 r_1 T_1^s)^n}{n!} \langle w^{n+1} \rangle_w\} \end{aligned} \tag{3.43}$$

If we substitute expression 3.30 into equation 3.43, after a lengthy but straightforward algebraic calculation (see Appendix A), we end up with:

$$\begin{aligned} & P(\mathcal{A}_{0,1}^{u,s}) = e^{-\gamma_1 r_1\left(d_s^{min} + l_s + \mu(x) T_0^u V_0^u\right)} e^{-\gamma_1 r_1\left(d_u^{min} + l_u + T_1^s V_1^s\right)} \left[1 + 0.5\Theta_0^u \left(\mu(x)\gamma_1 r_1 T_0^u\right)^2\right] \\ & \{\left[1 + \Lambda_1^s\left(d_u^{min} + l_u + T_1^s V_1^s\right)\right]\left[1 + 0.5\Theta_1^s\left(\gamma_1 r_1 T_1^s\right)^2\right] - \Lambda_1^s \gamma_1 r_1 (T_1^s)^2 \Theta_1^s\} \end{aligned} \tag{3.44}$$

Hence, the total merging probability for vehicle of class u is:

$$\pi_{0,1}^{u} = \sum_{s \in U} \frac{r_1^s}{r_1} e^{-\gamma_1 r_1 \left(d_s^{min} + l_s + \mu(x) T_0^u V_0^u\right)} \left[1 + 0.5\Theta_0^u \left(\mu(x)\gamma_1 r_1 T_0^u\right)^2\right] e^{-\gamma_1 r_1 \left(d_u^{min} + l_u + T_1^s V_1^s\right)}$$
$$\left\{\left[1 + \Lambda_1^s \left(d_u^{min} + l_u + T_1^s V_1^s\right)\right]\left[1 + 0.5\Theta_1^s \left(\gamma_1 r_1 T_1^s\right)^2\right] - \Lambda_1^s \gamma_1 r_1 (T_1^s)^2 \Theta_1^s\right\} \tag{3.45}$$

3.6.2 Diverging probability

It is straightforward to show that in the case of an off–ramp (Figure 3.2(b)), the diverging probability for vehicle of class u at location x and time instant t is determined by:

$$\pi_{1,0}^{u} = (\gamma_0)^2 r_0 \sum_{s \in U} r_0^s \langle \int_{d_{lead}^{u,1}(v)}^{\infty} \left[1 - F_0^s(h)\right] dh \rangle_v \langle \int_{d_{lag}^{s,0}(w)}^{\infty} \left[1 - F_0^s(h)\right] dh \rangle_w \tag{3.46}$$

Similar derivation as in the case of an on-ramp, we obtain:

$$\begin{aligned} \pi_{1,0}^{u} \;=\; & \sum_{s \in U} \frac{r_0^s}{r_0} e^{-\gamma_0 r_0 \left(d_s^{min} + l_s + \mu(x) T_1^u V_1^u\right)} \left[1 + 0.5\Theta_1^u \left(\mu(x)\gamma_0 r_0 T_1^u\right)^2\right] \\ & e^{-\gamma_0 r_0 \left(d_u^{min} + l_u + T_0^s V_0^s\right)} \left[1 + 0.5\Theta_0^s \left(\gamma_0 r_0 T_0^s\right)^2\right] \end{aligned} \tag{3.47}$$

From expression 3.45 and 3.47, we can see that the merging and diverging probability depend both on the traffic situation in the main carriageway and in the acceleration lane, such as density, mean speed, and mean speed variance. Furthermore, given traffic conditions in the target lane, it is rather straightforward to prove that the *mandatory lane-changing* probability decreases when drivers approach the end of the ramp. That is, $\pi_{i,j}^{u}$ is inversely proportional to $\mu(x)$. Consequently, drivers are more likely to merge/diverge when approaching the end of the ramp.

In Figure 3.8, we show a contour diagram of the merging probability, calculated at location $x = \frac{x_{end} - x_0}{2}$, with respect to the combination of the main carriageway flow rate and on–ramp flow rate. The figure is obtained from simulation results of the macroscopic traffic model proposed in Chapter 4.

In the developed model for lane-changing events, in addition to the gap distribution parameters, two other parameters are generated: the upper bound (μ_{max}) and lower bound (μ_{min}) for the *gap–acceptance* of the lane-changing vehicle in the merging and diverging zone. These parameters reflect the fact that the merging and diverging vehicles are willing to accept smaller gaps than in immediate lane-changing events, as a result of which they can disturb the traffic flow operations in the target lane more significantly.

In this section, we have only dealt with traffic interaction at on–and off–ramps. The lane–drops can also be modeled the same as in the case of merging. Cases where there is interaction between traffic that intends to exit a carriageway on the one hand, and other traffic that needs to enter that carriageway on the other hand (weaving) so far have not been covered. This restriction will be relaxed in the next section, where we model the *mandatory lane-changing* processes for weaving sections using the same approach as described above.

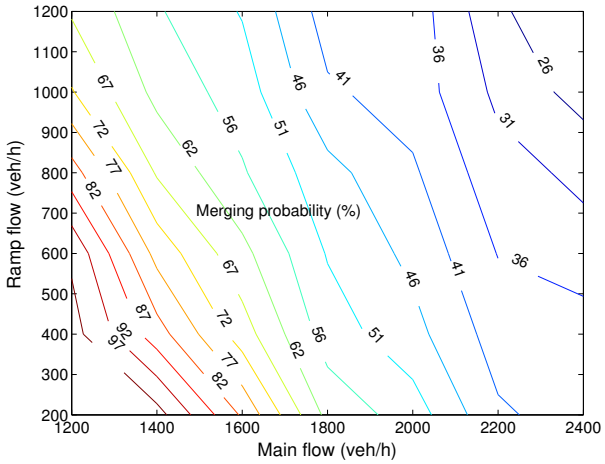

Figure 3.8: Contour diagram for the merging probability of on-ramp vehicle at the middle of the acceleration lane.

3.7 Weaving model

In the previous section, we determined the *mandatory lane-changing* probability for traffic flow at on– and off–ramps. This section deals with an extension of this model to describe traffic operations within weaving sections, where an on–ramp and an off–ramp are, as it where, combined. According to the Highway Capacity Manual (HCM2000 (2000)), weaving is defined as the crossing of several traffic streams moving on the freeway in the same direction. Due to the complexity of traffic interactions in a weaving area, weaving can lead to a significant capacity reduction, and, consequently, to a deterioration of the traffic operations. Thus, the importance of research, theory and modeling of the traffic operations at weaving sections of freeways is obvious .

In the 1970s, a research into the traffic operations in weaving areas was initiated in a U.S.' Highway Research Program to assess the capacity of freeways. In this study, an analytical method was developed by MacShane and Roess (1970) to model the lane-changing processes at weaving sections. Recently many researchers have been working on the capacity analysis of weaving sections and its dependence on the length of the weaving area. Makigami and Iizuka (1993) developed a method to evaluate the weaving traffic operation conditions and find a systematic way to determine the required weaving section length based on multiple merging probability theory. In this research, the weaving traffic considered only merging phenomena. Vermijs et al. (1995) used FOSIM (Freeway Operations SIMulation), a microscopic simulation model developed in the Netherlands for the section on symmetrical freeway weaving sections in the Dutch freeway capacity manual. Lately, Lertworawanich and Elefteriadou (2003) proposed a method to estimate the capacity of weaving sections based on a *gap-acceptance* theory and optimization technique. Almost all of the studies mentioned above use models at microscopic level and, therefore, require a large effort in calibration and validation. As a contribution to the research into traffic operations in weaving sections, in this thesis we aim to propose a continuum model to describe the traffic operations in weaving

sections. This is done by modeling the merging and diverging events occurring simultaneously in the same area, which are already a part of the gas-kinetic model presented in Section 3.4

3.7.1 Traffic dynamics at weaving section

In this section, a specific weaving section type (Figure 3.9) is considered in detail. In this type of weaving section (defined as type **B** according to HCM2000 (2000)), an on–ramp is connected with an off–ramp by an auxiliary lane.

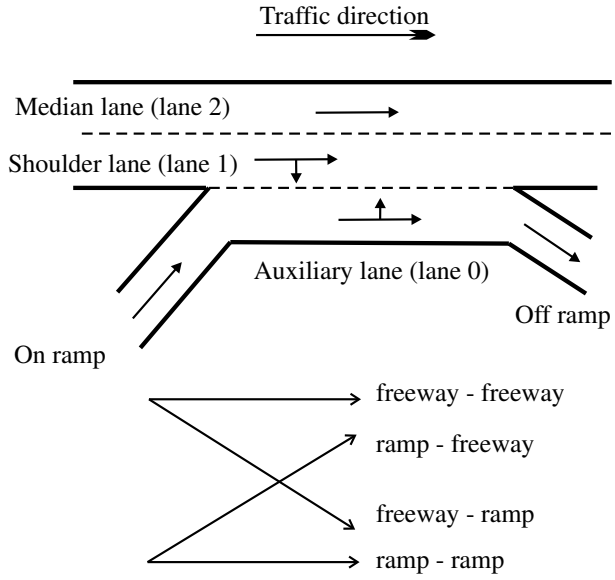

Figure 3.9: Layout of a weaving section.

Traffic operations within the considered weaving section include:

- Merging traffic from the on–ramp to the shoulder lane, specified by the fraction $\alpha^u_{0,1}$ (weaving flow).
- Diverging traffic from the shoulder lane to the off–ramp, specified by the fraction $\alpha^u_{1,0}$ (weaving flow).
- Through traffic in the shoulder lane with fraction $\alpha^u_{1,1}$ (non-weaving flow).
- Through traffic in the auxiliary lane (that is, traffic that continues from the on–ramp to the off–ramp) with fraction $\alpha^u_{0,0}$ (non-weaving flow).

Note $\alpha^u_{i,j}$ equals the ratio between the flow rate that intends to change from lane i to lane j and the total flow rate in lane i.

Obviously the merging and diverging probabilities depend on all of these traffic streams. The calculation methodology for merging and diverging probabilities is the same as in Section 3.6, for example, using the *gap-acceptance* model and *renewal theory*.

3.7.2 Merging probability

Let us consider a vehicle class u in the auxiliary lane trying to merge to the shoulder lane as shown in Figure 3.10. The decision to make a lane-change is based on the *gap-acceptance model*. As seen in Figure 3.10, there are four cases that may occur :

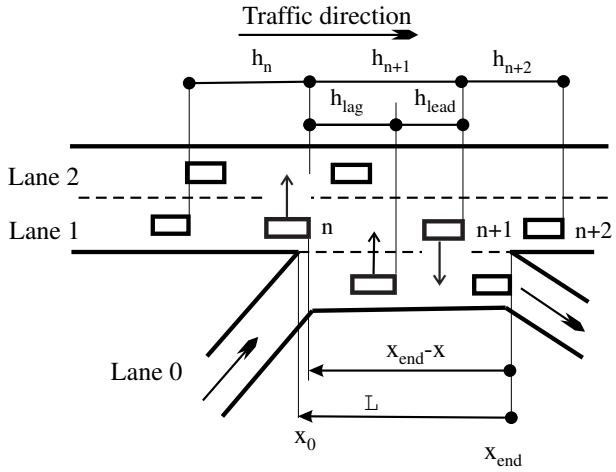

Figure 3.10: Merging process at a weaving section.

1. Case 1: In this case, both the follower and the leader are non-weaving vehicles. The probability that Case 1 occurs is $(\alpha^u_{1,1})^2$. There are two sub-cases:

   - Case 1.1: If the follower is willing to move to the adjacent lane in order to give way to a merging vehicle and is able to do so, the space available for merging is $(h_{n-1}+h_n)$. The probability that the follower finds a sufficient gap in the adjacent lane for a lane-change is calculated the same as in equation 3.31. Hence, in this case, the *c.d.f* of the *lag-gap* in the shoulder lane for merging is:

   $$F^u_{lag,1}\left(d^{u,1}_{lag}(w)\right) = 0.5\gamma_1 r_1 \int_0^{d^{u,1}_{lag}(w)} [1 - F^u_1(2h)]\, dh \tag{3.48}$$

   - Case 1.2: If the follower is unable to move to the adjacent lane in order to give way to a merging vehicle, the space available for merging remains h_n. The *lag-gap c.d.f* in the shoulder lane available for merging is determined as:

   $$F^u_{lag,2}\left(d^{u,1}_{lag}(w)\right) = \gamma_1 r_1 \int_0^{d^{u,1}_{lag}(w)} [1 - F^u_1(h)]\, dh \tag{3.49}$$

   With a summation of these two sub-cases we obtain the *lag-gap c.d.f* of vehicles of class u in the shoulder lane for Case 1 as:

   $$\begin{aligned} F^{u,1}_{lag}\left(d^{u,1}_{lag}(w)\right) &= \gamma_1 r_1 \{0.5\Omega^u_1 p^u_{1,2} \int_0^{d^{u,1}_{lag}(w)} [1 - F^u_1(2h)] \\ &+ \left(1 - \Omega^u_1 p^u_{1,2}\right) \int_0^{d^{u,1}_{lag}(w)} [1 - F^u_1(h)]\} dh \end{aligned} \tag{3.50}$$

2. Case 2: In this case, the follower is a weaving vehicle while its leader is a non-weaving vehicle. The probability that Case 2 occurs is $\alpha_{1,0}^{u}\alpha_{1,1}^{u}$. Because both vehicles in the shoulder lane do not change lanes at the moment of interaction, the space available for merging is h_n. Hence, the *lag-gap c.d.f* of vehicles of class u in the shoulder for Case 2 is determined as:

$$F_{lag}^{u,2}\left(d_{lag}^{u,1}(w)\right) = \gamma_1 r_1 \int_0^{d_{lag}^{u,1}(w)} \left[1 - F_1^u(h)\right] \tag{3.51}$$

3. Case 3: In this case, the follower is a non-weaving vehicle while the leader is a weaving vehicle. The probability that Case 3 occurs is $\alpha_{1,0}^{u}\alpha_{1,1}^{u}$. There are four sub-cases:

   - Case 3.1: If the follower is willing to move to the adjacent lane in order to give way to a merging vehicle and is able to do so, while the leader is able to move to the auxiliary lane immediately with probability $p_{1,0}$ when it finds a sufficient *lead-gap* in the auxiliary lane, the space available for merging is $(h_{n+1} + h_n + h_{n-1})$. Hence, in this case, the *c.d.f* of the *lag-gap* in the shoulder lane for merging is:

$$F_{lag,1}^{u}\left(d_{lag}^{u,1}\right) = \frac{1}{3}\gamma_1 r_1 \int_0^{d_{lag}^{u,1}(w)} \left[1 - F_1^u(3h)\right] dh \tag{3.52}$$

   - Case 3.2: If the follower is willing to move to the adjacent lane in order to give way to a merging vehicle and is able to do so, whereas the leader is unable to move to the auxiliary lane, the space available for merging is $(h_{n+1} + h_n)$. The *lag-gap c.d.f* for this sub-case is the same as equation 3.48
   - Case 3.3: If the follower is unable to move to the adjacent lane while the leader is able to move to the auxiliary lane, the space available for merging is $(h_n + h_{n-1})$. The *lag-gap c.d.f* for this sub-case is the same as equation 3.48
   - Case 3.4: If the follower is unable to move to the adjacent lane and the leader is unable to move to the auxiliary lane, the space available for merging now remains only h_n. The *lag-gap c.d.f* for this sub-case is the same as equation 3.49

   With a summation of these four sub-cases we obtain the *lag-gap c.d.f* of vehicles of class u in the shoulder lane for Case 3 as:

$$\begin{aligned}
F_{lag}^{u,3}\left(d_{lag}^{u,1}(w)\right) = \gamma_1 r_1 \{ & \frac{1}{3}\Omega_1^u p_{1,2}^u p_{1,0}^u \int_0^{d_{lag}^{u,1}(w)} \left[1 - F_1^u(3h)\right] \\
& + 0.5\Omega_1^u p_{1,2}^u \left(1 - p_{1,0}^u\right) \int_0^{d_{lag}^{u,1}(w)} \left[1 - F_1^u(2h)\right] \\
& + 0.5\left(1 - \Omega_1^u p_{1,2}^u\right) p_{1,0}^u \int_0^{d_{lag}^{u,1}(w)} \left[1 - F_1^u(2h)\right] \\
& + \left(1 - \Omega_1^u p_{1,2}^u\right)\left(1 - p_{1,0}^u\right) \int_0^{d_{lag}^{u,1}(w)} \left[1 - F_1^u(h)\right] \} dh
\end{aligned} \tag{3.53}$$

4. Case 4: In this case the follower and the leader are both weaving vehicles. The probability that Case 4 occurs is $(\alpha_{1,0}^{u})^2$. There are two sub-cases, which are as follows:

- Case 4.1: If the leader is able to move to the auxiliary lane with an immediate probability (that is, at the moment of interaction), the space available for merging is $(h_n + h_{n-1})$. The *lag-gap c.d.f* for this sub-case is calculated the same as in equation 3.48
- Case 4.2: If the leader is unable to move to the auxiliary lane, the space available for merging remains h_n. The *lag-gap c.d.f* for this sub-case is calculated the same as in equation 3.49

Summation of these two sub-cases leads to the *lag-gap c.d.f* of vehicles of class u in the shoulder lane for Case 4, thus:

$$\begin{aligned} F_{lag}^{u,4}\left(d_{lag}^{u,1}(w)\right) &= \gamma_1 r_1 \{0.5 p_{1,0}^u \int_0^{d_{lag}^{u,1}(w)} [1 - F_1^u(2h)] \\ &+ \left(1 - p_{1,0}^u\right) \int_0^{d_{lag}^{u,1}(w)} [1 - F_1^u(h)]\} dh \end{aligned} \tag{3.54}$$

From equations 3.50 to 3.54, we obtain the total *lag-gap c.d.f* of vehicles of class u in the shoulder lane for merging event as:

$$\begin{aligned} F_{lag}^u\left(d_{lag}^{u,1}(w)\right) &= (\alpha_{1,1}^u)^2 F_{lag}^{u,1}\left(d_{lag}^{u,1}(w)\right) + \alpha_{1,0}^u \alpha_{1,1}^u F_{lag}^{u,2}\left(d_{lag}^{u,1}(w)\right) \\ &+ \alpha_{1,0}^u \alpha_{1,1}^u F_{lag}^{u,3}\left(d_{lag}^{u,1}(w)\right) + (\alpha_{1,0}^u)^2 F_{lag}^{u,4}\left(d_{lag}^{u,1}(w)\right) \\ &= A_1^u \gamma_1 r_1 \int_0^{d_{lag}^{u,1}(w)} [1 - F_1^u(h)]\, dh \\ &+ B_1^u \gamma_1 r_1 \int_0^{d_{lag}^{u,1}(w)} [1 - F_1^u(2h)]\, dh \\ &+ C_1^u \gamma_1 r_1 \int_0^{d_{lag}^{u,1}(w)} [1 - F_1^u(3h)]\, dh \end{aligned} \tag{3.55}$$

Where

$$\begin{aligned} A_1^u &= \left(1 - \alpha_{1,1}^u \Omega_1^u p_{1,2}^u\right)\left(1 - \alpha_{1,0}^u p_{1,0}^u\right) \\ B_1^u &= 0.5[(\alpha_{1,1}^u)^2 \Omega_1^u p_{1,2}^u + \alpha_{1,1}^u \alpha_{1,0}^u \Omega_1^u p_{1,2}^u (1 - p_{1,0}^u) \\ &+ \alpha_{1,1}^u \alpha_{1,0}^u (1 - \Omega_1^u p_{1,2}^u) p_{1,0}^u + (\alpha_{1,0}^u)^2 p_{1,0}^u] \\ C_1^u &= \frac{1}{3} \alpha_{1,1}^u \alpha_{1,0}^u \Omega_1^u p_{1,2}^u p_{1,0}^u \end{aligned} \tag{3.56}$$

Given the gap distribution in the shoulder lane $F_1^u(h)$, the *c.d.f* $F_1^u(2h)$ and $F_1^u(3h)$ are determined using a *Laplace* transform, and the merging probability is obtained as follows:

$$\begin{aligned} &\tilde{\pi}_{0,1}^u = (\gamma_1)^2 r_1 \sum_{s \in U} r_1^s \langle \int_{d_{lead}^{u,0}(v)}^{\infty} [1 - F_1^s(h)]\, dh \rangle_v \\ &\langle \int_{d_{lag}^{s,1}(w)}^{\infty} \{A_1^s [1 - F_1^s(h)] + B_1^s [1 - F_1^s(2h)] + C_1^s [1 - F_1^s(3h)]\} dh \rangle_w \end{aligned} \tag{3.57}$$

By applying equation 3.13 in formulae 3.55 for $n = 1$, $n = 2$ and $n = 3$ the *lag-gap c.d.f* of vehicles of class u in the shoulder lane is determined as:

$$F_{lag}\left(d_{lag}^{u,1}\right) = 1 - e^{-\gamma_1 r_1 d_{lag}^{u,1}} - \tilde{A}_1^u d_{lag}^{u,1} e^{-\gamma_1 r_1 d_{lag}^{u,1}} - \tilde{B}_1^u \left(d_{lag}^{u,1}\right)^2 e^{-\gamma_1 r_1 d_{lag}^{u,1}} \tag{3.58}$$

Where

$$\begin{aligned}
\tilde{A}_1^u &= 0.5\left(\Omega_1^u p_{1,2}^u (1-\alpha_{1,0}^u)(1-\alpha_{1,0}^u p_{1,0}^u) + \alpha_{1,0}^u p_{1,0}^u\right)\gamma_1 r_1 \\
\tilde{B}_1^u &= \frac{1}{12}\alpha_{1,0}^u (1-\alpha_{1,0}^u)\Omega_1^u p_{1,2}^u p_{1,0}^u \left(\gamma_1 r_1\right)^2 \\
p_{1,0}^u &= e^{-\gamma_0 r_0 D^{u,1}}\left[1 + 0.5\Theta_0^s \left(\gamma_0 r_0 T_1^u\right)^2\right]
\end{aligned} \tag{3.59}$$

Hence, the average probability that a vehicle of class u finds a sufficient *lag-gap* between two vehicles of class s ($s \in U$) in the shoulder lane is:

$$\begin{aligned}
P\left(h > d_{lag}^{s,1}(w)\right) &= \langle e^{-\gamma_1 r_1 d_{lag}^{s,1}(w)}\rangle_w + \tilde{A}_1^s \langle d_{lag}^{s,1}(w) e^{-\gamma_1 r_1 d_{lag}^{s,1}(w)}\rangle_w \\
&+ \tilde{B}_1^s \langle \left(d_{lag}^{s,1}(w)\right)^2 e^{-\gamma_1 r_1 d_{lag}^{s,1}(w)}\rangle_w \\
&= e^{-\gamma_1 r_1\left(d_u^{min}+l_u\right)}\langle e^{-\gamma_1 r_1 T_1^s w}\rangle_w \\
&+ \tilde{A}_1^s \left(d_u^{min}+l_u\right) e^{-\gamma_1 r_1\left(d_u^{min}+l_u\right)}\langle e^{-\gamma_1 r_1 T_1^s w}\rangle_w \\
&+ \tilde{A}_1^s T_1^s e^{-\gamma_1 r_1\left(d_u^{min}+l_u\right)}\langle w e^{-\gamma_1 r_1 T_1^s w}\rangle_w \\
&+ \tilde{B}_1^s \left(d_u^{min}+l_u\right)^2 e^{-\gamma_1 r_1\left(d_u^{min}+l_u\right)}\langle e^{-\gamma_1 r_1 T_1^s w}\rangle_w \\
&+ 2\tilde{B}_1^s T_1^s \left(d_u^{min}+l_u\right) e^{-\gamma_1 r_1\left(d_u^{min}+l_u\right)}\langle w e^{-\gamma_1 r_1 T_1^s w}\rangle_w \\
&+ \tilde{B}_1^s \left(T_1^s\right)^2 e^{-\gamma_1 r_1\left(d_u^{min}+l_u\right)}\langle w^2 e^{-\gamma_1 r_1 T_1^s w}\rangle_w
\end{aligned} \tag{3.60}$$

After a lengthy but straightforward algebraic calculation (see Appendix A) we obtain the probability that a vehicle from the auxiliary lane finds an appropriate gap in the shoulder lane to merge:

$$\begin{aligned}
&P(\mathcal{A}_{0,1}^{u,s}) = e^{-\gamma_1 r_1\left(d_s^{min}+l_s+\mu(x)T_0^u V_0^u\right)}\left[1 + 0.5\Theta_0^u \left(\mu\gamma_1 r_1 T_0^u\right)^2\right] e^{-\gamma_1 r_1\left(d_u^{min}+l_u+T_1^s V_1^s\right)} \\
&\{\left[1 + \tilde{A}_1^s\left(d_u^{min}+l_u+T_1^s V_1^s\right) + \tilde{B}_s\left(d_u^{min}+l_u+T_1^s V_1^s\right)^2\right]\left(1 + 0.5\Theta_1^s\left(\gamma_1 r_1 T_1^s\right)^2\right) \\
&- \left[\tilde{A}_1^s \gamma_1 r_1 + 2\tilde{B}_1^s\left(d_u^{min}+l_u+T_1^s V_1^s\right) - \tilde{B}_1^s\right]\Theta_1^s \left(T_1^s\right)^2\}
\end{aligned} \tag{3.61}$$

and the merging probability of on-ramp vehicle:

$$\begin{aligned}
&\tilde{\pi}_{0,1}^u = \sum_{s\in U} \frac{r_1^s}{r_1} e^{-\gamma_1 r_1\left(d_s^{min}+l_s+\mu(x)T_0^u V_0^u\right)}\left[1 + 0.5\Theta_0^u \left(\mu\gamma_1 r_1 T_0^u\right)^2\right] e^{-\gamma_1 r_1\left(d_u^{min}+l_u+T_1^s V_1^s\right)} \\
&\{\left[1 + \tilde{A}_1^s\left(d_u^{min}+l_u+T_1^s V_1^s\right) + \tilde{B}_s\left(d_u^{min}+l_u+T_1^s V_1^s\right)^2\right]\left(1 + 0.5\Theta_1^s\left(\gamma_1 r_1 T_1^s\right)^2\right) \\
&- \left[\tilde{A}_1^s \gamma_1 r_1 + 2\tilde{B}_1^s\left(d_u^{min}+l_u+T_1^s V_1^s\right) - \tilde{B}_1^s\right]\Theta_1^s \left(T_1^s\right)^2\}
\end{aligned} \tag{3.62}$$

3.7.3 Diverging probability

Now let us consider a vehicle class u in the shoulder lane that intends to diverge to the auxiliary lane as shown in Figure 3.11. There are two cases that may occur :

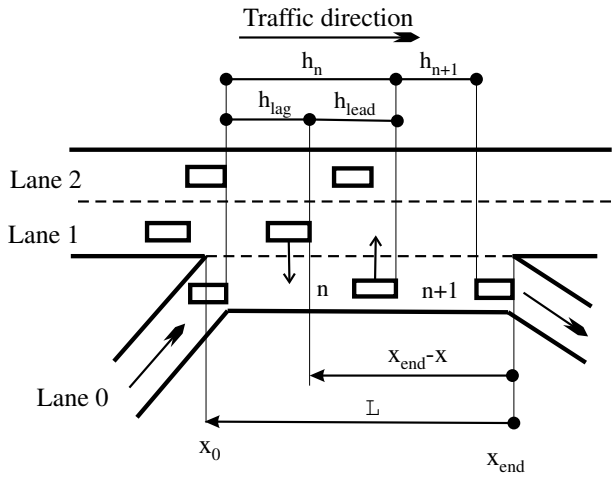

Figure 3.11: Diverging to the off-ramp.

1. Case 1: In this case, the leader doest not intend to weave. The probability that Case 1 occurs is $\alpha_{0,0}$. Then, the gap available for the diverging event is h_n. Hence, the *lag-gap c.d.f* in the ramp lane available for diverging is determined the same as in equation 3.51

2. Case 2: In this case, the leader is a weaving vehicle. The probability that Case 2 occurs is $(1 - \alpha_{0,0})$. There are two sub-cases that may occur:

   - Case 2.1: If the leader is unable to merge into the shoulder lane immediately with probability $(1 - p_{0,1})$, where $p_{0,1}$ is the probability to find a suitable *lead-gap* in the shoulder lane, the gap available for diverging remains h_n; hence, the *lag-gap c.d.f* in the ramp lane available for diverging is determined for this sub-case the same as in equation 3.49
   - Case 2.2: If the leader is able to merge into the shoulder lane immediately with probability $p_{0,1}$ the gap available for diverging becomes $(h_n + h_{n+1})$; hence, the *lag-gap p.d.f* in the auxiliary lane available for diverging is determined for this sub-case the same as in equation 3.48

   By a summation of these two sub-cases we obtain the *lag-gap c.d.f* of vehicles of class u in the auxiliary lane for Case 2 as:

$$\begin{aligned} F_{lag}^{u,2}\left(d_{lag}^{u,0}(v)\right) &= \gamma_0 r_0 \{0.5 p_{0,1}^{u} \int_0^{d_{lag}^{u,0}(v)} [1 - F_0^u(2h)] \\ &+ \left(1 - p_{0,1}^{u}\right) \int_0^{d_{lag}^{u,0}(v)} [1 - F_0^u(h)]\} dh \end{aligned} \tag{3.63}$$

From equations 3.51 and 3.63 we obtain:

$$\begin{aligned} F^u_{lag}\left(d^{u,0}_{lag}(v)\right) &= (1-\alpha^u_{0,1})F^{u,1}_{lag}\left(d^{u,0}_{lag}(v)\right) + \alpha^u_{0,1}F^{u,2}_{lag}\left(d^{u,0}_{lag}(v)\right) \\ &= \left(1-\alpha^u_{0,1}p^u_{0,1}\right)\gamma_0 r_0 \int_0^{d^{u,0}_{lag}(v)} \left[1-F^u_0(h)\right]dh \\ &+ 0.5\alpha^u_{0,1}p^u_{0,1}\gamma_0 r_0 \int_0^{d^{u,0}_{lag}(v)} \left[1-F^u_0(2h)\right]dh \end{aligned} \tag{3.64}$$

Given the gap distribution for the auxiliary lane $F^u_0(h)$, the *c.d.f* $F^u_0(2h)$ is determined using a *Laplace* transform, and the diverging probability is obtained as follows:

$$\begin{aligned} &\tilde{\pi}^u_{1,0} = (\gamma_0)^2 r_0 \sum_{s\in U} r^s_0 \langle \int_{d^{u,1}_{lead}(v)}^{\infty} \left[1-F^s_0(h)\right]dh\rangle_v \\ &\langle \int_{d^{s,0}_{lag}(w)}^{\infty} \{\left(1-\alpha^s_{0,1}p^s_{0,1}\right)\left[1-F^s_0(h)\right] + 0.5\alpha^s_{0,1}p^s_{0,1}\left[1-F^s_0(2h)\right]\}dh \end{aligned} \tag{3.65}$$

By applying equation 3.13 in formulae 3.64 for $n=1$ and $n=2$ the *lag-gap c.d.f* of vehicles of class u in the auxiliary lane is determined as:

$$F^u_{lag}\left(d^{u,0}_{lag}(v)\right) = 1 - e^{-\gamma_0 r_0 d^{u,0}_{lag}(v)} - \tilde{C}^u_0 d^{u,0}_{lag} e^{-\gamma_0 r_0 d^{u,0}_{lag}(v)} \tag{3.66}$$

Where

$$\begin{aligned} &\tilde{C}^u_0 = 0.5\alpha^u_{0,1}p^u_{0,1}\gamma_0 r_0 \\ &p^u_{0,1} = e^{-\gamma_1 r_1 D^{u,0}}\left[1+0.5\Theta^u_1\left(\gamma_1 r_1 T_0 u\right)^2\right] \end{aligned} \tag{3.67}$$

Hence, the average probability for a vehicle from the shoulder lane to find a sufficient *lag-gap* in the auxiliary lane is:

$$\begin{aligned} P\left(h > d^{s,0}_{lag}(w)\right) &= \langle e^{-\gamma_0 r_0 d^{s,0}_{lag}(w)}\rangle_w + \tilde{C}^s_0\langle d^{s,0}_{lag}(w) e^{-\gamma_0 r_0 d^{s,0}_{lag}(w)}\rangle_w \\ &= e^{-\gamma_0 r_0\left(d^{min}_u + l_u\right)}\langle e^{-\gamma_0 r_0 T^s_0 w}\rangle_w \\ &+ \tilde{C}^s_0\left(d^{min}_u + l_u\right)e^{-\gamma_0 r_0\left(d^{min}_u + l_u\right)}\langle e^{-\gamma_0 r_0 T^s_0 w}\rangle_w \\ &+ \tilde{C}^s_0 T^s_0 e^{-\gamma_0 r_0\left(d^{min}_u + l_u\right)}\langle w e^{-\gamma_0 r_0 T^s_0 w}\rangle_w \end{aligned} \tag{3.68}$$

By applying the same derivation as used for the calculation of the merging probability, we obtain the diverging probability as:

$$\begin{aligned} &\tilde{\pi}^u_{1,0} = \sum_{s\in U}\frac{r^s_0}{r_0} e^{-\gamma_0 r_0\left(d^{min}_s + l_s + \mu(x)T^u_1 V^u_1\right)}\left[1+0.5\Theta^u_1\left(\mu\gamma_0 r_0 T^u_1\right)^2\right] e^{-\gamma_0 r_0\left(d^{min}_u + l_u + T^s_0 V^s_0\right)} \\ &\{\left[1+\tilde{C}^s_0\left(d^{min}_u + l_u + T^s_0 V^s_0\right)\right]\left[1+0.5\Theta^s_0\left(\gamma_0 r_0 T^s_0\right)^2\right] - 0.5\tilde{C}^s_0\gamma_0 r_0\Theta^s_0\left(T^s_0\right)^2\} \end{aligned} \tag{3.69}$$

The *immediate lane–changing* and *mandatory lane–changing* probabilities are used to calculate the corresponding rates in the gas-kinetic model for interrupted traffic streams presented in Section 3.4.

3.8 Summary

In this chapter, we established a *MLMC* gas-kinetic model that describes the dynamics of traffic flow for interrupted freeways which include on–ramps, off–ramps, or a combinations of these (weaving sections).

In the model, the discontinuities due to traffic exiting and entering the freeways were described microscopically through the so-called *mandatory lane-changing* processes, which were determined from a *gap-acceptance* model and from *renewal theory*. While the former is used to calculate the probability to find an appropriate gap (namely, the *lead-gap* and the *lag-gap*) for making a lane-change, the latter is used to determine the distributions of these gaps. This approach was then extended to the calculation of the lane-changing probabilities within weaving sections, which connect an on–ramp and off–ramp with an auxiliary lane. In such a weaving area, the interaction of the merging flow and diverging flow plays an important role in the traffic operations of the main carriageway.

One of the main improvements of the developed model over existing approaches is the refinement of the immediate lane-changing probability, which, so far, has often been oversimplified in other continuum models. It has been shown that the derived probabilities converge into a region of physical values $[0, 1]$ with respect to different traffic conditions. For analytical purposes of this chapter, we have assumed that the gaps are exponentially distributed. However, the *mandatory lane-changing* rates can be solved numerically as long as the gap distributions are known.

We have argued that the proposed gas-kinetic model can deal in detail with the interactions among merging flow, diverging flow and the main flow . In the new model, the give-way behavior of the vehicles in the shoulder lane (namely, changing a lane to the left) is taken into account explicitly. Due to this behavior, the *spontaneous lane-changing* rate between the shoulder lane and the median lane also increases near on–ramps. Moreover, the model also considers the willingness to accept smaller gaps by merging and diverging drivers when approaching the end of a ramp, which, consequently, can disturb traffic flow in the target lane more significantly than in the case of an immediate lane-changing event. In the derived model, interactions between user classes in lane-changing processes are taken into account through user specific reaction time, which contributes among the others significantly to lane-changing probabilities.

The derived gas-kinetic model enables the development of a *MLMC* macroscopic model for interrupted traffic flow dynamics. This will be shown in the next chapter.

Chapter 4

Generalized *MLMC* macroscopic model for interrupted traffic flow

This chapter will establish a macroscopic model for interrupted traffic streams. The derivation is based on the gas-kinetic model developed in Chapter 3, and uses the *method of moments* presented in Chapter 2 to derive the macroscopic model from the mesoscopic one. That is:

$$\int_0^\infty \text{gas-kinetic model} \;\; dv \rightarrow \text{macroscopic model}$$

Compared to the gas-kinetic model, the macroscopic model is more suitable for theoretical and numerical analysis of traffic phenomena and real-time application in traffic control. The derivation of macroscopic traffic flow models from gas-kinetic traffic models using the *method of moments* has been applied by many researchers such as Leutzbach (1988), Helbing (1997a), Hoogendoorn (1999a), Hoogendoorn and Bovy (1999b), and so on. With the application of the *method of moments* we can obtain the equations for the dynamics of density (first order), mean speed (second order), speed variance (third order), etcetera. These equations are often of a hyperbolic type which can be solved by a number of dedicated numerical solutions (Chapter 5).

This chapter will show that the proposed model is able to replicate congested traffic states as other macroscopic models are able to do so. Furthermore, we will prove that the developed model can show analytically the impact of acceleration lane length on congested traffic patterns, which has been neglected in the current macroscopic models. That is, in the proposed model the acceleration lane length acts as a 'distributor' of disturbances caused by traffic from the on–ramp over the acceleration lane.

The outline of this chapter is as follows. The link between phase space density and the macroscopic traffic variables is described in Section 4.1. Section 4.2 briefly presents the application of the *method of moments* for the *MLMC* gas-kinetic traffic flow model. In Section 4.3 we describe the *MLMC* continuum model for an interrupted traffic stream. In Section 4.4 we show the properties of the developed model in simulating congested traffic states for different traffic demands and on-ramp flows, as well as with different ramp-lengths. Section

4.5 analytically derives the impact of the acceleration lane length on the dynamics of the traffic flow based on a linear stability method. Section 4.6 summarizes this chapter.

4.1 Derivation of macroscopic traffic variables

Since the aim of this thesis is to formulate equations that describe the dynamics of macroscopic *MLMC* traffic flow variables, this section establishes the relation between the phase space density and macroscopic traffic variables.

The macroscopic traffic flow variables are categorized into a so-called *conservative* and *primitive* type. The latter type reflects directly observable macroscopic quantities of the traffic flow, such as speed and speed variance, whereas the former type describes the state of the collective flow, such as density and flow rate. The conservative traffic variables reflect the conservative nature of the variables. That is, only the convective process is considered. Traffic density and flow rate are conserved. Although the conservative type is violated due to interaction (the acceleration and deceleration process), its use yields advantages in establishing the macroscopic continuum equations from the gas-kinetic equation developed in Chapter 3 and in deriving numerical solutions for these equations (see Chapter 5).

By definition, the macroscopic traffic variables for a *MLMC* traffic flow are:

- A lane and class specific density ($r_i^u(x,t)$). Let $f(x,v,t)$ denote the probability density function of speed v, the density is defined by: $\rho_i^u(x,v,t) = f(x,v,t)r_i^u(x,t)$. If we take the integral of this relation over the speed v we have
  $\int_0^\infty \rho_i^u(x,v,t)dv = r_i^u(x,t)\int_0^\infty f(x,v,t)dv$.
  By definition, $\int_0^\infty f(x,v,t)dv = 1$; hence:

$$r_i^u(x,t) = \int_0^\infty \rho_i^u(x,v,t)dv \tag{4.1}$$

- A lane and class specific speed ($V_i^u(x,t)$). The mean speed V is defined as $V = \langle v \rangle = \int_0^\infty v f(x,v,t)dv$; hence:

$$V_i^u(x,t) = \frac{1}{r_i^u(x,t)}\int_0^\infty \rho_i^u(x,v,t)vdv \tag{4.2}$$

- A lane and class specific speed variance ($\Theta_i^u(x,t)$). The speed variance Θ is defined as $\Theta = \langle (v-V)^2 \rangle$; hence:

$$\Theta_i^u(x,t) = \frac{1}{r_i^u(x,t)}\int_0^\infty \rho_i^u(x,v,t)(v-V_i^u)^2dv \tag{4.3}$$

- Let $V_{i,u}^{\pm}(x,t)$ denote the mean speed of vehicle class u entering lane i (with a plus sign) or exiting from lane i (with a minus sign) respectively at location x and time instant t. The following relation is applied:

$$V_{i,u}^{\pm}(x,t) = \langle v \rangle_{i,u}^{\pm} \tag{4.4}$$

- A lane and class specific traffic flow rate ($q_i^u(x,t)$) is deduced as:

$$q_i^u = r_i^u V_i^u \tag{4.5}$$

4.2 Method of moments

This section presents the application of the *method of moments* for the derivation of the macroscopic model from the gas-kinetic model developed in Chapter 3. Accordingly, we multiply both sides of equation 3.17 with v^k ($k = 0, 1, 2, \ldots$), then integrate them over the range of speed $v \in [0, \infty)$. That is:

$$\begin{aligned} &\frac{\partial}{\partial t}\int_0^\infty \rho_i^u v^k dv + \frac{\partial}{\partial x}\int_0^\infty \rho_i^u v^{k+1} dv + \frac{\partial}{\partial v}\int_0^\infty \left(\rho_i^u \frac{v^k V_i^{u,max} - v^{k+1}}{\tau_i^u}\right) dv = \\ &\int_0^\infty \left[\left(\frac{\partial \rho_i^u v^k}{\partial t}\right)_{int} + \left(\frac{\partial \rho_i^u v^k}{\partial t}\right)_{lc}^{int} + \left(\frac{\partial \rho_i^u v^k}{\partial t}\right)_{lc}^{spon} + \left(\frac{\partial \rho_i^u v^k}{\partial t}\right)_{lc}^{man}\right] dv \end{aligned} \tag{4.6}$$

Let $m_{i,k}^u(x,t) = \int_0^\infty \rho_i^u(x,v,t) v^k dv = r_i^u \langle v^k \rangle_i$ and $m_{i,k}^{u,0}(x,t) = r_i^u V_i^{u,max} \langle v^{k-1} \rangle_i$. The *LHS* of equation 4.6 then becomes:

$$\begin{aligned} &\frac{\partial}{\partial t}\int_0^\infty \rho_i^u v^k dv + \frac{\partial}{\partial x}\int_0^\infty \rho_i^u v^{k+1} dv + \frac{\partial}{\partial v}\int_0^\infty \left(\rho_i^u \frac{v^k V_i^{u,max} - v^{k+1}}{\tau_i^u}\right) dv \\ = \;& \frac{\partial m_{i,k}^u}{\partial t} + \frac{\partial m_{i,k+1}^u}{\partial x} - k\int_0^\infty \left(\rho_i^u \frac{v^{k-1} V_i^{u,max} - v^k}{\tau_i^u}\right) dv \\ = \;& \frac{\partial m_{i,k}^u}{\partial t} + \frac{\partial m_{i,k+1}^u}{\partial x} + k\frac{m_{i,k}^u - m_{i,k}^{u,0}}{\tau_i^u} \end{aligned} \tag{4.7}$$

For the *RHS* of equation 4.6, all the first three terms were already described in Chapter 2. The last term is determined below:

$$\int_0^\infty \left(\frac{\partial \rho_i^u v^k}{\partial t}\right)_{lc}^{man} dv = \nu_{i,u}^+(x,t)\langle v^k \rangle_i^+ + \nu_{i,u}^-(x,t)\langle v^k \rangle_i^- \tag{4.8}$$

Where

$$\begin{aligned} \nu_{i,u}^{\pm}(x,t) &= \int_0^\infty \tilde{\nu}_{i,u}^{\pm}(x,v,t) dv \\ \langle v^k \rangle_{i,u}^{\pm} &= \int_0^\infty \frac{\tilde{\nu}_{i,u}^{\pm}(x,v,t)}{\nu_{i,u}^{\pm}(x,t)} v^k dv \end{aligned} \tag{4.9}$$

From the obtained results, we come up with a *MLMC* macroscopic model for interrupted traffic stream when we set $k = 0$ for the first order model, $k = 1$ for the second order model, or an even higher order model if $k = 2$. In the next section, we present equations for the dynamics of density, flow rate, and/or mean speed.

4.3 *MLMC* macroscopic traffic model for interrupted freeways

This section describes the equations for the dynamics of traffic density and flow rate (conservative variables) for interrupted freeways. Third order models have not yet shown superior performance in describing traffic dynamics compared to second order models, which made, for example, Helbing et al. (1999a) return to the latter type. Therefore, this chapter only focuses on the second order model type, and the system is closed by assuming that the speed variance is a pre-determined function of speed and density. By substituting expressions 4.1–4.5 into the *RHS* of equation 4.7 for $k = 0$ and $k = 1$, we obtain the corresponding expressions for density and speed momentum dynamics as described in equation 4.10 and equation 4.11, respectively.

In equation 4.10 and equation 4.11, the interaction rate $\Pi_i^{u,s}$ between vehicles of class u and vehicles of class s in lane i is calculated by equation 2.55 in Chapter 2. $\alpha_{i,i-1}^u$ is the fraction of vehicles of class u exiting the freeway at an off–ramp or weaving section. At these 'exit areas', $\alpha_{i,i-1}^u \pi_{i,i-1}^u$ denotes the probability that vehicles of class u in the shoulder lane have exited to the acceleration lane or the auxiliary lane, and $\left(1 - \alpha_{i,i-1}^u\right) p_{i,i+1}^u$ denotes the probability that those vehicles have changed lanes to the left on the main carriageway. Consequently, the probability that vehicles of class u remain in the shoulder lane is $1 - \alpha_{i,i-1}^u \pi_{i,i-1}^u - \left(1 - \alpha_{i,i-1}^u\right) p_{i,i+1}^u$, which contributes to the *braking* term in equation 4.11.

The set of equations 4.10 and 4.11 are of a hyperbolic type and can be solved using a number of numerical solutions presented in Chapter 5.

Conservation law ($k = 0$)

$$\begin{aligned} \frac{\partial r_i^u}{\partial t} + \underbrace{\frac{\partial q_i^u}{\partial x}}_{\text{convection}} &= \underbrace{\sum_{s \in U} \sum_{j=i\pm1} \left(p_{j,i}^u \Psi_j^{u,s} - p_{i,j}^u \Psi_i^{u,s} \right)}_{\text{immediate lane-changing}} \\ &+ \underbrace{\sum_{j=i\pm1} \left(\triangle_{j,i}^u r_j^u - \triangle_{i,j}^u r_i^u \right)}_{\text{spontaneous lane-changing}} \\ &+ \underbrace{\nu_{i,u}^+(x,t) + \nu_{i,u}^-(x,t)}_{\text{mandatory lane-changing}} \end{aligned} \tag{4.10}$$

Momentum dynamics ($k = 1$)

$$\begin{aligned}
\frac{\partial q_i^u}{\partial t} + \underbrace{\frac{\partial r_i^u \left[(V_i^u)^2 + \Theta_i^u\right]}{\partial x}}_{\text{convection}} &= \underbrace{\frac{r_i^u V_i^{u,max} - q_i^u}{\tau_i^u}}_{\text{relaxation}} \\
&- \underbrace{\left[1 - \alpha_{i,i-1}^u \pi_{i,i-1}^u - \left(1 - \alpha_{i,i-1}^u\right) p_{i,i+1}^u\right] \sum_{s \in U} \Pi_i^{u,s}}_{\text{braking}} \\
&+ \underbrace{\sum_{s \in U} \sum_{j=i\pm 1 J} \left(p_{j,i}^u \Phi_j^{u,s} - p_{i,j}^u \Phi_i^{u,s}\right)}_{\text{immediate lane-changing}} \\
&+ \underbrace{\sum_{j=i\pm 1} \left(\triangle_{j,i}^u q_j^u - \triangle_{i,j}^u q_i^u\right)}_{\text{spontaneous lane-changing}} \\
&+ \underbrace{\nu_{i,u}^+(x,t) V_{i,u}^+ + \nu_{i,u}^-(x,t) V_{i,u}^-}_{\text{mandatory lane-changing}} \qquad (4.11)
\end{aligned}$$

The *mandatory lane–changing* rate is determined for different situations such as at on–ramps, off–ramps, and weaving sections:

- In the case of an on–ramp:

$$\begin{aligned}
\nu_{i,u}^+(x,t) &= (-1)^{i+1} \frac{\delta(x)}{L} \pi_{0,1}^u(x,t) \int_0^\infty \rho_0^u(x,v,t) v dv \\
&= (-1)^{i+1} \frac{\delta(x)}{L} \pi_{0,1}^u(x,t) q_0^u(x,t) \qquad (4.12)
\end{aligned}$$

- In the case of an off–ramp:

$$\begin{aligned}
\nu_{i,u}^-(x,t) &= (-1)^{i} \frac{\delta(x)}{L} \pi_{1,0}^u(x,t) \alpha_{1,0}^u \int_0^\infty \rho_1^u(x,v,t) v dv \\
&= (-1)^{i} \frac{\delta(x)}{L} \pi_{1,0}^u(x,t) \alpha_{1,0}^u q_1^u(x,t) \qquad (4.13)
\end{aligned}$$

- In the case of a weaving section:

$$\begin{aligned}
\nu_{i,u}^+(x,t) &= (-1)^{i+1} \frac{\delta(x)}{L} \tilde{\pi}_{0,1}^u(x,t) \alpha_{0,1}^u \int_0^\infty \rho_0^u(x,v,t) v dv \\
&= (-1)^{i+1} \frac{\delta(x)}{L} \tilde{\pi}_{0,1}^u(x,t) \alpha_{0,1}^u q_0^u(x,t) \\
\nu_{i,u}^-(x,t) &= (-1)^{i} \frac{\delta(x)}{L} \tilde{\pi}_{1,0}^u(x,t) \alpha_{1,0}^u \int_0^\infty \rho_1^u(x,v,t) v dv \\
&= (-1)^{i} \frac{\delta(x)}{L} \tilde{\pi}_{1,0}^u(x,t) \alpha_{1,0}^u q_1^u(x,t) \qquad (4.14)
\end{aligned}$$

Equation 4.11 can also be reformulated in the so-called *primitive* form, as presented below:

Speed dynamics

$$
\begin{aligned}
r_i^u \frac{\partial V_i^u}{\partial t} + r_i^u V_i^u \frac{\partial V_i^u}{\partial x} &= -\frac{\partial r_i^u \Theta_i^u}{\partial x} + \frac{r_i^u V_i^{u,max} - q_i^u}{\tau_i^u} \\
&- \left[1 - \alpha_{i,i-1}^u \pi_{i,i-1}^u - \left(1 - \alpha_{i,i-1}^u\right) p_{i,i+1}^u\right] \sum_{s \in U} \Pi_i^{u,s} \\
&+ \sum_{s \in U} \sum_{j=i\pm1} \left[p_{j,i}^u \left(\Phi_j^{u,s} - V_i^u \Psi_i^u\right) - p_{i,j}^u \left(\Phi_i^{u,s} - V_i^u \Psi_i^u\right)\right] \\
&+ \sum_{j=i\pm1} \triangle_{j,i}^u \left(q_j^u - r_j^u V_i^u\right) \\
&+ \nu_{i,u}^+(x,t) \left(V_{i,u}^+ - V_i^u\right) + \nu_{i,u}^-(x,t) \left(V_{i,u}^- - V_i^u\right) \qquad (4.15)
\end{aligned}
$$

In equation 4.15, the term $\nu_{i,u}^+(x,t) \left(V_{i,u}^+ - V_i^u\right)$ or $\nu_{i,u}^-(x,t) \left(V_{i,u}^- - V_i^u\right)$ results in speed adaptation of traffic from the on–ramp to the main carriageway, or of traffic from the main carriageway to the off–ramp, respectively.

Vehicle balance condition

The vehicle balance condition at merging and/or diverging areas is given as below:

$$\int_{x_0}^{x_{end}} \nu_{i,u}^{\pm}(x,t)dx = \text{merging/diverging flow} \qquad (4.16)$$

In case of merging, we have:

$$\int_{x_0}^{x_{end}} \nu_{i,u}^{\pm}(x,t)dx = \int_{x_0}^{x_{end}} \frac{\delta(x)}{L} \pi_{0,1}^u(x,t) q_0^u(x,t)dx \qquad (4.17)$$

In an ideal condition, when all on–ramp vehicles can merge into the main carriageway, we have $\pi_{0,1}^u(x,t) = 1$ and $q_0^u(x,t) = q_0^u(t)$; hence:

$$\int_{x_0}^{x_{end}} \nu_{i,u}^{\pm}(x,t)dx = q_0^u(t) \int_{x_0}^{x_{end}} \frac{\delta(x)}{L} dx = q_0^u(t) \qquad (4.18)$$

which satisfies the aforementioned vehicle balance condition.

The derived *MLMC* macroscopic model for interrupted traffic flow refines the generalized model of Hoogendoorn (1999a) by including driver behavior (that is, *gap-acceptance model*) in immediate lane-changing process. At discontinuities the derived model demonstrates plausible behavior characteristics and takes into account explicitly the impact of road design (that is, acceleration lane length) on the driving behavior. Interactions between user classes are modeled through user specific reaction time, which contributes among the others significantly to the lane-changing probabilities. In the next sections we show qualitatively and quantitatively the properties of the derived model.

4.4 Model performance

It is expected that the proposed model is able to replicate the congested traffic states, such as, moving localized clusters, stop–and–go waves, and homogeneous jams, which have been discussed in Treiber et al. (2000) and Helbing et al. (2002). Furthermore, the simulation results will show the influence of acceleration lane length on the dynamics of the main traffic flow, to be analyzed mathematically in Section 4.5.

Before model performance is covered in detail, let us briefly discuss the empirical features of a number of main congested traffic states (Treiber et al. (2000) and Helbing et al. (2002)) that will be reproduced by our model:

- Pinned Localized Cluster: this congested pattern is characterized by a localized reduction of speed with a high density. It often occurs nearby freeway bottlenecks during peak periods and is fixed at this location. This pattern is normally caused by lane-changes of vehicles along the bottleneck (such as, an on–ramp). Traffic upstream and downstream of the pinned localized cluster is often free.

- Moving Localized Cluster: this congested state is more or less the same as the pinned localized cluster but the jam, instead of being stationary, propagates upstream with a speed of approximately 15km/h. This pattern is often induced by a perturbation due to traffic from an on–ramp when the traffic on the main carriageway is already heavy.

- Stop–and–Go Waves: these waves consist of a sequence of traffic jams with free traffic in between, which are often localized and propagate in the upstream direction with the speed of approximately 15km/h. The propagation of these waves normally ends in a free traffic state or as a pinned localized cluster.

- Homogeneous Congested Traffic: this state occurs on heavily congested freeways due to, for example, high traffic demand from an on–ramp to an already congested main carriageway. In a homogeneous congested state, the speed is very low and remains almost unchanged over a long section of freeway. The traffic operations are usually non-congested downstream of the homogeneous congested state, however, upstream of the bottleneck, the congested traffic regime grows in time.

- Oscillating Congested Traffic, which has the same features as the homogeneous congested state with respect to its mechanism. However, the speed within the congestion area is oscillating with a frequency and amplitude that are constant during a certain period.

To get an idea of the model performance in replicating the aforementioned traffic congested states in the presence of an on–ramp, we simulated the proposed model (for aggregate lane and aggregate class) with a two lanes freeway that is 10km in length and contains an on–ramp at location $x = 5km$. The duration of the simulation was 30 minutes. A dedicated numerical

scheme, namely HLLE (shorthand for Harten-van Leer- Lax and Einfeldt), was adopted. This scheme was proven to be robust, reliable and fast with second order traffic models (see Chapter 5). The road was divided into cells with a length of 100m. The simulation time step was 2 seconds. These values were chosen to satisfy the numerical stability condition as well (Courant-Friedrichs-Lewy condition, see Sod (1985)). The model parameters for this simulation are given in Table 4.1

Table 4.1: Model parameters. Note that the sum of safe distance and vehicle length $(d_{min} + l)$ is equal to the inverse of the jam density $(1/r_{max})$.

Notations	Values	Units
Free speed V_{max}	120	km/h
Jam density r_{max}	145	veh/km
Relaxation time τ	15	sec
Reaction time T	1.2	sec
α_0	0.008	
$\delta\alpha$	0.03	
δr	5	veh/km

In this simulation, open boundary conditions were imposed. The simulation scenarios and results are given in Table 4.2

Table 4.2: Simulation scenarios and results.

Scenarios	Main density (veh/km)	Main flow (veh/h/lane)	Ramp flow (veh/h/lane)	Results
1	30	2100	100	Traffic cluster
2	30	2100	300	Double clusters
3	30	2100	450	Stop-and-go
4	30	2100	600	Homogeneous

Because in this section we mainly focus on an analysis of the impact of ramp flow and acceleration lane length on the traffic in the main carriageway, we set the main flow to 2100 veh/h/lane. Figure 4.1 – Figure 4.4 show the congested traffic patterns produced by the proposed model when the acceleration lane length is fixed to 200m.

- Scenario 1. In this case, only a small perturbation of the ramp flow (100veh/h/lane) results in the formation of a cluster that gradually moves upstream (Figure 4.1). This type of congested state is called a Moving Localized Cluster, which is reported in Helbing and Treiber (1998).

- Scenario 2. If the ramp flow is further increased to 300veh/h/lane, a jam is formed in the same way as in scenario 1, but when the first Moving Localized Cluster travels upstream, it triggers another cluster that forms a second one (Figure 4.2). This process can be repeated if the ramp flow is further increased.

- Scenario 3. The (distance) interval between the clusters is shorter and, therefore, the number of clusters increases when the ramp flow is equal to 450 veh/h. The so-called Triggered Stop-and-Go waves are formed (Figure 4.3). This type of congested state is also obtained if the upstream inflow is decreased (1950 veh/h) but the ramp flow is increased (600veh/h) so that the total demand at the bottleneck is unchanged.

- Scenario 4. A still further increase of ramp flow results in the disappearance of waves inside the congested area, that is, the speed inside the congested area is reduced to jam speed (Figure 4.4). This jam formation is called Homogeneous Congested Traffic. By imposing a temporary and short peak in the on-ramp demand, we can also obtain the so-called recurring hump state found in Lee et al. (1999) and the hysteretic phenomenon can be obtained. The explanation for these instability phenomena can be found in, for example, Tampere (2004).

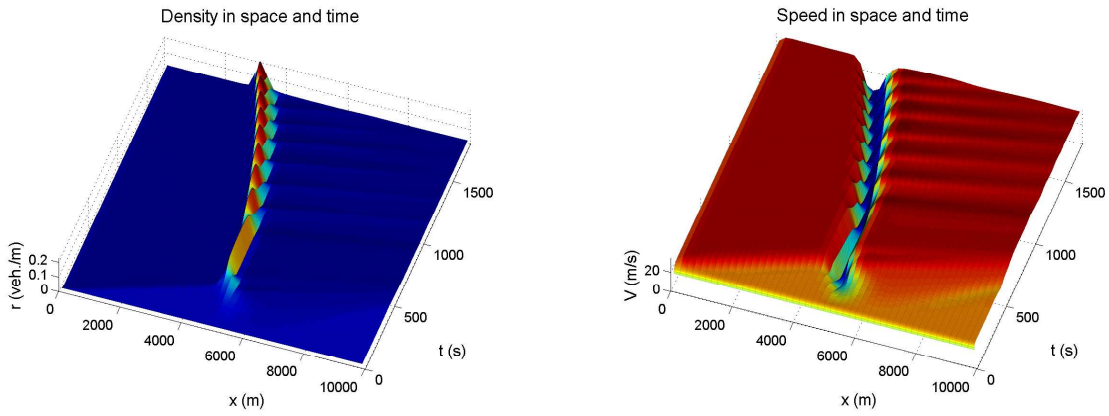

(a) (b)

Figure 4.1: Single moving traffic cluster on main carriageway due to perturbation of on-ramp traffic (Scenario 1).

Overall, the model results for congested traffic states nearby the bottleneck caused by the ramp flow are consistent with findings in the literature. To support the improvement of the derived model with respect to the description of the impact of acceleration lane length on the traffic operations, let us simulate scenario 2 with different acceleration lane lengths, namely, 50m and 2000m. The simulation results (Figure 4.5) show the different traffic states. When the acceleration lane is too short (L=50m), the transition from the two moving clusters state to the triggered stop-and-go state occurs (Figure 4.5(a)). In this scenario, the considered freeway was divided into cells with a length of 50m, and the simulation time step was 1sec. The transition from the two moving clusters to the triggered stop-and-go waves reflects the fact that the acceleration lane is not long enough to spread out small disturbances caused

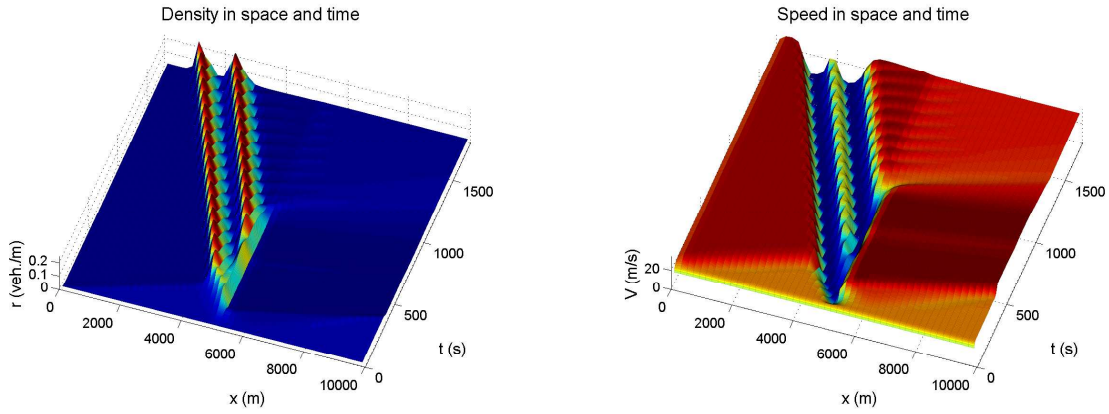

(a) (b)

Figure 4.2: Double moving traffic clusters on main carriageway due to perturbation of on-ramp traffic (Scenario 2).

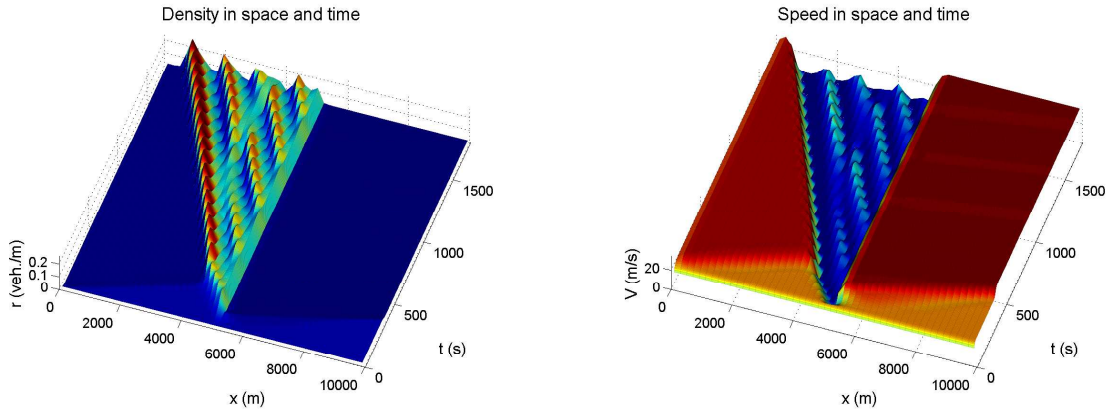

(a) (b)

Figure 4.3: Stop and go congested state on main carriageway due to perturbation of on-ramp traffic (Scenario 3).

by the on–ramp traffic, leading to more unstable operations for the main carriageway. In contrast, when the acceleration lane length is set to a very high value (L=2000m), the traffic from the on–ramp has no impact on the traffic in the main carriageway and a stable state results (Figure 4.5(b)). These simulation results will be supported by the stability analysis in Section 4.5, in which the acceleration lane length is recognized as an important factor for the model stability, which explains why the different congested traffic states are obtained at different observation locations relative to the ramp.

4.5 Linear stability analysis of the model

This section derives the stability conditions based on the 'linear method' for the continuum model developed in this chapter. The linear method refers to linear Taylor approximations, which are used throughout the analysis. The consequence of these approximations is that

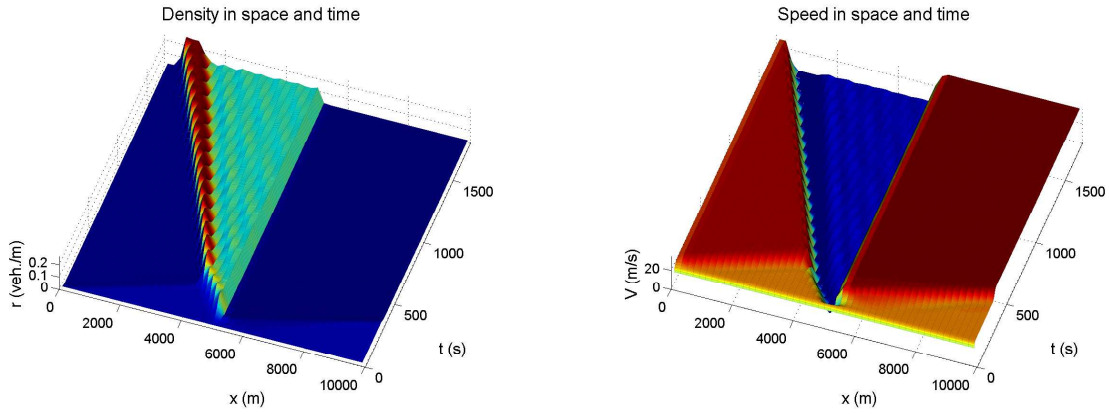

(a) (b)

Figure 4.4: Homogeneous congested state on main carriageway due to perturbation of on-ramp traffic (Scenario 4).

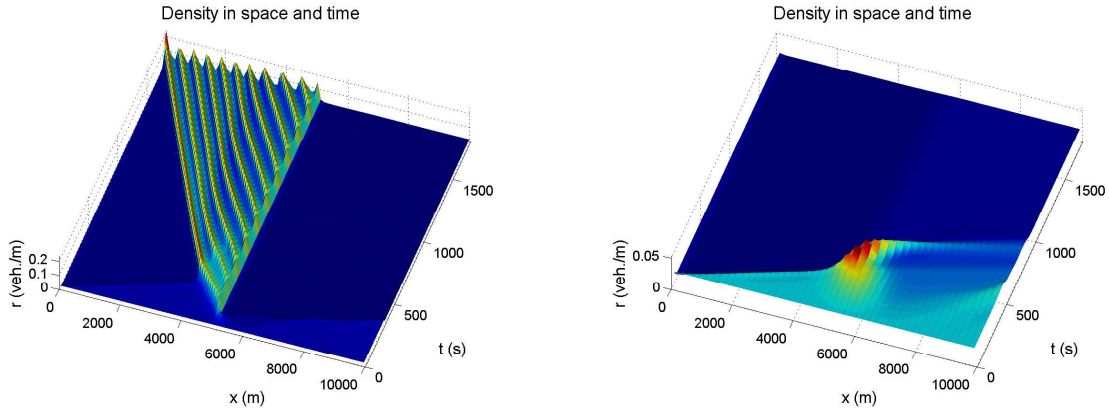

(a) Unstable traffic state with L= 50m (b) Stable traffic state with L= 2000m

Figure 4.5: Effect of acceleration lane length on main carriageway traffic dynamics.

conditions that are stable according to this analysis might actually still show non-linear instability. However, in general the linear analysis gives sound insights into the general behavior of the model in the presence of an on–ramp. To this purpose, equations 4.10 and 4.15 are used. Further information about the linear method for the stability analysis of second order macroscopic traffic flow models is found in Helbing (1997a) and Tampere (2004).

To facilitate the stability analysis of the proposed model but without loss of generality, we only focus on the on–ramp model while aggregating the main lane, as well as the vehicle classes; it is not necessary to also show the results for the off–ramp model, because in the off–ramp model, we only change the sign of the ramp-flow demand, that is, the flow rate desired to exit. Let us first start with the linear stability analysis of the model with the main focus on disturbances due to traffic from the on–ramp and the impact of the acceleration lane length on distributing and spreading out these disturbances. The on–ramp traffic model for the aggregated main lanes and aggregated vehicle classes proposed in equations 4.10 and

4.11 is:

$$\frac{\partial r}{\partial t} + V\frac{\partial r}{\partial x} + r\frac{\partial V}{\partial x} = \delta\frac{q_0}{L}\pi_{0,1} \tag{4.19}$$

$$\frac{\partial V}{\partial t} + V\frac{\partial V}{\partial x} + \frac{1}{r}\frac{\partial P}{\partial x} = \frac{V_e - V}{\tau} + \delta\frac{q_0\left(V_0 - V\right)}{rL}\pi_{0,1} \tag{4.20}$$

where $P = r\Theta$ denotes the traffic pressure on the main carriageway. L denotes the acceleration lane length.

Let us suppose a *stationary* and *spatially homogeneous* solution with index ss of the system of equations 4.19 and 4.20 with constant density r_{ss} and corresponding speed $V_{ss} = V_e(r_{ss})$. This is obvious because at this solution the merging probability $\pi_{0,1}\left(r_{ss}, V_{ss}|x,t\right) \rightarrow 0$ due to the infinite space factor γ as shown in Section 3.4.2 ($\lim_{\gamma\rightarrow\infty}\pi_{0,1} = 0$). Hence, the right hand side of equation 4.20 limits to zero at the solution pair (r_{ss} and V_{ss}).

Now we consider large perturbations around the solution pair (r_{ss} and V_{ss}), denoted by $\check{r}(x,t)$ and $\check{V}(x,t)$, which leads to:

$$\begin{aligned} r(x,t) &= r_{ss} + \check{r}(x,t) \\ V(x,t) &= V_{ss} + \check{V}(x,t) \end{aligned} \tag{4.21}$$

The region of instability can be found by a linear stability analysis as follows. Let the perturbations be determined as the cosine functions with frequency λ and wave number κ as shown below:

$$\begin{aligned} \check{r}(x,t) &= \tilde{r}e^{\lambda t + i\kappa x} \\ \check{V}(x,t) &= \tilde{V}e^{\lambda t + i\kappa x} \end{aligned} \tag{4.22}$$

where i denotes the imaginary unit.

By substituting system 4.21 and 4.22 into the system of equations 4.19 and 4.20, given the acceleration lane length L and ramp flow q_0 we obtain:

$$\begin{aligned} \frac{\partial\check{r}}{\partial t} + V_{ss}\frac{\partial\check{r}}{\partial x} + r_{ss}\frac{\partial\check{V}}{\partial x} - \frac{\delta q_0}{L}\left(\frac{\partial\pi_{0,1}}{\partial r}\check{r} + \frac{\partial\pi_{0,1}}{\partial V}\check{V}\right) = 0 \\ \frac{\partial\check{V}}{\partial t} + V_{ss}\frac{\partial\check{V}}{\partial x} + \frac{1}{r_{ss}}\left(\frac{\partial P}{\partial r}\frac{\partial\check{r}}{\partial x} + \frac{\partial P}{\partial V}\frac{\partial\check{V}}{\partial x}\right) - \left(\frac{\partial\psi}{\partial r}\check{r} + \frac{\partial\psi}{\partial V}\check{V}\right) = 0 \end{aligned} \tag{4.23}$$

where ψ denotes the *RHS* of equation 4.20 .

If we substitute expression 4.22 into system 4.23 we obtain:

$$\underbrace{\begin{pmatrix} \lambda - a_{11} & a_{12} \\ a_{21} & \lambda - a_{22} \end{pmatrix}}_{\mathbf{A}} \begin{pmatrix} \check{r} \\ \check{V} \end{pmatrix} = 0 \tag{4.24}$$

where

$$\begin{aligned} a_{11} &= \frac{\delta q_0}{L}\frac{\partial \pi_{0,1}}{\partial r} - i\kappa V_{ss} \\ a_{12} &= -\frac{\delta q_0}{L}\frac{\partial \pi_{0,1}}{\partial V} + i\kappa r_{ss} \\ a_{21} &= -\frac{\partial \psi}{\partial r} + \frac{1}{r_{ss}}\frac{\partial P}{\partial r} i\kappa \\ a_{22} &= \frac{\partial \psi}{\partial V} - \frac{1}{r_{ss}}\frac{\partial P}{\partial V} i\kappa - i\kappa V_{ss} \end{aligned} \tag{4.25}$$

The system is stable if and only if: 1) the deviation pair ($\check{r}$ and $\check{V}$) is a solution for the equations 4.19 and 4.20 and 2) if the amplitude of the perturbation 4.22 is decreasing with time. The latter is true if and only if the real part of frequency λ is strictly negative. Condition 1 is satisfied if and only if the determinant of matrix A is zero, that is:

$$det|\mathbf{A}| = 0 \;\Leftrightarrow\; \lambda^2 - (a_{11} + a_{22})\,\lambda + (a_{11}a_{22} - a_{12}a_{21}) = 0 \tag{4.26}$$

The solutions of equation 4.26 are:

$$\lambda_{1,2} = 0.5\left(a_{11} + a_{22} \pm \sqrt{(a_{11} - a_{22})^2 + 4a_{12}a_{21}}\right) \tag{4.27}$$

The following formula for the real part **R** and complex part **I** of expression $\sqrt{(a_{11} - a_{22})^2 + 4a_{12}a_{21}}$ is used:

$$\sqrt{\mathbf{R} + i\mathbf{I}} = \sqrt{0.5\left(\sqrt{\mathbf{R}^2 + \mathbf{I}^2} + \mathbf{R}\right)} + i\sqrt{0.5\left(\sqrt{\mathbf{R}^2 + \mathbf{I}^2} - \mathbf{R}\right)} \tag{4.28}$$

For simplicity, we assume that the speed variance Θ is a density-dependent function; after a lengthy but straightforward algebraic calculation (see Appendix B), inequality $Real\,(\lambda_{1,2}) < 0$ becomes:

$$\left(\frac{\partial \psi}{\partial V} + \frac{q_0}{L}\frac{\partial \pi_{0,1}}{\partial r}\right)^2 \frac{\partial P}{\partial r} > \left(r_{ss}\frac{\partial \psi}{\partial r} + \frac{1}{r_{ss}}\frac{q_0}{L}\frac{\partial \pi_{0,1}}{\partial V}\frac{\partial P}{\partial r}\right)^2 \tag{4.29}$$

- In case of uninterrupted traffic flow, that is $q_0 = 0$, equation 4.29 becomes:

$$\left(\frac{\partial \psi}{\partial V}\right)^2 \frac{\partial P}{\partial r} > \left(r_{ss}\frac{\partial \psi}{\partial r}\right)^2 \tag{4.30}$$

  For the Payne-type model (see Section 2.3), $V_e = V_e(r)$ and $P = P_e(r)$, we obtain:

$$\frac{\partial \psi}{\partial V} = -\frac{1}{\tau} \;\text{ and }\; \frac{\partial \psi}{\partial r} = \frac{1}{\tau}\frac{dV_e}{dr} \tag{4.31}$$

  which is substituted into equation 4.30, resulting in:

$$r_{ss}\left|\frac{dV_e}{dr}\right| > \sqrt{\frac{dP_e}{dr}} \tag{4.32}$$

  This condition is consistent with the one derived by Helbing (1997a).

- In case of interrupted traffic flow, solving 4.29 (see Appendix B) gives two solutions:

$$q_0 < \frac{L \mid \partial\psi/\partial V \mid}{\mid \partial\pi_{0,1}/\partial r \mid} \tag{4.33}$$

$$r_{ss} < \frac{\mid \partial\psi/\partial V \mid \sqrt{\partial P/\partial r}}{\mid \partial\psi/\partial r \mid} \tag{4.34}$$

It is clear that in the presence of on–ramps, there are two stability conditions for traffic flow. On the one hand, the condition of the density regime 4.34 must be satisfied. On the other hand, the condition for the ramp flow and acceleration lane length 4.33 needs to be fulfilled as well. From condition 4.33, we can see that, given that condition 4.34 is satisfied, the fluctuation of the inflow from the on–ramp may cause instability of the main traffic flow which results in congestion. This is also supported by the simulation results shown in Section 4.4. For a fixed acceleration lane length, below a certain critical value of ramp flow, the free traffic state may survive but when the on–ramp flow is higher, traffic becomes unstable, leading to the stop-and-go state, oscillatory congested state, or even homogeneous congested state if the main carriageway is heavily used already. However, the acceleration lane length is also an important factor, which spreads the perturbations from on-ramps. Obviously the longer the acceleration lane, the more stable the main traffic flow is. This finding is consistent with Helbing et al. (1999b), since when the ramp flow goes to zero or the acceleration lane length goes to infinite, condition 4.33 is always satisfied. That means that the ramp flow has no influence on the main carriageway traffic operations. Last but not least, based on simulation we found that closer to the end of a ramp, the gradient of merging probability with respect to the density increases, giving rise to the smaller *RHS* of condition 4.33. This means that the main traffic is more unstable, which supports the conclusion that when approaching the end of a ramp, drivers are willing to make more precarious decisions when merging (that is, accept smaller gaps when changing lanes), and, consequently, disturb the main traffic flow more significantly.

From the model stability analysis in this section, we can draw a contour diagram for the necessary acceleration lane length (in terms of model stability according to equation 4.33) in order to distribute the on–ramp flow and the corresponding combination of main flow and ramp flow (Figure 4.6). It can be seen that the longer the acceleration lane length is, the more on–ramp flow the main traffic can carry. For a short acceleration lane length, the main traffic can be unstable even when traffic demand from the on–ramp is low.

4.6 Summary

In this chapter, we introduced an improved *MLMC* macroscopic model for interrupted traffic flow dynamics on freeways. The model was obtained from the gas-kinetic model for interrupted traffic flow from Chapter 3 using the so-called *method of moments*. The developed model is able to explicitly take into account the lane-changing process between a ramp lane (exit or entry) and the shoulder lane of the main carriageway. The derived model is also

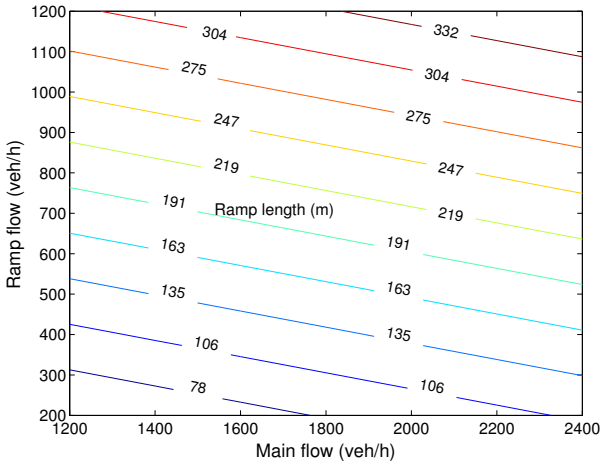

Figure 4.6: Contour diagram for minimum acceleration lane lengths to keep main traffic flow stable (Simulation with 2-lane main road and 1-lane ramp).

applied for other cases of bottlenecks like lane–drops, which are modeled the same as in the case of an on–ramp. In this model, the *mandatory lane-change* is performed along a considerable stretch of roadway, while other macroscopic models treat this merging or diverging zone as a point, that is, traffic merges or diverges immediately. This property also allows the simulation of traffic dynamics in weaving sections, which had yet to be implemented accurately in current macroscopic models.

Because the applied approach to model discontinuities, such as at on– and off–ramps, lane–drops, and so on, stems from microscopic driving behavior, the developed model is able to take into account some situations which are often neglected in other macroscopic models, such as:

- Vehicles that want to enter from an on–ramp or to exit to an off–ramp may travel along a considerable stretch of roadway (acceleration lane) before they find a suitable *lead-gap* and *lag-gap* in the target lane and, thus, can merge or diverge.
- Drivers are willing to accept smaller gaps as they approach the end of on–/off–ramps or lane–drops, and, as a consequence, in those cases disturb the traffic on the main carriageway more significantly.
- Drivers in the shoulder lane are cooperative by changing to the adjacent lane in order to give way for merging vehicles.

Since the model is derived from microscopic principles, it is more elaborate than the current macroscopic models in terms of modeling the inflow from on–ramps and outflow to off–ramps. In the developed model, interactions between user classes in lane-changing processes are taken into account through user specific reaction time, which contributes among the others significantly to the lane-changing probabilities. However, the derived model generates

only two additional parameters compared to the original model of Hoogendoorn (1999a): the upper bound (μ_{max}) and lower bound (μ_{min}) for the *gap–acceptance* of the lane–changing vehicle in the merging and diverging zone. Moreover, the derived model obviously requires much fewer parameters than microscopic models.

We have shown with simulation that the proposed model can replicate several congested traffic states which have been identified in the literature. Furthermore, we have analyzed, both mathematically and numerically, the importance of the acceleration lane length on the stability of traffic operations based on the developed continuum model. According to this analysis, there are two conditions for model stability that need to be fulfilled in the presence of on–ramps. Firstly, the stability condition for the initial condition of the main traffic must be satisfied. Secondly, the condition for ramp flow demand (amplitude of disturbance) and the acceleration lane length must be fulfilled as well. This explicit condition is consistent with the findings of Helbing et al. (1999b) about the dependency of the traffic states on acceleration lane length and ramp flow. Therefore, the advantage of the new approach to on–ramp modeling compared to other models proposed in the past is that it analytically shows the influence of the disturbance from on–ramps on the traffic operations in the main carriageway. We have also shown that the linkage between merging probability and acceleration lane length in the proposed model is useful to design optimal acceleration lane lengths.

The developed *MLMC* continuum model is of a hyperbolic type. Therefore, it can be solved numerically by a number of finite volume schemes that will be described in the next chapter.

Chapter 5

Numerical solution for second order macroscopic traffic models

This chapter describes novel numerical solution approaches for general second order continuum (macroscopic) traffic flow models presented in Chapter 2. Application of these solutions to the macroscopic model developed in Chapter 4 is straightforward.

In general, second order macroscopic models consist of two partial differential equations which are of the hyperbolic kind. Information (density and speed) propagates along the so-called characteristic curves with a certain characteristic speed. Focusing and dispersion of the characteristics lead to the formation of, respectively shock and rarefaction waves. Furthermore, from the possible directions in which the characteristics can move it follows that flow information can travel both downstream and upstream, depending on prevailing traffic conditions (free flow or congestion). The latter is of importance when considering the conditions at the cell boundaries of a roadway section (that is, the roadway is divided into cells, all with the same length small enough so as the traffic dynamics within a cell can be neglected), to decide which information is required at the boundary to ensure the correct flow conditions.

Numerical solution schemes must consider the different phenomena and situations which are related to the focusing and dispersion of the characteristics, and handle them adequately, which is certainly a requirement for an accurate and reliable scheme. Two classes of techniques that are often used to obtain approximation solutions are finite volume methods and finite element methods (see Hirsch (1990a) and Hirsch (1990b)). The former are the topic of this chapter. Due to the fact that a small perturbation in the traffic flow may result in formation of traffic congestion, an inappropriate choice of numerical schemes can result in very poor performance of the model. This is illustrated in Lyrintzis et al. (1994), where it is argued that, though the second order model is superior to the simple kinematic model in some aspects, Payne (1979) failed to show this in his simulation because of a poor choice for the applied numerical solution approach, namely, the Euler-like space-central finite difference scheme.

While the robust scheme of Godunov has been proposed by Leo and Pretty (1992), Daganzo (1994), Lebacque (1996) to numerically solve the first-order model of Lighthill and Whitham (1955), generally applicable numerical methods that are able to efficiently solve general second-order models so far have not been established. Different approaches have been proposed (see Leo and Pretty (1992), Hoogendoorn (1999a), Helbing and Treiber (1999c)), but the definitive answer on their applicability in terms of accuracy and reliability has not yet been given. For this reason, we propose in this chapter a novel numerical scheme and make a cross-comparison with other schemes for second-order macroscopic models. To ensure an unbiased comparison between the schemes, the model parameters are calibrated using dedicated optimization techniques and real data collected in the Netherlands for each considered numerical scheme using an automated calibration algorithm. The corresponding optimal parameters are then used to simulate the chosen model with another data set (validation process) in order to make a cross-comparison of model predictions with different schemes (see Ngoduy and Hoogendoorn (2003b), Ngoduy et al. (2004a)).

This chapter is organized as follows. In Section 5.1 we discuss the characteristics of the second order continuum traffic model. Section 5.2 presents the general concept of the so-called *finite volume method* and its application to traffic flow. Section 5.3 describes two typical numerical schemes for second order macroscopic traffic models with their drawbacks in certain traffic situations. In Section 5.4 we propose an improved numerical solution that can guarantee positively conservative traffic variables (that is, prevent traffic from moving backwards). Section 5.5 discusses the results of model simulations with different calibrated and validated numerical schemes. Finally, Section 5.6 summarizes this chapter.

5.1 Governing equations

This section presents some important characteristics of general second order macroscopic traffic flow models of the hyperbolic type presented in Chapter 2 (in general, the model of Kerner and Konhauser (1993) is not of the hyperbolic type). This system consists of two partial differential equations that describe the dynamics of traffic density and flow rate, which can be reformulated in the conservation vector form as follows:

$$\frac{\partial \mathbf{U}}{\partial t} + \frac{\partial \mathbf{F}}{\partial x} = \mathbf{S} \tag{5.1}$$

In equation 5.1, **U**, **F**, **S** are defined by:

$$\mathbf{U} = \begin{bmatrix} r \\ q \end{bmatrix}, \mathbf{F} = \begin{bmatrix} q \\ E \end{bmatrix}, \mathbf{S} = \begin{bmatrix} 0 \\ (q_e - q)/\tau \end{bmatrix} \tag{5.2}$$

Where $E = r(V^2 + C^2)$ with C is determined for different models as (see Chapter 2 for more details on these models):

- For Payne's model (Payne (1971)), $C = \sqrt{-\frac{1}{2\tau}\frac{dV_e}{dr}}$

- For Philips' model (Philips (1979)), $C = \sqrt{\Theta_0(1 - 2r/r_{max})}$
- For Treiber's model (Treiber et al. (1999)), $C = V\left[A(r) \pm \sqrt{A^2(r) + A(r) + r\frac{dA(r)}{dr}}\right]$

Equation 5.1 can recast into the so-called *quasi-linear* form as given below:

$$\frac{\partial \mathbf{U}}{\partial t} + \frac{\partial \mathbf{F}}{\partial U}\frac{\partial \mathbf{U}}{\partial x} = \mathbf{S} \tag{5.3}$$

System 5.3 has two real and different eigenvalues, for which it is called strictly hyperbolic. These eigenvalues are used to determine the characteristic wave speeds of the listed second order models. These eigenvalues are determined from the Jacobian matrix $\mathcal{J} = \partial\mathbf{F}/\partial\mathbf{U}$ by the following equations:

$$\lambda_{min}^{max} = V \pm |C| \tag{5.4}$$

In expression 5.4, λ_{min}^{max} denote the wave speeds of the models. Corresponding to each eigenvalue, there is a family of shocks (shock and expansion waves). This is an important property of second order models, which is analyzed as follows.

Let e_1 and e_2 be the corresponding eigenvectors of the Jacobian matrix $\mathcal{J}$, which are determined as: $e_1 = (r/(2C), 1/2)$ and $e_2 = (-r/(2C), 1/2)$. We define the matrix of eigenvectors $\mathcal{E}$ as :

$$\mathcal{E} = \begin{pmatrix} r/(2C) & -r/(2C) \\ 1/2 & 1/2 \end{pmatrix} \quad \text{with} \quad \mathcal{E}^{-1} = \begin{pmatrix} C/r & 1 \\ -C/r & 1 \end{pmatrix} \tag{5.5}$$

By using these matrices, equation 5.3 becomes:

$$\mathcal{E}^{-1}\frac{\partial \mathbf{U}}{\partial t} + \mathcal{E}^{-1}\mathcal{J}\frac{\partial \mathbf{U}}{\partial x} = \mathcal{E}^{-1}\mathbf{S} \tag{5.6}$$

Let z denote the so-called Riemann variables and let us consider any variation $\delta\mathbf{U}$ in $\mathbf{U}$ and define: $\delta z = \mathcal{E}^{-1}\delta\mathbf{U}$, which is equivalent to: $\delta\mathbf{U} = \mathcal{E}\delta z$. These definitions lead to:

$$\mathcal{E}\frac{\partial z}{\partial t} = \frac{\partial \mathbf{U}}{\partial t} \quad \text{and} \quad \mathcal{E}\frac{\partial z}{\partial x} = \frac{\partial \mathbf{U}}{\partial x} \tag{5.7}$$

which means that equation 5.6 can be rewritten as follows:

$$\frac{\partial z}{\partial t} + \Lambda\frac{\partial z}{\partial x} = \tilde{\mathbf{S}} \tag{5.8}$$

where $\tilde{\mathbf{S}} = \mathcal{E}^{-1}\mathbf{S}$ and:

$$\Lambda = \begin{pmatrix} V + C & 0 \\ 0 & V - C \end{pmatrix} \tag{5.9}$$

The definition of the Riemann variables results in:

$$\delta z_1 = \delta V + \frac{C}{r}\delta r \quad \text{and} \quad \delta z_2 = \delta V - \frac{C}{r}\delta r \tag{5.10}$$

For Payne's model, $C = C_0$, the Riemann variables equal: $z_1 = V + C_0 ln(r)$ and $z_2 = V - C_0 ln(r)$, which depend on the shape of the fundamental diagram.

Equation 5.8 is decoupled into:

$$\frac{\partial z_1}{\partial t} + \lambda_{max}\frac{\partial z_1}{\partial x} = \tilde{\mathbf{S}}_1 \quad (5.11)$$

$$\frac{\partial z_2}{\partial t} + \lambda_{min}\frac{\partial z_2}{\partial x} = \tilde{\mathbf{S}}_2 \quad (5.12)$$

These equations show that the quantities $z_{1,2}$ propagate along the corresponding characteristics with speed λ_{min}^{max}. These characteristic curves are defined as:

$C^+ : dx = \lambda_{max} dt$ and $C^- : dx = \lambda_{min} dt$.

Let us consider any point **Y**(x,t) at location x and time t, the density and speed at this point are determined from the quantities $z_{1,2}$ transported with speed λ_{min}^{max} along the curves $C^{\pm}$, that is:

$$(z_1)_{\mathbf{Y}} = (V + C_0 ln(r))_{\mathbf{Y}^+} = (z_1)_{\mathbf{Y}^+} \quad (5.13)$$

$$(z_2)_{\mathbf{Y}} = (V - C_0 ln(r))_{\mathbf{Y}^-} = (z_2)_{\mathbf{Y}^-} \quad (5.14)$$

Figure 5.1 describes the domain of dependence for both *subsonic* and *supersonic* traffic flow operations. Here, the terms *subsonic* and *supersonic* are used in analogy to continuous media. That is, *subsonic* flow conditions occur when the speed of the particles V is lower than the speed of sound C, while the *supersonic* flow conditions occur when the speed V is higher than the speed of sound c. When the traffic operations are *subsonic*, the characteristic curve moves in the opposite direction of traffic (since the slope of the characteristic curve C^- is negative). Hence, the density, speed and pressure are transported not only downstream by the curve C^+ but also upstream by the curve C^- (Figure 5.1).

Because the solution of the wave speed that corresponds to λ_{max} travels faster than traffic itself resulting in downstream propagation of the shock wave, this property violates the anisotropic condition, that is, drivers only react to downstream stimuli . This drawback has been identified by several authors, such as Daganzo (1995), Del Castillo et al. (1993). However, these arguments have been invalidated by others, such as Helbing (1995), Helbing (1996), Helbing (1997b), Helbing et al. (2002), Zhang (2003). Furthermore, simulations described in this chapter will also show that a perturbation that travels faster than traffic decays quickly with time.

By using linear stability analysis (see Section 4.5), it can be shown that second order models are stable if the following condition is satisfied: $r|dV/dr| \leq C$ (Helbing (1997b)). For Payne's model, the stability criteria is: $r \leq (\tau|dV_e/dr|)^{-1/2}$. Obviously, the stability of the traffic conditions increases when the relaxation time τ decreases. That is, the more time drivers have to react to the prevailing traffic conditions, the more unstable the traffic flow conditions are. Note that when $\tau \rightarrow 0$, Payne's model is always stable (see Section 4.5 for details on the derivation).

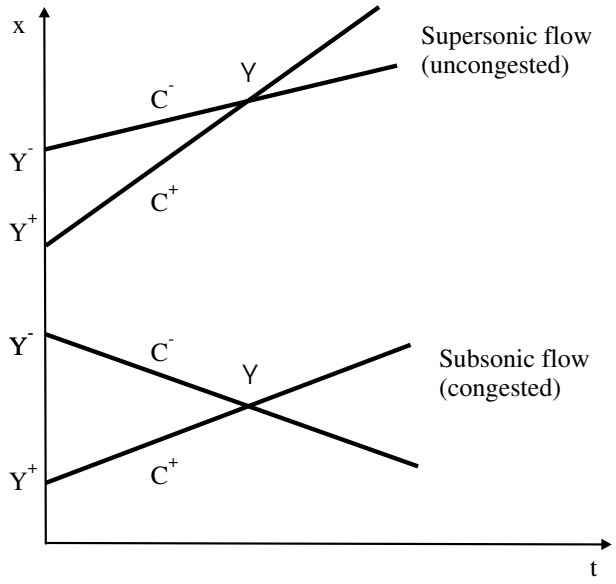

Figure 5.1: Propagation of flow quantities. The points Y^+ and Y^- indicate the origin of the respective unique characteristic curves C^+ and C^- stemming from these points that reach point Y. The upper part shows the case of *supersonic* flow when the curve C^- has a positive slope, while the lower part illustrates the case of *subsonic* flow when the curve C^- has a negative slope.

There are plenty of numerical schemes to solve hyperbolic systems 5.3, which are suitable for a specific model. In the remainder of chapter, we mainly focus on finite volume methods for hyperbolic conservation equations. These methods are often used by traffic theorists (Leo and Pretty (1992), Hoogendoorn (1999a), Helbing and Treiber (1999c)) to simulate high(er) order macroscopic traffic flow models.

5.2 Finite volume methods

According to Hirsch (1990b), finite volume methods allow a direct discrimination of variables in the physical space, for arbitrary mesh configurations, without the necessity of an explicit computation of metric coefficients. In finite volume methods, the integral conservation laws are discretized over a control volume cell ABCD (Figure 5.2). With different choices for this control volume cell, and according to the way the fluxes are computed on each cell interface, many possible finite volume methods can be generated.

As seen from Figure 5.2, the element ABCD is attached to the mesh point (i, j). The mass conservation law is integrated as follows:

$$\begin{aligned} &\oint_{ABCD} \vec{F}.d\vec{Z} = 0 \\ &\Leftrightarrow \left(\vec{F}.\vec{Z}\right)_{AB} + \left(\vec{F}.\vec{Z}\right)_{BC} + \left(\vec{F}.\vec{Z}\right)_{CD} + \left(\vec{F}.\vec{Z}\right)_{DA} = 0 \end{aligned} \tag{5.15}$$

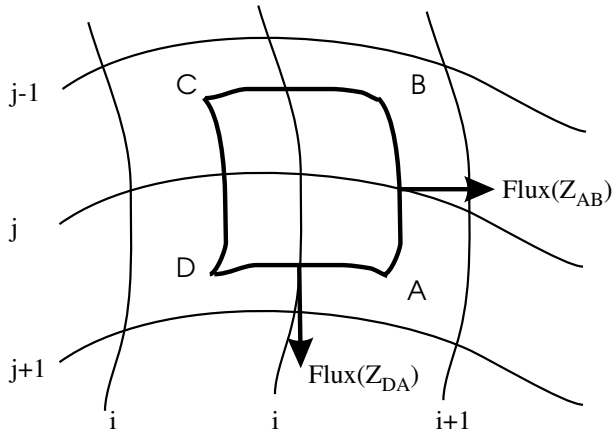

Figure 5.2: Finite volume discrimination in physical space.

Where $\vec{F}$ denotes the flux vector and $\vec{Z}$ denotes the surface vector, which both point outwards. Equation 5.15 is used to determine the fluxes in the context of the traffic flow on the freeway, as shown in the ensuing of this chapter.

To numerically solve the conservative system 5.3, time and space (one dimension), respectively, are divided into time steps $t_k = kt$ and segments (cells) $x_i = ix$ (see Figure 5.3).

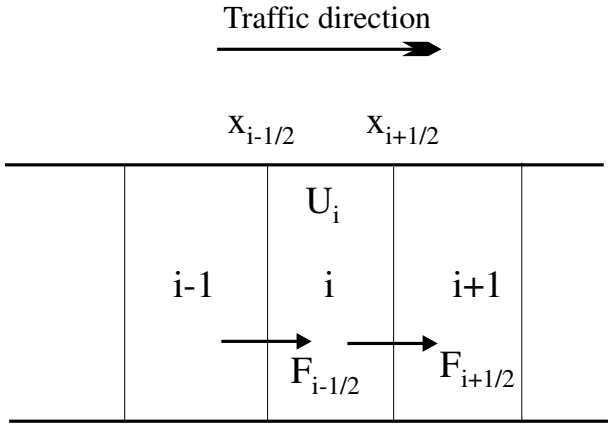

Figure 5.3: Illustration of the finite volume method for a roadway.

The space-averaged conservative vector U in system 5.3 over cell i at time instant k is defined as:

$$\tilde{U}_{i,k} = \frac{1}{\Delta x} \int_{x_{i-1/2}}^{x_{i+1/2}} U(x, t_k) dx \tag{5.16}$$

These values represent the mean conservative variables per unit of roadway length. The time-averaged conservative flux over time interval $[t_k, t_{k+1}]$ at location x_i is defined as:

$$\tilde{F}_{i,k} = \frac{1}{\Delta t} \int_{t_k}^{t_{k+1}} F(x_i, t) dt \tag{5.17}$$

Finally, the time-space-averaged source term S over a space and time interval is defined as:

$$\tilde{S}_{i,k} = \frac{1}{\Delta t \Delta x} \int_{x_{i-1/2}}^{x_{i+1/2}} \int_{t_k}^{t_{k+1}} S(x,t) dx dt \tag{5.18}$$

To determine the space-averaged conservative variables, the total fluxes $\tilde{F}_{i,k}$ and source term $\tilde{S}_{i,k}$ are computed first. These numerical fluxes are determined by the conditions in the cell upstream and the cell downstream of the cell interface (i.e. cells i and $i+1$ for determining the conditions at the boundary $i+1/2$). The computed fluxes to a large extent determine the changes in the conservative variables **U** (that are, density and flow), since the changes in **U** are determined by the balance of the inflow and outflow of density and traffic momentum at the boundaries of cell i. For instance, the density $r_i(k)$ in cell i increases due to the density flux (flow) into the cell (at the boundary $x_i - 1/2$), while it decreases due to the density flux at the downstream cell boundary (at $x_i + 1/2$). Note that **U** also changes due to non-conservative dynamic processes (for example, due to relaxation of the speed to the equilibrium speed) which are not described by the fluxes. The most important point in a finite volume scheme is thus the computation of the numerical fluxes. From the apparent inability to determine a definite solver for second-order macroscopic flow models, it should be clear that this specification is by no means self-evident. Several approximation schemes have been developed for second order models. Simple schemes as Lax-Friedrichs or upwind schemes were often used in the past to compute approximation solutions of certain models as the Payne model (Hoogendoorn (1999a)). However, these schemes yield a numerical diffusion, which causes smoothing of shock fronts. This effect may cause vehicles to drive backwards into the empty region, which is not realistic. As argued by Zhang (2001), the main problem to the development of reliable and robust numerical schemes for the high(er) order models is the treatment of various kinds of waves that occur in this type of models. Discussions of several numerical schemes can be found in Helbing and Treiber (1999c). We will discuss a number of different schemes in Section 5.3 that are often used in simulations with second order macroscopic traffic flow models (of hyperbolic type).

5.3 Numerical solutions

For numerical analysis of fluid dynamics, many solutions exist (Hirsch (1990a) and Hirsch (1990b)). Application of some second order solutions which are often used to solve high order macroscopic traffic flow models is discussed in the ensuing of this section.

5.3.1 MacCormack scheme

The MacCormack numerical scheme was used by Helbing and Treiber (1999c) to simulate a non-local second order macroscopic model (Treiber et al. (1999)). This scheme consists of two step, namely *Predictor* and *Corrector* as described below:

- Predictor:

$$\tilde{r}(i,k) = r(i,k) - \frac{\Delta t}{\Delta x}\left(q(i,k) - q(i-1,k)\right) \tag{5.19}$$

$$\begin{aligned}\tilde{q}(i,k) &= q(i,k) - \frac{\Delta t}{\Delta x}\left(E(i,k) - E(i-1,k)\right) \\ &+ \Delta t \frac{q_e(i,k) - q(i,k)}{\tau}\end{aligned} \tag{5.20}$$

- Corrector:

$$r(i,k+1) = 0.5\left[\tilde{r}(i,k) + r(i,k) - \frac{\Delta t}{\Delta x}\left(\tilde{q}(i+1,k) - \tilde{q}(i,k)\right)\right] \tag{5.21}$$

$$\begin{aligned}q(i,k+1) &= 0.5\left[\tilde{q}(i,k) + q(i,k) - \frac{\Delta t}{\Delta x}\left(\tilde{E}(i+1,k) - \tilde{E}(i,k)\right)\right] \\ &+ 0.5\Delta t \frac{\tilde{q}_e(i,k) - \tilde{q}(i,k)}{\tau}\end{aligned} \tag{5.22}$$

Note that in the corrector step the source term is evaluated as $\tilde{S} = S(\tilde{U})$.

Order of accuracy: If Δx and Δt are decreased simultaneously by the factor ε, the upper bound of the local error is proportional to ε^2 (second order accuracy).

This scheme is reported to produce no smoothing of the shock fronts, and, therefore, it can prevent vehicles from moving backward from a jam into the empty region. However, there is strong oscillation around the shock. The resulting errors occurring in the shock region indicate how this scheme treats discontinuities. This kind of scheme is more sensitive to nonlinear instabilities than the methods with first order accuracy like the *Upwind* method or *Lax- Friedrichs* method (see Hirsch (1990a)). It is suggested that one should always implement different numerical schemes and compare their simulation results because oscillations, which act as perturbations, may cause additional traffic jams that do not occur in reality (Helbing and Treiber (1999c)).

5.3.2 Steger-Warming Flux Splitting scheme

This scheme was used by Hoogendoorn (1999a) and Hoogendoorn and Bovy (1999b), in which the fluxes at boundaries are determined based on the traffic conditions in the cell considered and the cell downstream as given below:

$$r(i,k+1) = r(i,k) - \frac{\Delta t}{\Delta x}\left(q(i+1/2,k) - q(i-1/2,k)\right) \tag{5.23}$$

$$\begin{aligned}q(i,k+1) &= q(i,k) - \frac{\Delta t}{\Delta x}\left(E(i+1/2,k) - E(i-1/2,k)\right) \\ &+ \Delta t \frac{q_e(i,k) - q(i,k)}{\tau}\end{aligned} \tag{5.24}$$

Where $q_{i+1/2}$ and $E_{i+1/2}$ are numerical fluxes at interface $i+1/2$, which are determined as follows:

$$\begin{aligned} q(i+1/2,k) &= q^{+}(i,k)+q^{-}(i+1,k) \\ E(i+1/2,k) &= E^{+}(i,k)+E^{-}(i+1,k) \end{aligned} \tag{5.25}$$

The specification of $q^{\pm}(i,k)$ and $E^{\pm}(i,k)$ depends on the traffic conditions of the considered cell i and the downstream cell $i+1$, as described with:

- If $V(i,k) > C(i,k)$, the traffic in cell i is uncongested or free flowing, and all characteristics move downstream, thus, in the same direction as the traffic flow; this means that no momentum or energy is transported upstream. In other words, the numerical fluxes at a cell interface, say $x_{i+1/2}$, are only determined by the conditions in the upstream cell i, which is reflected in the Steger-Warming specification of the numerical fluxes:

$$q^{+}(i,k) = q(i,k) \text{ and } q^{-}(i,k) = 0 \tag{5.26}$$

$$E^{+}(i,k) = E(i,k) \text{ and } E^{-}(i,k) = 0 \tag{5.27}$$

- If $V(i,k) < C(i,k)$ then traffic in cell i is congested. This implies that information moves both downstream and upstream, that is, momentum or energy are also transported upstream. This property is respected by the Steger-Warming scheme, as can be concluded from the specification of the numerical fluxes that show that the numerical fluxes, say at cell interface $x_{i+1/2}$, is determined from the conditions at cell i and cell $i+1$:

$$q^{+}(i,k) = r(i,k)\left(V(i,k)+C(i,k)\right)/2 \tag{5.28}$$

$$q^{-}(i,k) = r(i,k)\left(V(i,k)-C(i,k)\right)/2 \tag{5.29}$$

$$E^{+}(i,k) = r(i,k)\left(V^{2}(i,k)+C^{2}(i,k)\right)/2 \tag{5.30}$$

$$E^{-}(i,k) = r(i,k)\left(V^{2}(i,k)-C^{2}(i,k)\right)/2 \tag{5.31}$$

Briefly, in both situations of traffic operations (free moving or congested), the numerical fluxes at the cell interface are determined.

Order of accuracy: If Δx and Δt are decreased simultaneously by the factor ε, the upper bound of the local error is proportional to ε (first order accuracy).

Hoogendoorn (1999a) reported that this scheme produces little numerical diffusion, that is, after releasing the vehicles, drivers at the head of a queue drive away with realistic speeds while the vehicle at the tail of the queues remain at their locations. This property also prevents vehicles from moving backward from a jam into the empty region. However, he also found that this scheme yields some artifacts at the tails of a queue, that is, some vehicles are able to drive into the jam. This unrealistic effect is caused by the discontinuity in the numerical flux functions.

5.4 An improved numerical scheme

In this section we propose an improved numerical scheme for second order continuum traffic flow models. We will show mathematically that this scheme can prevent traffic from moving backwards. This property of the scheme is very important for the simulation of congested traffic, as is shown via simulation results in Section 5.5 .

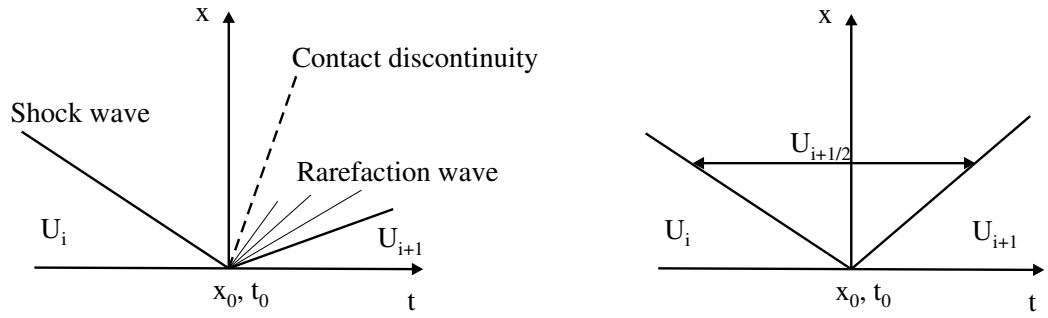

(a) The exact Riemann solution (b) The approximation solution

Figure 5.4: Illustration of the Riemann-based numerical solution.

The proposed *HLLE* scheme (*HLLE* shorthand for Niemann-based Harten-van Leer- Lax and Einfeldt), was developed by Einfeldt (1988) for gas dynamics. Let us briefly discuss the working of the scheme and its most important properties with respect to second order traffic models. The scheme computes an approximation of the exact solution of the Riemann problem (Figure 5.4(a)), in which intermediate states are averaged and the contact waves are ignored (contact waves occur when two traffic states that have the same speed but different densities come in contact with each other). It thus consists of three states, as illustrated in Figure 5.4(b). The value of the traffic variable vector at cell i $\mathbf{U}_i(k)$ is approximated to the mean value of the exact solution $\mathbf{U}$ of equation 5.3 as given below:

$$\mathbf{U}_i(k) = \frac{1}{\Delta x} \int_{-\infty}^{+\infty} \mathbf{U}(x,t)dx \tag{5.32}$$

The solution of equation 5.3 is then obtained by solving a series of Riemann problems at the cell boundaries. From the theory of divergence, equation 5.3 is rewritten as follows:

$$\frac{d}{dt} \int_{x_i-1/2}^{x_i+1/2} \mathbf{U}(x,t)dx + \frac{F\left(\mathbf{U}(x_{i+1/2},t)\right) - F\left(\mathbf{U}(x_{i-1/2},t)\right)}{\Delta x} = 0 \tag{5.33}$$

where the numerical flux $F\left(\mathbf{U}(x_{i+1/2},t)\right)$ is determined at each cell interface and each time step. To approximate this numerical flux, a value of $\mathbf{U}(x,t)$ needs to be determined at the interfaces. The Riemann problem is then described as follows:

$$\begin{aligned} \frac{\partial \mathbf{U}}{\partial t} + \frac{\partial F(\mathbf{U})}{\partial x} &= 0 \\ \mathbf{U}(x,0) &= \mathbf{U}_l \quad \text{with} \quad x < 0 \\ \mathbf{U}(x,0) &= \mathbf{U}_r \quad \text{with} \quad x > 0 \end{aligned} \tag{5.34}$$

Now let $\tilde{\mathbf{U}}\left(\frac{x-x_0}{t-t_0}\right)$ denote the Riemann solution of equation 5.34. This solution consists of three waves (Figure 5.4) that separate two constant states. For long it has been argued that it is costly to determine the exact solutions, or that it involves in an unnecessary amount of details for most numerical methods of the *Godunov* type. Moreover, an implicit numerical scheme requires a differentiable flux in order to arrive at a linearized set of algebraic equations at each iteration. However, the exact solution is not available in any closed form (Batten et al. (1993)). The solution introduced in this section, therefore, will approximate the Riemann solution (Figure 5.4(a)) by using a single state (Figure 5.4(b)) which is calculated in such a way that the mean value of the exact solution is the same as the mean value of the approximation solution. Then the approximation solution of the Riemann problem 5.34 is determined as follows:

$$\tilde{\mathbf{U}}_{i+1/2}\left(\frac{x-x_{i+1/2}}{t}\right) = \begin{array}{ll} \mathbf{U}_i & \left(x - x_{i+1/2} < \chi^l_{i+1/2} t\right) \\ \mathbf{U}_{i+1/2} & \left(\chi^l_{i+1/2} t < x - x_{i+1/2} < \chi^r_{i+1/2} t\right) \\ \mathbf{U}_{i+1} & \left(x - x_{i+1/2} > \chi^r_{i+1/2} t\right) \end{array} \tag{5.35}$$

The variables $\chi^r(i+1/2,k)$ and $\chi^l(i+1/2,k)$ in equation 5.35 denote the numerical approximations for the largest and smallest physical wave speeds, respectively, of the propagation of the physical waves in the exact solution of the Riemann problem, determined as follows:

$$\begin{aligned} \chi^r(i+1/2,k) &= \max\left(\chi^{max}(i+1/2,k), \chi^{max}(i+1,k)\right) \\ \chi^l(i+1/2,k) &= \min\left(\chi^{min}(i+1/2,k), \chi^{min}(i,k)\right) \end{aligned} \tag{5.36}$$

Where $\chi^{max}(i+1/2,k)$ and $\chi^{min}(i+1/2,k)$ denote the maximum and minimum of the eigenvalues of the Jacobian matrix defined by equation 5.4 at cell interface $x_{i+1/2}$, respectively.

In equation 5.35, the average intermediate state is determined in such a way that the conservation law is satisfied, as follows:

$$\int_{-\Delta x/2}^{+\Delta x/2} \tilde{\mathbf{U}}_{i+1/2}(x/t)dx = \int_{-\Delta x/2}^{+\Delta x/2} \tilde{\mathbf{U}}(x/t)dx \tag{5.37}$$

Hence $\mathbf{U}_{i+1/2}$ is calculated by:

$$\begin{aligned} \mathbf{U}(i+1/2,k) &= \frac{\chi^r(i+1/2,k)\mathbf{U}(i+1,k) - \chi^l(i+1/2,k)\mathbf{U}(i,k)}{\chi^r(i+1/2,k) - \chi^l(i+1/2,k)} \\ &- \frac{\mathbf{F}(i+1,k) - \mathbf{F}(i,k)}{\chi^r(i+1/2,k) - \chi^l(i+1/2,k)} \end{aligned} \tag{5.38}$$

The approximation solution at the next time step $(k+1)$ is then obtained by averaging these solutions:

$$\mathbf{U}(i,k+1) = \frac{1}{\Delta x}\int_{0}^{+\Delta x/2} \tilde{\mathbf{U}}_{i+1/2}(x/t)dx + \frac{1}{\Delta x}\int_{-\Delta x/2}^{0} \tilde{\mathbf{U}}_{i-1/2}(x/t)dx \tag{5.39}$$

Which can be written in the conservation form as:

$$\mathbf{U}(i,k+1) = \mathbf{U}(i,k) - \frac{\Delta t}{\Delta x}\left(\mathbf{F}(i+1/2,k) - \mathbf{F}(i-1/2,k)\right) \tag{5.40}$$

In which the fluxes are determined as follows:

$$\begin{aligned}\mathbf{F}(i+1/2,k) &= \frac{\chi^+(i+1/2,k)\mathbf{F}(i,k) - \chi^-(i+1/2,k)\mathbf{F}(i+1,k)}{\chi^+(i+1/2,k) - \chi^-(i+1/2,k)} \\ &+ \frac{\chi^+(i+1/2,k)\chi^-(i+1/2,k)}{\chi^+(i+1/2,k) - \chi^-(i+1/2,k)}\left(\mathbf{U}(i+1,k) - \mathbf{U}(i,k)\right)\end{aligned} \tag{5.41}$$

In equation 5.41, $\chi^+(i+1/2,k)$ and $\chi^-(i+1/2,k)$ denote the upper bounds and lower bounds of the largest and smallest physical wave speeds, respectively, determined as given below:

$$\begin{aligned}\chi^+(i+1/2,k) &= \max\left(\chi^r(i+1/2,k),0\right) \\ \chi^-(i+1/2,k) &= \min\left(\chi^l(i+1/2,k),0\right)\end{aligned} \tag{5.42}$$

The expression 5.42 captures the differences between free-flow and congested flow conditions: in case of free-flow, disturbances in the flow travel in the upstream direction(along the two characteristics). By applying this scheme to the Payne-like models, we end up with the following equations:

$$r(i,k+1) = r(i,k) - \frac{\Delta t}{\Delta x}\left(q(i+1/2,k) - q(i-1/2,k)\right) \tag{5.43}$$

$$\begin{aligned}q(i,k+1) &= q(i,k) - \frac{\Delta t}{\Delta x}\left(E(i+1/2,k) - E(i-1/2,k)\right) \\ &+ \frac{q_e(i,k) - q(i,k)}{\tau}\end{aligned} \tag{5.44}$$

Properties of the proposed scheme: Let us discuss the properties of the proposed newly approximation scheme in two extreme cases: upstream congested / downstream free flow and upstream free flow / downstream congested.

- upstream free flow / downstream congested: let us assume that the density of cell i approaches to zero at time instant $t_0 = k\Delta t$ (the traffic conditions approach the free-flow situation), that is $r(i,k) \to 0$, we have:

$$\frac{\partial r}{\partial t} = \frac{1}{\Delta x}\left(q(i-1/2,k) - q(i+1/2,k)\right) \tag{5.45}$$

Where $q(i+1/2,k)$ and $q(i-1/2,k)$ are determined from equation 5.41 :

$$\begin{aligned} q(i+1/2,k) &= \frac{-\chi^-(i+1/2,k)r(i+1,k)}{\chi^+(i+1/2,k)-\chi^-(i+1/2,k)} \\ &\quad \big(V(i+1,k)-\chi^+(i+1/2,k)\big) \qquad (5.46) \\ q(i-1/2,k) &= \underbrace{\frac{\chi^+(i-1/2,k)q(i-1,k)}{\chi^+(i-1/2,k)-\chi^-(i-1/2,k)}}_{\geq 0} \\ &+ \underbrace{\frac{-\chi^+(i-1/2,k)\chi^-(i-1/2,k)}{\chi^+(i-1/2,k)-\chi^-(i-1/2,k)}r(i-1,k)}_{\geq 0} \geq 0 \qquad (5.47) \end{aligned}$$

By using the following Roe's approximation for traffic variables:

$$V(i+1/2,k)=\frac{V(i,k)\sqrt{r(i,k)}+V(i+1,k)\sqrt{r(i+1,k)}}{\sqrt{r(i,k)}+\sqrt{r(i+1,k)}} \qquad (5.48)$$

after a straightforward algebraic calculation we obtain the upper limit of the wave speed as:$\chi^+(i+1/2,k)=V(i+1,k)+C(i+1,k)$. Hence, the density flux (flow rate) at the downstream cell interface is:

$$q(i+1/2,k)=\frac{\chi^-(i+1/2,k)r(i+1,k)}{\chi^+(i+1/2,k)-\chi^-(i+1/2,k)}C(i+1,k)\leq 0 \qquad (5.49)$$

Therefore, $\partial r/\partial t \geq 0$ $\Leftrightarrow$r(x,t)$\geq$ 0 at every time instant $t > t_0$. Because traffic in cell i is uncongested, $\partial q/\partial t$ has the same sign as $\partial r/\partial t$, which means that $\partial q/\partial t \geq 0$ $\Leftrightarrow$q(x,t)$\geq$ 0 at every time instant $t > t_0$.

- upstream congested / downstream free flow: if the density of cell i approaches the jam density at time instant $t_0 = k\Delta t$ (the traffic conditions approach the congested/standstill situation), that is $r(i,k) \to r_{max}$, we have:

$$\frac{\partial q}{\partial t}=\frac{1}{\Delta x}\left(E(i-1/2,k)-E(i+1/2,k)\right) \qquad (5.50)$$

Where $E(i+1/2,k)$ and $E(i-1/2,k)$ are determined from equation 5.41 as :

$$\begin{aligned} E(i+1/2,k) &= \frac{-\chi^-(i+1/2,k)r(i+1,k)}{\chi^+(i+1/2,k)-\chi^-(i+1/2,k)} \\ &\quad \left[V^2(i+1,k)+C^2(i+1,k)-\chi^+(i+1/2,k)V(i+1,k)\right] \qquad (5.51) \\ E(i-1/2,k) &= \underbrace{\frac{\chi^+(i-1/2,k)E(i-1,k)}{\chi^+(i-1/2,k)-\chi^-(i-1/2,k)}}_{\geq 0} \\ &+ \underbrace{\frac{-\chi^+(i-1/2,k)\chi^-(i-1/2,k)}{\chi^+(i-1/2,k)-\chi^-(i-1/2,k)}q(i-1,k)}_{\geq 0} \geq 0 \qquad (5.52) \end{aligned}$$

By using Roe's approximation for traffic variables, we obtain the flux of the flow rate at the downstream cell interface as:

$$E(i+1/2,k) = \frac{\chi^-(i+1/2,k)r(i+1,k)}{\chi^+(i+1/2,k)-\chi^-(i+1/2,k)} \times C(i+1,k)\left[V(i+1,k)-C(i+1,k)\right] \leq 0 \quad (5.53)$$

since in the uncongested region of cell $(i+1)$, $V(i+1,k) > C(i+1,k)$. Hence, $\partial q/\partial t \geq 0 \Leftrightarrow$q(x,t)$\geq 0$ at every time instant $t > t_0$. Because traffic in cell i is congested, $\partial q/\partial t$ has the opposite sign as $\partial r/\partial t$, which means that $\partial r/\partial t \leq 0$ $\Leftrightarrow$r(x,t)$\leq r_{max}$ at every time instant $t > t_0$.

In sum, in both extreme cases the traffic does not move backwards, that is, from downstream to upstream, and the proposed scheme guarantees the positivity constraints over all the time of computation.

In order to visualize the property of the proposed scheme, let us simulate Payne's model using this scheme. We assume that there is a congested region in the middle of a 6km roadway (from KM1-KM3) at time instant $t = 0$. The cell length and time step are 100m and 2sec, respectively. There is no traffic demand from upstream when the traffic starts to dissipate from the congestion. The output of the simulation in Figure 5.5 shows that the congestion region gradually dissipates and that there is no traffic moving from the congestion area to the empty road upstream (vehicle at the tail of the queues are standstill), as well as from the empty road downstream to the congestion area (the jam is not filled with more traffic, that is, the maximum density is not exceeded). This property shows the advantage of the proposed scheme in satisfying conservatively the positive traffic variables. In the next section, we will cross-compare this numerical solution with the others in calibrating and validating Payne's model.

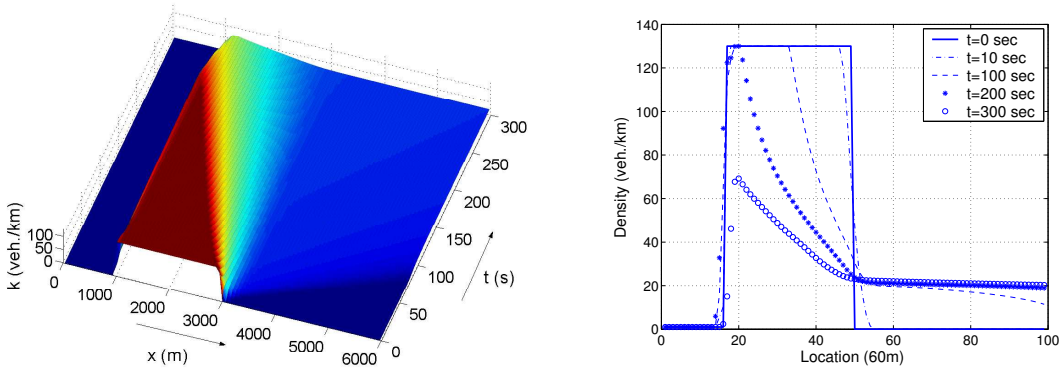

(a) Time-space density (b) Space density

Figure 5.5: Simulation results with the HLLE scheme.

Order of accuracy: In the proposed scheme, if Δx and Δt are decreased simultaneously by the factor ε , the upper bound of the local error is proportional to ε (first order accuracy).

5.5 Cross-comparison of numerical schemes for Payne-type models

In this section, we cross-compare the performance of three numerical schemes, namely *MacCormack*, *Steger-Warming* and the newly proposed scheme for Payne's model using real-life data. The extension of our approach to the other second order macroscopic models is straightforward (Tampere (2004)).

5.5.1 Numerical stability and boundary conditions

Let us start with discussing conditions for numerical stability and the choice of the boundary conditions as follows.

- *Numerical stability*: A numerical solution is unstable if the errors grow exponentially, which in turn may lead to oscillation of the traffic variables with very short wave lengths. The condition for the stability of the finite volume methods for the flux is the so-called Courant-Friedrichs-Lewy condition (Sod (1985)). This condition states that the domain for the approximation of $\mathbf{U}(i, k+1)$ in equation 5.38 must be able to include all the physical information which influences the behavior of the system at this point. To this end, the following inequality must be fulfilled $\Delta t \leq \Delta x / V_{max}$. In addition, the instability can also occur if Δt is larger than one of the local relaxation times $1/\epsilon_k$, where ϵ_k are the eigenvalues of the functional matrix of the sink and source terms $\mathbf{S}$. With this condition, the additional restriction of Δt, which depends on the maximum density in the simulation, needs to be fulfilled as well (Helbing and Treiber (1999c)).

- *Boundary conditions*: Four types of the time-dependent boundary conditions are illustrated in this chapter as follows (Helbing and Treiber (1999c)):

  1. The periodic boundary condition assumes that the density and flow at the entry and exit of the considered freeway are equal, as: $\mathbf{U}(x_0, t) = \mathbf{U}(x_{end}, t)$ and $\partial \mathbf{U}/\partial x|_{(x_0,t)} = \partial \mathbf{U}/\partial x|_{(x_{end},t)}$
  2. The Neumann boundary condition reflects the case where the density and flow are constant at the entry and exit of the considered freeway, as: $\partial \mathbf{U}/\partial x|_{(x_0,t)} = \partial \mathbf{U}/\partial x|_{(x_{end},t)} = 0$
  3. The open boundary condition describes the situation when the traffic state is smooth at the boundary, as: $\partial^2 \mathbf{U}/\partial x^2|_{(x_0,t)} = \partial^2 \mathbf{U}/\partial x^2|_{(x_{end},t)} = 0$
  4. The Dirichlet boundary condition is given by the empirically measured data $\mathbf{U}(x_0, t)$ and $\mathbf{U}(x_{end}, t)$ at the entry and exit of the freeway.

  In this chapter, we adopt the combination of Dirichlet boundary condition and Neumann boundary condition for the simulation with all mentioned numerical schemes. The reason for our choice is illustrated in detail in Helbing and Treiber (1999c).

5.5.2 Simulation and calibration/validation results

The data used in this chapter is obtained from the Dutch Ministry of Transport, Public Works and Water Management. These data contain the time-dependent (every 5 minutes) traffic flow rate and mean speed at each detector on the two-lane freeway A1 from KM 87.3 to KM108.6. For the purpose of this chapter, a homogeneous part of the A1 without on–ramps and off–ramps, from KM 96.3 to KM 104.6 has been used. During the period from 14.00h to 19.00h in September and October 2002, this part of freeway was heavily congested from KM97.8 to KM 104.0 due to a bottleneck in the form of a bridge. The detectors were located as shown in Figure 5.6

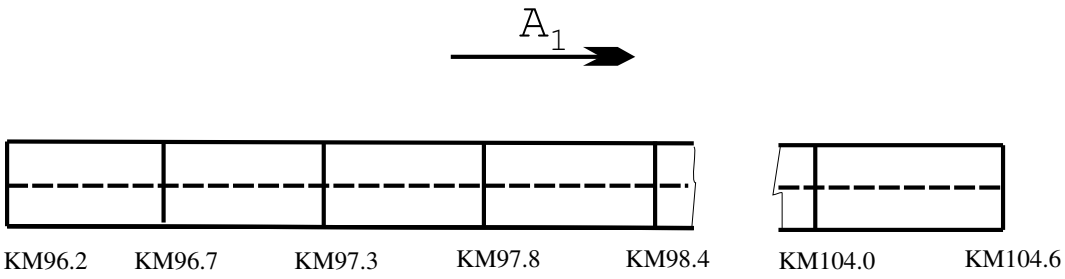

Figure 5.6: Lay-out of the roadway for simulation.

Payne's model was first calibrated with the different numerical schemes mentioned above using the traffic data from 22 September 2002, then it was validated with data from 4 October 2002. The model parameters to be calibrated were the following:

1. The local wave speed c
2. The fundamental diagram's factors: the free speed V_{max}, the critical density r_{cr} and the jam density r_{max}
3. The relaxation time τ

The objective function to be optimized was formulated as the weighted total mean square error of the mean speed and flow rate:

$$Z = \frac{1}{D \times N} \sum_{d=1}^{D} \sum_{t=1}^{N} \{ [V_m(d,t) - V(d,t)]^2 + \tilde{\mu} \, [q_m(d,t) - q(d,t)]^2 \} \tag{5.54}$$

where $(0 \leq \tilde{\mu} \leq 1)$ is the weighted factor, d is the location of detectors, q_m and V_m are the measured flow rate and mean speed at the detectors.

The length of the cells equaled 200 m, while the time-step equaled 5 s for the *HLLE* method and 1 s for the other methods, because the MacCormack scheme and the Steger-Warming scheme need a smaller time-step to guarantee numerical stability. Note that the larger time step used in the *HLLE* method will have a slight negative impact on the accuracy of the model predictions (which obviously depends on the size of the time step). The data used to feed

the model were given at KM 96.2 and KM 104.6 (boundary conditions) and the objective function was calculated with the data at the remaining detectors. Since we simulated the model with a cell-length of 200m, the traffic data were interpolated within the detectors upstream and downstream of the cell.

To calibrate Payne's model with these numerical schemes, we set up an automated calibration procedure for macroscopic traffic models. This procedure is described in detail in Chapter 7. The automated calibration process was successfully carried out with data set from 22 September 2002 for the considered numerical approximation schemes. The results are shown in Table 5.1. If we consider the estimated model parameters (Table 5.1), we can conclude that different optimal values are found for the different numerical schemes tested. In particular, the estimated values of the local wave speed somehow differ. The reason is that different schemes result in different model predictions, especially near the large gradients of flow and speed (emphasized by the big difference of local wave speed). It is also noteworthy that the total mean square errors do not differ strongly. In this step, the total relative mean square errors of the *HLLE* scheme are slightly higher than that of the MacCormack scheme due to the fact that, as explained earlier, the time step of the former is much higher than that of the latter. The obtained parameters, such as, free speed, jam density, critical density and relaxation time are well-comparable with the values found in calibrating and validating the METANET model (Ngoduy and Hoogendoorn (2003a)).

Table 5.1: Results of parameter calibration process (TMSE = Total relative Mean Square Errors).

Schemes	Wave speed (km/h)	Free speed (km/h)	Jam density (veh/km)	Critical density (veh/km)	Rel. time (second)	TMSE (%)
Max-Min	0-150	80-100	100-200	20-40	5-40	
HLLE	81.7	124.5	167.4	35.0	17.3	5.3
MacCormack	96.8	122.5	165.5	33.9	17.1	4.8
Steger-Warming	101.8	120.4	159.1	34.8	16.1	7.8

To investigate the performances of the model with the different numerical schemes, we performed simulations with the three calibrated schemes and compared them with the collected data from 4 October 2002 (validation process). To make a cross-comparison, the real data and outputs were interpolated to obtain the same time and space intervals. The simulation outputs of the model with *HLLE* scheme are shown in Figures 5.7 and 5.8. Figure 5.9 shows the results of the simulation with the MacCormack method. Figure 5.10 shows the results of the simulation with the Steger-Warming Flux Splitting method. The simulation results in both the calibration and validation process show that the *HLLE* scheme is very stable during the whole simulation, while the Steger-Warming scheme produces oscillations both upstream and downstream of the congestion. The MacCormack scheme produces equally good results but requires a much smaller time step - in this case 1 s - compared to the HLLE scheme - in

this case 5 s - in order to ensure the numerical stability. As a result, traffic simulation and the automated calibration with the *HLLE* scheme require much shorter time. The benefits of using the proposed *HLLE* scheme are thus clear, providing good accuracy, while being more robust and much faster than the other schemes.

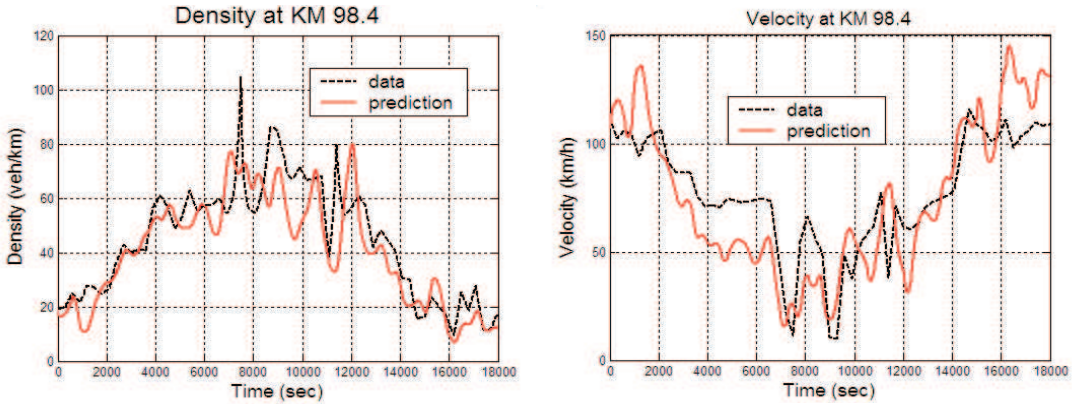

(a) Density (b) Speed

Figure 5.7: Validation with the *HLLE* method versus real data.

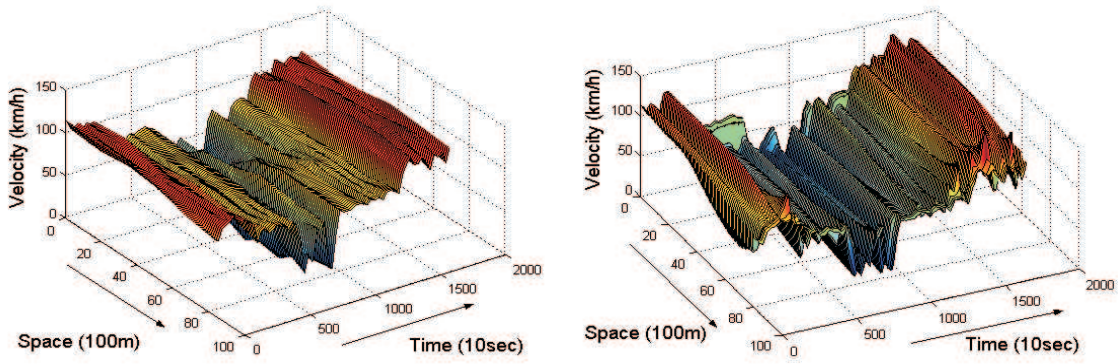

(a) Observation (b) Estimation

Figure 5.8: Spatial and temporal evolution of the mean speed with the *HLLE* method.

5.6 Summary

Second order macroscopic traffic models are systems of partial differential equations (PDE's) that consist of the conservation of vehicles equation, and of a dynamic equation that describes the dynamics of the speed (or the flow). These systems of partial differential equations are of the hyperbolic type. To use this type of model to simulate traffic flow operations , traffic engineers have often used finite volume methods to numerically approximate the exact solution of these PDE's, with various degrees of success. Assuming that the underlying model is accurate, an appropriate choice of numerical scheme results in good model performance.

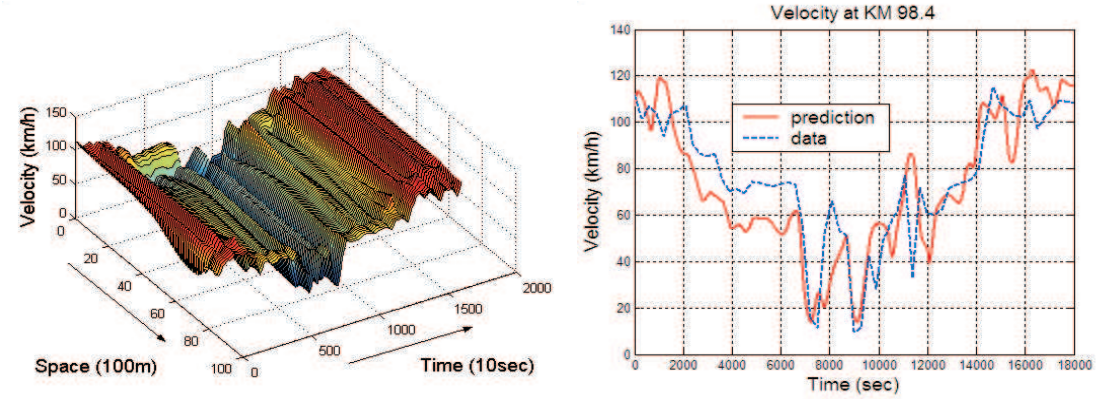

(a) Observation (b) Estimation

Figure 5.9: Spatial and temporal evolution of the mean speed and density with the *MacCormack* method.

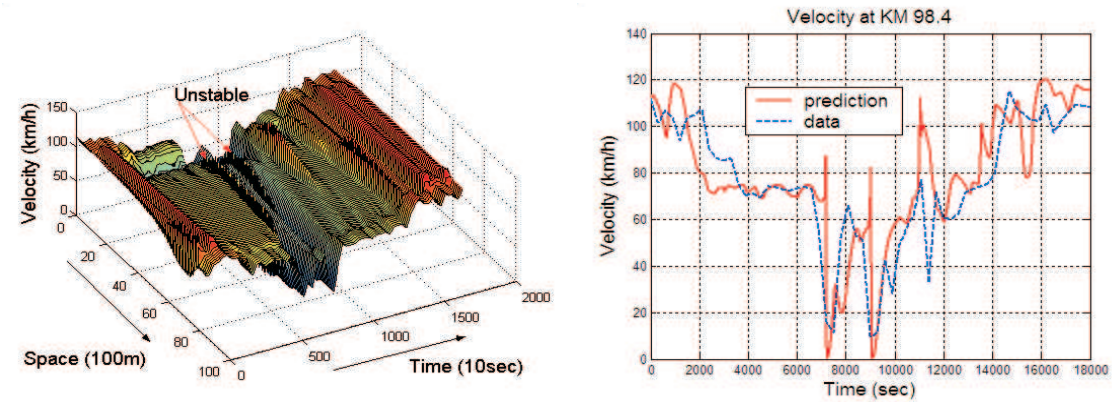

(a) Observation (b) Estimation

Figure 5.10: Spatial and temporal evolution of the mean speed and density with the *Steger-Warming* method.

In this chapter, we proposed a numerical solution that guarantees all positivity variable constraints, and we presented an approach to cross-compare different numerical approaches for second-order macroscopic traffic models. The approach consists of an automated calibration procedure and cross-comparison of the model predictions of these numerical schemes using real-life data. The used data was collected in 2002 from the A1, a freeway in the Netherlands. In particular, a period with traffic congestion was considered (from September for the calibration and from October for the validation).

In this chapter we considered three numerical models based on the second-order model, namely, the Steger-Warming solver, the MacCormack solver, and a novel approach: the so-called extended *HLLE* scheme. The simulations covered a 5-hour period. The optimization processes were terminated successfully and good optimal model parameters were estimated for the different schemes. In general, the three considered numerical schemes produced comparable mean square errors, although the estimated parameter values were somehow different (in particular the parameter that describes the local wave speed). However, the MacCormack

and Steger-Warming method require much smaller time steps than the new numerical model proposed in this chapter, and thus required much more computational time. On top of this, the *HLLE* method appears very stable while the others produced unrealistic oscillations in regions with large gradients (upstream and downstream of the congestion period). From the same original model, the different numerical schemes resulted in different simulation outputs. The new scheme proposed in this chapter proved to be the most reliable in terms of computational time and numerical stability compared to the others, in particular when the occurrence of traffic congestion was simulated. The scheme improves the performance of the model significantly, and thus provides an effective and reliable approach to simulate traffic flow under congestion. This scheme is applied to approximate the *MLMC* model developed in Chapter 4 in an extended calibration and validation process in Chapter 7.

Chapter 6

MLMC macroscopic model for urban networks

The current macroscopic traffic flow models for urban networks presented in Chapter 2, such as METACOR (Elloumi et al. (1994)) and STRADA (Buisson et al. (1996)), rarely distinguish user classes, nor do they consider the lateral dynamics between lanes (lane changing and overtaking maneuvers). However, due to the large differences between vehicle classes it is expected that the explanatory and predictive power of contemporary macroscopic traffic models for urban networks may be improved significantly by distinguishing user classes with their specific flow characteristics. Furthermore, distinguishing user-classes is essential when class-specific or priority control is applied, or when different types of traffic information are available to different user-classes.

To enable the generalized description of traffic flow dynamics in urban networks, in this chapter we will deal with (macroscopic) modeling discontinuities of multiclass traffic flow at multilane intersections. That is, the way traffic flows in and flows out at multilane intersections will be handled taking into account the traffic composition. In Chapter 4, we have introduced a generalized macroscopic continuum model dealing with discontinuities at on– and off–ramps on multilane freeways based on a *gap-acceptance* model and on *renewal theory*. In this chapter, we will show the extension of this approach to model traffic operations in *MLMC* urban networks.

The main purpose of this chapter is the development of a new macroscopic model to describe the class-specific traffic flow operations in a multilane urban network, with intersections that consist of exclusive lanes for right-turning and left-turning traffic, etcetera. A multilane model is expected to improve the predictive accuracy (improved blocking back modeling, reduced capacity due to left-turning vehicles blocking the road, and so on), which will be beneficial to both control applications and class-specific dynamic assignment problems (Bliemer (2001)). For these reasons, this chapter aims to develop an operational model to support the analysis of network operations (estimation and prediction) under a variety of circumstances based on the *MLMC* traffic flow theory. To this end, a dedicated numerical scheme is required, in which the boundary conditions at the intersections need to be defined and handled

adequately. In the developed model (Ngoduy et al. (2005a)), we need to determine the traffic flow rate incoming from or outgoing to a link at nodes based on the *gap-acceptance* model and *renewal theory* from Chapter 3, which are applied in Chapter 4. This, in turn, plays an important role in the determination of the boundary conditions for that link.

The outline of this chapter is follows. In Section 6.1 a *MLMC* continuum model for links is described. Section 6.2 presents a model to describe traffic operations at intersections. Finally, we conclude this chapter in Section 6.3.

6.1 Macroscopic model for *MLMC* links

This section presents a *MLMC* macroscopic traffic model for links in an urban network. We will show the governing equations for the dynamics of multiclass traffic on multilane links and describe a robust numerical solution for these equations.

6.1.1 Governing equation

The main traffic phenomena on urban links are not due to the inherent traffic flow dynamics as on freeway links but, in most cases, due to intersections, unsignalized, or signalized, at which the switching of the traffic lights or the influence of stop lines lead to the corresponding shock waves generated by the stop–and–go movements of the vehicles upstream of the intersections. As a result, the queue formation at intersections play a major role in determining the dynamics of traffic flow on an urban link. The dynamics of queue at intersections are determined based on the traffic inflows and outflows of such intersections. Due to the mentioned difference between traffic operations on freeways and urban links, in the context of urban networks, only the first order macroscopic *MLMC* model presented in Chapter 4 for traffic flow of vehicle class u ($u \in U$) in lane i ($i \in I$), at link a ($a \in L$) is employed. The model consists of the following partial differential equation that describes the time-space dynamics of aggregate traffic variables: flow $q = q(x,t)$, mean speed $V = V(x,t)$ and density $r = r(x,t)$:

$$\begin{aligned} \frac{\partial r^a_{i,u}}{\partial t} + \underbrace{\frac{\partial q^a_{i,u}}{\partial x}}_{\text{convection}} &= \underbrace{\sum_{s\in U}\sum_{j=i\pm1}\left(p^a_{j,i,u}\Psi^a_{j,u,s} - p^a_{i,j,u}\Psi^a_{i,u,s}\right)}_{ILC} \\ &+ \underbrace{\sum_{j=i\pm1}\left(\triangle^a_{j,i,u} r^a_{j,u} - \triangle^a_{i,j,u} r^a_{i,u}\right)}_{SLC} \\ &+ \underbrace{\nu^{a,+}_{i,u}(x,t) + \nu^{a,-}_{i,u}(x,t)}_{MLC} \end{aligned} \tag{6.1}$$

With the assumption of equilibrium traffic conditions (first-order theory), the traffic flow rate $q(x,t)$ is considered a function of density, $q(x,t) = q_e(r(x,t))$, which is determined

empirically. Therefore, the basic traffic variable is density while the traffic flow is the derived variable. Note in equation 6.1 that the *mandatory lane-changing* term accounts for the lane-drops on links (permanent or due to accidents). The *immediate lane-changing* probability $p^a_{i,j,u}$ of vehicle class u from lane i to the adjacent lane j ($j = i \pm 1$) of link a is determined the same as with equation 3.32, while the *mandatory lane-changing* rate from lane i to lane j ($j > i$) in case of lane–drops is determined the same as the merging rate at on-ramps in equation 4.12.

To simulate equation 6.1 we use a dedicated numerical scheme, namely the Godunov scheme (see Leo and Pretty (1992), Daganzo (1994), Lebacque (1996)). In this scheme, the Godunov numerical flux is calculated based on the cell supply and demand rule as described in the next section.

6.1.2 Numerical solution

In this section, we briefly describe the working of the Godunov scheme for the *MLMC* continuum traffic model presented in Section 6.1.1. In order to numerically solve the conservative equation 6.1, time and space are divided into time steps $t_k = k * \Delta t$ and segments (cells) $x_m = m * \Delta x$ (Figure 6.1). In the context of a multilane link, due to the exchanges of flow between the lanes, the traffic density of vehicle class u in lane i of link a, at cell m and time instant $k + 1$ is determined in two steps as follows:

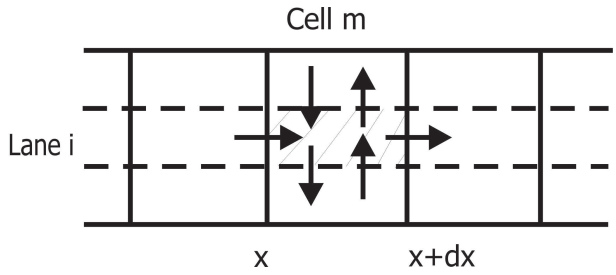

Figure 6.1: Traffic flowing into and out of a cell m in lane i of link a.

Longitudinal dynamics : This step calculates the dynamics of the density due to the movement of the vehicles along the road.

$$\tilde{r}^a_{i,u}(m,k) = r^a_{i,u}(m,k) - \frac{\Delta t}{\Delta x}\left[q^a_{i,u}(m+1/2,k) - q^a_{i,u}(m-1/2,k)\right] \tag{6.2}$$

Lateral dynamics : This step updates the dynamics of the density over lanes due to overtaking and lane-changing processes (immediate, spontaneous and mandatory lane-changes).

$$\begin{aligned} r^a_{i,u}(m,k+1) &= \tilde{r}^a_{i,u}(m,k) \\ &+ \underbrace{\sum_{s\in U}\sum_{j=i\pm1}\left[(\tilde{p}^a_{j,i,u}(m,k)\tilde{\Psi}^a_{j,u,s}(m,k) - \tilde{p}^a_{i,j,u}(m,k)\tilde{\Psi}^a_{i,u,s}(m,k)\right]}_{ILC} \\ &+ \underbrace{\sum_{j=i\pm1}\left[\tilde{\Delta}^a_{j,i,u}(m,k)\tilde{r}^a_{j,u}(m,k) - \tilde{\Delta}^a_{i,j,u}(m,k)\tilde{r}^a_{i,u}(m,k)\right]}_{SLC} \\ &+ \underbrace{\tilde{\nu}^{a,+}_{i,u}(m,k) + \tilde{\nu}^{a,-}_{i,u}(m,k)}_{MLC} \end{aligned} \tag{6.3}$$

Where $\tilde{q}$, $\tilde{\Delta}$, $\tilde{\Psi}$, $\tilde{\pi}$, $\tilde{p}$, and $\tilde{\nu}$ are determined with respect to $\tilde{r}$.

To calculate the density due to longitudinal processes, the density fluxes at cell interface $q^a_{i,u}(m+1/2,k)$ must be computed first. In order to take into account the effect of downstream congestion, the flux in the current cell m is estimated according to the downstream density in section $m+1$. This enables the representation of the change in driver behavior with respect to downstream traffic conditions. This means that the shockwave direction at each point x_m corresponding to the discrete space representation has to be defined. Thus, the input flow to section m of link a during $k\Delta t < t < (k+1)\Delta t$ is estimated based on the traffic densities of section m and $m+1$. According to the cell supply and cell demand rule (Daganzo (1994), Lebacque (1996), Lebacque and Khoshyaran (1998)), these numerical fluxes are determined as:

$$q^a_{i,u}(m+1/2,k) = \min\left(\Xi^a_{i,u}(m,k), \Sigma^a_{i,u}(m+1,k)\right) \tag{6.4}$$

Where $\Xi^a_{i,u}(m,k)$ and $\Sigma^a_{i,u}(m+1,k)$ are the traffic demand and traffic supply of the considered cell m and the downstream cell $m+1$, respectively (see Section 2.3.6 for the definition of the traffic supply and traffic demand in the numerical solution). These are computed as functions of density by the following equations:

Traffic demand

$$\Xi^a_{i,u}(m,k) = \begin{cases} q^e_u(m,k) & \text{if } r^a_i(m,k) \le r^{a,cr}_i \\ q^{a,max}_i & \text{else} \end{cases} \tag{6.5}$$

Traffic supply

$$\Sigma^a_{i,u}(m,k) = \begin{cases} q^e_u(m,k) & \text{if } r^a_i(m,k) > r^{a,cr}_i \\ q^{a,max}_i & \text{else} \end{cases} \tag{6.6}$$

In equations 6.5 and 6.6, the equilibrium flow rate is considered a function of all class specific densities, $r^{a,cr}_i$ and $q^{a,max}_i$ denote the critical density, respectively, the capacity of lane i

on link a. There are a few models proposed to calculate the equilibrium speed (hence, equilibrium flow rate) with respect to all vehicle classes such as Logghe (2003), Daganzo (1997) , Wong and Wong (2002). The fundamental diagrams must appropriately represent the difference between vehicle classes. For example, let us consider two vehicle classes (trucks and cars) in the traffic flow. If the fraction of trucks increases, the lane-changing due to interaction between cars (fast vehicles) and trucks (slow vehicles) should increase, and, obviously, the speed should decrease.

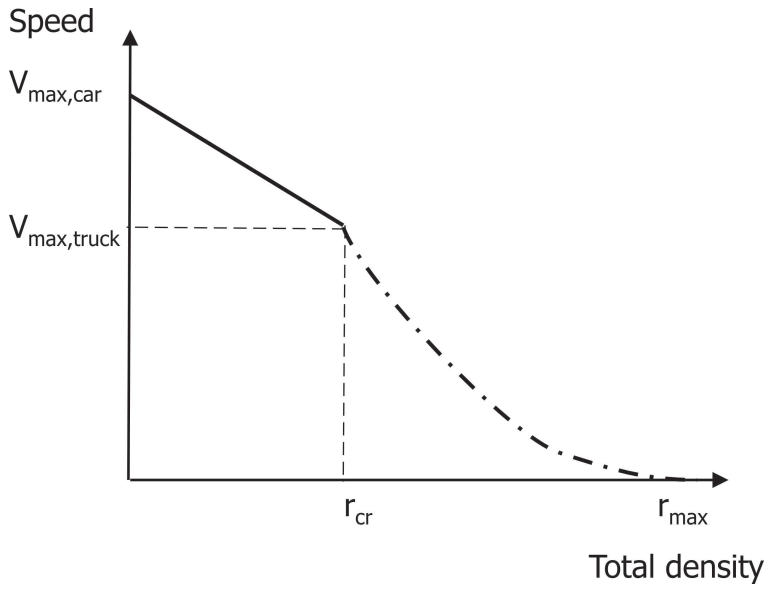

Figure 6.2: Equilibrium speed relations for cars and trucks.

Figure 6.2 illustrates that in congested states the speed is the same for trucks and cars. That is due to the fact that in the congested regime there is no space for overtaking, and, thus, the cars must slow down to the speed of the trucks. This property has been assumed in Bliemer (2001), Zhang and Jin (2002), Logghe (2003). From Figure 6.2, it is clear that the speed of cars decreases from free speed to the critical speed (corresponding to the total critical density), whereas the speed of trucks is rather steady until traffic becomes congested. Based on these features, Chanut (2005) has constructed fundamental diagrams for multiclass traffic flow.

Obviously, from equations 6.2 and 6.3, the major question is how to determine the boundary conditions of the link at nodes (inflow and outflow). For instance, how to compute $q^a_{i,u}(1/2, k)$ or $q^a_{i,u}(M + 1/2, k)$ when i is equal to 1 or M, respectively (Figure 6.3)

In the next section, we will present a model which enables the determination of the inflow and outflow at multilane intersections based on the *gap-acceptance* model and the *renewal theory* presented in Chapter 3.

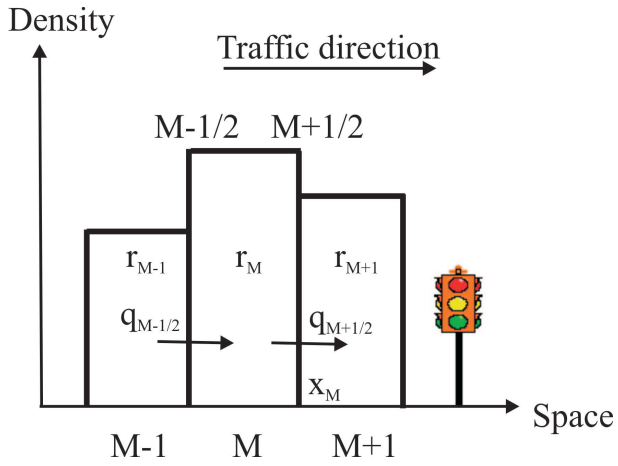

Figure 6.3: Computation of density fluxes at an intersection.

6.2 Macroscopic model for *MLMC* intersections

This section describes a new model to determine inflows and outflows at multilane urban intersections. The inner space of the intersection is divided into spatial zones, corresponding to each allowed turning movement. Figure 6.4 depicts all allowed turning movements for vehicles going from link 1 in the case of a four-leg intersection: left-turning vehicles from link 1 to link 4, right-turning vehicles to link 2, and through vehicles to link 3. The spatial zones within the inner space of the intersection, and associated with each turning movement, play the same role as the cells of an urban link as described in Section 6.1.2.

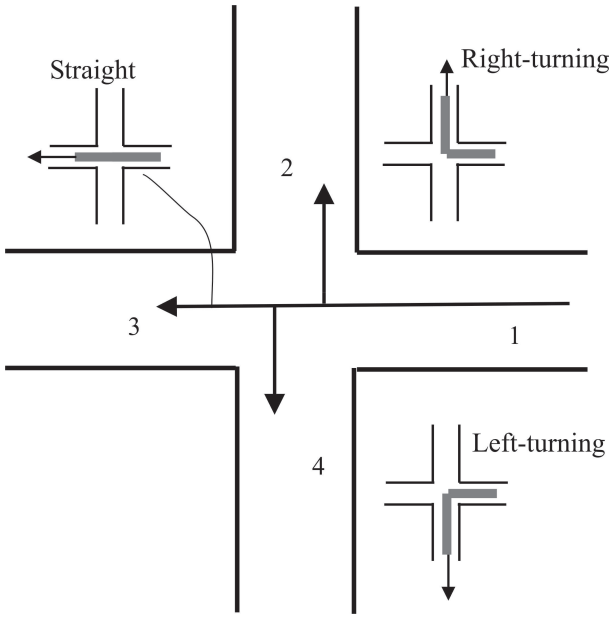

Figure 6.4: Turning movements at a 4 leg intersection.

In order to model the traffic dynamics at intersections, all the nodes are considered to consist

of three links. The approach can easily be extended to a situation with more than three links by using the so-called *dummy* link in order to split this node into nodes with less than three links. In the *dummy* link, there are no dynamics in the traffic flow. We regard a node as a merging node if there are two incoming links and one outgoing link at that node, and as a diverging node if there are two outgoing links and one incoming link.

The inflow to each spatial zone is estimated taking into account the traffic conditions in the first cell of the destination link and those in the last cell of the origin link, and the percentage of each turning movement. The outflow from the spatial zone is estimated based on the traffic conditions within the inner space of the intersection and those in the first cell of the destination link, and the percentage of each turning movement. This enables to take into account queue spill-back from downstream links which influence the traffic flow at the intersection.

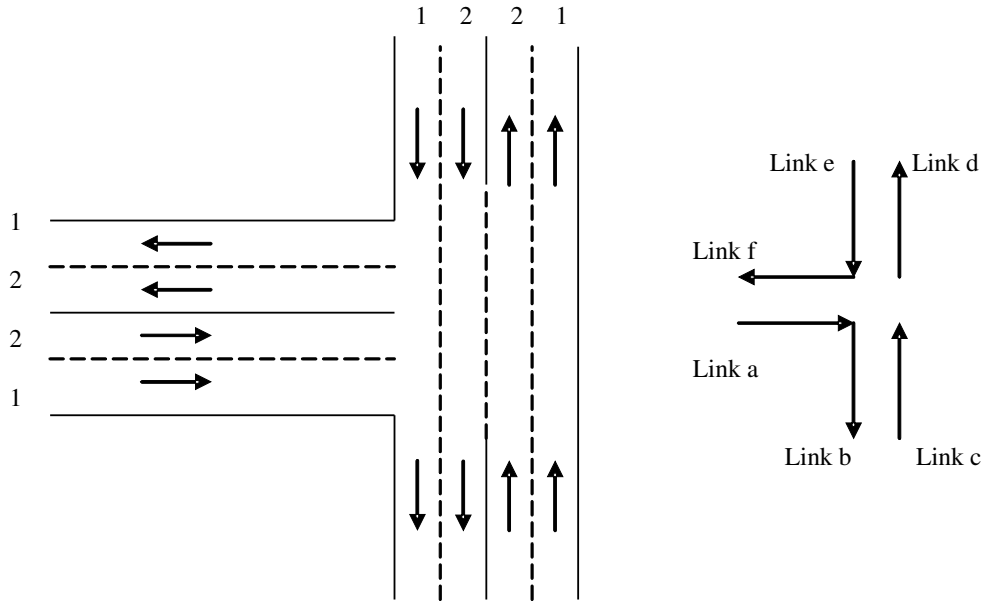

Figure 6.5: Layout of a two-lane T -junction. The traffic flowing out of link a, link c and link e as well as the traffic flowing to link b, link d and link f are determined based on *gap-acceptance* theory.

Let us consider a T-intersection, where the incoming and outgoing links have two-lanes (the generalization of links having more than two links is straightforward) as seen in Figure 6.5. The probability of making a left (right) turn depends on the traffic conditions in a crossing stream (if there is any) and the traffic conditions in the target lane. Vehicles that intend to make a left (right) turn will occupy lanes that lead to their target lanes, while the through vehicles can occupy both lanes. Therefore, the congestion in the right-turning lane will not immediately influence the left-turning probability, and vice versa. Furthermore, the priority rule is also applied in modeling left (right) turning traffic. For instance, left-turning traffic has to give way to through traffic in the opposite direction or the right-turning direction. When both vehicles want to make a left-turn, the vehicle that comes from the minor street must give

way to the other.

For an uncontrolled two-lane T-junction in Figure 6.5 , the traffic flowing in and out of a link is determined in the ensuing of this section.

6.2.1 Inflowing traffic

In this subsection we show how to determine the inflow of vehicles of class u to link d from link a and link c, which consists of traffic making a left-turn from lane ia on link a and through traffic from lane ic on link c (Figure 6.5). From Figure 6.6 , it can be seen that the left-turning traffic from link a to link d depends on the probability to cross the traffic stream on link e, on the probability to find a sufficient *lag-gap* of traffic stream on link c (this is, the merging probability) and on the traffic supply of link d. The crossing and merging probability are calculated from the *lag-gap* probability distribution function (*p.d.f*) of traffic on link e and link c regardless of user classes while the traffic supply of link d is calculated by equation 6.6

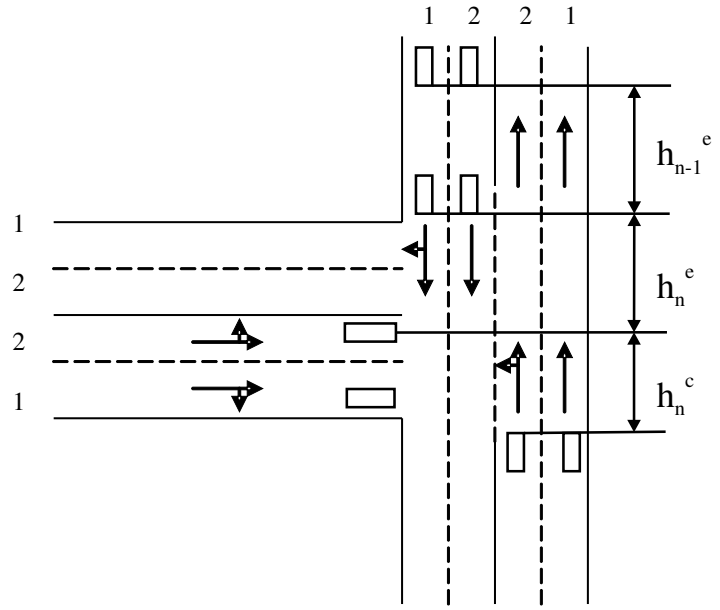

Figure 6.6: Inflows from upstream links *a* and *c* to link *d*.

Let us consider a vehicle of class u from link a going to link d. It interacts with arriving vehicles of class s from link e and from link c. The probability to find sufficient a *lag-gap* for vehicle class s from lane ie of link e and from lane ic of link c, respectively, is $P\left(h > d^e_{ie,s}(w)\right)$ and $P\left(h > d^c_{ic,s}(w)\right)$. The probability that a vehicle in lane ie of link e or in lane ic of link c interacting with a left-turning vehicle that belongs to class s is $r^e_{ie,s}/r^e_{ie}$ or $r^c_{ic,s}/r^c_{ic}$, respectively. The resulting probability of left-turning vehicle class u from lane ia of link a to lane id of link d is as follows:

$$\pi^{a,d}_{ia,id,u} = \prod_{ie} \sum_{s \in U} \frac{r^e_{ie,s}}{r^e_{ie}} \underbrace{P\left(h > d^e_{ie,s}(w)\right)}_{\text{sufficient lag-gap on link } e} \prod_{ic} \sum_{s \in U} \frac{r^c_{ic,s}}{r^c_{ic}} \underbrace{P\left(h > d^c_{ic,s}(w)\right)}_{\text{sufficient lag-gap on link } c} \tag{6.7}$$

The *lag-gap* on link e that is sufficient for left-turning traffic also depends on the fraction of vehicles to turn right from this link to lane if of link f since the right-turning traffic from link e to link f does not conflict with the left-turning traffic from link a to link d. Let $\alpha^{e,f}_{ie,u}$ denote the fraction of right-turning vehicles of class u from lane ie on link e to link f. That is, a fraction $(1 - \alpha^{e,f}_{ie,u})$ of vehicles of class u in lane ie of link e interacts with left-turning vehicles from lane ia of link a to link d. Let us consider two cases below:

- If the arriving vehicle from link e is right-turning, the gap available for a left-turning vehicle from link a to link d is $h^e_n + h^e_{n-1}$. By using the *renewal theory* presented in Chapter 3, the *lag-gap p.d.f* of vehicles of class u arriving from link e is calculated as

$$f^{ie,e}_{lag,u}(h) = 0.5\gamma^e_{ie} r^e_{ie} \left[1 - F^{ie,e}_u(2h)\right] \tag{6.8}$$

  hence the corresponding *lag-gap* cumulative distribution function (c.d.f) is:

$$F^{ie,e}_{lag,1}(d^{ie,e}_{lag,u}) = 0.5\gamma^e_{ie} r^e_{ie} \int_0^{d^{ie,e}_{lag,u}} \left[1 - F^{ie,e}_u(2h)\right] dh \tag{6.9}$$

- If the arriving vehicle from link e is not right-turning, the gap available for a left-turning vehicle from link a to link d is h^e_n, the *lag-gap p.d.f* of vehicles of class u arriving from link e is calculated as:

$$f^{ie,e}_{lag,u}(h) = \gamma^e_{ie} r^e_{ie} \left[1 - F^{ie,e}_u(h)\right] \tag{6.10}$$

  hence the corresponding *lag-gap c.d.f* is:

$$F^{ie,e}_{lag,2}(d^{ie,e}_{lag,u}) = \gamma^e_{ie} r^e_{ie} \int_0^{d^{ie,e}_{lag,u}} \left[1 - F^{ie,e}_u(h)\right] dh \tag{6.11}$$

The total *lag-gap c.d.f* of traffic arriving from link e available for left-turning traffic from link a becomes:

$$\begin{aligned} F^{ie,e}_{lag,u}(d^e_{ie,u}(w)) &= 0.5\alpha^{e,f}_{ie,u}\gamma^e_{ie} r^e_{ie} \int_0^{d^{ie,e}_{lag,u}} \left[1 - F^{ie,e}_u(2h)\right] dh \\ &+ \left(1 - \alpha^{e,f}_{ie,u}\right) \gamma^e_{ie} r^e_{ie} \int_0^{d^{ie,e}_{lag,u}} \left[1 - F^{ie,e}_u(h)\right] dh \end{aligned} \tag{6.12}$$

From expression 6.12, the average probability that a vehicle on link a finds a sufficient *lag-gap* between two successive vehicles of class s on link e to cross is calculated as:

$$\begin{aligned} P\left(h > d^e_{ie,s}(w)\right) &= \langle 1 - F^{ie,e}_{lag,s}(d^e_{ie,s}(w)) \rangle \\ P\left(h > d^e_{ie,s}(w)\right) &= 1 - 0.5\alpha^{e,f}_{ie,s}\gamma^e_{ie} r^e_{ie} \langle \int_{d^{ie,e}_{lag,s}(w)}^{\infty} \left[1 - F^{ie,e}_s(2h)\right] dh \rangle_w \\ &- \left(1 - \alpha^{e,f}_{ie,s}\right) \gamma^e_{ie} r^e_{ie} \langle \int_{d^{ie,e}_{lag,s}(w)}^{\infty} \left[1 - F^{ie,e}_s(h)\right] \} dh \rangle_w \end{aligned} \tag{6.13}$$

Because both the left-turning vehicles from link c to link f and through vehicles from link c to link d conflict with left-turning vehicles from link a to link d. The gap available for a left-turning vehicle from link a to link d is h_n^c. The *lag-gap p.d.f* of vehicles of class u arriving from link c is calculated as:

$$f_{lag}^{ic,c}(h) = \gamma_{ic}^c r_{ic}^c \left[1 - F_u^{ic,c}(h)\right] \tag{6.14}$$

hence the *lag-gap c.d.f* is:

$$F_{lag,u}^{ic,c}(d_{lag,u}^{ic,c}) = \gamma_{ic}^c r_{ic}^c \int_0^{d_{lag,u}^{ic,c}} \left[1 - F_u^{ic,c}(h)\right] dh \tag{6.15}$$

and the average probability that a vehicle on link a finds a sufficient *lag-gap* on link c is calculated as:

$$\begin{aligned} P\left(h > d_{ic,s}^c(w)\right) &= \langle 1 - F_{lag,s}^{ic,c}(d_{ic,s}^c(w))\rangle \\ P\left(h > d_{ic,s}^c(w)\right) &= 1 - \gamma_{ic}^c r_{ic}^c \langle \int_{d_{lag,s}^{ic,c}(w)}^{\infty} \left[1 - F_s^{ic,c}(h)\right]\} dh\rangle_w \end{aligned} \tag{6.16}$$

From equations 6.13 and 6.16, we obtain the left-turning probability as follows:

$$\begin{aligned} \pi_{ia,id,u}^{a,d}(k) = & \prod_{ic} \sum_{s\in U} \frac{r_{ic,s}^c}{r_{ic}^c} \{1 - \gamma_{ic}^c r_{ic}^c \langle \int_{d_{lag,s}^{ic,c}(w)}^{\infty} \left[1 - F_s^{ic,c}(h)\right] dh\rangle_w\}_{(Mc,k)} \\ & \prod_{ie} \sum_{s\in U} \frac{r_{ie,s}^e}{r_{ie}^e} \{1 - \left(1 - \alpha_{ie,s}^{e,f}\right) \gamma_{ie}^e r_{ie}^e \langle \int_{d_{lag,s}^{ie,e}(w)}^{\infty} \left[1 - F_s^{ie,e}(h)\right] dh\rangle_w \\ & -0.5\alpha_{ie,s}^{e,f} \gamma_{ie}^e r_{ie}^e \langle \int_{d_{lag,s}^{ie,e}(w)}^{\infty} \left[1 - F_s^{ie,e}(2h)\right] dh\rangle_w\}_{(Me,k)} \end{aligned} \tag{6.17}$$

Where Me and Mc are the last cell of link e and link c, respectively.

Given the class specific gap distributions $F_u^{ic,c}(h)$ of vehicles of class u in lane ic of link c and $F_u^{ie,e}(h)$ of vehicles of class u in lane ie of link e, the corresponding *c.d.f* $F_u^{ic,c}(2h)$ and $F_u^{ie,e}(2h)$ are calculated with the *Laplace* transform presented in Chapter 3. Consequently, the left-turning probability of vehicle of class u from link a to link d is determined from expression 6.17

By using assumption of exponential distribution of gaps, after a lengthy but straightforward algebraic calculation (see Appendix A), expression 6.13 reduces to:

$$\begin{aligned} P\left(h > d_{ie,s}^e(w)\right) = & exp\left[-\gamma_{ie}^e r_{ie}^e \left(d_u^{min} + l_u + T_{ie,s}^e V_{ie,s}^e\right)\right] \\ & \left[1 + 0.5\alpha_{ie,s}^{e,f} \gamma_{ie}^e r_{ie}^e \left(d_0^u + l_u + T_{ie,s}^e V_{ie,s}^e\right)\right] \end{aligned} \tag{6.18}$$

Expression 6.16 reads:

$$P\left(h > d_{ic,s}^c(w)\right) = exp\left[-\gamma_{ic}^c r_{ic}^c \left(d_u^{min} + l_u + T_{ic,s}^c V_{ic,s}^c\right)\right] \tag{6.19}$$

and equation 6.17 reduces to:

$$\begin{aligned}\pi^{a,d}_{ia,id,u}(k) &= \prod_{ic}\sum_{s\in U}\frac{r^c_{ic,s}}{r^c_{ic}}exp\left[-\gamma^c_{ic}r^c_{ic}\left(d^{min}_u+l_u+T^c_{ic,s}V^c_{ic,s}\right)\right]_{(Mc,k)}\\ &\prod_{ie}\sum_{s\in U}\frac{r^e_{ie,s}}{r^e_{ie}}exp\left[-\gamma^e_{ie}r^e_{ie}\left(d^{min}_u+l_u+T^e_{ie,s}V^e_{ie,s}\right)\right]\\ &\left[1+0.5\alpha^{e,f}_{ie,s}\gamma^e_{ie}r^e_{ie}\left(d^{min}_u+l_u+T^e_{ie,s}V^e_{ie,s}\right)\right]_{(Me,k)}\end{aligned} \tag{6.20}$$

Now let us consider the dynamics of traffic at the last cell Ma of link a. The total traffic demand in lane ia of this cell at time step k is $\Xi^a_{ia}(Ma,k)$. Let $\beta^{a,d}_{ia,id,u}$ and $\beta^{c,d}_{ic,id,u}$ be the split coefficient of the traffic supply at the first cell of lane id of link d to incoming vehicles of class u from lane ia of link a and from lane ic of link c, respectively. The flux of vehicles of class u entering cell 1 of lane id at time step k from link a, denoted by $q^{a,d}_{id,u}(1/2,k)$, is determined as below:

$$q^{a,d}_{id,u}(1/2,k)=\min\left[\alpha^{a,d}_{ia,id,u}\Xi^a_{ia,u}(Ma,k),\pi^{a,d}_{ia,id,u}(k)\beta^{a,d}_{ia,id,u}\Sigma^d_{id,u}(1,k)\right] \tag{6.21}$$

Where

$$\begin{aligned}\Xi^a_{ia,u}(Ma,k) &= \frac{r^a_{ia,u}(Ma,k)}{r^a_{ia}(Ma,k)}\Xi^a_{ia}(Ma,k)\\ \Sigma^d_{id,u}(1,k) &= \frac{r^a_{id,u}(1,k)}{r^d_{id}(1,k)}\Sigma^d_{id}(1,k)\end{aligned} \tag{6.22}$$

From equation 6.21, it can be seen that, when the crossing traffic is busy (e.g. $\pi^{a,d}_{ia,id,u}\to 0$), $q^{a,d}_{id,u}(1/2,k)\to 0$ no matter the traffic conditions in the target lane id. That is, there is still a queue in the left-turning lane even if the first cell of the target lane is empty. Therefore, the proposed model is more accurate than the current network models in the sense that the latter allow traffic to exit a link if the first cell of the target link is empty.

Let us consider through traffic from link c, the flux of vehicles of class u entering cell 1 of lane id at time step k from link c is determined as given below:

$$q^{c,d}_{id,u}(1/2,k)=\min\left[(\alpha^{c,d}_{ic,id,u}\Xi^c_{ic,u}(Mc,k),\beta^{c,d}_{ic,id,u}\Sigma^d_{id,u}(1,k)\right] \tag{6.23}$$

Hence, the total flux of vehicles of class u entering cell 1 of lane id at time step k is:

$$q^d_{id,u}(1/2,k)=q^{a,d}_{id,u}(1/2,k)+q^{c,d}_{id,u}(1/2,k) \tag{6.24}$$

There are different models proposed for the value of β such as Lebacque (1996), Buisson et al. (1996). A simple calculation for this split coefficient is:

$$\beta^{d,c}_{id,ic}=\frac{\alpha^{c,d}_{ic,id}\Xi^c_{ic}(Mc,k)}{\alpha^{c,d}_{ic,id}\Xi^c_{ic}(Mc,k)+\alpha^{a,d}_{ia,id}\Xi^a_{ia}(Ma,k)} \tag{6.25}$$

The above derivation process can be applied to determine the inflow to link f from link c and link e, and the inflow to link b from link a and link e. Another boundary condition needed to be determined is the outflow from a link, which is described in the next section.

6.2.2 Outflowing traffic

Following the approach in Section 6.2.1, in this section we calculate the outflow of vehicles of class u from lane ia of link a to link b and link d, which consists of traffic making a right-turn to lane ib of link b and a left -turn to lane id of link d. The outflow of vehicles of class u from lane ia to lane id is calculated by equation 6.21.

Now let us consider right-turning traffic from lane ia of link a to lane ib of link b. The average probability that a right-turning vehicle from link a finds a sufficient *lag-gap* of vehicles of class u arriving from lane ie of link e is determined in equation 6.13. Therefore, the right-turning probability of vehicles of class u $\pi^{a,b}_{ia,ib,u}$ from lane ia of link a to lane ib of link b is calculated as:

$$\begin{aligned}\pi^{a,b}_{ia,ib,u}(k) &= \prod_{ie}\sum_{s\in U}\frac{r^e_{ie,s}}{r^e_{ie}}\{1-\left(1-\alpha^{e,f}_{ie,s}\right)\gamma^e_{ie}r^e_{ie}\langle\int_{d^{ie,e}_{lag,s}(w)}^{\infty}\left[1-F^{ie,e}_s(h)\right]dh\rangle_w \\ &\quad -0.5\alpha^{e,f}_{ie,s}\gamma^e_{ie}r^e_{ie}\langle\int_{d^{ie,e}_{lag,s}(w)}^{\infty}\left[1-F^{ie,e}_s(2h)\right]dh\rangle_w\}_{(Me,k)} \end{aligned} \tag{6.26}$$

By using assumption of the exponential distribution of gaps, equation 6.26 reduces to:

$$\begin{aligned}\pi^{a,b}_{ia,ib,u}(k) &= \prod_{ie}\sum_{s\in U}\frac{r^e_{ie,s}}{r^e_{ie}}exp\left[-\gamma^e_{ie}r^e_{ie}\left(d^{min}_u+l_u+T^e_{ie,s}V^e_{ie,s}\right)\right] \\ &\quad \left[1+0.5\alpha^{e,f}_{ie,s}\gamma^e_{ie}r^e_{ie}\left(d^{min}_u+l_u+T^e_{ie,s}V^e_{ie,s}\right)\right]_{(Me,k)} \end{aligned} \tag{6.27}$$

From equation 6.26 and equation 6.27 the outflow of vehicles of class u from lane ia to link b, denoted by $q^{a,b}_{ia,u}(Ma+1/2,k)$ is calculated as:

$$q^{a,b}_{ia,u}(Ma+1/2,k)=\min\left[\alpha^{a,b}_{ia,ib,u}\Xi^a_{ia,u}(Ma,k),\pi^{a,b}_{ia,ib,u}(k)\beta^{b,a}_{ib,ia,u}\Sigma^b_{ib,u}(1,k)\right] \tag{6.28}$$

Hence, the total outflow of vehicles of class u from lane ia of link a is:

$$q^a_{ia,u}(Ma+1/2,k)=q^{a,b}_{ia,u}(Ma+1/2,k)+q^{a,d}_{ia,u}(Ma+1/2,k) \tag{6.29}$$

It is clear from equation 6.29 that in multilane intersections when there are exclusive lanes for left-turning and/or right-turning traffic, if either of these lanes is blocked, the total outflow will be equal to the outflow from the other lane. In single lane intersections, link a has only one lane (that is, $ia=1$), the outflow of vehicles of class u from link a is:

$$q^a_{ia,u}(Ma+1/2,k)=\min\left[q^{a,b}_{ia,u}(Ma+1/2,k),q^{a,d}_{ia,u}(Ma+1/2,k)\right] \tag{6.30}$$

Obviously, in this case if either of the turning traffic streams is blocked, the whole traffic in lane ia is blocked too.

6.2.3 Traffic signals

The influence of a traffic signal on the link can be taken into account in a simple way by setting the probability of finding a corresponding sufficient gap to a fixed value. For example, when the signal is red, the traffic outflow of link a is simply equal to zero. When the traffic light turns to green, the traffic out-flowing of this link only depends on the traffic condition at the entry of the target link d as well as the traffic arriving from link c if the light for this link is green too.

This section described the development of a model for multiclass traffic dynamics at multilane intersections. In order to incorporate the model proposed here and the model presented in Chapter 4 to model the dynamics of traffic flow in an entire network, these two model concepts need to be facilitated through a multilane multiclass network representation. The representation is based on the object-oriented network model HELENA (see Appendix C), which enables intersection modeling and - as a prelude to future work, intersection control.

6.3 Summary

In this chapter, we developed a macroscopic traffic flow model for *MLMC* urban networks. Especially, we introduced an approach to develop a model for a multilane intersection based on the implementation of the probability of left-turning and right-turning rates. The implementation was derived mathematically from microscopic driving principles in which the *renewal theory* was used. The proposed approach provides a solution to bridge the gap between the microscopic traffic models and macroscopic traffic models in modeling traffic interactions at nodes. The developed model has been implemented in the urban part of the computer-based network model, namely HELENA, which can predict *MLMC* traffic conditions given static network parameters, initial network state, the route flow demand patterns (to calculate the turning fraction factor), and the prevailing control settings (to determine the probability of lane-changing processes at nodes). The improvement of the developed model over other models is that it can deal adequately with the multiplicity of control objectives and user-classes in different street lanes. This model is not only more elaborate than the current macroscopic network models in terms of modeling the multi user class traffic flow going in and out of intersections but also requires fewer parameters than microscopic models.

Chapter 7

Model calibration and validation

This chapter presents the performance of the *MLMC* model derived in Chapter 4 with respect to empirical data. To this end, firstly, an automated procedure to calibrate macroscopic traffic models is proposed. The resulting, calibrated model is then used for comparison with results obtained from other macroscopic traffic flow model. For the comparison, we model a 7.5 km segment of one direction of a 2x2 lane freeway during the morning peak. This segment contains three on–ramps and three off–ramps.

Basically, to obtain insight into the dynamics of traffic flow operations on multilane roadways, dedicated data sets are required. That is, observations that reflect lane-changing processes are needed. To this end, data from the 2x2 lane freeway A9 in the Netherlands were analyzed. The data set contained the dynamics of macroscopic traffic variables, such as flow rate and speed, for each lane. Based on these data, all relevant model parameters were estimated using an optimization technique (model calibration). The optimal parameters obtained were used to simulate the model with another data set of the same freeway (model validation). It was found that the proposed model corresponds well to the empirical data. These results were cross-compared with results obtained from a macroscopic simulator, namely METANET (Technical University of Crete (2001)). It is concluded that the developed model is able to more correctly predict traffic congestion states on the considered freeway section than METANET.

This chapter is organized as follows. Section 7.1 briefly presents the dynamics of macroscopic traffic variables on a two-lane freeway carriageway. In Section 7.2 we discuss the meanings of the model parameters, and we consider which values are feasible. Section 7.3 describes the optimization algorithm used for model calibration. In Section 7.4 we show simulation results of the (calibrated and validated) model with empirical data. These results are cross-compared with results obtained from METANET, shown in Section 7.5. Section 7.6 concludes this chapter.

7.1 Data collection and analysis

In this section we discuss the observations needed for the extended model calibartion/validation. Accordingly, data were collected at the Dutch 4-lane freeway A9, near the city of Badhoevedorp.

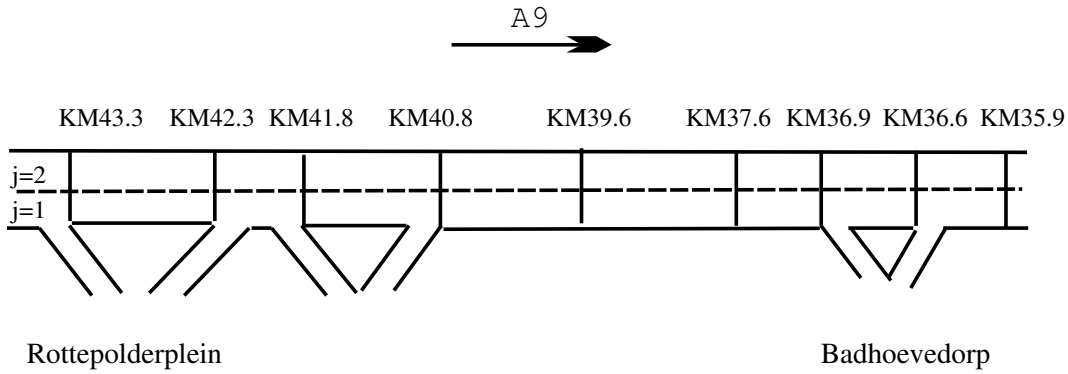

Figure 7.1: Lay-out of the roadway for calibration of the developed *MLMC* model.

Figure 7.1 shows the location of the detectors that were used to measure the data. The data consisted of flow rates, speeds and vehicle lengths in each lane. Based on the vehicle lengths, the vehicles were classified as cars ($< 6m$) or trucks ($> 6m$). Because this chapter mainly focuses on calibrating/validating the lane-changing processes at bottlenecks, the aggregate vehicle class data were used and the detectors from KM39.6 to KM35.9 were used to represent the dynamics of the traffic operations. An exhaustive analysis of the traffic congestion occurring in this segment was already carried out in Logghe (2003). In this section, we discuss some congested states that can be replicated by the developed model.

It was found that during the morning peak, from 7AM to 10AM, on 18 October 1994, there was a transition from free-flow to the congested traffic state due to congestion spill-back caused by the downstream on-ramp at KM36.6.

Figure 7.2 clearly shows the dynamics of the speed and density for each lane. In free flow, the speeds in the left lane (lane 2) are generally higher than in the right lane (lane 1). This accounts for the fact that in free-flow, passenger cars interact with trucks more often and, as a consequence, change to the left lane. Consequently, there are more passenger cars in the left lane than in the right lane, and there are more trucks in the right lane than in the left lane. When the traffic conditions deteriorate, the speed in the left lane drops to the speed in the right lane. During congestion (7.45AM–9.15AM), so-called stop-and-go waves are observed. These waves are characteristic for traffic flow when the density has exceeded a certain critical value.

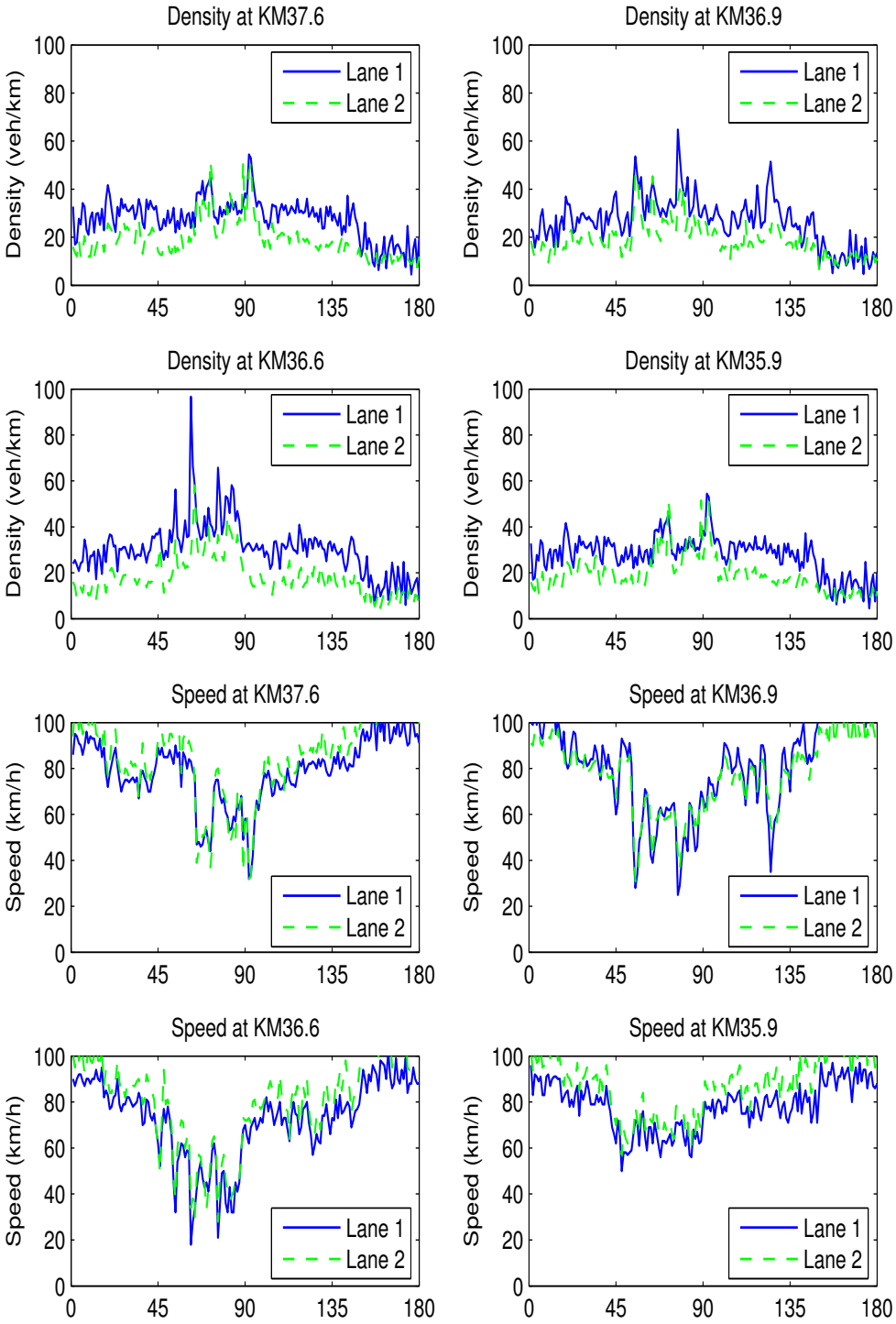

Figure 7.2: Dynamics of mean speed in both lanes of the Dutch freeway A9 (18 October 1994).

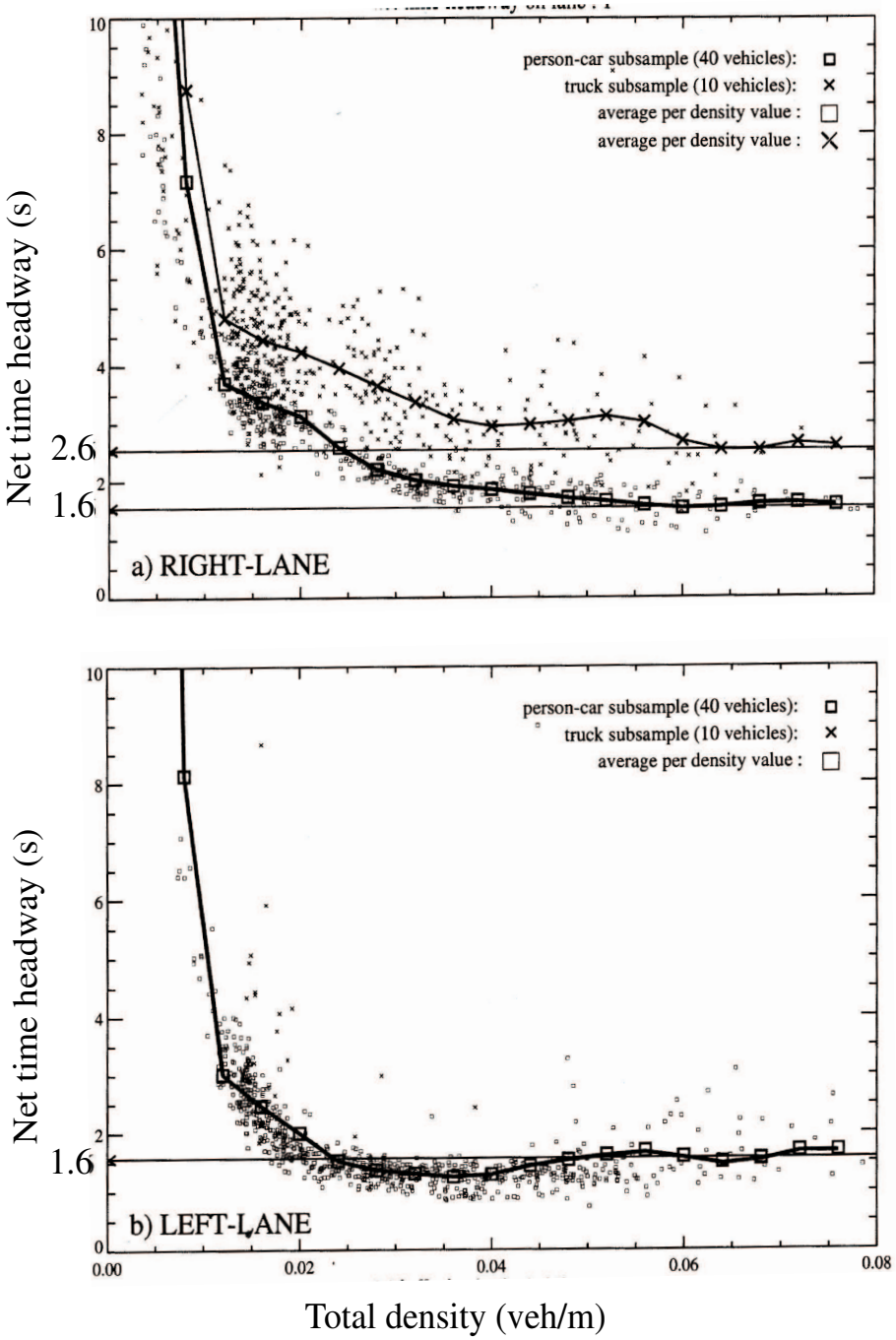

Figure 7.3: Net time gap of traffic in both lanes of the 2x2 lane Dutch freeway A9 (KM40.8-KM37.6). Source: Hoogendoorn (1999a).

Another interesting indication from Figure 7.2 is that in stop-and-go waves, the speed in the right lane (that is lane 1, with a higher fraction of trucks) is lower than the speed in the left lane (that is lane 2, with a higher fraction of passenger cars). Obviously, this is due to the fact that it is more difficult for trucks to accelerate within short waves than for passenger cars.

Figure 7.3 shows the net time headway (denoted by T) for both lanes. Because trucks in general require longer time headways than passenger cars, the net time headway in the right lane is larger than in the left lane. As can be seen in this figure, the net time headways are approximately $2.1sec$ and $1.6sec$ for the right lane (lane 1) and the left lane (lane 2), respectively.

7.2 Model parameters

This section discusses the lane-specific and aggregate class model parameters and their meaning in traffic flow dynamics. The model parameters that need to be calibrated are:

1. Lane specific free speeds, $V_{i,max}$ (km/h)
2. Lane specific jam density, $r_{i,max}$ (veh/km)
3. Lane specific reaction time, T_i (sec)
4. Lane specific relaxation time, τ_i (sec)
5. Lane specific coefficients for speed variance: $A_{i,0}$, δA_i, δr_i (veh/km) and critical density $r_{i,cr}$ (veh/km)
6. Lane specific coefficient for spontaneous lane change: $g_{i,3-i}$ (h) and β.

The factor that accounts for the willingness to accept smaller gaps when drivers approach the end of a ramp is approximated as a linear function of location x, that is:

$$\mu(x) = \mu_{min} + (\mu_{max} - \mu_{min}) \frac{x_{end} - x}{L} \tag{7.1}$$

The speed variance parameters (which also influence the immediate lane changing factor functions Ψ and Φ) $A_{i,0}$, δA_i, δr_i and $r_{i,cr}$ play an important role in the determination of the equilibrium speed-density relation. Besides, the free speed, reaction time and jam density also influence the equilibrium speed-density relation. The free speed can be obtained by fitting the speed-density relation for low densities while the jam density is determined by fitting this relation for high densities. It is reported that the aggregate class jam density is in the range between $160veh/km$ and $180veh/km$ (Kuhne (1991)). If there is a high proportion of fast vehicles, the free speed and jam density increases, and vice versa.

The relaxation time τ is calibrated systematically by means of the dynamic properties of traffic flow. As shown in Section 4.5, the relaxation time influences the stability of the model:

the higher the value of τ, the more unstable the model is. That is, the outflow from the bottleneck is decreased with an increased relaxation time because the increased value of τ leads to lower accelerations. The outflow also decreases with increased time headways because the time headway is the inverse of the flow.

Because of the intuitive meaning of the parameters, a reasonable range of values can be chosen in advance. According to Helbing et al. (2002), T should be compatible with the average time headway kept in homogeneous congested traffic, which is in the range of $[1.0s, 2.5s]$. τ should be in the range of $[10s, 40s]$, where the higher value is chosen for freeways and the lower value is chosen for urban traffic. r_{max} must be consistent with the average length of vehicles plus the safe distance d_{min} of about $2.0m$. The parameters that influence the spontaneous lane-changing processes are g and β. The primary use of the right lane at small densities ($g_{right} > g_{left}$) reflects European traffic rules. Concerning the immediate and mandatory lane-changing processes, the reaction time is the main factor, which reflects the type of driving behavior. For example, the truck drivers in general require longer reaction times than passenger car drivers, bad weather conditions cause more careful driving, resulting in higher reaction times.

7.3 Automated calibration procedure

This section illustrates an automated calibration procedure for macroscopic traffic models (Ngoduy and Hoogendoorn (2003a)). For some years already, there are several automated calibration procedures that have been applied with success to macroscopic models in some cases (Cremer and Papageorgiou (1981)). In this thesis, we propose another procedure based on a well-known Nelder-Mead simplex optimization algorithm. The procedure's main quality is its ability to also be used with other macroscopic models, with relevant modifications. The calibration process is performed as described in Figure 7.4.

In Figure 7.4 the main part is the optimization procedure. The proposed Nelder-Mead algorithm uses a simplex with $(n + 1)$ vertices in n dimensions, and evaluates the objective function in each vertex. Let us consider the problem:

$$\text{Min} : f(x), x \in \Re^n \tag{7.2}$$

where x presents the vector of the model parameters to be calibrated, $f(x)$ is the objective function, defined as the total mean square errors between model simulation results and measurements, which is to be minimized.

The algorithm starts with each iteration k that constitutes a vertex x^k, $k = 1, 2, \ldots, n+1$ (to be selected randomly), and the corresponding objective function value being $f(x^k)$. Then, the vertices with, respectively, the lowest values (x^k_{low}), highest values $(x^k_{high,1})$ and next-to-highest $(x^k_{high,2})$ values are determined.

Let x^k_{rest} be the remaining vertices at iteration k. The objective function is evaluated via the new vertex x^k_{ref}, namely *reflection vertex*, that is determined by the following equation:

$$x^k_{ref} = (1 + \lambda)\, x^k_{rest} - \lambda x^k_{high,1} \tag{7.3}$$

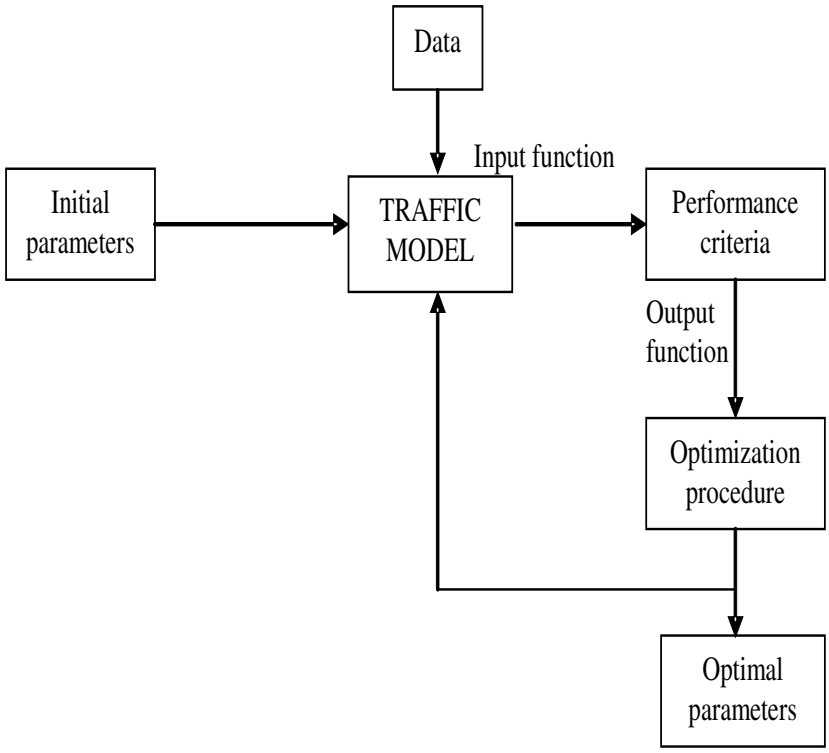

Figure 7.4: Automated calibration procedure for macroscopic traffic flow models.

Where λ is the reflection factor ($\lambda \geq 0$).

1. Step 1: If $f(x^k_{ref}) \geq f(x^k_{high,1})$, the objective function is evaluated again in the vertices determined between x^k_{rest} and x^k_{high} as:

$$x^k_1 = (1-\gamma)\, x^k_{rest} + \gamma x^k_{high,1} \quad \text{with} \quad 0 \leq \gamma \leq 1 \tag{7.4}$$

   If $f(x^k_1) \leq f(x^k_{high,1})$, the new simplex is found by replacing $x^k_{high,1}$ with x^k_1; else the new simplex is found by shrinking the current vertex nearby x^k_{low}, namely *contraction vertex*, replacing x^k_m with $(1-\eta)\, x^k_{low} + \eta x^k_m$ in which $0 \leq \eta \leq 1$ and $x^k_m \neq x^k_{low}$. Where η is contraction factor.

2. Step 2: If $f(x^k_{high,2}) < f(x^k_{ref}) < f(x^k_{high,1})$ the objective function is evaluated in the vertex between x^k_{new} and x^k_{rest} determined by:

$$x^k_2 = (1-\gamma)\, x^k_{rest} + \gamma x^k_{ref} \tag{7.5}$$

   if $f(x^k_2) \leq f(x^k_{ref})$ the new simplex is found by replacing $x^k_{high,1}$ with x^k_2 else the new simplex is found by replacing $x^k_{high,1}$ with x^k_{ref}, then shrinking the resulting simplex nearby x^k_{low}, replacing x^k_m with $(1-\eta)\, x^k_{low} + \eta x^k_m$

3. Step 3: If $f(x^k_{low}) < f(x^k_{ref}) < f(x^k_{high,2})$ the new simplex is found by replacing $x^k_{high,1}$ with x^k_{ref}

4. Step 4: If $f(x^k_{ref}) < f(x^k_{low})$ the objective function is evaluated in an expanded vertex x^k_{exp}, namely the *expansion vertex*, determined by:

$$x^k_{exp} = (1-\theta)\, x^k_{rest} + \theta x^k_{ref} \quad \text{with} \quad \theta \geq 1 \tag{7.6}$$

   If $f(x^k_{exp}) < f(x^k_{low})$, the new simplex is found by replacing $x^k_{high,1}$ with x^k_{exp}; else the new simplex is found by replacing $x^k_{high,1}$ with x^k_{ref}. Where θ is the expansion factor.

The next iteration is $(k+1)$ in which the optimal vertex found from the previous one is used as x^{k+1}_{low}. This loop is carried out until the stopping criteria is satisfied.

Figure 7.5 summarizes all optimization steps.

The algorithm described above was coded in MATLAB as an extension of the built-in *fminsearch* function (Appendix D illustrates the MATLAB code).

The automated procedure presented in this section was tested successfully with the METANET model using data collected from the Dutch freeway A1 (see Ngoduy and Hoogendoorn (2003a) and Hegyi et al. (2003)). The next section will show the application of this procedure to the calibration of the model developed in this thesis, with the data mentioned in Section 7.1.

7.4 Calibration results

In this section, we show the calibration results of the developed model. Several properties of the model in replicating reality are discussed.

In order to simulate the derived model, the numerical scheme *HLLE*, which is described in Chapter 5, was applied. Accordingly, the selected section of the A9 freeway (approximately 4km) was divided into cells of 100m each and a time step of 2 s was applied. These values were also selected to satisfy the numerical stability condition (see more details in Chapter 5).

The data input for the simulation is shown in Figure 7.6. Using this data input, the proposed model (both for multilane and for aggregate lane type) was calibrated successfully using the optimization algorithm presented in Section 7.3. The objective function that was minimized concerns the total mean square error, as in equation 5.54

The optimal parameters of the model are summarized in Tables 7.1 and 7.2. These parameters correspond to a total relative mean square error between the measured and estimated data of 8.0% and 12%, respectively, for multilane model (7.4% and 8.6% for the left lane and the right lane, respectively) and for aggregate lane model, and will be used for the validation of the model in the next section.

As can be seen in Table 7.1, the model parameters show obvious difference between the two lanes. These can be explained by the fact that there is a high fraction of cars in the left lane (lane 2) and a high fraction of trucks in the right lane (lane 1). Consequently, for example, the free speed and jam density in the left lane are higher than in the right lane, while the reaction time in the left lane is lower than in the right lane (since trucks require longer reaction times than passenger cars). For sake of validation, the optimal parameter values in Tables 7.1 and 7.2 were used to simulate the model again with data collected in the same period on 20 October 1994, when the same type of congestion occurred. This data set was also simulated with METANET. The results are shown in Section 7.5

Table 7.1: Optimal parameters for the two-lane, single class model, obtained from calibration with traffic data from the Dutch freeway A9 (all the values are rounded).

Parameters	Notation/Unit	Right lane (i=1)	Left lane (i=2)
Ramp factor	μ_{max}	0.90	
	μ_{min}	0.20	
Free speed	$V_{i,max}$ (km/h)	105	120
Jam density	$r_{i,max}$ (veh/km)	120	160
Reaction time	T_i (sec)	2.2	1.6
Relaxation time	τ_i (sec)	35	18
Speed variance coefficients	$A_{i,0}$	0.008	0.01
	δA_i	0.05	0.08
	δr_i (veh/km)	3	6
	$r_{i,cr}$ (veh/km)	32	38
SLC coefficients	$g_{i,3-i}$	120	30
	β_i	8	8

Table 7.2: Optimal parameters for the aggregate lane, single class model, obtained from calibration with traffic data from the Dutch freeway A9 (all the values are rounded).

Parameters	Notation/Unit	Values
Ramp factor	μ_{max}	0.90
	μ_{min}	0.20
Free speed	V_{max} (km/h)	112
Jam density	r_{max} (veh/km)	150
Reaction time	T (sec)	1.8
Relaxation time	τ (sec)	28
Speed variance coefficients	A_0	0.01
	δA	0.07
	δr (veh/km)	4.5
	r_{cr} (veh/km)	35

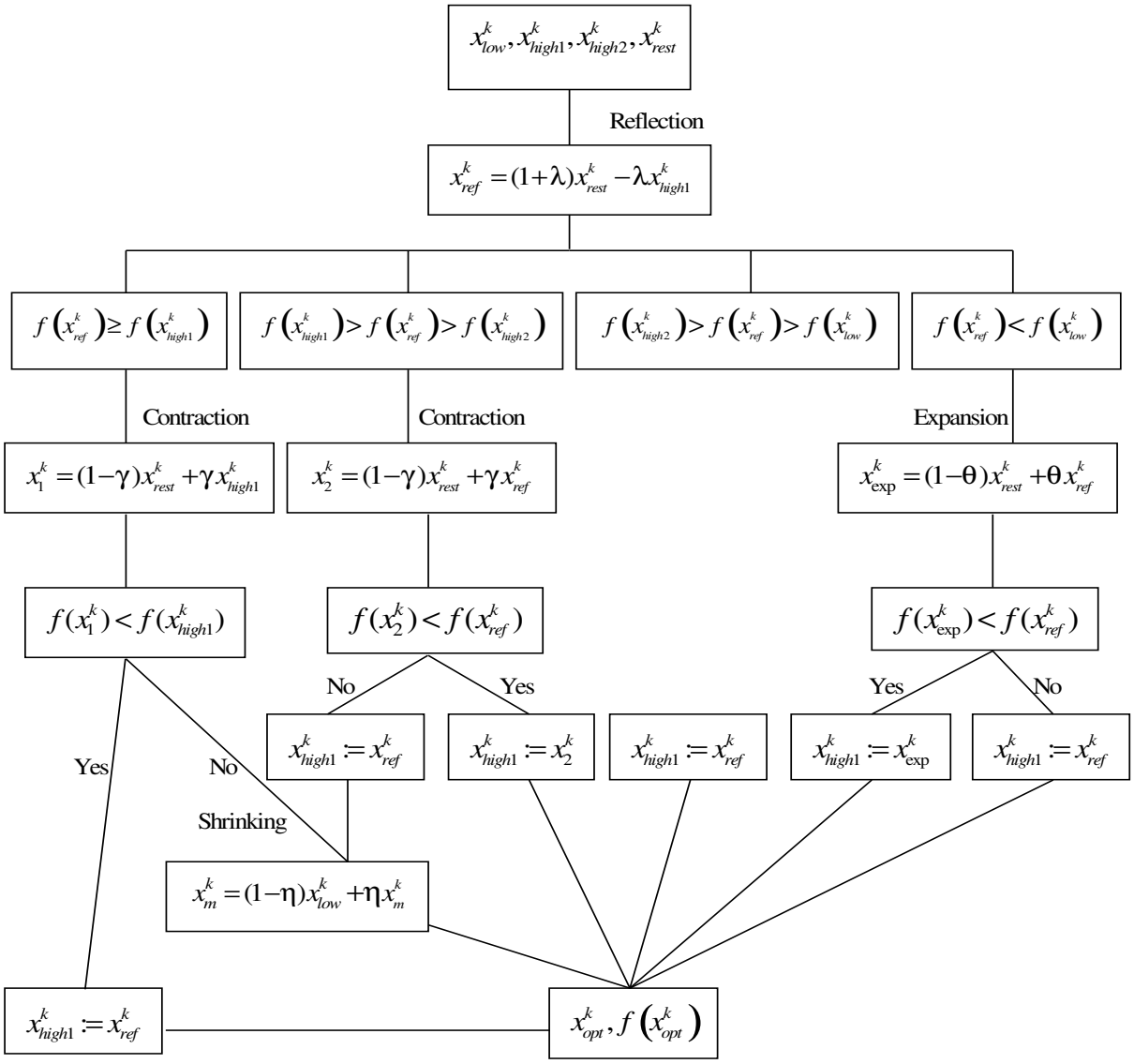

Figure 7.5: Flow chart for iteration k of the Nelder-Mead Algorithm.

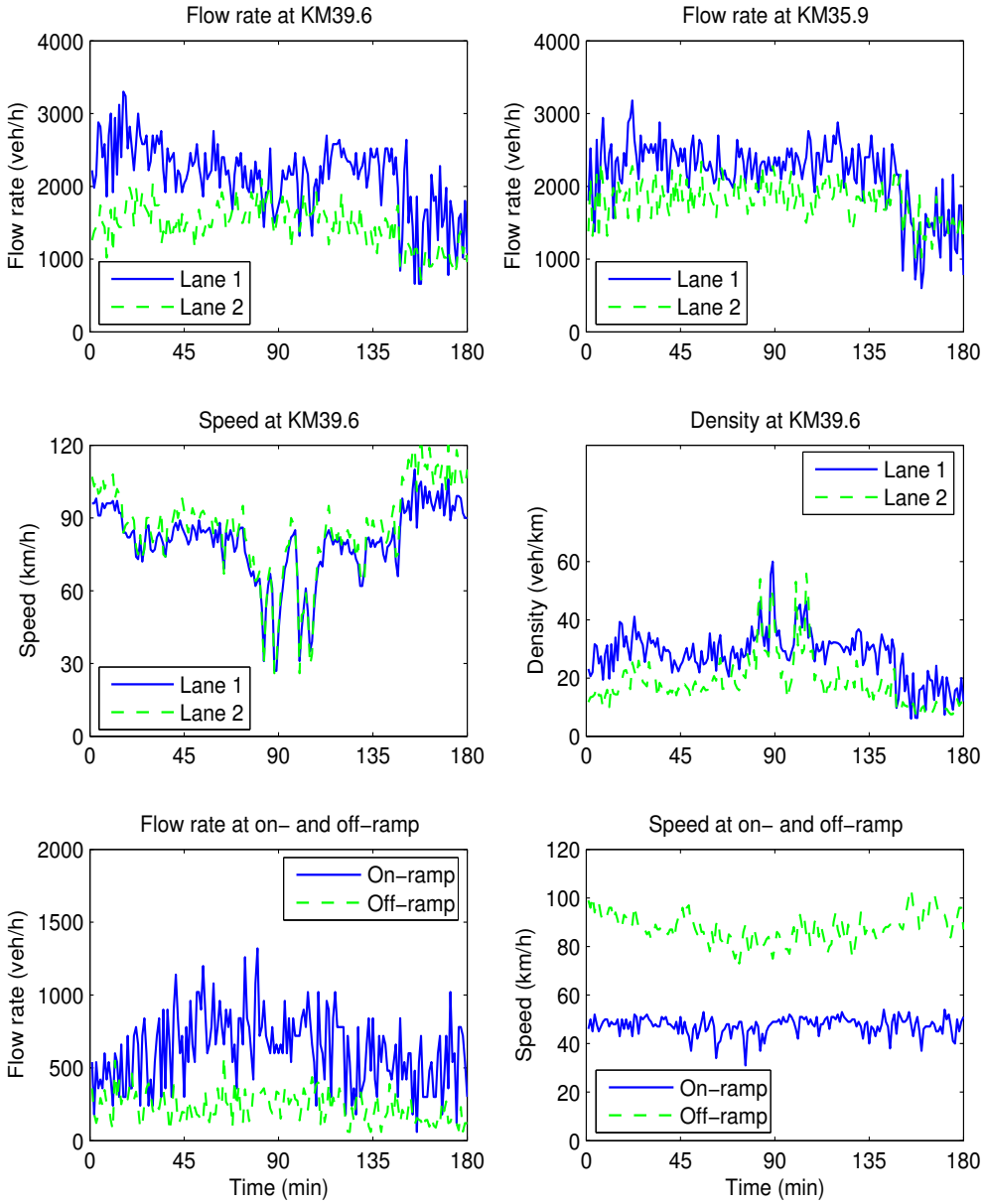

Figure 7.6: Boundary conditions include 2 conditions at the entrance (flow and speed), a condition at the exit (flow) of the chosen freeway section, and 2 conditions at the on- and off-ramp (flow rate and speed).

7.5 Cross-comparison of model performance

This section shows the validation results of the proposed model, which were cross-compared with the simulation results obtained from METANET (Technical University of Crete (2001)). For this comparison, let us first explain shortly the working of METANET with the data set given in Section 7.1.

METANET is software for the simulation of traffic networks based on Payne's macroscopic model, developed by Technical University of Crete (2001). The main outputs of the model are the traffic density, traffic flow rate and mean speed at all network locations. The basic equations used to evaluate the above variables for every cell i of link a at time step k are described in form of a discretization as follows:

$$r_{i,a}(k+1) = r_{i,a}(k) - \frac{\Delta t}{I_a \Delta x_a}\left[q_{i,a}(k) - q_{i-1,a}(k)\right] \tag{7.7}$$

Where $r_{i,a}(k)$ is the density in cell i of link a at time step k, $q_{i,a}(k)$ is the flow rate, determined by $q_{i,a}(k) = I_a r_{i,a}(k) V_{i,a}(k)$. I_a is the number of lanes on link a. Δt and Δx_a are the simulation step and the length of each cell on link a, respectively. $V_{i,a}(k)$ is the mean speed in cell i of link a. The dynamics equation for the mean speed is:

$$\begin{aligned} V_{i,a}(k+1) &= \max\{V_{min}, V_{i,a}(k) - \frac{\Delta t}{\Delta x_a} V_{i,a}(k)\left[V_{i,a}(k) - V_{i-1,a}(k)\right] \\ &- \frac{\nu \Delta t}{\tau \Delta x_a}\frac{r_{i+1,a}(k) - r_{i,a}(k)}{r_{i,a}(k) + \kappa} + \frac{\Delta t}{\tau}\left[V^e_{i,a}(k) - V_{i,a}(k)\right] \\ &- \underbrace{\frac{\delta \Delta t}{I_a \Delta x_a}\frac{q_m(t)(k) V_{1,a}(k)}{r_{1,a}(k) + \kappa}}_{\text{Merging effect}} - \underbrace{\frac{\phi \Delta t}{I_a \Delta x_a}\frac{\Delta I_a r_{l,a}(t)}{r_{cr,a}}(V_{l,a})^2}_{\text{Lane drop effect}}\} \end{aligned} \tag{7.8}$$

Where τ is the relaxation time, ν is the anticipation factor, and the last two terms represent the effect of merging (factor δ) and lane drops (factor ϕ) phenomena on speed. The index m and l delineate the merging link and the last cell of the considered link, and ΔI is the number of dropped lanes. $V^e_{i,a}$ is the equilibrium speed, determined by:

$$V^e_{i,a} = V_{a,max} exp\left[-\frac{1}{\vartheta}\left(\frac{r_{i,a}}{r_{cr,a}}\right)^{\vartheta}\right] \tag{7.9}$$

Where $V_{a,max}$ denotes the free speed of link a.

The global parameters of the METANET model are: ν, τ, κ, δ, ϕ, V_{min} and r_{max}, in which V_{min} and r_{max} are the minimum speed and jam density. These parameters, including the fundamental diagram parameters, such as, the constant ϑ, free speed V_{max} and critical density r_{cr}, are considered the variables to be calibrated. Note that in METANET, three distinct fundamental diagrams apply to upstream off-ramp (KM37.6-KM36.9), downstream on-ramp (KM36.6-KM35.9) and between off-ramp and on-ramp (KM36.9-KM36.6).

To calibrate METANET, the same procedure was applied as used for the calibration of our model. The following discritization steps were used: $\Delta x = 100m$ and $\Delta t = 2sec$. The optimal parameters for METANET are shown in Tables 7.3 and 7.4

Table 7.3: Optimal parameter values obtained from the calibration of METANET (all the values are rounded).

Parameters	Notation/Unit	Values
Jam density	r_{max} (veh/km)	138
Relaxation time	τ_i (sec)	24
Anticipation factor ν	(km$^2/h$)	52
Merging factor δ		0.2
κ	(veh/km)	0
Min speed V_{min}	(km/h)	10

Table 7.4: Optimal parameter values of fundamental diagram in METANET (all the values are rounded).

Parameters	Notation/Unit	Values
Free speed	$V_{i,max}$ (km/h)	110
Critical density r_{cr}	(veh/km)	
Upstream		27
Bottleneck		25
Downstream		30
ϑ		
Upstream		2.89
Bottleneck		3.14
Downstream		2.77

The input for the validation process was data collected on 20 October 1994. The morning peak from 7.00AM to 10.00AM was used. In this period, the characteristics of the traffic congestion were similar to the congested period from which the data used for the calibration process originated. The simulation results show that all the models correctly reflect the duration of the congested period (see Figures 7.7, 7.8, 7.9 and Table 7.5).

Figures 7.8 and 7.9 show the performance of the developed model for 2 lanes data set. It is found from Table 7.5 that the multilane ramp model demonstrates little improvements over the aggregate lane ramp model in the considered freeway due to the fact that there is few (immediate and spontaneous) lane-changing manoeuver between two lanes when traffic becomes congested.

From Table 7.5 (see also Figures 7.7) it is clear that in general the proposed model (both multilane and aggregate lane) is more accurate than METANET in estimating the dynamics of (macroscopic) traffic variables (flow rate and speed) for each lane. Performance differences with respect to mean speeds are striking between the developed model and METANET. With

Table 7.5: Cross-comparison of our multilane and aggregate lane model prediction with METANET (in terms of total mean square errors).

	Method	Total	Lane 1	Lane 2	KM37.6	KM36.9	KM36.6	KM35.9
Flow	Multilane Model	510	343	291	405	522	582	608
	Agg. lane Model	483	347	391	433	488	608	607
	METANET	478	402	458	415	416	767	420
Speed	Multilane Model	8.72	9.80	9.47	6.32	9.42	10.04	11.17
	Agg. lane Model	9.20	9.76	9.72	6.99	10.23	10.89	11.45
	METANET	16.17	16.76	16.80	17.22	15.25	13.26	10.36

respect to the traffic flow rate, performance differences between the developed model and METANET are not striking. The number of parameters to be calibrated in the proposed model for aggregate lane data set is 10 compared to 13 in METANET and 23 in the proposed model for 2 lane date set. Therefore, in case of aggregate type, the developed model requires less computational effort than METANET.

Although the transition "free-synchronization-wide jam" near the bottleneck is well captured by two models, the reduction of speed within the congested regime in each lane is overestimated by METANET (Table 7.5 and Figure 7.7). At an intermediate density regime (from 30veh/km to 40veh/km), there was a so–called linearly unstable traffic state (stop–and–go waves) which was well-replicated by the proposed model. This is consistent with the findings of Helbing (2001), that is, in reality traffic is only stable at very small densities and extreme densities. This property was not described by METANET.

Figures 7.10 and 7.11 illustrate the dynamics of phase-space speed estimated by our model in each lane compared with observations.

Figures 7.12 illustrates the dynamics of phase-space speed estimated by METANET compared with real data.

As far as the lane distribution of the traffic is concerned (Figure 7.13), the proposed model is able to predict the lane-changing processes (immediate, spontaneous and mandatory lane changes) rather accurately during the congestion regime (this is not described by METANET).

7.6 Summary

This chapter presented an automated calibration procedure for general macroscopic traffic models based on a direct search optimization algorithm (Nelder-Mead algorithm). The proposed procedure was applied successfully to calibrate METANET model (a macroscopic simulator) and the model developed in Chapter 4 with empirical data from KM39.6 to KM35.9 (including an on–ramp and an off–ramp) of the Dutch 2x2 lanes freeway A9 collected from 7.00AM to 10.00AM, 18 October 1994.

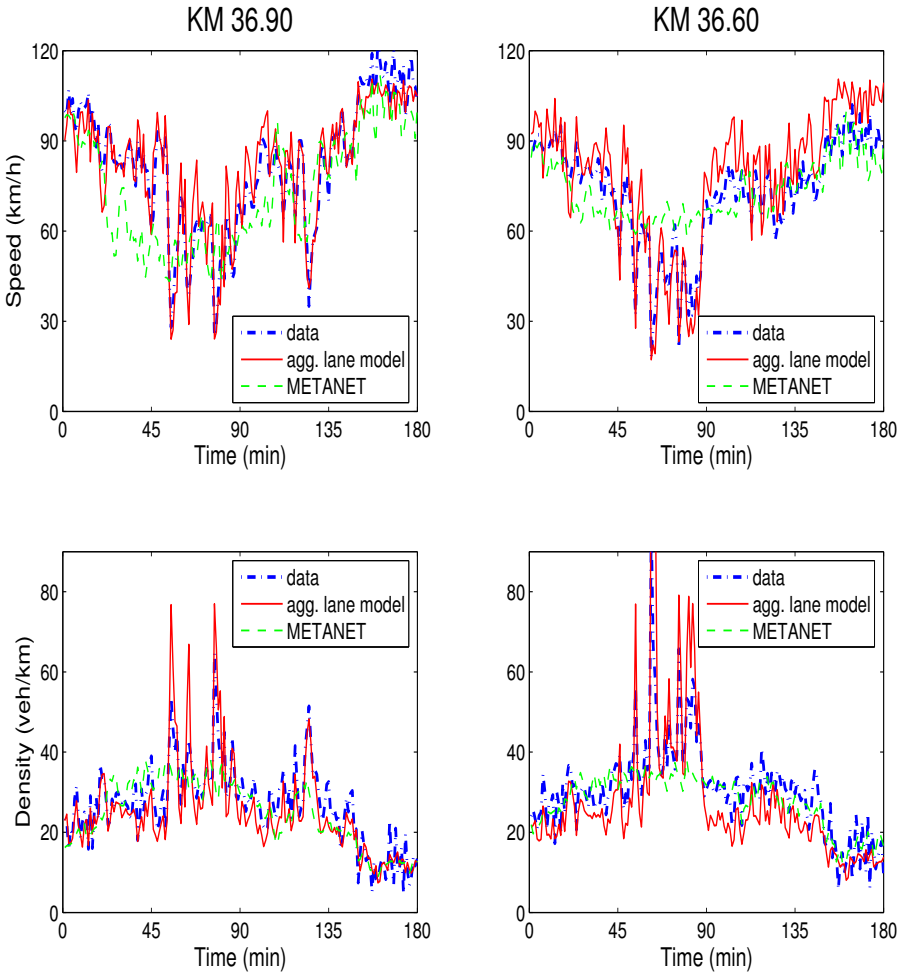

Figure 7.7: Dynamics of the mean speed and density at on– and off–ramp location.

The optimal parameter values were used to validate the developed model with a data set from the same measurement location, but this time from 20 October 1994. The simulation results were consistent with the empirical data in replicating the congestion duration. The validation results also showed that the lane-changing processes was represented accurately by the developed model. These results were cross–compared with the outputs of METANET model. We found that the proposed model (both for multilane and for aggregate lane context) was more accurate than METANET in terms of estimating the dynamics of macroscopic traffic variables (flow rate and speed). Due to the generation of parameters of the multilane model compared to METANET model, the multilane model must demand more calibration effort than METANET model. However, this drawback can be remedied by using fast computers or other parallel computing solutions.

Furthermore, the proposed model was able to represent the stop–and–go waves induced near the on–ramp. The transition of congested traffic states from free flow-congested traffic was also well replicated by the proposed model.

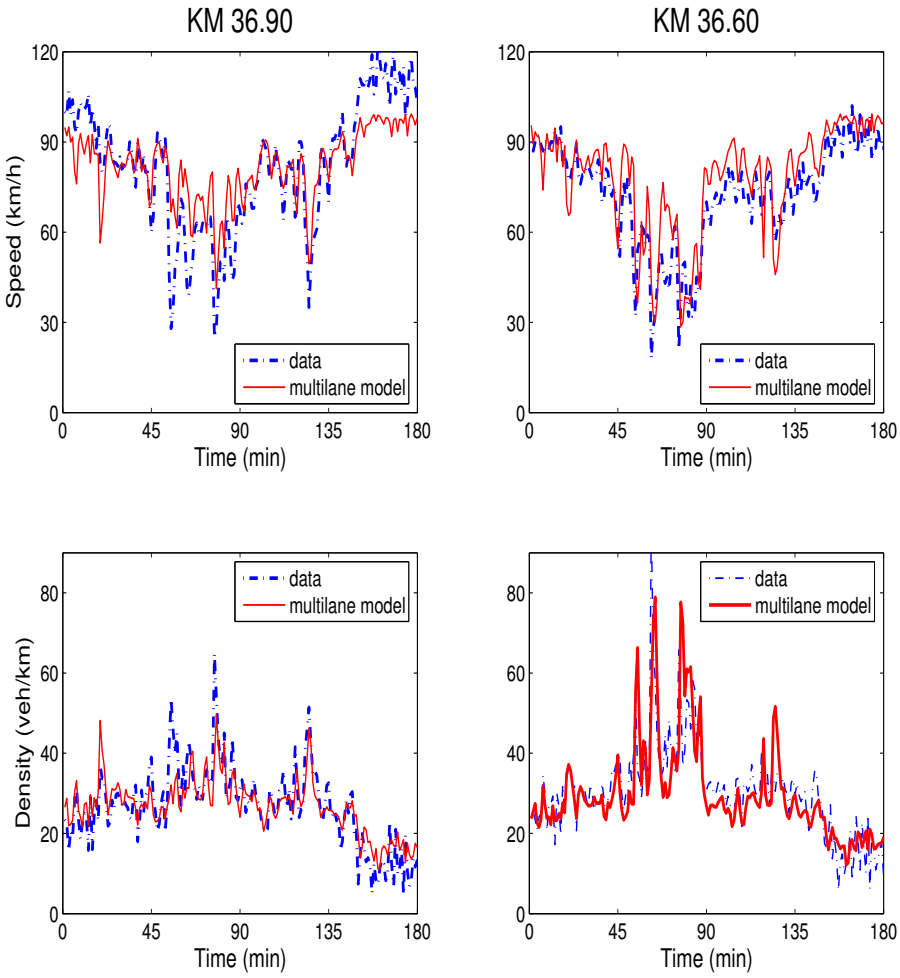

Figure 7.8: Dynamics of the mean speed and density in left lane (lane 1) at on- and off-ramp location.

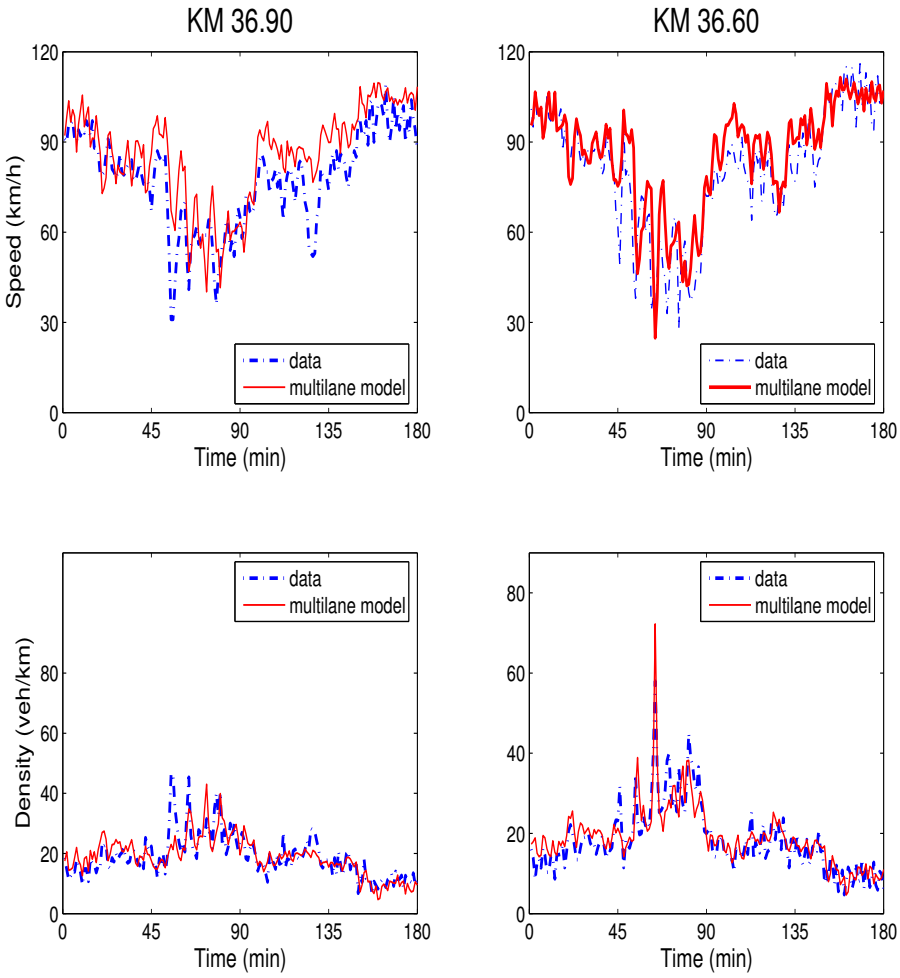

Figure 7.9: Dynamics of the mean speed and density in right lane (lane 2) at on- and off-ramp location.

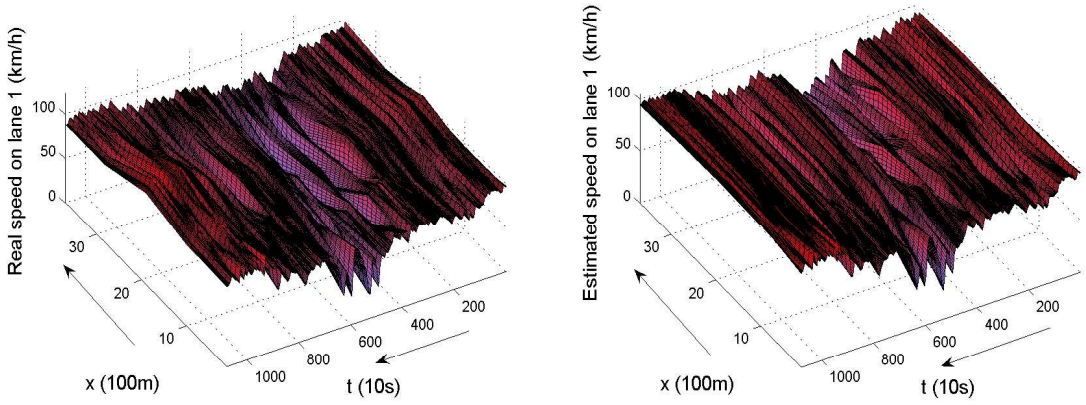

(a) Observation (b) Estimation

Figure 7.10: Spatial and temporal dynamics of observed speed versus estimated speed (by our model) in left lane (lane 1).

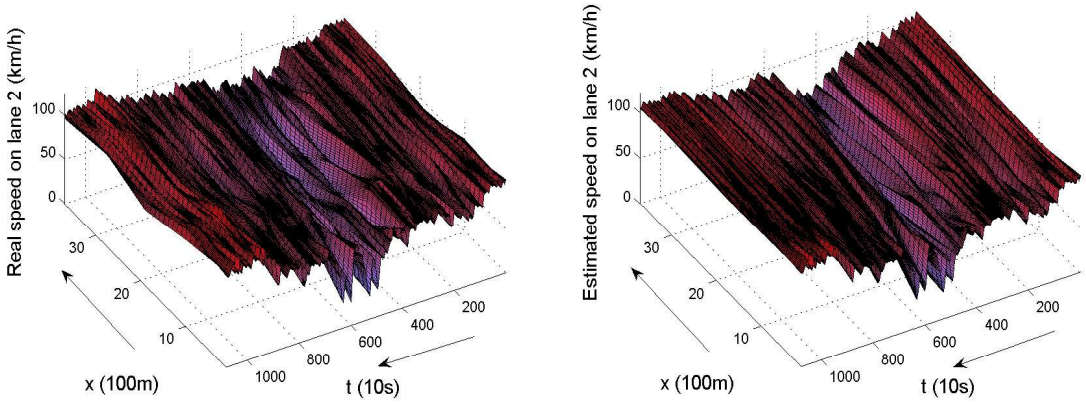

(a) Observation (b) Estimation

Figure 7.11: Spatial and temporal dynamics of observed speed versus estimated speed (by our model) in right lane (lane 2).

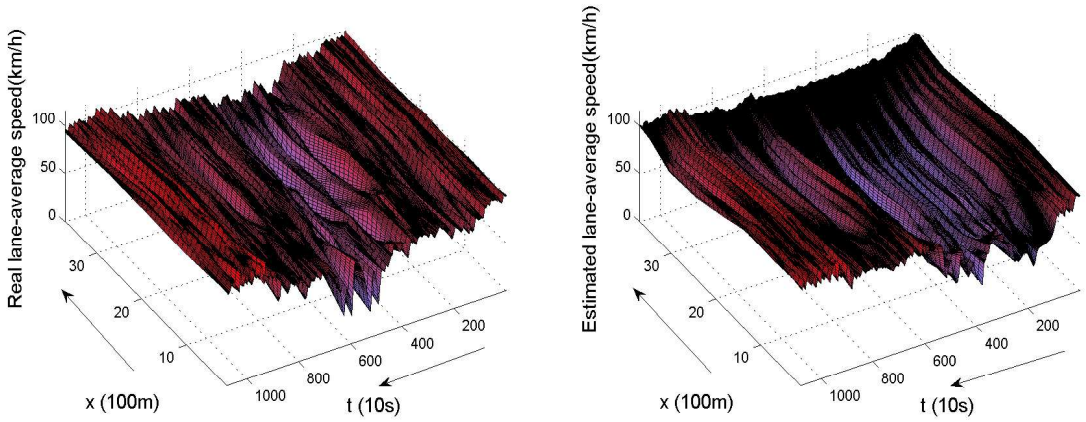

(a) Observation (b) Estimation

Figure 7.12: Spatial and temporal dynamics of observed speed versus estimated speed (by METANET).

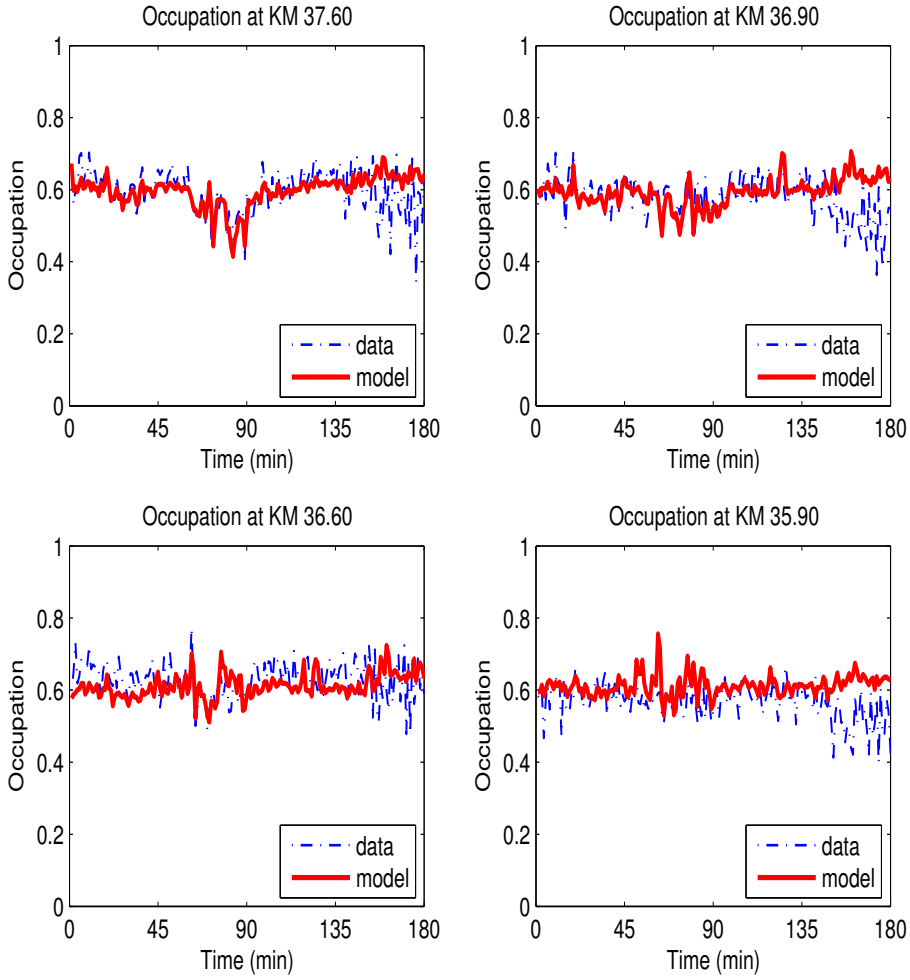

Figure 7.13: Occupation of traffic in the left lane (%), predicted by our multilane model.

Chapter 8

Conclusions and further research

In this concluding chapter, we summarize the conceptual framework of the research. The main contributions of this thesis to traffic flow theory, continuum traffic modeling, numerical solutions and model application results are described. Further, some directions for follow up research are discussed.

8.1 Summary of research

In this thesis we established a new approach to model discontinuities in continuum traffic models, developed a suitable numerical solution for general macroscopic continuum models, analyzed mathematical properties of the newly developed model, and presented some interesting results in the calibration and validation process of the model. Correspondingly, this thesis is summarized into three categories: theory development, numerical solutions, and model calibration/validation.

8.1.1 Theory development

The main result of this thesis is the development of a (macroscopic) realistic modeling approach to describe discontinuities of traffic dynamics at bottlenecks such as at on–ramps, off–ramps and intersections. The newly developed macroscopic model provides insight into the interactions of multiclass vehicles between the main lanes and the acceleration lanes on freeways, as well as between traffic streams, such as left-turning, right-turning and through streams at multilane intersections. The basis for the derivation of this model is a *gap-acceptance* model. That is, a vehicle is able to change to the target lane when both the *lead-gap* and the *lag-gap* are accepted. The *lead-gap* is accepted if the space between the lane-changing vehicle after the lane-change and its leader in the target lane is larger than a certain threshold distance (*critical lead-gap*). The *lag-gap* is accepted if the space between the lane-changing vehicle after the lane-change and its follower in the target lane is larger than the *critical lag-gap*. At discontinuities, drivers are willing to accept smaller gaps as

they approach the end of current lane. That is, the remaining distance to the end of current lane influences the *gap-acceptance* behavior. In order to determine the gap distributions in various traffic situations at on–ramps (lane–drops), off–ramps, weaving, and intersections, the so-called *renewal process* was applied.

Based on the new modeling approach, we established generalized *MLMC* gas-kinetic equations that describe the dynamics of the so-called *phase-space density* of multilane traffic flow on freeways with discontinuities. In these equations, continuum processes reflect the changes of the *phase-space density* in terms of convection and acceleration, whereas non-continuum processes account for non-smooth changes in speeds, such as, braking (deceleration) and lane-changing events. At discontinuities, the traditional gas-kinetic equations over-simplify the merging and diverging processes (for example, the effect of geometry is not taken into account explicitly). In contrast, the new equations introduce the so-called *mandatory lane-changing* processes in which microscopic lane-changing behavior has been implemented. Consequently, the following situations are represented by the new model:

- Drivers merge and/or diverge along a considerable stretch of freeway (acceleration lane).
- Drivers are willing to accept smaller gaps as they approach the end of on–/off–ramps or lane–drops.
- Drivers in the shoulder lane are cooperative by changing to a lane to the left to give way to merging vehicles.

In the developed gas-kinetic model, interactions between user classes in lane-changing processes are taken into account through reaction time, which contributes among the others significantly to lane-changing probabilities.

From the developed gas-kinetic equations a *MLMC* macroscopic continuum model was derived based on the *method of moments*. Compared to the gas-kinetic model, the macroscopic continuum model is more suitable for theoretical and numerical analysis of traffic phenomena. Furthermore, due to the small number of parameters, simplifying the calibration process, the macroscopic continuum model is very suitable for real-time applications in traffic control. The new model is not only more elaborate than the current macroscopic models in terms of modeling the inflow from on–ramps/lane–drops and outflow to off–ramps, but also requires fewer parameters than microscopic models.

Simulation results of the developed *MLMC* macroscopic model show that the model is able to replicate several congested traffic states under various scenarios of traffic demand from the ramp and different acceleration lane lengths. These congested states include patterns such as Moving Localized Clusters, Stop–and–Go Waves, Homogeneous Congested Traffic, etcetera. Furthermore, the influence of acceleration lane length on the operation of the main traffic flow was described. That is, the longer the acceleration lane length, the better traffic operation on the main carriageway. This property was shown mathematically by using linear stability analysis. The results analytically show the impact of acceleration lane length and ramp flow

on the dynamics of traffic flow on the main carriageway of a freeway, which previously had not been included in macroscopic models. Accordingly, in the presence of an on–ramp, not only do the traffic conditions in the main lanes contribute to the model stability, but the same is also achieved by the on-ramp flow and acceleration lane length. While the former acts as a disturbance source, the latter plays a role in spreading out this source on the main traffic. That explains the different congested traffic states obtained at different observation locations relative to the ramp location.

The developed macroscopic model was extended in the context of urban networks, in which the dynamics of traffic flowing in and out of multilane intersections was modeled in detail based on the modeling approach proposed to model the mandatory lane-changing process on freeways . The resulting model was shown to be able to deal even with traffic in opposite directions at multilane intersections. Consequently, the macroscopic models developed in this thesis can yield a better understanding of traffic operations both on freeways and in urban networks than current macroscopic models, while generating only two more parameters than the original model of Hoogendoorn (1999a).

8.1.2 Numerical solution

In this thesis, we showed that in high(er) order macroscopic models (of the hyperbolic type) information (density and speed) propagates along the so-called characteristic curves with a certain characteristic speed. Focussing and dispersion of the characteristics lead to the formation of, respectively, shock waves and rarefaction waves. Furthermore, the possible directions in which the characteristics move show that flow information can travel both downstream and upstream, depending on the prevailing traffic conditions (free flow or congestion). The latter is of importance when considering the conditions at the cell boundaries of the considered roadway section, that is, deciding which information is required on the boundary to ensure correct flow conditions. Numerical solution schemes must consider these different phenomena and situations, and handle them adequately, which is arguably a requirement for an accurate and reliable scheme. Due to the fact that a small perturbation in the traffic flow may result in the formation of traffic congestion, an inappropriate choice of numerical schemes can result in very poor performance of the model (for instance, traffic jams that never occur in reality). To this end, we proposed a numerical solution which always satisfies the positivity constraints of all traffic variables. That is, the proposed numerical solution is able to prevent traffic from moving backwards. This property was proven both analytically and numerically in this thesis.

To evaluate the different numerical approaches, we compared the solutions proposed in this thesis with two other solutions which have often been used by traffic theorists, using empirical data. For simplicity, we chose Payne's model for this purpose. The obtained results show that, in general, the three numerical schemes considered produce comparable mean square errors, although the estimated parameter values are somehow different (in particular the parameter that describes the local wave speed). However, the methods other than the proposed one require much smaller time steps, and thus require much more computational time. On

top of this, the proposed method is very stable while the others produce unrealistic oscillations in regions with large gradients (upstream and downstream of the congestion period). From the same original model, the different numerical schemes result in different simulation outputs. The scheme proposed in this thesis proved to be the most reliable in terms of computational time and numerical stability compared to the others, in particular when simulating the occurrence of traffic congestion. The scheme improves the performance of the model significantly, and thus provides an effective and reliable approach to simulate traffic flow under congestion.

8.1.3 Model calibration/validation

The developed macroscopic model was calibrated with empirical data collected from KM39.6 to KM35.9 (including an on–ramp and an off–ramp) of the Dutch 2x2 lanes freeway A9, from 7.00AM to 10.00AM on 18 October 1994. To facilitate the calibration process, we proposed an automated calibration procedure for general traffic flow models based on a direct search optimization algorithm (Nelder-Mead algorithm). This procedure was previously applied successfully to the calibration of the METANET model (a macroscopic simulator) and, in this thesis, to the calibration of the developed more complex model.

The optimal parameter values obtained in case of the 2 lanes and of the aggregate lane data set were used to validate the developed model with a data set from the same measurement location, but this time from 20 October 1994. The simulation results were consistent with the empirical data in replicating the congestion duration. The validation results also show that the lane-changing processes are represented accurately by the developed model. These results were cross–compared with the outputs of METANET model. We found that the proposed model was more accurate than METANET in terms of estimating the dynamics of macroscopic traffic variables (flow rate and speed). Furthermore, the proposed model was able to represent the stop–and–go waves induced near the on–ramp. The transition of congested traffic states from free flow-wide jams was also well replicated by the proposed model. In case of aggregate lane type, the developed model requires fewer parameters than METANET, therefore demand less computational effort.

8.2 Model applications

In this section some application areas of the newly developed macroscopic model are discussed. Application areas are:

1. Automated incident and congestion detection
2. Dynamic multiclass travel time prediction
3. Multiclass, multilane data checking and completion

4. Optimal design of roadway geometry

5. Development of advanced multi–agent control strategies for multi–class traffic networks

While the first three applications previously have been covered in Hoogendoorn (1999a), the last two will be discussed in the ensuing of this section

8.2.1 Optimal design of roadway geometry

In this thesis we showed mathematically and numerically that the geometrical design of the roadway plays an important role in the traffic operations on freeways and in urban networks. That is, choosing an appropriate layout of the roadway at discontinuities yields better traffic operations. Let us discuss the application of the developed model in the context of both freeways and urban networks.

- Optimal geometrical design of ramps: at on–and off–ramps or weaving sections, the length of the acceleration lane is a factor that influences the dynamics of the traffic flow within these areas. To some extent, the longer the acceleration lane is, the better the resulting traffic operations. We have shown that the necessary length of the acceleration lane depends on some combinations between the traffic demand of the main carriageway and of on–ramp. Therefore, given a fixed O-D matrix and an objective function the necessary length of ramps can be obtained.

- Optimal geometrical design of multilane intersections: traffic operations at multilane intersections consist of many traffic streams, which are captured by the developed model. Application of the developed model shows that the operation of these streams can be improved by suitable lane allocation, for example, designing exclusive lanes for right-turning or left-turning movements. This property has been shown mainly in microscopic models but not yet in macroscopic models.

8.2.2 Development of advanced multi–agent control strategies for multi–class traffic networks

This application is the topic of project 3 within the framework of AMICI program. Let us briefly summarize the aims of this project and its connection with the research presented in this thesis.

The performance of traffic networks can be influenced by many control measures, such as ramp metering, variable speed limits, and traffic signals. To improve the network's performance, a traffic control scheme can be used that results in a more efficient use of the existing infrastructure. The current traffic control schemes often only act on an isolated scale, while they seldom take the varying objectives of different user classes into account. Current traffic

control measures often alleviate the congestion on a highway section or a part of the freeway by moving it to another part of the freeway network or to the local street network. To further improve traffic conditions, we need to simultaneously consider both the freeways and the urban roads. Hence, we require a coordinated network–wide traffic control set up for hybrid networks that also takes multi-class characteristic of traffic flows into account. To this end, an innovative control theory is needed that is specifically suited to the coordinated control of heterogeneous traffic flow in hybrid networks. There are two control approaches, namely, soft control measures (for instance, providing traffic information or route directives), and hard control measures (ramp-metering, intersection control, exit control, etcetera). The hard control measures lead to fast dynamics in the traffic system, while the soft measures give slow re-routing dynamics. In order to develop a control structure that can effectively handle both fast and slow dynamics, it is necessary to combine existing control design techniques from the fields of distributed and hierarchical control, supervisory control, hybrid systems control and multi-agent control, and to apply them to coordinated control of multi-class traffic networks. This work should result in a control strategy that has several advantages: it should take the influence of information into account, distinguish different driver classes, describe mixed urban/freeway networks, be flexible and robust to local hardware failures, have good scaling properties, and be easily extended. For the hard control measures, the macroscopic model developed in this thesis is an appropriate tool.

8.3 Recommendations

In this final section we aim to give some directions for the further research following from the study performed in this thesis. These directions are categorized into two groups: modeling approach and model calibration/validation.

8.3.1 Modeling approach

Some assumptions made while developing the macroscopic model presented in this thesis can be released by considering the following research directions:

- In order to account for the fact that traffic flow consists of constrained and unconstrained vehicles, another type of distance gap distributions can be used, namely the Cowan M3 distribution type (Cowan (1975)). This distribution consists of two parts which reflect the gap distribution of unconstrained and constrained vehicle. Consequently, the obtained macroscopic model is divided into two parts. The first part consists of equations that describe the dynamics of unconstrained vehicles, whereas the other part consists of equations for the dynamics of constrained vehicles.

- In the context of multilane freeways, we have only considered the lane–changes of vehicles from the shoulder lane to the median lane in order to give-way to merging vehicles. However, the reduction of speed of those vehicles in order to create more

gaps for merging vehicles should also be included in the *mandatory lane-changing* processes.

- Multiple merging/diverging phenomena (that is, several vehicles merge or diverge into the same gap between two successive vehicles in the target lanes) should be considered in the further development of the model.

- Acceleration and/or deceleration of (mandatory) lane-changing vehicles to adapt their speeds to the speeds of vehicles on the destination lane should be taken into account.

- In this thesis, we modeled traffic inflow and outflow at multilane intersection by considering uniform arrival rate. However, the contribution of random delay (that is, stochastic arrival rate) to traffic dynamics at intersection can also be taken into account.

8.3.2 Model calibration/validation

To enhance the ability of the model applications proposed in this thesis to more accurately predict the (macroscopic) lane-changing processes at bottlenecks under various geometrical characteristics, the model should be calibrated with richer data than used in this thesis. That is:

- The impact of the length of the acceleration lane on the *mandatory lane-changing* processes should be observed and the model should be calibrated using data from different sites with different layouts.

- Using the data that contain lane-changing information can make the calibrated values of lane-changing model parameters more precise.

- Using different objective functions to see if the result is robust.

- Using other minimization algorithms to investigate how the result depends on the choice of the algorithm.

- So far, the model has only been calibrated/validated using data collected from a single freeway. There is a need for detailed data measured in an urban network, in which all the lane-changing processes should be observed, especially the turning movements at (controlled and uncontrolled) multilane intersections.

- Data including the dynamics of traffic compositions should be observed so that the developed model can be calibrated in order to describe the interactions between vehicle types and their effects on the traffic evolution in the main lanes.

A more extensive calibration/validation of the model developed for freeways and urban networks should be performed. Further cross-comparisons of the developed model with others (both macroscopic and microscopic) models should be carried out in terms of accuracy and computational efforts.

We envisage that the proposed modeling approach will yield improved (continuum) macroscopic models to describe traffic operations on freeways and in urban networks. The ability of the developed models to take into account in detail the influence of (infrastructure) discontinuities in traffic flow dynamics enables a more efficient utilization of the existing infrastructure and of the available traffic control measures.

Bibliography

Ahmed, K. I. (1999). *Modelling Drivers' Acceleration and Lane Changing Behavior.* PhD thesis, Massachusetts Institute of Technology, USA.

Aw, A., and Rascle, M. (2000). Resurrection of Second Order Models of Traffic Flow. *SIAM Journal of Applied Mathematics*, *60*, 916-938.

Bando, M., Hasebe, K., Nakanishi, K., and Nakayama, A. (1998). Analysis of Optimal Velocity Model with Explicit Delay. *Physical Review E*, *58*, 5429-5435.

Bando, M., Hasebe, K., Nakayama, A., Shibata, A., and Sugiyama, Y. (1995). Dynamical Model of Traffic Congestion and Numerical Simulation. *Physical Review E*, *51*, 1035-1042.

Barcelo, J., Casas, J., Ferrer, J. L., and Garcia, D. (1998). Modelling Advanced Transport Telematic Applications with Microscopic Simulators: The Case with AIMSUN2. In *Proceedings of the workshop Verkehr und Mobilitat, Forschungsverbund Verkehrssimulation und Umweltswirkungen* (p. 137-143).

Batten, P., Clarke, N., Lambert, C., and Causon, D. M. (1993). On the Choice of Wave Speeds for the HLLC Riemann Solver. *SIAM Journal of Science Computing*, *18*, 1553-1570.

Ben-Akiva, M., and Lerman, S. (1995). *Discrete Choice Analysis.* Cambridge: MIT Press.

Bliemer, M. J. C. (2001). *Analytical Dynamic Traffic Assignment with Interacting User-classes: Theoretical Advances and Applications Using a Variation Inequality Approach.* PhD thesis, Delft University of Technology, Netherlands.

Brackstone, M., and McDonald, M. (2000). Car-following: A Historical Review. *Transportation Research F*, *2*, 181-196.

Buisson, C., Lebacque, J. P., and Lesort, J. B. (1996). STRADA, a Discretized Macroscopic Model of Vehicular Traffic Flow in Complex Networks Based on the Godunov Scheme. In *Symposium on Modeling, Analysis and Simulation* (p. 976-981).

Chadler, R. E., Herman, R., and Montroll, E. W. (1958). Traffic Dynamics: Studies in Car Following. *Operations Research*(6), 165-184.

Chanut, S. (2005). First order macroscopic traffic flow model for mixed traffic including moving bottleneck effects. In *Proceedings of the 16th International Symposium on Transportation and Traffic Theory* (p. 365-386).

Cowan, R. J. (1975). Useful Headway Models. *Transportation Research*, *9*, 371-375.

Cox, D. R. (1962). *Renewal Theory.* London: Birkbeck College University of London.

Cremer, M., and Ludwig, J. (1986). A Fast Simulation Model for Traffic Flow on Basic of Boolean Operations. *Mathematics and Computers in Simulation*, *28*, 297-303.

Cremer, M., and Papageorgiou, M. (1981). Parameter identification for a traffic flow model. *Automatica*, *17*, 837-843.

Daganzo, C. F. (1994). The Cell Transmission Model, Part II: Network Traffic. *Transportation Research B*, *28*, 279-293.

Daganzo, C. F. (1995). Requiem for Second-order Fluid Approximations of Traffic Flow. *Transportation Research B*, *29*, 277-286.

Daganzo, C. F. (1997). A Continuum Theory of Traffic Dynamics for Freeways with Special Lanes. *Transportation Research B*, *31*, 83-102.

Del Castillo, J. M. (1996). A Car Following Model Based on the Lighthill-Whitham Theory. In *Proceedings of the 13th International Symposium on Transportation and Traffic Theory* (p. 517-538).

Del Castillo, J. M., Pintado, P., and Benitez, F. G. (1993). A Formulation for the Reaction Time of Traffic Flow Models. In *Proceedings of the 12th International Symposium on Transportation and Traffic Theory* (p. 387-405).

Einfeldt, B. (1988). On Godunove-type Methods for Gas Dynamics. *SIAM Journal of Numerical Analysis*, *25*, 294-318.

Elloumi, N., Hadj-Salem, H., and Papageorgiou, M. (1994). METACOR, a Macroscopic Modelling Tool for Urban Corridors. In *Proceedings of the 2nd Triennial Symposium on Transportation Analysis* (p. CD ROM).

Forbes, T. W., Zagorski, H. J., Holshouser, E. L., and Deterline, W. A. (1958). Measurement of Driver Reaction to Tunnel Conditions. In *Proceedings of Highway Research Board* (p. 345-357).

Gipps, P. G. (1981). A Behavioural Car Following Model for Computer Simulation. *Transportation Research B*, *15*, 105-111.

Hegyi, A., Ngoduy, D., Schutter, B. de, Hellendoorn, J., Hoogendoorn, S. P., and Stramigioli, S. (2003). Suppressing Shock Waves on the A1 in The Netherlands-Model Calibration and Model-Based Predictive Control. In *Proceedings of the 6th International Incollection on Intelligent Transportation Systems* (p. 672-677).

Helbing, D. (1995). Improved Fluid-dynamic Model for Vehicular Traffic. *Physical Review E*, *51*, 3164-3169.

Helbing, D. (1996). Gas-kinetic Derivation of Navier-Stokes-like Traffic Equations. *Physical Review E*, *53*, 2366-2381.

Helbing, D. (1997a). *Verkehrsdynamik.* Berlin: Springer-Verlag.

Helbing, D. (1997b). Modelling Multilane Traffic Flow with Queuing Effects. *Physica A*, *242*, 175-194.

Helbing, D. (2001). Traffic and Related Self-driven Many-particle Systems. *Reviews of modern physics*, *33*(4), 1067-1141.

Helbing, D., Hennecke, A., Shvetsov, V., and Treiber, M. (1999a). MASTER: Macroscopic Traffic Simulation Based on a Gas-kinetic Non-local Traffic Model. *Transportation Research B*, *35*(2), 183-211.

Helbing, D., Hennecke, A., Shvetsov, V., and Treiber, M. (2002). Micro-and Macrosimulation of Freeway Traffic. *Mathematical and Computer Modelling*, *35*, 517-547.

Helbing, D., Hennecke, A., and Treiber, M. (1999b). Phase Diagram of Traffic States in the Presence of Inhomogeneities. *Physical Review Letters*, *82*(21), 4360-4363.

Helbing, D., and Treiber, M. (1998). Gas-kinetic Based Traffic Flow Models Explaining Observed Hysteretic Phase Transition. *Physical Review Letters*, *81*, 3042-3045.

Helbing, D., and Treiber, M. (1999c). Numerical Simulation of Macroscopic Traffic Equations. *Computing in Science and Engineering*, *1*, 89-99.

Herman, R., Montrol, E. W., Potts, R., and Rothery, R. W. (1959). Traffic Dynamics: Analysis of Stability in Car-Following. *Operations Research*(7), 86-106.

Herman, R., and Rothery, R. W. (1963). Microscopic and Macroscopic Aspects of Single Lane Traffic Flow. *Journal of Operations Research Society of Japan*(5), 74-93.

Highway Capacity Manual. (2000). Washington D.C.

Hilliges, M., and Weidlich, W. (1995). A Phenomenological Model for Dynamic Traffic Flow in Networks. *Transportation Research B*, *29*, 407-431.

Hirsch, C. (1990a). *Numerical Computation of Internal and External Flow. Volume 1: Fundamentals of Numerical Discretization.* Brussel: John Wiley and Sons.

Hirsch, C. (1990b). *Numerical Computation of Internal and External Flow. Volume 2: Computational Methods for Inviscid and Viscous Flows.* Brussel: John Wiley and Sons.

Hoogendoorn, S. P. (1999a). *Multiclass Continuum Modelling of Multilane Traffic Flow*. PhD thesis, Delft University of Technology, Netherlands.

Hoogendoorn, S. P., and Bovy, P. H. L. (1999b). Multiclass Macroscopic Traffic Flow Modelling: A Multilane Generalization Using Gas-kinetic Theory. In *Proceedings of the 14th International Symposium on Transportation and Traffic Theory* (p. 27-50).

Hoogendoorn, S. P., Bovy, P. H. L., and Lint, H. van. (2002). Short-term Prediction of Traffic Flow Conditions in a Multilane Multi-class Network. In *Transportation and Traffic Theory in the 21st Century* (p. 625-651).

Jepsen, M. (1998). On the Speed-Flow Relationships in Road Traffic: A Model of Driver Behaviour. In *Proceedings of the Third International Symposium on Highway Capacity* (p. 297-319).

Kerner, B. S. (1998). Experimental Features of Self-Organization in Traffic Flow. *Physical Review Letters*, *81*, 3797-3800.

Kerner, B. S. (2002). Empirical Macroscopic Features of Spatial-Temporal Traffic Patterns at Highway Bottlenecks. *Physical Review E*, *65*, 046138-046167.

Kerner, B. S., and Klenov, S. L. (2003). Microscopic Theory of Spatial-Temporal Congested Traffic Patterns at Highway Bottlenecks. *Physical Review E*, *68*, 036130-036149.

Kerner, B. S., and Konhauser, P. (1993). Cluster Effect in Initially Homogeneous Traffic Flow. *Physical Review E*, *48*, R2335-R2338.

Kerner, B. S., and Konhauser, P. (1994). Structure and Parameters of Clusters in Traffic Flow. *Physical Review E*, *50*, 54-83.

Kerner, B. S., Konhauser, P., and Schilke, M. (1995). Deterministic Spontaneous Appearance of Traffic Jam in Slightly Inhomogeneous Traffic Flow. *Physical Review E*, *51*, R6243-R6246.

Kerner, B. S., Konhauser, P., and Schilke, M. (1996b). Dipole-layer Effect in Dense Traffic Flow. *Physical Letter A*, *215*, 45-56.

Kerner, B. S., and Rehborn, H. (1996a). Experimental Features and Characteristics of Traffic Jams. *Physical Review E*, *53*(2), 1297-1300.

Kerner, B. S., and Rehborn, H. (1997). Experimental Properties of Phase Transitions in Traffic Flow. *Physical Review Letters*, *79*, 4030-4033.

Klar, A., and Wegener, R. (1997). Enskog-like Kinetic Models for Vehicular Traffic. *Journal of Statistical Physics*, *87*, 91-114.

Krauss, S. (1998). *Microscopic Modeling of Traffic Flow: Investigation of Collision Free Vehicle Dynamics* (Tech. Rep. No. 98-08). DLR-Deutsches Zentrum fur Luft-und Raumfahrt e.V., Cologne.

Kuhne, R. D. (1991). Traffic Patterns in Unstable Traffic Flow for Freeways. In Brannolte (Ed.), *Highway Capacity and Level of Service.* Rotterdam.

Lebacque, J. P. (1984). Semimacroscopic simulation of urban traffic. In *Proceedings of the International Minneapolis Summer Conference.*

Lebacque, J. P. (1996). The Godunov Scheme and What It Means for First Order Traffic Flow Models. In *Proceedings of the 13th International Symposium on Transportation and Traffic Theory* (p. 647-677).

Lebacque, J. P. (2005). First Order Macroscopic Traffic Flow Models: Intersection Modeling, Network Modeling. In *Proceedings of the 16th International Symposium on Transportation and Traffic Theory* (p. 365-386).

Lebacque, J. P., and Khoshyaran, M. M. (1998). First Order Macroscopic Traffic Flow Models for Networks in the Context of Dynamic Assignment. In *Proceedings of the 6th Meeting of the Euro Working Group on Transportation* (p. 119-139).

Lee, H. Y., Lee, H. W., and Kim, D. (1999). Dynamic States of a Continuum Traffic Equation with On-ramp. *Physical Review E*, *59*, 5101-5111.

Leo, C. J., and Pretty, R. L. (1992). Numerical Simulation of Macroscopic Continuum Traffic Flow Models. *Transportation Research B*, *26*, 207-220.

Lertworawanich, P., and Elefteriadou, L. (2003). A Methodology for Estimating Capacity at Ramp Weaves Based on Gap-acceptance Theory and Linear Optimization. *Transportation Research B*, *37*, 459-483.

Leutzbach, W. (1988). *An Introduction to the Theory of Traffic Flow*. Berlin: Springer-Verlag.

Lighthill, M. H., and Whitham, G. B. (1955). On Kinematic Waves 2: A Theory of Traffic Flow on Long, Crowded Roads. In *Proceedings of the Royal Society of London* (p. 317-345).

Liu, G., Lyrintzis, A. S., and Michalopoulos, P. G. (1996). Modelling of Freeway Merging and Diverging Flow Dynamics. *Applied Mathematic Modelling*, *20*, 459-469.

Logghe, S. (2003). *Dynamic Modeling of Heterogeneous Vehicular Traffic*. PhD thesis, Katholieke University of Leuven, Belgium.

Lyrintzis, A. S., Liu, G., and Michalopoulos, P. G. (1994). Development and Comparative Evaluation of High Order Traffic Flow Models. *Transportation Research Records*, *1547*, 174-183.

MacShane, W. R., and Roess, R. P. (1970). Capacity Analysis of Freeway Weaving Sections. In (p. 236-261). Traffic Engineering.

Makigami, Y., and Iizuka, T. (1993). Evaluation of Weaving Traffic Stream Using Merging Probability. In *Proceedings of the 12th International Symposium on Transportation and Traffic Theory* (p. 53-69).

Mason, A. D., and Woods, A. W. (1998). The Effect of Speed Controls on Traffic. *Mathematics in Transport Planning and Control*, 351-360.

Michalopoulos, P. G., Beskov, D. E., and Yamauchi, Y. (1984). Multilane Traffic Flow Dynamics: Some Macroscopic Considerations. *Transportation Research B*, *18*, 377-395.

Michalopoulos, P. G., Yi, P., and Lynrintzis, A. S. (1993). Continuum Modeling of Traffic Dynamics for Congested Freeways. *Transportation Research B*, *27*(4), 315-332.

Minderhoud, M. M. (1999). *Supported Driving: Impacts on Motorway Traffic Flow*. PhD thesis, Delft University of Technology, Netherlands.

Munjal, P., Hsu, Y. S., and Lawrence, R. L. (1971b). Analysis and Validation of Lane-drop Effects on Multilane Freeways. *Transportation Research*, *5*, 257-266.

Munjal, P., and Pahl, J. (1969). An Analysis of the Boltzmann-type Statistical Models for Multilane Traffic Flow. *Transportation Research*, *3*, 151-163.

Munjal, P., and Pipes, L. A. (1971a). Propagation of On-ramp Density Perturbations on Unidirectional Two and Three-Lane Freeways. *Transportation Research*, *5*, 241-255.

Nelson, P. (1995). A Kinetic Theory of Vehicular Traffic and its Associated Bimodal Equilibrium Solutions. *Transport Theory and Statistical Physics*, *24*, 383-409.

Newell, G. F. (1961). Nonlinear Effects in the Dynamics of Car Following. *Operations Research*(9), 209-229.

Ngoduy, D. (2005b). A Continuum Traffic Model for Weaving Sections on Freeways. *Journal of Transportmetrica*, To appear.

Ngoduy, D., and Hoogendoorn, S. P. (2003a). An Automated Calibration Procedure for Traffic Flow Models. In *Proceedings of the 10th International Federation of Automatic Control* (p. 295-300).

Ngoduy, D., and Hoogendoorn, S. P. (2003b). Positively Conservative Numerical Scheme for Macroscopic Traffic Flow Models. In *Proceedings of the 10th International Federation of Automatic Control* (p. 301-306).

Ngoduy, D., Hoogendoorn, S. P., and Lint, J. W. C. van. (2005a). Modeling Traffic Flow Operations in Multilane and Multiclass Urban Networks. *Journal of Transportation Research Records*, *1923*, 73-81.

Ngoduy, D., Hoogendoorn, S. P., and Zuylen, H. J. van. (2004a). Cross-comparison of Numerical Schemes for Macroscopic Traffic Flow Models. *Journal of Transportation Research Records*, *1876*, 52-61.

Ngoduy, D., Hoogendoorn, S. P., and Zuylen, H. J. van. (2004b). Modelling and Simulation of Multilane and Multiclass Traffic Flow at On and Off Ramps. In *Proceedings of the 5th Triennial Symposium on Transportation Analysis.* CD ROM.

Ngoduy, D., Hoogendoorn, S. P., and Zuylen, H. J. van. (2004c). Multiclass Traffic Flow Theory for Modelling of Multilane Motorway Networks. In *Proceedings of the 10th World Conference in Transportation Research.* in press.

Ngoduy, D., Hoogendoorn, S. P., and Zuylen, H. J. van. (2004d). Macroscopic Traffic Flow Modeling of Weaving Sections on Freeways. In *Proceedings of the 8th TRAIL Congress* (p. 331-354).

Ngoduy, D., Hoogendoorn, S. P., and Zuylen, H. J. van. (2006). New Continuum Traffic Model for Freeway with On- and Off-ramp to Explain Different Traffic Congested States. *Journal of Transportation Research Records*, To appear.

Ossen, S. J. L., and Hoogendoorn, S. P. (2005). Car-following Behavior Analysis from Microscopic Trajectory Data. *Journal of Transportation Research Records*, To appear.

Ossen, S. J. L., Hoogendoorn, S. P., and Gorte, B. G. H. (2006). Inter-driver Differences in Car-following: A Vehicle Trajectory Based Study. *Journal of Transportation Research Records*, To appear.

Papageorgiou, M., Blosseville, J. M., and Hadi-Salem, H. (1989). Macroscopic Modelling of Traffic Flow on the Boulevard Peripherique in Paris. *Transportation Research B*, *23*, 29-47.

Papageorgiou, M., Blosseville, J. M., and Hadi-Salem, H. (1990). Modelling and real-time control of traffic flow on the southern part of Boulevard Peripherique in Paris: Part I: Modelling. *Transportation Research A*, *24*, 345-359.

Paveri-Fontana, S. L. (1975). On Boltzmann-like Treatments for Traffic Flow: A Critical Review of the Basic Model and an Alternative Proposal for Dilute Traffic Analysis. *Transportation Research B*, *9*, 225-235.

Payne, H. J. (1971). Models for Freeway Traffic Control. *Mathematical Models of Public Systems*, *1*, 51-61.

Payne, H. J. (1979). FREFLO: A Macroscopic Simulation Model of Freeway Traffic. *Transportation Research Records*, *722*, 68-77.

Philips, W. F. (1977). *Kinetic Model for Traffic Flow* (Tech. Rep.). National Technical Information Service, Springfield, VA 22161.

Philips, W. F. (1979). Kinetic Model for Traffic Flow with Continuum Implications. *Transportation Research Planning and Technology*, *5*, 131-138.

Pipes, L. A. (1953). An Operational Analysis of Traffic Dynamics. *Applied Physics*, *24*(1), 274-287.

Prigogine, I. (1961). A Boltzmann-like Approach to the Statistical Theory of Traffic Flow. In R. Herman (Ed.), *Theory of Traffic Flow.*

Prigogine, I., and Andrews, F. C. (1960). A Boltzmann-like Approach for Traffic Flow. *Operations Research*, *8*, 789-797.

Prigogine, I., and Herman, R. (1971). *Kinetic Theory of Vehicular Traffic.* New-York: American Elsevier.

Reuschel, A. (1950). Fahrzeugbewegungen in der Kolonne. *Osterr. Ingen. -Archiv*, *4*, 193-215.

Richards, P. I. (1956). Shock Waves on the Highway. *Operations Research*, *4*, 42-51.

Rorbech, J. (1976). *The Multilane Traffic Flow Process.* PhD thesis, Technical University of Denmark, Denmark.

Rothery, R. W. (1999). Car Following Models. In Gartner, Messer, and Rathi (Ed.), *Traffic Flow Theory, a State of the Art Report.*

Shvetsov, V., and Helbing, D. (1999). Macroscopic Dynamics of Multilane Traffic. *Physical Review E*, *59*, 6328-6339.

Sod, G. A. (1985). *Numerical Methods in Fluid Dynamics.* USA: Cambridge University Press.

Tampere, C. M. J. (2004). *Human-kinetic Multiclass Traffic Flow Theory and Modelling.* PhD thesis, Delft University of Technology, Netherlands.

Tanner, J. C. (1962). A theoretical Analysis of Delays at an Uncontrolled Intersection. *Biometrica*, *49*, 163-170.

Technical University of Crete. (2001). *METANET, A SIMULATION PROGRAM FOR MOTORWAY NETWORKS.* Greece: Technical University of Crete.

Toledo, T. (2003). *Integrated Driving Behavior Modeling.* PhD thesis, Massachusetts Institute of Technology, USA.

Tomer, E., Safonov, L., and Havlin, S. (2000). Presence of Many Stable Nonhomogeneous States in an Inertial Car-following Model. *Physical Review Letters*, *75*, 382-385.

Treiber, M., Hennecke, A., and Helbing, D. (1999). Derivation, Properties and Simulation of a Gas-kinetic-based, Non-local Traffic Model. *Physical Review E*, *59*, 239-253.

Treiber, M., Hennecke, A., and Helbing, D. (2000). Congested Traffic States in Empirical Observations and Microscopic Simulations. *Physical Review E*, *62*, 1805-1824.

Vermijs, R. G. M. M., Papendrecht, H. J., Lutje Spelberg, R. F., and Toetenel, W. J. (1995). Short-term Forecasting of the Level of Service on a Motorway Network, by Using a Microscopic Simulation Model. In *Proceedings of the 2nd Eramus-Network Incollection on Transportation and Traffic engineering.* Kerkrade.

Wegener, R., and Klar, A. (1996). A Kinetic Model for Vehicular Traffic Derived from a Stochastic Microscopic Model. *Transport Theory and Statistics of Physics*, *25*, 785-798.

Wiedemann, R. (1974). *Simulation des Strassenverkehrsflusses* (Tech. Rep.). Institute for Traffic Engineering, University of Karlsruhe.

Wolf, D. E. (1999). Cellular Automata for Traffic Simulations. *Physica A*, *263*, 438-451.

Wong, G. C. K., and Wong, S. C. (2002). A Multiclass Traffic Flow Model-an Extension of LWR Model with Heterogeneous Drivers. *Transportation Research A*, *36*, 763-848.

Zhang, H. M. (2000). Structural Properties of Solutions Arising from a Nonequilibrium Traffic Flow Theory. *Transportation Research B*, *34*, 583-603.

Zhang, H. M. (2001). A Finite Difference Approximation of a Non-equilibrium Traffic Flow Model. *Transportation Research B*, *35*, 337-365.

Zhang, H. M. (2003). Anisotropic Property Revisited-Does It Hold in Multilane Traffic? *Transportation Research B*, *37*, 561-577.

Zhang, H. M., and Jin, W. L. (2002). A Kinematic Wave Traffic Flow Model for Mixed Traffic. *Transportation Research Records*, *1802*, 197-204.

Appendix A

Formulation for lane-changing probabilities

In this appendix, we show the applied method to determine lane-changing probabilities. In the developed model, the lane-changing probabilities consist of an immediate and mandatory lane-changing process. While the former occurs due to interactions between fast and slow vehicles, the latter occurs when vehicles are forced to change lanes, for example, due to the geometry of the roadway.

A.1 Immediate lane-changing probability

Let us consider a vehicle of class u driving in lane i that intends to change to the adjacent lane $j = i \pm 1$ (Figure 3.5 in Chapter 3).

Let $\mathcal{A}_{i,j}^{u,s}(v|x,t)$ be the event that a vehicle from class u that drives in lane i finds a sufficient gap between vehicles from class s in lane j. The probability that $\mathcal{A}_{i,j}^{u,s}(v|x,t)$ occurs is calculated by the following equation:

$$\begin{aligned} P\left(\mathcal{A}_{i,j}^{u,s}\right) &= exp\left[-\gamma_j r_j \left(d_u^{min} + l_u\right)\right] \sum_0^\infty \frac{(-1)^n (\gamma_j r_j T_j^s)^n}{n!} \langle w^n \rangle_w \\ & \quad exp\left[-\gamma_j r_j \left(d_s^{min} + l_s\right)\right] \sum_0^\infty \frac{(-1)^n (\gamma_j r_j T_i^u)^n}{n!} \langle v^n \rangle_v \end{aligned} \tag{A.1}$$

As long as the distribution of the speed is Gaussian, we have:

$$\langle v^k \rangle_v = V^k + 0.5k(k-1)V^{k-2}\Theta \tag{A.2}$$

Now let us consider the following expression:

$$\begin{aligned}
& \sum_{0}^{\infty} \frac{(-1)^n(\gamma r T)^n \langle v^n \rangle_v}{n!} = 1 - \gamma r T V \\
+ & \sum_{2}^{\infty} \frac{(-1)^n (\gamma r T)^n \left[V^n + 0.5n(n-1)V^{n-2}\Theta\right]}{n!} \\
= & \sum_{0}^{\infty} \frac{(-1)^n (\gamma r T V)^n}{n!} + 0.5\Theta \sum_{2}^{\infty} \frac{(-1)^n (\gamma r T)^n V^{n-2}}{(n-2)!} \\
= & e^{-\gamma r T V} + 0.5\Theta (\gamma r T)^2 \sum_{2}^{\infty} \frac{(-1)^{n-2} (\gamma r T V)^{n-2}}{(n-2)!} \\
= & e^{-\gamma r T V} + 0.5\Theta (\gamma r T)^2 e^{-\gamma r T V} = e^{-\gamma r T V} \left[1 + 0.5\Theta (\gamma r T)^2\right] \qquad \text{(A.3)}
\end{aligned}$$

By substituting expression A.3 into equation A.1 we obtain:

$$\begin{aligned}
P(\mathcal{A}_{i,j}^{u,s}) = & e^{-\gamma_j r_j \left(d_s^{min} + l_s + T_i^u V_i^u\right)} \left[1 + 0.5\Theta_i^u \left(\gamma_j r_j T_i^u\right)^2\right] \\
& e^{-\gamma_j r_j \left(d_u^{min} + l_u + T_j^s V_j^s\right)} \left[1 + 0.5\Theta_j^s \left(\gamma_j r_j T_j^s\right)^2\right] \qquad \text{(A.4)}
\end{aligned}$$

A.2 Mandatory lane-changing probability

A.2.1 Merging at on–ramp

The probability that a vehicle from the on–ramp finds a sufficient gap (both *lead-gap* and *lag-gap*) in the shoulder lane in order to merge is determined as (see equation 3.43 in Chapter 3):

$$\begin{aligned}
P(\mathcal{A}_{0,1}^{u,s}) = & exp\left[-\gamma_1 r_1 \left(d_s^{min} + l_s\right)\right] \sum_{0}^{\infty} \frac{(-1)^n (\mu(x)\gamma_1 r_1 T_0^u)^n}{n!} \langle v^n \rangle_v \\
& \left\{\left[1 + \Lambda_1^s \left(d_u^{min} + l_u\right)\right] exp\left[-\gamma_1 r_1 \left(d_u^{min} + l_u\right)\right] \sum_{0}^{\infty} \frac{(-1)^n (\gamma_1 r_1 T_1^s)^n}{n!} \langle w^n \rangle_w \right. \\
+ & \left. \Lambda_1^s T_1^s \sum_{0}^{\infty} \frac{(-1)^n (\gamma_1 r_1 T_1^s)^n}{n!} \langle w^{n+1} \rangle_w \right\} \qquad \text{(A.5)}
\end{aligned}$$

Let us consider the following expression:

$$\begin{aligned}
&\sum_{0}^{\infty} \frac{(-1)^n(\gamma r T)^n \langle v^{n+1}\rangle_v}{n!} \\
&= V - \sum_{1}^{\infty} \frac{(-1)^n (\gamma r T)^n \left[V^{n+1} + 0.5n(n+1)V^{n-1}\Theta\right]}{n!} \\
&= V - \sum_{1}^{\infty} \frac{(-1)^n (\gamma r T)^n V^{n+1}}{n!} + 0.5\Theta \sum_{1}^{\infty} \frac{(-1)^n (\gamma r T)^n V^{n-1}(n+1)}{(n-1)!} \\
&= V\left[1 - \sum_{1}^{\infty} \frac{(-1)^n (\gamma r T V)^n}{n!}\right] - 0.5\Theta\gamma r T \sum_{0}^{\infty} \frac{(-1)^n (\gamma r T V)^n (n+2)}{n!} \\
&= V e^{-\gamma r T V} - 0.5\Theta\gamma r T \sum_{0}^{\infty} \frac{(-1)^n (\gamma r T V)^n (n+2)}{n!}
\end{aligned} \tag{A.6}$$

Now let us consider the following expansions:

$$\begin{aligned}
\sum_{0}^{\infty} \frac{X^n(n+2)}{n!} &= 2 + 3X + 4\frac{X^2}{2!} + 5\frac{X^3}{3!} + \dots \\
e^X = \sum_{0}^{\infty} \frac{X^n}{n!} &= 1 + X + \frac{X^2}{2!} + \frac{X^3}{3!} + \dots
\end{aligned} \tag{A.7}$$

Hence,

$$\begin{aligned}
\sum_{0}^{\infty} \frac{X^n(n+1)(n+2)}{n!} - 2e^X &= X + X^2 + \frac{X^3}{2!} + \frac{X^4}{3!} \dots \\
&= X\left(1 + X + \frac{X^2}{2!} + \frac{X^3}{3!} + \dots\right) \\
&= X e^X
\end{aligned} \tag{A.8}$$

That is,

$$\sum_{0}^{\infty} \frac{X^n(n+2)}{n!} = e^X (2 + X) \tag{A.9}$$

By substituting expression A.9 into expression A.6, we obtain:

$$\sum_{0}^{\infty} \frac{(-1)^n(\gamma r T)^n \langle v^{n+1}\rangle_v}{n!} = e^{-\gamma r T V}\left[V - 0.5\Theta\gamma r T\left(2 - \gamma r T V\right)\right]$$

This expression together with expression A.3 is substituted into equation A.5, which results in the following expression for the average probability that a merging vehicle finds a sufficient gap in the shoulder lane:

$$
\begin{aligned}
P(\mathcal{A}_{0,1}^{u,s}) &= e^{-\gamma_1 r_1\left(d_s^{min}+l_s+\mu(x)T_0^uV_0^u\right)}e^{-\gamma_1 r_1\left(d_u^{min}+l_u+T_1^sV_1^s\right)}\left[1+0.5\Theta_0^u\left(\mu(x)\gamma_1 r_1 T_0^u\right)^2\right] \\
&\quad \left\{\left(1+\Lambda_1^s\left[d_u^{min}+l_u+T_1^sV_1^s\right)\right]\left[1+0.5\Theta_1^s\left(\gamma_1 r_1 T_1^s\right)^2\right]\right. \\
&- \left.\Lambda_1^s\gamma_1 r_1 (T_1^s)^2\Theta_1^s\right\} \qquad \text{(A.10)}
\end{aligned}
$$

A.2.2 Merging at weaving section

The probability that a vehicle from the auxiliary lane finds a sufficient lag-gap in the shoulder lane in order to merge is determined as (see equation 3.60 in Chapter 3):

$$
\begin{aligned}
P\left(h > d_{lag}^{s,1}(w)\right) &= \{e^{-\gamma_1 r_1\left(d_u^{min}+l_u\right)}\langle e^{-\gamma_1 r_1 T_1^s w}\rangle_w \\
&+ \tilde{A}_1^s\left(d_u^{min}+l_u\right)e^{-\gamma_1 r_1\left(d_u^{min}+l_u\right)}\langle e^{-\gamma_1 r_1 T_1^s w}\rangle_w \\
&+ \tilde{A}_1^s T_1^s e^{-\gamma_1 r_1\left(d_u^{min}+l_u\right)}\langle we^{-\gamma_1 r_1 T_1^s w}\rangle_w \\
&+ \tilde{B}_1^s\left(d_u^{min}+l_u\right)^2 e^{-\gamma_1 r_1\left(d_u^{min}+l_u\right)}\langle e^{-\gamma_1 r_1 T_s w}\rangle_w \\
&+ 2\tilde{B}_1^s T_1^s\left(d_u^{min}+l_u\right)e^{-\gamma_1 r_1\left(d_u^{min}+l_u\right)}\langle we^{-\gamma_1 r_1 T_1^s w}\rangle_w \\
&+ \tilde{B}_1^s\left(T_s\right)^2 e^{-\gamma_1 r_1\left(d_u^{min}+l_u\right)}\langle w^2 e^{-\gamma_1 r_1 T_1^s w}\rangle_w\} \qquad \text{(A.11)}
\end{aligned}
$$

Note that so far we have calculated the following expression:

$$
\begin{aligned}
\langle e^{-\gamma r T v}\rangle_v &= e^{-\gamma r T V}\left[1+0.5\Theta\left(\gamma r T\right)^2\right] \\
\langle v e^{-\gamma r T v}\rangle_v &= e^{-\gamma r T V}\left[V-0.5\Theta\gamma r T\left(2-\gamma r T V\right)\right] \qquad \text{(A.12)}
\end{aligned}
$$

Now let us consider the following expression:

$$
\begin{aligned}
\langle v^2 e^{-\gamma r T v}\rangle_v &= \langle v^2\sum_0^\infty\frac{(-1)^n\left(\gamma r T v\right)^n}{n!}\rangle_v = \sum_0^\infty\frac{(-1)^n\left(\gamma r T\right)^n}{n!}\langle v^{n+2}\rangle_v \\
&= \sum_0^\infty\frac{(-1)^n\left(\gamma r T\right)^n}{n!}\left[V^{n+2}+0.5(n+1)(n+2)V^n\Theta\right] \\
&= V^2\sum_0^\infty\frac{(-1)^n\left(\gamma r T V\right)^n}{n!}+0.5\Theta\sum_0^\infty\frac{(-1)^n\left(\gamma r T V\right)^n(n+1)(n+2))}{n!} \\
&= V^2 e^{-\gamma r T V}+0.5\Theta\sum_0^\infty\frac{(-1)^n\left(\gamma r T V\right)^n(n+1)(n+2))}{n!} \qquad \text{(A.13)}
\end{aligned}
$$

Where the following expansion is used:

$$\sum_{0}^{\infty} \frac{X^n(n+1)(n+2)}{n!} = 2 + 6X + 12\frac{X^2}{2!} + 20\frac{X^3}{3!} + \dots \tag{A.14}$$

Hence,

$$\begin{aligned} \sum_{0}^{\infty} \frac{X^n(n+2)}{n!} - 2e^X &= 4X + 5X^2 + 6\frac{X^3}{2!} + 7\frac{X^4}{3!}\dots \\ &= X\left(4 + 5X + 6\frac{X^2}{2!} + 7\frac{X^3}{3!} + \dots\right) \end{aligned} \tag{A.15}$$

In which:

$$4 + 5X + 6\frac{X^2}{2!} + 7\frac{X^3}{3!} + \dots - 4e^X = Xe^X \tag{A.16}$$

That is:

$$\sum_{0}^{\infty} \frac{X^n(n+1)(n+2)}{n!} = e^X\left(2 + 4X + X^2\right) \tag{A.17}$$

which results in the following expression:

$$\left\langle v^2 e^{-\gamma r T v}\right\rangle_v = e^{-\gamma r T V}\left[V^2 + 2 - 4\gamma r T V + (\gamma r T V)^2\right] \tag{A.18}$$

Expressions A.9 and A.18 are substituted into equation A.11 in order to obtain the average probability that a vehicle from the auxiliary lane finds a sufficient gap in the shoulder lane for merging:

$$\begin{aligned} &P(\mathcal{A}_{0,1}^{u,s}) = e^{-\gamma_1 r_1\left(d_s^{min} + l_s + \mu(x) T_0^u V_0^u\right)}\left[1 + 0.5\Theta_0^u\left(\mu(x)\gamma_1 r_1 T_0^u\right)^2\right] e^{-\gamma_1 r_1\left(d_u^{min} + l_u + T_1^u V_1^u\right)} \\ &\{\left[1 + \tilde{A}_1^s\left(d_u^{min} + l_u + T_1^u V_1^u\right) + \tilde{B}_s\left(d_u^{min} + l_u + T_1^u V_1^u\right)^2\right]\left(1 + 0.5\Theta_1^s\left(\gamma_1 r_1 T_1^s\right)^2\right) \\ &- \left[\tilde{A}_1^s\gamma_1 r_1 + 2\tilde{B}_1^s\left(d_u^{min} + l_u + T_1^u V_1^u\right)\right]\Theta_1^s\left(T_1^s\right)^2 + \tilde{B}_1^s\left(T_1^s\right)^2\Theta_1^s\} \end{aligned} \tag{A.19}$$

A.2.3 Diverging probability

The average probability that a vehicle from the shoulder lane finds a sufficient gap in the auxiliary lane for diverging can be calculated by the same derivation, which is:

$$\begin{aligned} &P(\mathcal{A}_{1,0}^{u,s}) = e^{-\gamma_0 r_0\left(d_s^{min} + l_s + \mu(x) T_1^u V_1^u\right)}\left[1 + 0.5\Theta_1^u\left(\mu(x)\gamma_0 r_0 T_1^u\right)^2\right] e^{-\gamma_0 r_0\left(d_u^{min} + l_u + T_0^s V_0^s\right)} \\ &\{\left(1 + \tilde{C}_0^s\left(d_u^{min} + l_u + T_0^s V_0^s\right)\right)\left[1 + 0.5\Theta_0^s\left(\gamma_0 r_0 T_0^s\right)^2\right] - 0.5\tilde{C}_0^s\gamma_0 r_0\Theta_0^s\left(T_0^s\right)^2\} \end{aligned} \tag{A.20}$$

When the probabilities that vehicles find sufficient gaps in the target lanes have been determined, the merging/diverging probabilities can be calculated because in the mandatory lane-changing processes, the target lanes are always fixed.

Appendix B

Linear Stability Analysis of the developed Model

This appendix derives the stability conditions for the macroscopic model developed in this thesis based on a 'linear' method. That is, linear Taylor approximations are used throughout the analysis. The consequence of these approximations is that conditions that are stable according to this analysis might actually still show non-linear instability. However, in general linear analysis give good insights in the general behavior of the model in the presence of an on–ramp.

Before going into the details of the derivation, let us summarize the procedure to obtain the linearized stability conditions.

- Defining an equilibrium solution (k_{ss}, V_{ss}) of the system of partial differential equations (here, $V_{ss} = V_e(r_{ss})$);
- Considering large perturbations around the equilibrium solution, which is denoted as $\check{r}(x,t)$ and $\check{V}(x,t)$
- Choice of the functional form of perturbations. If the model is stable with any sine or cosine function it will also be stable with any linear combination of these functions. Therefore, since any function can be considered a linear combination of sine and cosine functions, the stability conditions of the model with sine or cosine perturbations also are the general stability conditions with any functional form of the perturbations. Consequently, we have:

$$\begin{aligned} \check{r}(x,t) &= \tilde{r}e^{\lambda t + i\kappa x} \\ \check{V}(x,t) &= \tilde{V}e^{\lambda t + i\kappa x} \end{aligned} \tag{B.1}$$

Where i denotes the imaginary unit, λ is the frequency and κ is the wave number.

- The stability conditions of the model are twofold. On the one hand, the pair $\check{r}(x,t)$ and $\check{V}(x,t)$ is a solution of the model. On the other hand, the amplitude of the perturbations decreases with time.

In the ensuing of this appendix we apply this procedure to the system of partial differential equations that describes the dynamics of traffic flow at an on–ramp.

Now let us consider the following system:

$$\underbrace{\begin{pmatrix} \lambda - a_{11} & a_{12} \\ a_{21} & \lambda - a_{22} \end{pmatrix}}_{\mathbf{A}} \begin{pmatrix} \check{r} \\ \check{V} \end{pmatrix} = 0 \tag{B.2}$$

Where

$$\begin{aligned} a_{11} &= \frac{\delta q_0}{L}\frac{\partial \pi_{0,1}}{\partial r} - i\kappa V_{ss} \\ a_{12} &= -\frac{\delta q_0}{L}\frac{\partial \pi_{0,1}}{\partial V} + i\kappa r_{ss} \\ a_{21} &= -\frac{\partial \psi}{\partial r} + \frac{1}{r_{ss}}\frac{\partial P}{\partial r} i\kappa \\ a_{22} &= \frac{\partial \psi}{\partial V} - \frac{1}{r_{ss}}\frac{\partial P}{\partial V} i\kappa - i\kappa V_{ss} \end{aligned} \tag{B.3}$$

The first condition is satisfied if and only if the determinant of matrix A is zero, that is:

$$det|\mathbf{A}| = 0 \;\Leftrightarrow\; \lambda^2 - (a_{11} + a_{22})\,\lambda + (a_{11}a_{22} - a_{12}a_{21}) = 0 \tag{B.4}$$

The solutions of equation B.4 are:

$$\lambda_{1,2} = 0.5\left(a_{11} + a_{22} \pm \sqrt{(a_{11} - a_{22})^2 + 4a_{12}a_{21}}\right) \tag{B.5}$$

The second condition is satisfied if and only if $Real\,(\lambda_{1,2}) < 0$. We have:

$$Real\,(a_{11} + a_{22}) = \frac{\delta q_0}{L}\frac{\partial \pi_{0,1}}{\partial r} + \frac{\partial \psi}{\partial V} \tag{B.6}$$

and:

$$Real\left(\sqrt{(a_{11} - a_{22})^2 + 4a_{12}a_{21}}\right) = \sqrt{0.5\left(\sqrt{\mathbf{R}^2 + \mathbf{I}^2} + \mathbf{R}\right)} \tag{B.7}$$

Where:

$$\begin{aligned} \mathbf{R} &= \left(\frac{\delta q_0}{L}\frac{\partial \pi_{0,1}}{\partial r} - \frac{\partial \psi}{\partial V}\right)^2 - \left(\frac{1}{r_{ss}}\frac{\partial P}{\partial V}\kappa\right)^2 + 4\frac{\delta q_0}{L}\frac{\partial \pi_{0,1}}{\partial V}\frac{\partial \psi}{\partial r} - 4\frac{\partial P}{\partial r}\kappa^2 \\ \mathbf{I} &= -2\frac{1}{r_{ss}}\frac{\partial P}{\partial V}\kappa\left(\frac{\delta q_0}{L}\frac{\partial \pi_{0,1}}{\partial r} - \frac{\partial \psi}{\partial V}\right) - 4\kappa\left(r_{ss}\frac{\partial \psi}{\partial r} + \frac{1}{r_{ss}}\frac{\delta q_0}{L}\frac{\partial \pi_{0,1}}{\partial V}\frac{\partial P}{\partial r}\right) \end{aligned} \tag{B.8}$$

From expression B.6 and B.7, $Real\,(\lambda_{1,2}) < 0$ if:

$$\begin{aligned}
& \frac{\delta q_0}{L}\frac{\partial \pi_{0,1}}{\partial r} + \frac{\partial \psi}{\partial V} < -\sqrt{0.5\left(\sqrt{\mathbf{R}^2+\mathbf{I}^2}+\mathbf{R}\right)} \\
\Leftrightarrow \quad & \left(\frac{\delta q_0}{L}\frac{\partial \pi_{0,1}}{\partial r} + \frac{\partial \psi}{\partial V}\right)^2 > 0.5\left(\sqrt{\mathbf{R}^2+\mathbf{I}^2}+\mathbf{R}\right) \\
\Leftrightarrow \quad & 4\left(\frac{\delta q_0}{L}\frac{\partial \pi_{0,1}}{\partial r} + \frac{\partial \psi}{\partial V}\right)^4 - 4\left(\frac{\delta q_0}{L}\frac{\partial \pi_{0,1}}{\partial r} + \frac{\partial \psi}{\partial V}\right)^2 R > \mathbf{I}^2 \\
\Leftrightarrow \quad & \left(\frac{\partial \psi}{\partial V} + \frac{\delta q_0}{L}\frac{\partial \pi_{0,1}}{\partial r}\right)^2 \frac{\partial P}{\partial r} > \left(r_{ss}\frac{\partial \psi}{\partial r} + \frac{1}{r_{ss}}\frac{\delta q_0}{L}\frac{\partial \pi_{0,1}}{\partial V}\frac{\partial P}{\partial r}\right)^2
\end{aligned} \tag{B.9}$$

After an intermediate algebraic calculation, we obtain the following inequality:

$$\begin{aligned}
\left(\frac{\partial \psi}{\partial r}\right)^2 (r_{ss})^4 \quad - \quad & \left[\left(\frac{\partial \psi}{\partial V}\right)^2 + \left(\frac{\delta q_0}{L}\frac{\partial \pi_{0,1}}{\partial r}\right)^2\right]\frac{\partial P}{\partial r}(r_{ss})^2 \\
+ \quad & \left(\frac{\delta q_0}{L}\frac{\partial \pi_{0,1}}{\partial V}\frac{\partial P}{\partial r}\right)^2 < 0
\end{aligned} \tag{B.10}$$

Solving this inequality, we obtain the following criteria for the stability of the on–ramp model:

$$q_0 < \frac{L \mid \partial \psi/\partial V \mid}{\mid \partial \pi_{0,1}/\partial r \mid} \tag{B.11}$$

$$r_{ss} < \frac{\mid \partial \psi/\partial V \mid \sqrt{\partial P/\partial r}}{\mid \partial \psi/\partial r \mid} \tag{B.12}$$

Appendix C

HELENA Traffic Flow Network Model

In order to incorporate the models proposed in this thesis to model traffic operations on intersections and freeways, in this appendix we describe the working of the applied computer-based network model, namely HELENA (Hoogendoorn and Bovy (1999b)) – as a prelude to future work, namely, for intersection control.

As a basis, a road network is represented as a directed graph (Figure C.1), in which nodes (origins, destinations and intermediate nodes) are connected through directed links. Each link is build up of a set of 1 to I lanes.

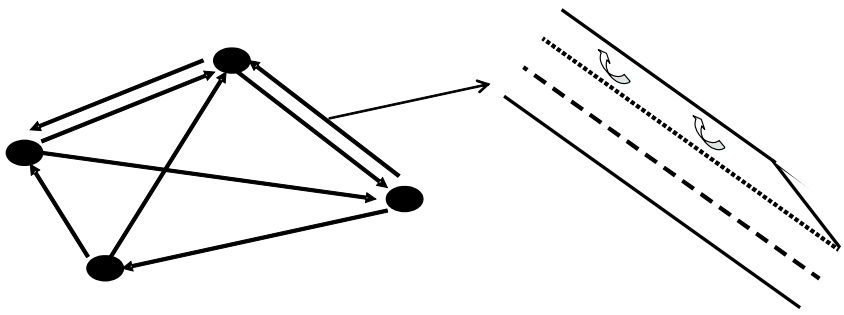

Figure C.1: Network description of HELENA: a directed graph.

In the longitudinal direction, a lane is sliced up into a set of $1 \ldots N$ cells. In the data-object model shown in Figure C.2 solid lines with the aggregation symbol depict ownership (for instance, a link owns lane objects), while solid with dots depict reference (for instance, a link contains references (pointers) to node objects). Furthermore, dotted lines denote the "kin" type of relationship (for instance, volume and density are user class specific, but do not themselves own or contain a reference to a user class object). Finally, the numbers at the start and endpoint of each relation ($1, 2, \ldots, M$ for any number > 0) denote the hierarchy of the relationship: a link is connected to two nodes; whereas a node may contain references to any number of connected links).

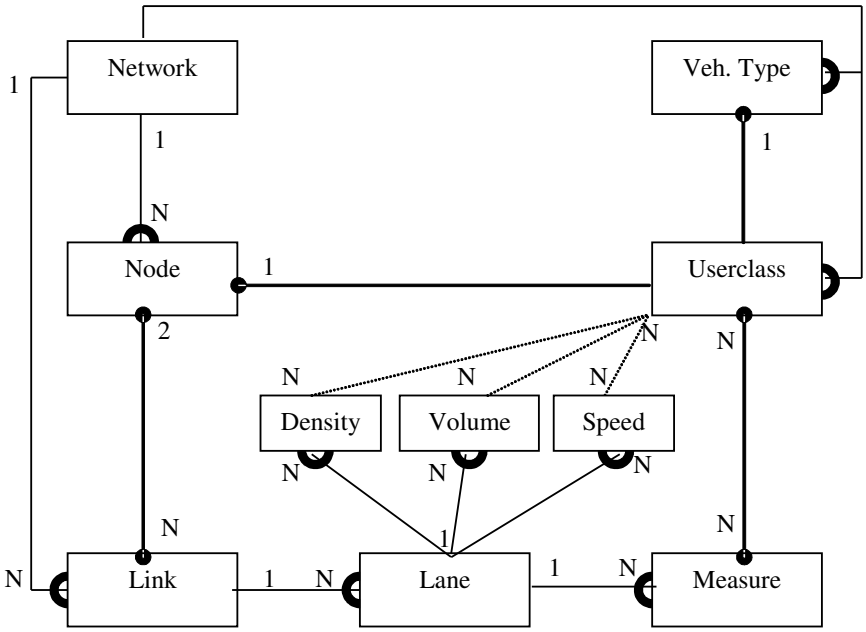

Figure C.2: Data-object model of HELENA.

As outlined in the data-object model (Figure C.2), a road network contains nodes and links. The propagation of flow on multi-lane links is governed by so-called Link flow procedures, which implement the *MLMC* equations, described in Chapter 6. All external lane-specific influences on traffic flow are modeled through the concept of Measures. A lane may contain any number of measures. Measures are user class specific, that is: a measure may operate on one or more (or all) user classes. In general, two classes of measures exist. The first class operates on infrastructure or basic driver related parameters (designated truck lanes, overtaking prohibitions, and lane closures). In a sense, these measures may be considered "low-level" measures. The second class of measures operates on "higher-level" driver behavior, such as, choice of free-speed or lane changing behavior (for instance, speed-reduction, pay lanes). Some measures (of the first class) are inherently introduced by the infrastructure (such as shunt zones at left lane drops). They are generated automatically as a result of network design. Other "low-level" measures are created dynamically as a result of route choice behavior (for instance, shunt zones before intersections). All other measures (for instance, intelligent driver assistant systems) can be created by the user and can be assigned to any or all user classes. Measures that are created as a result of network design always prevail over user-created measures.

Traffic demand external to the network under consideration is modeled at the nodes, through a so-called feeder object (Figure C.3). A feeder simply places traffic of various user classes at a node at each simulation step. At the nodes, also traffic supply is governed, yielding boundary conditions at the downstream end of links. In case a node represents an intersection, the available gaps in the conflicting traffic stream restrict the outflow out of the incoming links at the node, according to the equations presented in Section 6.2. In case of a

signalized controlled intersection, outflow is determined by the available green time. During red phases, traffic supply is zero, inevitably leading to queues. A node of type intersection thereto contains a Traffic Control object, which implements all kinds of traffic control, such as, traffic lights at urban intersections. User class-specific split fractions are not the result of a multiclass-dynamic traffic assignment, but are based on normative user class specific route choice models based on habit, experience and possibly the effect of traffic management, such as, VMS's. A node may contain a VMS object, which influences the route choice. The response to VMS's is user class specific and user-adjustable.

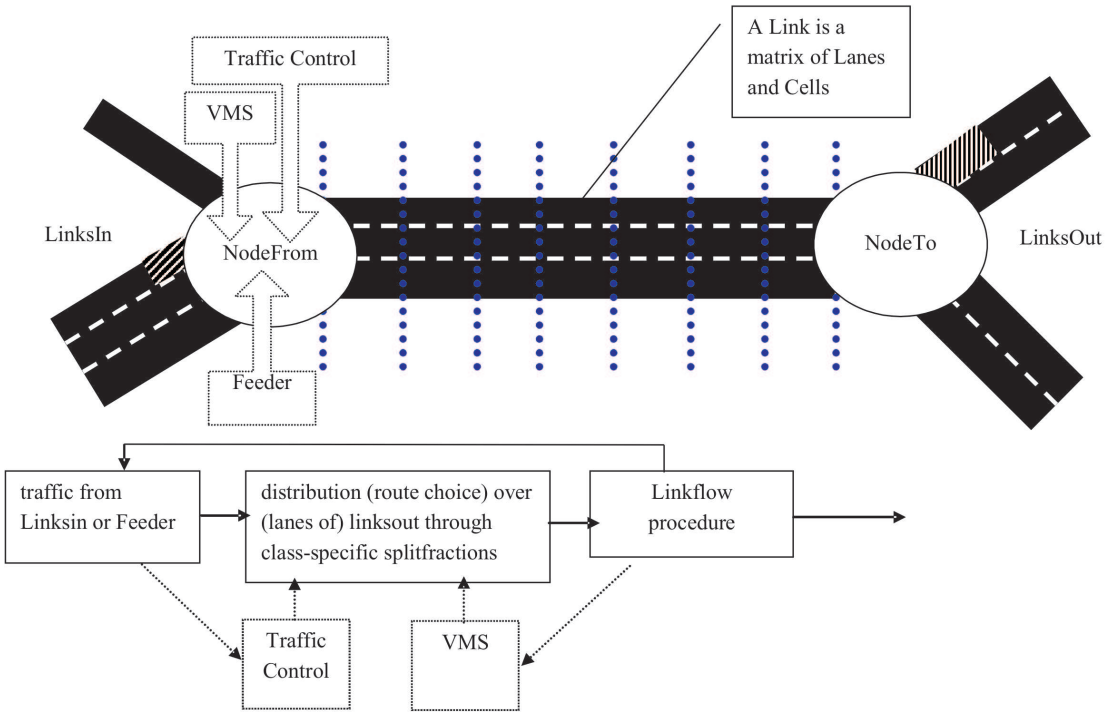

Figure C.3: Dynamics of route choice and link flow in HELENA.

As shown in Figure C.3, each link contains lanes, which are subsequently divided into cells. A link-specific cell-size or a link-specific number of cells determines the number of cells in a specific lane. Cells are not modeled as objects, since all the necessary characteristics (geometry) are available in the lane or link object. All lane objects of a specific link maintain matrices of size [Nr of Cells x Nr of User classes] of the dynamic variables that are updated in the Link flow procedure (for instance, *MLMC* Link equations). These include class specific densities, speeds, flows.

Finally, a user class object is modeled as a combination of a vehicle type object and a node (destination) object. The latter may be omitted. This implies that there may be as much as ($nr.$ of vehicle types) x (nr of destinations + 1) different user classes for a specific network. A vehicle type object incorporates all parameters associated with different types of driver-vehicle combinations. These include physical attributes, such as, vehicle length and maximum density; driver related attributes, such as, reaction time, spontaneous lane changing rates. As elaborated in Chapter 4 and Chapter 6, these parameters are used in the *MLMC*

equations. Since the extension of the HELENA model with the lane-changing and intersection specific equations is still ongoing, we reserve empirical results with the simulator for near future research.

Appendix D

MATLAB-based Nelder-Mead Algorithm

This appendix presents the working of the Nelder-Mead optimization algorithm in the MATLAB environment. The code was written based on the built-in function *fminsearch* of MATLAB.

if $nargin < 2$

    error('two input arguments are required');

end

$sizex = size(x)$;
$transpose = (length(sizex) == 2 \ \& \ sizex(2) == 1)$;

if transpose

    $x = x'$;

end

if $nargin < 3$

    $ix = 1 : prod(sizex)$;

end

$ix = unique(ix)$; $lx = length(ix)$;
if $nargin < 4$

    $options = []$;

end

if $nargin < 5$

$vlb = -Inf + zeros(size(1, lx));$

end

if $nargin < 6$

$vub = Inf + zeros(size(1, lx));$

end

$options = foptions(options);$
$prnt = options(1);$

if $options(14)$

$options(14) = 50 * lx;$

end

$tolx = options(2);$
$tolf = options(3);$
$maxfcalls = options(14);$

$varargs = \{vlb, vub, fun, varargin\{:\}\};$

$xx = x(ix)';$
if $all(abs(xx) < eps)$

$xx = xx + eps;$

end

$d = 0.1;$

$v = repmat(xx, 1, lx + 1) + [diag(d * xx)\ zeros(lx, 1)];$
$fcalls = 0;\ dv = Inf;$

if prnt

$fprintf('\%7s\%10s\%12s','f - COUNT','FUNCTION','x - TOL');$

end
$i = 0;$

while $(i < lx)$ & $(dv >= tolx)$

```
    [y, fmin, tmp4] = fminmod(v, tolf, maxfcalls, x, ix, varargs{:});
y = y'; x(ix) = y;
fcalls = fcalls + tmp4;
if prnt
        fprintf('%7d%10.5f', fcalls, fmin);
end
    if lx == 1
        break
end
    if lx == 2
        v(:, 1) = y;
else
        for j = 1 : lx - 1
            j1 = [jj + 1];
         [y(j1), fmin, tmp4] = fminmod([xx(j1) y(j1) [xx(j1(1))
         y(j1(2))]'], ...
                tolf, maxfcalls, ...
            x, ix(j1), varargs{:});
         x(ix) = y; v(:, j) = y;
         fcalls = fcalls + tmp4;
      end
end
    j1 = [1 lx];
[y(j1), fmin, tmp4] = fminmod([xx(j1) y(j1) [xx(j1(1)) y(j1(2))]'], ...
        tolf, maxfcalls, ...
    x, ix(j1), varargs{:});
x(ix) = y; v(:, lx) = y;
fcalls = fcalls + tmp4;
    if lx > 3
        j1 = [2lx - 1];
end
[y(j1), fmin, tmp4] = fminmod([xx(j1) y(j1) [y(j1(1)) xx(j1(2))]'], ...
        tolf, maxfcalls, ...
    x, ix(j1), varargs{:});
```

$x(ix) = y; v(:, lx + 1) = y;$
$fcalls = fcalls + tmp4;$
$dv = max(tol(min(v, [], 2), max(v, [], 2)));$
if prnt
$fprintf('\%7d\%10.5f\%12.6f', fcalls, fmin, dv);$
end
$i = i + 1;$
end
if prnt
$fprintf('');$
end
$options(8) = fmin;$
$options(10) = fcalls;$
if transpose
$x = x';$
end

return

function $[x, fmin, fcalls] = fminmod(v, tolf, maxfcalls, varargin)$

$rho = 1; chi = 2; psi = 0.5; sigma = 0.5;$
$n = length(v(:, 1));$
$onesn = ones(1, n);$
$two2np1 = 2 : n + 1;$
$one2n = 1 : n;$
$zerosn = zeros(1, n);$
$x = zerosn;$
$fv = zeros(1, n + 1);$

for $j = 1 : n + 1$
$x(:) = v(:, j);$
$fv(j) = wrapper(x, varargin\{:\});$
end

$[fv, jj] = sort(fv);$
$v = v(:, jj);$
$fmin = fv(1); fcalls = n + 1;$

while $(fcalls < maxfcalls)\& \ldots$

```
        (tol(fmin, fv(n + 1)) > tolf)
    shrink = 0;
    xbar = sum(v(:, one2n), 2)/n;
    xr = (1 + rho) * xbar − rho * v(:, n + 1);
    x(:) = xr;
    fxr = wrapper(x, varargin:);
    fcalls = fcalls + 1;

  if fxr < fv(1)
      xe = (1 + rho * chi) * xbar − rho * chi * v(:, n + 1);
   x(:) = xe;
   fxe = wrapper(x, varargin:);
   fcalls = fcalls + 1;
      if fxe < fxr
          v(:, n + 1) = xe;
       fv(n + 1) = fxe;
   else
          v(:, n + 1) = xr;
       fv(n + 1) = fxr;
   end
  elseif fxr < fv(n)
      v(:, n + 1) = xr;
   fv(n + 1) = fxr;
else
      if fxr < fv(n + 1)
          xc = (1 + psi * rho) * xbar − psi * rho * v(:, n + 1);
       x(:) = xc;
       fxc = wrapper(x, varargin:);
       fcalls = fcalls + 1;
          if fxc <= fxr
             v(:, n + 1) = xc;
         fv(n + 1) = fxc;
      else
             shrink = 1;
      end
   else
          xcc = (1 − psi) * xbar + psi * v(:, n + 1);
      x(:) = xcc;
      fxcc = wrapper(x, varargin{:});
      fcalls = fcalls + 1;
          if fxcc < fv(n + 1)
```

$v(:, n+1) = xcc;$
$fv(n+1) = fxcc;$
else
$shrink = 1;$
end
end
if shrink
for $j = two2np1$
$v(:, j) = v(:, 1) + sigma * (v(:, j) - v(:, 1));$
$x(:) = v(:, j);$
$fxcc = wrapper(x, varargin\{:\});$
end
$fcalls = fcalls + n;$
end
end
$[fv, jj] = sort(fv);$
$v = v(:, jj);$
fmin=fv(1);

end
$x(:) = v(:, 1);$

return

function $r = tol(a, b)$

$c = (abs(b) + abs(a))/2;$
$j = find(c < eps);\ c(j) = ones(size(j));$
$r = abs(b - a)./c;$

return

function $fmin = wrapper(x, x0, ix, vlb, vub, funfcn, varargin)$

$x1 = zeros(1, prod(size(x0)));$
$x1(:) = x0;$
$x1(ix) = x;$
$x0(:) = max(min(x1, vub), vlb);$

$funfcn = fcnchk(funfcn, 1 + length(varargin));$
$[fmin, fconstr] = feval(funfcn, x0, varargin\{:\});$

$fconstr = [vlb - x1, x1 - vub, fconstr];$
$fmin = fmin + 1e6 * sum(fconstr(find(fconstr > 0)));$

return

About the Author

Dong NGODUY was born on 14 August 1975 in Vietnam. He finished his high school in 1991 and received his Bachelor degree (with honor) in Civil Engineering from the Hanoi University of Transportation in 1996. He started to work for the Vietnamese Research Institute of Transportation Science and Technology from 1996 to 1999. In August 1999, he attended the International Master Program specialized in traffic safety at the Linkoping University of Technology (Sweden). His master thesis concerned the development of a mathematical model to predict the trajectories of vehicles in a freeway when overtaking or after crashing, which was defended successfully (with distinction) in 2001. Then he started to work as a research assistant at the Napier University (United Kingdom) under the leadership of Professor Mike Maher for a year. In this period, he conducted a research in Accident Minimizing Traffic Flow Patterns in Urban Networks.

Since 1 May 2002, he has been employed by the Transportation and Planning Section of the Delft University of Technology (The Netherlands) to conduct a research in the AMICI project (Advanced Multi–agent Information and Control for Integrated multi–class traffic networks). The AMICI research program focuses on traffic congestion management in and around large cities, such as Beijing, Rotterdam, Amsterdam and Shanghai. This research, under the supervision of Professor Henk van Zuylen and Dr. Serge Hoogendoorn, resulted in his PhD dissertation and publications in the Journals such as Transportation Research Records, Transportation Research part B, Transportmetrica, and Applied Mathematical Modeling, as well as in several international conferences in Asia, Europe and North America. In 2005 he received a certificate for the excellence of research at the 10th HKSTS International Conference. His PhD dissertation concerned the development of a generalized continuum traffic model describing the (infrastructure) discontinuities of multiclass traffic flow on multilane freeways and in multilane urban networks. His research interests are continuum traffic flow models and their numerical solutions, traffic control and optimization algorithm, model-based traffic stability analysis.

Author's publications

A series of author's publications in traffic flow theory:

In Journals

1. Ngoduy, D., Hoogendoorn, S., and Zuylen, H. J. van. (2004a). Cross-comparison of Numerical Schemes for Macroscopic Traffic Flow Models. *Journal of Transportation Research Records*, Vol. 1876, pp. 52–61.

2. Ngoduy, D., Hoogendoorn, S., and Zuylen, H. J. van. (2004c). Multiclass Traffic Flow Theory for Modeling of Discontinuities on Multilane Freeways. Revised for *Journal of Transportation Research B*.

3. Ngoduy, D., Hoogendoorn, S., and Lint, J. W. C. van. (2005a). Modeling Traffic Flow Operation in Multilane and Multiclass Urban Networks. *Journal of Transportation Research Records*, Vol. 1923, pp. 73–81.

4. Ngoduy, D. (2005b). Derivation of Continuum Traffic Model for Weaving Sections on Freeways. Accepted for *Journal of Transportmetrica*.

5. Ngoduy, D., Hoogendoorn, S., and Zuylen, H. J. van. (2006a). New Continuum Traffic Model for Freeway with On-and Off-ramp to Explain Different Traffic Congested States. Accepted for *Journal of Transportation Research Records*.

In Proceedings

1. Ngoduy, D., and Hoogendoorn, S. (2003a). An Automated Calibration Procedure for Traffic Flow Models. In *Proceedings of the 10th International Federation of Automatic Control*, Tokyo, pp. 295–300.

2. Ngoduy, D., and Hoogendoorn, S. (2003b). Positively Conservative Numerical Scheme for Macroscopic Traffic Flow Models. In *Proceedings of the 10th International Federation of Automatic Control*, Tokyo, pp. 301–306.

3. Hegyi, A., Ngoduy, D., Schutter, B. de, Hellendoorn, J., Hoogendoorn, S. P., and Stramigioli, S. (2003). Suppressing Shock Waves on the A1 in The Netherlands–Model Calibration and Model-Based Predictive Control. In *Proceedings of the 6th International Incollection on Intelligent Transportation Systems*, Shanghai, pp. 672–677.

4. Ngoduy, D., Hoogendoorn, S., and Zuylen, H. J. van. (2004b). Cross-comparison of Numerical Schemes for Macroscopic Traffic Flow Models. In *Annual Meeting of Transportation Research Boards*, Washington D.C.

5. Ngoduy, D., Hoogendoorn, S., and Zuylen, H. J. van. (2004b). Modeling and Simulation of Multilane and Multiclass Traffic Flow at On and Off Ramps. In *Proceedings of the 5th Triennal Symposium onTransportation Analysis*, Guadeloupe, CD-ROM.

6. Ngoduy, D., Hoogendoorn, S., and Zuylen, H. J. van. (2004c). Multiclass Traffic Flow Theory for Modeling of Multilane Motorway Networks. In *Proceedings of the 10th World Conference in Transportation Research*, Istanbul, in press.

7. Ngoduy, D., Hoogendoorn, S., and Zuylen, H. J. van. (2004d). Macroscopic Traffic Flow Modeling of Weaving Sections on Freeways. In *Proceedings of the 8th TRAIL Congress*, Rotterdam, pp. 331–354.

8. Ngoduy, D., Hoogendoorn, S., and Lint, J. W. C. van. (2005b). Modeling Traffic Flow Operation in Multilane and Multiclass Urban Networks. In *Annual Meeting of Transportation Research Boards*, Washington D.C.

9. Ngoduy, D. (2005b). Derivation of Continuum Traffic Model for Weaving Sections on Freeways. In *Proceedings of the 10th HKSTS International Conference*, Hongkong, pp.328-337

10. Ngoduy, D., Hoogendoorn, S., and Zuylen, H. J. van. (2006a). New Continuum Traffic Model for Freeway with On-and Off-ramp to Explain Different Traffic Congested States. *Annual Meeting of Transportation Research Boards*, Washington D.C.

Submitted to Journals

1. Ngoduy, D., and Hoogendoorn, S. Derivation and Stability Analysis of a Macroscopic Model at an On and Off ramp. *Journal of Applied Mathematical Modeling*

Summary

Congestion in traffic networks causes severe problems in and around large cities. It is the source of important economic inefficiencies, both on the level of individual persons and of the society as a whole. However, societal and environmental constraints prohibit large-scale extensions of the currently available network infrastructure. Consequently, solutions need to be sought in using the existing traffic networks more efficiently. Dynamic Traffic Management (DTM) plays an important role in this, providing the possibilities to aim for a sustainable transportation system. Empirical studies have also shown that solving traffic problems locally frequently only amounts to relocating bottlenecks, either within the freeway network, or from a freeway to the underlying urban network. Improving traffic conditions on a ring road around a city may also increase the use of this ring road by urban traffic. This is why the net profit of isolated DTM measures if often small, and integrated approaches are needed. At the same time, currently synergetic effects between different DTM measures are not fully utilized for improving network-wide traffic conditions effectively. We envisage that to effectively deploy DTM to resolve congestion on freeways and in urban networks, an integrated and coordinated approach to DTM is required. To develop such a control method, an analytical model-based approach is required. To this purpose, an elaborate model describing the dynamics of traffic flow on freeways and in urban networks is necessary.

In this thesis, we establish a new approach to model the (infrastructure) discontinuities of heterogeneous traffic flow operations on multilane freeways and in multilane urban networks. The model provides insight into the interactions of vehicles between lanes near to a bottleneck (that is, on–ramps, off–ramps, weaving areas, and intersections). Research conducted in this thesis involves three parts: the development of a generalized gas-kinetic and macroscopic model for interrupted traffic flow, the development of a dedicated numerical scheme for general high(er) order macroscopic traffic models (of the hyperbolic type), and the development and application of an automated calibration procedure for general macroscopic traffic models, used to cross-compare the performance of the proposed model with other models. In this summary, we present the main achievements of this thesis.

The theories and models developed in this thesis are based on the concepts of *gap-acceptance* theory and the *renewal process*. The *gap-acceptance* theory is used to determine how lane-changing processes take place, such as, immediate lane-changing and mandatory lane-changing. While the former reflects the fact that when a faster driver approaches a slower vehicle, he has to change to either adjacent lane in order to maintain his current speed, the latter describes forced lane-changes when the current lane stops being available (that is, when a driver ap-

proaches the downstream end of an on–ramp, off–ramp, weaving area or intersection). According to the *gap-acceptance* theory, a vehicle is able to change to the target lane when both the *lead-gap* and *lag-gap* are accepted by the driver. The *lead-gap* is accepted if the space between the lane-changing vehicle after the lane-change and its leader in the target lane is larger than a certain threshold distance (*critical lead-gap*). The *lag-gap* is accepted if the space between the lane-changing vehicle after the lane-change and its follower in the target lane is larger the than *critical lag-gap*. At bottlenecks, drivers are willing to accept smaller gaps as they approach the end of the current lane. That is, the remaining distance to the end of current lane influences the *gap-acceptance* behavior. In order to determine these gap distributions in various traffic situations at bottlenecks, the *renewal process* is applied. We implement the concept of gap-acceptance theory and of renewal processes into the existing multilane and multiclass (MLMC) gas-kinetic traffic model, which describes the dynamics of the MLMC phase-space density (defined as the probability distribution of traffic densities). This newly developed gas-kinetic model is able to describe the dynamics of interrupted traffic flow at bottlenecks.

For the application of model-based control, we derive a tractable macroscopic model from the developed generalized gas-kinetic model using the method of moments. This model allows to explicitly take into account the relation between the road geometry and the traffic operations, which has been often neglected in existing macroscopic models. We show by simulation that the new model can replicate traffic congested states similar to current macroscopic models. Furthermore, using the linear stability analysis of the new model, we mathematically show the impact of acceleration lane length and ramp flow on the dynamics of main traffic flow, which so far has not been covered by existing macroscopic models. This analytical result is also illustrated with simulation. The acceleration lane length necessary for a adequate, that is, stable, operations of the main traffic depends on the combination of traffic demand from the on–ramp and from the upstream of the main carriageway. This finding is important for the design of control measures for the on-ramp (such as, ramp metering) or the necessary acceleration lane length given an O-D matrix.

To numerically solve the developed macroscopic model, it is essential to have a suitable numerical solution. In this thesis, we show that a small perturbation in the traffic flow may result in formation of traffic congestion which never occurs in reality, thus, an inappropriate choice of a numerical scheme can result in very poor performance of the model. Different approaches have previously been proposed, but the definitive answer on their applicability in terms of accuracy and reliability has so far not been given. For this reason, in this thesis, we propose a numerical scheme that is able to prevent traffic from moving backwards. This novel numerical scheme is based on an approximation of the exact solution of the Riemann problem, in which intermediate states are averaged and the contact waves are ignored (contact waves occur when two traffic states that have the same speed but different densities come in contact with each other). We show both numerically and analytically that the proposed solution can satisfy all positivity conservative variable constraints under various traffic situations. The proposed solution is cross-compared with other numerical schemes using real data. Based on the obtained results, we show that the proposed scheme is the most

reliable in terms of computational time and numerical stability compared to the other considered solutions, in particular when the occurrence of traffic congestion is concerned. The scheme improves the performance of the model significantly, and thus provides an effective and reliable approach to simulate traffic flow under congestion.

The new modeling approach presented in this thesis is also used to describe the operations of heterogeneous traffic at multilane intersections in an urban network. This leads to a new model that is able to take explicitly into account the interaction between traffic streams at intersections, such as left-turning, right-turning and through movements. This allows to model the traffic flow at an intersection more accurately than is possible with existing macroscopic modeling approaches.

Finally, we present the results of an application of the developed model for a real network. In order to calibrate/validate the developed model with empirical data, we propose an automated calibration procedure for general macroscopic models based on the generalization of a direct search optimization algorithm (Nelder-Mead-Delft algorithm). The validated results of the developed model are then compared with the (validated) results obtained from other simulators, namely a macroscopic model (METANET). Conclusions that follow from this comparison are that the developed model is more accurate than the other in terms of estimating the dynamics of macroscopic traffic variables (density and speed). Furthermore, the proposed model can represent stop–and–go waves induced near the on–ramp. The transition to congested traffic states from free flow-wide jams is also replicated well by the proposed model.

TRAIL Thesis Series

A series of The Netherlands TRAIL Research School for thesis on transport, infrastructure and logistics.

Nat, C.G.J.M., van der, *A Knowledge-based Concept Exploration Model for Submarine Design*, T99/1, March 1999, TRAIL Thesis Series, Delft University Press, The Netherlands

Westrenen, F.C., van, *The Maritime Pilot at Work: Evaluation and Use of a Time-to-boundary Model of Mental Workload in Human-machine Systems*, T99/2, May 1999, TRAIL Thesis Series, Eburon, The Netherlands

Veenstra, A.W., *Quantitative Analysis of Shipping Markets*, T99/3, April 1999, TRAIL Thesis Series, Delft University Press, The Netherlands

Minderhoud, M.M., *Supported Driving: Impacts on Motorway Traffic Flow*, T99/4, July 1999, TRAIL Thesis Series, Delft University Press, The Netherlands

Hoogendoorn, S.P., *Multiclass Continuum Modelling of Multilane Traffic Flow*, T99/5, September 1999, TRAIL Thesis Series, Delft University Press, The Netherlands

Hoedemaeker, M., *Driving with Intelligent Vehicles: Driving Behaviour with Adaptive Cruise Control and the Acceptance by Individual Drivers*, T99/6, November 1999, TRAIL Thesis Series, Delft University Press, The Netherlands

Marchau, V.A.W.J., *Technology Assessment of Automated Vehicle Guidance - Prospects for Automated Driving Implementation,* T2000/1, January 2000, TRAIL Thesis Series, Delft University Press, The Netherlands

Subiono, *On Classes of Min-max-plus Systems and their Applications*, T2000/2, June 2000, TRAIL Thesis Series, Delft University Press, The Netherlands

Meer, J.R., van, *Operational Control of Internal Transport*, T2000/5, September 2000, TRAIL Thesis Series, Delft University Press, The Netherlands

Bliemer, M.C.J., *Analytical Dynamic Traffic Assignment with Interacting User-Classes: Theoretical Advances and Applications using a Variational Inequality Approach*, T2001/1, January 2001, TRAIL Thesis Series, Delft University Press, The Netherlands

Muilerman, G.J., *Time-based logistics: An analysis of the relevance, causes and impacts*, T2001/2, April 2001, TRAIL Thesis Series, Delft University Press, The Netherlands

Roodbergen, K.J., *Layout and Routing Methods for Warehouses*, T2001/3, May 2001, TRAIL Thesis Series, The Netherlands

Willems, J.K.C.A.S., *Bundeling van infrastructuur, theoretische en praktische waarde van een ruimtelijk inrichtingsconcept,* T2001/4, June 2001, TRAIL Thesis Series, Delft University Press, The Netherlands

Binsbergen, A.J., van, J.G.S.N. Visser, *Innovation Steps towards Efficient Goods Distribution Systems for Urban Areas*, T2001/5, May 2001, TRAIL Thesis Series, Delft University Press, The Netherlands

Rosmuller, N., *Safety analysis of Transport Corridors*, T2001/6, June 2001, TRAIL Thesis Series, Delft University Press, The Netherlands

Schaafsma, A., *Dynamisch Railverkeersmanagement, besturingsconcept voor railverkeer op basis van het Lagenmodel Verkeer en Vervoer*, T2001/7, October 2001, TRAIL Thesis Series, Delft University Press, The Netherlands

Bockstael-Blok, W., *Chains and Networks in Multimodal Passenger Transport. Exploring a design approach*, T2001/8, December 2001, TRAIL Thesis Series, Delft University Press, The Netherlands

Wolters, M.J.J., *The Business of Modularity and the Modularity of Business,* T2002/1, February 2002, TRAIL Thesis Series, The Netherlands

Vis, F.A., *Planning and Control Concepts for Material Handling Systems*, T2002/2, May 2002, TRAIL Thesis Series, The Netherlands

Koppius, O.R., *Information Architecture and Electronic Market Performance*, T2002/3, May 2002, TRAIL Thesis Series, The Netherlands

Veeneman, W.W., *Mind the Gap; Bridging Theories and Practice for the Organisation of Metropolitan Public Transport*, T2002/4, June 2002, TRAIL Thesis Series, Delft University Press, The Netherlands

Van Nes, R., *Design of multimodal transport networks, a hierarchical approach*, T2002/5, September 2002, TRAIL Thesis Series, Delft University Press, The Netherlands

Pol, P.M.J., *A Renaissance of Stations, Railways and Cities, Economic Effects, Development Strategies and Organisational Issues of European High-Speed-Train Stations*, T2002/6, October 2002, TRAIL Thesis Series, Delft University Press, The Netherlands

Runhaar, H., *Freight transport: at any price? Effects of transport costs on book and newspaper supply chains in the Netherlands*, T2002/7, December 2002, TRAIL Thesis Series, Delft University Press, The Netherlands

Spek, S.C., van der, Connectors. *The Way beyond Transferring*, T2003/1, February 2003, TRAIL Thesis Series, Delft University Press, The Netherlands

Lindeijer, D.G., *Controlling Automated Traffic Agents*, T2003/2, February 2003, TRAIL Thesis Series, Eburon, The Netherlands

Riet, O.A.W.T., van de, *Policy Analysis in Multi-Actor Policy Settings. Navigating Between Negotiated Nonsense and Useless Knowledge*, T2003/3, March 2003, TRAIL Thesis Series, Eburon, The Netherlands

Reeven, P.A., van, *Competition in Scheduled Transport*, T2003/4, April 2003, TRAIL Thesis Series, Eburon, The Netherlands

Peeters, L.W.P., *Cyclic Railway Timetable Optimization*, T2003/5, June 2003, TRAIL Thesis Series, The Netherlands

Soto Y Koelemeijer, G., *On the behaviour of classes of min-max-plus systems*, T2003/6, September 2003, TRAIL Thesis Series, The Netherlands

Lindveld, Ch..D.R., *Dynamic O-D matrix estimation: a behavioural approach*, T2003/7, September 2003, TRAIL Thesis Series, Eburon, The Netherlands

Weerdt, de M.M., *Plan Merging in Multi-Agent Systems*, T2003/8, December 2003, TRAIL Thesis Series, The Netherlands

Langen, de P.W, *The Performance of Seaport Clusters*, T2004/1, January 2004, TRAIL Thesis Series, The Netherlands

Hegyi, A., *Model Predictive Control for Integrating Traffic Control Measures*, T2004/2, February 2004, TRAIL Thesis Series, The Netherlands

Lint, van, J.W.C., *Reliable Travel Time Prediction for Freeways*, T2004/3, June 2004, TRAIL Thesis Series, The Netherlands

Tabibi, M., *Design and Control of Automated Truck Traffic at Motorway Ramps*, T2004/4, July 2004, TRAIL Thesis Series, The Netherlands

Verduijn, T.M., *Dynamism in Supply Networks: Actor switching in a turbulent business environment*, T2004/5, September 2004, TRAIL Thesis Series, The Netherlands

Daamen, W. *Modelling Passenger Flows in Public Transport Facilities*, T2004/6, September 2004, TRAIL Thesis Series, The Netherlands

Zoetman, A., *Railway Design and Maintenance from a Life-Cycle Cost Perspective: A Decision-Support Approach*, T2004/7, November 2004, TRAIL Thesis Series, The Netherlands

Bos, D.M., *Changing Seats: A Behavioral Analysis of PR Use*, T2004/8, November 2004, TRAIL Thesis Series, The Netherlands

Versteegt, C., *Holonic Control For Large Scale Automated Logistic Systems*, T2004/9, December 2004, TRAIL Thesis Series, The Netherlands

Wees, K.A.P.C. van *Juridische Aspecten van ADAS (Advanced Driver Assistance Systems)*, T2004/10, December 2004, TRAIL Thesis Series, The Netherlands

Tampere, C.M.J. *Human-Kinetic Multiclass Traffic Flow Theory and Modelling: With Application to Advanced Driver Assistance Systems in Congestion*, T2004/11, December 2004, TRAIL Thesis Series, The Netherlands

Rooij, R.M. *The Mobile City. The planning and design of the Network City from a mobility point of view*, T2005/1, February 2005, TRAIL Thesis Series, The Netherlands

Le-Anh, T. *Intelligent Control of Vehicle-Based Internal Transport Systems*, T2005/2, April 2005, TRAIL Thesis Series, The Netherlands

Zuidgeest, M.H.P. *Sustainable Urban Transport Development: a Dynamic Optimization Approach*, T2005/3, April 2005, TRAIL Thesis Series, The Netherlands

Hoogendoorn-Lanser, S. *Modelling Travel Behavior in Multimodal Networks*, T2005/4, May 2005, TRAIL Thesis Series, The Netherlands

Dekker, S. *Port Investment - Towards an Integrated Planning of Port Capacity*, T2005/5, June 2005, TRAIL Thesis Series, The Netherlands

Koolstra, K. *Transport Infrastructure Slot Allocation*, T2005/6, June 2005, TRAIL Thesis Series, The Netherlands

Vromans, M. *Reliability of Railway Systems*, T2005/7, July 2005, TRAIL Thesis Series, The Netherlands

Oosten, W. *Ruimte voor een democratische rechtsstaat. Geschakelde sturing bij ruimtelijke investeringen*, T2005/8, September 2005, TRAIL Thesis Series, The Netherlands

Le-Duc, T. *Design and control of efficient order picking*, T2005/9, September 2005, TRAIL Thesis Series, The Netherlands

Goverde, R. *Punctuality of Railway Operation and Timetable Stability Analysis*, T2005/10, October 2005, TRAIL Thesis Series, The Netherlands

Kager, R. *Design and implementation of a method for synthesis of travel diary data*, T2005/11, October 2005, TRAIL Thesis Series, The Netherlands

Boer, C. *Distributed Simulation in Industry*, T2005/12, November 2005, TRAIL Research School, The Netherlands

Pielage, P. *Conceptual Design of Automated Freight Transport Systems. Methodology and Practice*, T2005/14, November 2005, TRAIL Research School, The Netherlands

Groothedde, B. *Collaborative Logistics and Transportation Networks. A Modeling Approach to Hub Network Design*, T2005/15, November 2005, TRAIL Research School, The Netherlands

Valk, J.M., *Coordination among Autonomous Planners*, T2005/16, December 2005, TRAIL Thesis Series, The Netherlands

Krogt, R.P.J. van der, *Plan Repair in Single-Agent and Multi-Agent Systems*, T2005/17, December 2005, TRAIL Thesis Series, The Netherlands

Bontekoning, Y.M., *Hub exchange operations in intermodal hub-and-spoke networks. A performance comparison of four types of rail-rail exchange facilities*,T2006/1, February 2006, TRAIL Thesis Series, The Netherlands

Lentink, R., *Algorithmic Decision Support for Shunt Planning*, T2006/2, February 2006, TRAIL Thesis Series, The Netherlands

Ngoduy, D., *Macroscopic Discontinuity Modeling for Multiclass Multilane Traffic Flow Operations*, T2006/3, April 2006, TRAIL Thesis Series, The Netherlands